Dissertations - ALL

5-14-2017

Design and Behavior of Steel Delta Girders

Omar El Masri
Syracuse University

Recommended Citation

Abstract

In steel structures, I-sections are commonly used for beams and columns. These cross-sections usually lack lateral rigidity and torsional stiffness. An effective method to improve their lateral rigidity and overall flexural resistance is to weld two inclined rectangular plates to the compression flange and the compression portion of the web of hot-rolled or welded I-section to form what is known as a Delta girder. This mixed cross-section, i.e., cross-section composed of an open profile attached to a closed profile, can provide enhanced torsional stiffness and hence noticeably higher lateral-torsional buckling (LTB) capacity for the beam. While Delta girders can be used for any beams, their main applications are the design of crane runway and bridge beams and strengthening of existing beams.

The main objectives of this dissertation are to study the static behavior of these girders and to provide a set of design equations for their nominal flexural and shear capacities. The research includes deriving closed-form equations for the cross-section properties of Delta girders. These equations are then verified against solutions obtained numerically. Using these cross-section properties, the theoretical lateral-torsional buckling capacity of Delta girders are determined and compared against results obtained from a finite element (FE) analysis. The results show that the theoretical LTB equation derived for general monosymmetric sections can be applied to these Delta girders. Additionally, it is shown that a simplified expression for the coefficient of monosymmetry β_x derived for I-sections can be used in the computation of the elastic LTB capacity of Delta girders. A parametric study is then performed based on elastic LTB capacity to demonstrate the effectiveness of Delta girders in achieving a favorable capacity-to-weight ratio when compared to standard I-section members.

A refined three-dimensional (3D) nonlinear inelastic FE models are then developed to examine the capacity of simply-supported Delta girders under uniform bending and pure shear. The models take into considerations the effects of initial geometrical imperfections and residual stresses on the behavior of Delta girders. The FE model and the modeling techniques used are verified against the experimental result of a test beam that failed by inelastic LTB. The analysis covers a comprehensive range of Delta girder dimensions based on the dimensions of standard hot-rolled European H- and I-sections. A sensitivity study on the effects of using reduced imperfections magnitudes shows up to 18.2% increase in the LTB capacity of the girder.

Based on the FE LTB simulation results, it is shown that the buckling curve in the AISC (2016a) specifications overestimates the buckling capacity of Delta girders by an average of 9% and a maximum value of 21%. On the other hand, buckling curves "a" and "b" for rolled sections or equivalent welded sections case in the EuroCode 3 (2005) for Delta girders with $d/b_c \leq 2$ and $d/b_c > 2$, respectively, provide an average difference of only 2% and a maximum difference of 7% in comparison to the FE results. Hence, these two curves are recommended for the LTB design of Class 1 (compact) Delta girders. Additionally, design recommendations are provided for selecting the proper delta stiffeners dimensions based on the cross-section geometries of the corresponding I-sections.

Shear capacity equations for Class 1 (compact) Delta girders are proposed based on FE simulation results. The equations provide the option of selecting a conservative value that ignores strain hardening in the cross-section or a value that allows for some strain hardening to occur. In comparison to I-sections, the Delta girders analyzed in this study show an increase in shear capacity in the range of 41% to 89%. Furthermore, it is shown that in contrast to I-sections,

yielding is a gradual process in Delta girders due to the presence of a non-uniform elastic shear stress distribution in the cross-section.

Design and Behavior of Steel Delta Girders

by

Omar Youssef El Masri

B.E., Lebanese American University, 2012
M.S., Lebanese American University, 2014

Dissertation
Submitted in partial fulfillment of the requirements for the degree of
Doctor of Philosophy in Civil Engineering

Syracuse University
May 2017

In the name of God, The Most Compassionate, The Most Merciful

Dedication

To my beloved family

Acknowledgments

I am grateful to have had so many great people support me for the last three years to complete my Ph.D. journey. Without them, this dissertation could not have been undertaken and completed.

First and foremost, I wish to express my deepest gratitude and admiration to my advisor, Dr. Eric M. Lui, without whose knowledge, contributions, guidance and availability this dissertation would not have seen the light. His remarkable knowledge of structural engineering, his perpetual energy and his accessibility to his students are exceptional. My interaction with him has driven me to dig deeper and push the frontier further.

I also want to extend my gratitude to my dissertation committee members - Dr. Riyad Aboutaha, Dr. Hossein Ataei, Dr. Junho Chun, Dr. James Mandel and Dr. Teng Zhang - for their encouragements, comments and support. I also wish to thank Dr. Barry D. Davidson who was a committee member of my qualifying and candidacy examinations, but was away on sabbatical and was not able to attend my Ph.D. defense.

I would like to thank Mr. Abdallah Yabroudi for his generous financial support through the Yabroudi & Al-Bitar Fellowship during my first two years of study.

During my graduate study, I was fortunate to have peers and friends who offered their continuous support and encouragement. To list them all would not be possible, but among them I am especially thankful for Dr. James Mandel and his wife, Mrs. Carolyn Mandel, for sharing their home and family time on holidays and special events with me and for the warm welcome they offered me whenever I was in their house. I would like to thank Dr. Gebran Karam and Dr.

Samir El Zein for their heartfelt encouraging words. I would also like to thank Ms. Elizabeth Buchanan and Ms. Maja Macura for their help and support at various stages of this dissertation.

Finally, I wish to acknowledge the unconditional love and moral support I have received from my parents and siblings, and the unswerving financial support of my father. Also, I would like to thank my grandmother and my aunt for their love, care and continuous encouragement over the years. To all of them, I am forever indebted.

Above all, I thank God, The Creator and The Maker, for his continuous work in my life. To Him is due all glory.

Table of Contents

List of Tables

xvi

List of Figures

Chapter 1

Introduction

"The scientific man does not aim at an immediate result. He does not expect that his advanced ideas will be readily taken up. His work is like that of the planter – for the future. His duty is to lay the foundation for those who are to come, and point the way. He lives and labors and hopes."

Nikola Tesla (1856-1943)

1.1 <u>Background</u>

I-sections are one of the most commonly used structural shapes for steel beams and columns. Although these sections possess good flexural strength and rigidity when bent about the major axis, they often lack minor axis strength and have weak torsional stiffness. As a result, if these members are slender, local buckling or lateral-torsional buckling (LTB) often governs the design. To improve their load carrying capacity, lateral bracing or longitudinal stiffeners can be added. However, lateral bracing can only be installed on site and so LTB can still be a problem during transportation and erection. On the other hand, longitudinal stiffeners can enhance the strength and stiffness of the web, but do not always add appreciable torsional rigidity to the section (Szewczak, Smith, & DeWolf, 1983). Furthermore, if the sections are to be used as crane runway or bridge beams, LTB is often a limiting design condition because unlike bridge girders they usually lack lateral supports. Since thin-walled closed-sections have much higher torsional stiffness than open-sections, several studies have been conducted to add a closed region to a

1

typical I-section. One example is reinforcing the I-sections by welding an equal-leg angle (L-section) on top of the compression flange in the form of a hat (O'Connor, Goldsmith, & Ryall, 1965). Another example is to use hollow tubular flange plate girders (Hassanein, Kharoob, & El Hadidy, 2013).

Research work on adding stiffeners to plates and plate girders to enhance their stability can be traced back to the work of Timoshenko (1921) and Chwalla (1936). At present, transverse and/or longitudinal stiffeners are often used in the design of plate girders. The primary reasons to employ transverse stiffeners are to improve the buckling resistance of the web to shear forces and/or concentrated loads and to develop postbuckling strength. On the other hand, longitudinal stiffeners are required for plate girders with slender webs to control web lateral flexing and increase the web bend-buckling resistance. Analytical, experimental and numerical research work on transverse and longitudinal stiffeners is abundant in the literature (Kim & White, 2013; Maiorana, Pellegrino, & Modena, 2011; Owen, Rockey, & Skaloud, 1970; Plum & Svensson, 1993; Takabatake, 1988; Takabatake, Kusumoto, & Inoue, 1991; White & Baker, 2008). Other forms of stiffeners include inclined web stiffeners that can increase the LTB capacity of girders (Yang & Lui, 2012) . In lieu of adding stiffeners, Chen and Das (2009) examined reinforcing steel I-beams with carbon fiber reinforced polymers (CFRP) while Egilmez and Yormaz (2011) examined using glass fiber reinforced polymers (GFRP) to reinforce steel I-beams.

A Delta girder is formed by welding two inclined rectangular plates to the compression flange and the compression portion of the web of a hot-rolled or welded I-section as shown in Figure 1.1. This hybrid cross-section, i.e., section composed of a combination of open and closed profiles, is monosymmetric and greatly enhances the section's torsional stiffness, and hence increases the beam's LTB capacity. The main advantages of Delta girders are:

2

- Improving the lateral-torsional buckling capacity of the girder

- Increasing the shear resistance of the cross-section

- Reducing the width-to-thickness ratios of both the compression flange and the web

- Replacing the longitudinal and transverse stiffeners if they are needed

- Enhancing the girder resistance to eccentric loading

- Facilitating the transportation and erection processes

- Strengthening the existing beams or girders in retrofitting projects.
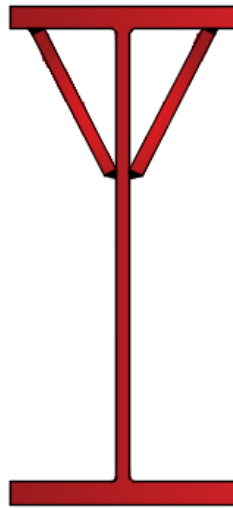
Figure 1.1 Typical Delta girder

The main anticipated applications for Delta girders are the design of new crane runway and bridge beams and retrofitting of existing beams. For crane runway and bridge beams, standard hot-rolled H- or I-sections are often used for light to medium load carrying capacity cranes as shown in Figure 1.2. Because these beams often span large distances without lateral supports, lateral-torsional instability is an important limiting factor in their design. Figure 1.3 shows a crane bridge beam that was designed to carry a maximum load of 5 tons over a span of 18 m. A standard HEB 450 H-section was used. The limiting unbraced length for inelastic lateral-

torsional buckling, L_r, of this beam is 11.5 m. As a result, the design of this beam is governed by elastic lateral-torsional buckling. The addition of delta stiffeners to this cross-section will greatly enhance its load carrying capacity, as long as the bottom flange can carry the additional wheel load; or allow it to span longer distances. This retrofitting process can be performed on site with relative ease.
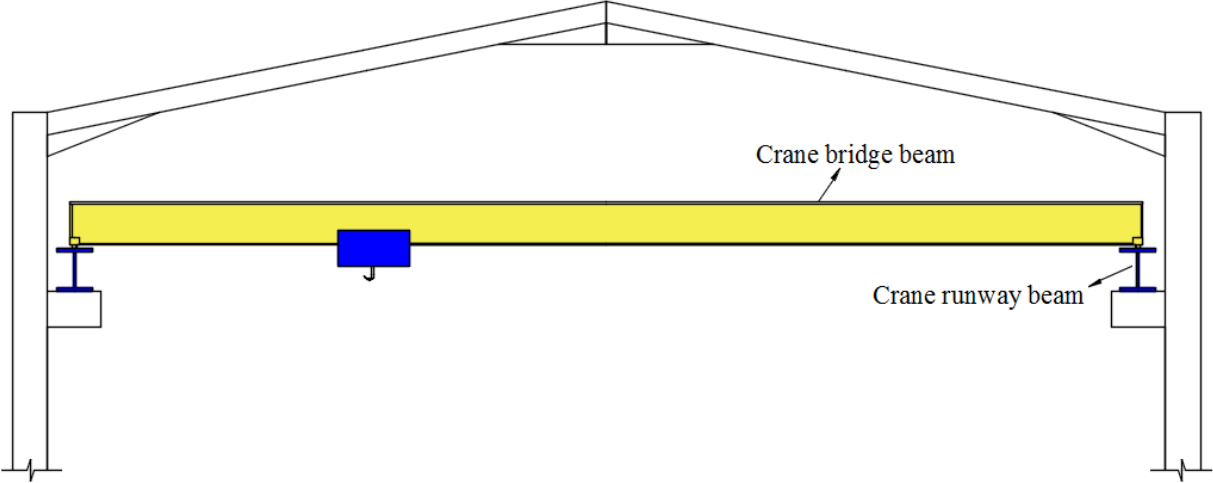
Figure 1.2 Top running crane with underhung hoist

Figure 1.3 A crane bridge beam employing a standard H-section

1.2   <u>Objectives and Research Scope</u>

The numerous advantages of Delta girders have been experimentally and numerically demonstrated. However, equations that govern the design and behavior of Delta girders have not been derived or developed. Thus, the primary goal of this research is to provide engineers with a set of design equations for determining the capacity of Delta girders. With such equations, Delta girders can be implemented in actual design applications especially in the cases for crane runway and bridge girders and in retrofitting projects where they might prove more desirable than other alternative solutions.

In order to achieve this goal, the following objectives are to be accomplished for this research:

1) Derive closed-form equations for the geometric and torsion cross-section properties of Delta girders and verify it against finite element results.

2) Check the accuracy of the theoretical LTB equation of monosymmetric simply-supported beams under uniform bending in predicting the elastic critical LTB moment of Delta girders. The check is performed through comparisons with finite element results obtained through an eigenvalue buckling analysis. This elastic LTB moment is important because it provides the design moment for slender beams in AISC (2016a) and forms the basis for the inelastic LTB moment in EuroCode 3 "EC3" (2005).

3) Develop refined nonlinear inelastic finite element models to determine the flexural and shear capacities of Delta girders. The models will take into account the effects of initial geometric imperfections and residual stresses. To this end, a residual stress pattern for Delta girders will be created based on available residual stress patterns for

monosymmetric I-sections and rectangular steel plates. The accuracy of the finite element

models will be verified against theoretical and experimental work.

4) Develop design equations for the flexural and shear capacities of Delta girders based on

finite element simulation results.

5) Provide design examples and recommendations for Delta girders to facilitate their use in

practical cases.

The scope of this research is summarized as follows:

1) This research only considers straight, prismatic and homogeneous cross-sections.

2) Delta girders are only examined for their strength limit states. In particular, the flexural

and shear limit states are investigated in this research.

3) The LTB capacity of Delta girders is studied only for the cases of uniform bending

moment and simply-supported boundary conditions

4) The proposed residual stress pattern for Delta girders used in the analysis assumes the

base I-section is a welded section. The recommended LTB equations are likely to

produce conservative results if the delta stiffeners are added to a hot-rolled I-section.

5) The recommended LTB equations for Delta girders are limited to compact cross-sections

as per AISC (2016a) classifications, or to Class 1 sections in accordance with EC3 (2005)

classifications for flexural members, i.e., cross-sections without non-compact or slender

component elements and can develop full plastic moments.

6) The proposed shear resistance equations are only applicable to compact or Class 1 cross-

sections, i.e., cross-sections that can develop full shear yielding capacity.

1.3   <u>Research Approach</u>

Experimental testing is an important research component to determine the behavior and capacity of a structural element. However, nonlinear finite element analysis software that are currently available have demonstrated to be a reliable tool for capturing the elastic and inelastic behavior of metal structures. For example, the lateral-torsional buckling curves in EC3 (2005) are largely based on calibrations against refined nonlinear finite element model results. Furthermore, experimental testing is generally expensive and allow only for a few key design parameters to be physically examined. These parameters include different geometric configurations, material strengths, load types and boundary conditions. At present, many researchers are making use of the accuracy of refined nonlinear finite element models to study the behavior of a structural element, perform large parametric studies and recommend design equations. These equations can subsequently be verified against experimental results.

In this dissertation, the proposed design equations and design recommendations are based primarily on finite element simulation results for simply-supported Delta girders subjected to uniform bending moment or vertical shear. The accuracy of the finite element models is checked against theoretical elastic buckling solutions of Delta girders and rectangular plates as well as against experimental results of I-sections that failed by inelastic LTB. These checks are provided in Chapters 4, 5 and 7. The FE models are then used to assess the capability of AISC (2016a) and EC3 (2003) design equations to predict the flexural and shear capacities of Delta girders, and to assess the newly developed equations for Delta girders. Based on these assessments, recommendations are made to determine the buckling resistance curve of Delta girders and new equations are proposed to determine the shear yielding capacity of these girders. The

7

recommended and proposed equations will follow the format of the EC3 (2005) design equations.

1.4 <u>Organization</u>

This dissertation provides analytical and numerical work on the design and behavior of Delta girders with compact component elements. Chapter 2 provides a summary of previous experimental and numerical work on Delta girders and reviews the limit state of lateral-torsional buckling of I-sections. This chapter also provides reviews on some residual stress patterns and measurements for hot-rolled, welded and monosymmetric I-sections.

In Chapter 3, equations for the geometric and torsion properties of Delta girders are derived and verified against numerical solutions obtained using the commercial finite element software ShapeBuilder. The chapter starts with a verification of the software output against various open and closed cross-sections with known cross-sectional properties. In addition, simplified equations for the torsional cross-section properties of Delta girders that have been used in previous work are checked against the numerical solutions.

Chapter 4 describes the elastic finite element model developed using the commercial finite element software Abaqus to perform eigenvalue analysis. The numerical LTB results of Delta girders are compared to the theoretical LTB moments for monosymmetric simply-supported beams under uniform bending. Thereafter, sensitivity studies are performed to examine an available simplification for the coefficient of monosymmetry β_x, as well as to compare the LTB moments of Delta girders to I-sections and an alternative solution. Recommendations for some key design parameters are then made based on the results of a parametric study using the theoretical elastic LTB solution.

Chapter 5 describes the details of the refined nonlinear finite element models developed in this research. The discussions include key modeling techniques, material properties, initial geometrical imperfections, and a proposed residual stress pattern for Delta girders. This chapter also includes a verification of the finite element model against the experimental results of a test girder (Dux & Kitipornchai, 1983). The finite element model is then used to study the sensitivity of the lateral-torsional buckling capacity of Delta girders to the magnitude of initial imperfections and residual stresses used in the model.

Chapter 6 provides recommended design equations for the flexural capacity of Delta girders along with recommendations for delta stiffener configurations. These equations are assessed against FE simulation results, and the flexural capacities of Delta girders are then compared with the corresponding I-sections. This chapter also provides an overview of and a comparison between the lateral-torsional buckling design equations in the AISC (2016a) specifications and EC3 (2005) provisions, along with equations derived for the plastic section modulus of Delta girders.

Chapter 7 starts with an overview of the shear design equations in AISC (2016a) and EC3 (2005). This is followed by a description of the nonlinear finite element model developed to simulate shear yielding of Delta girders. Based on the numerically obtained elastic shear stress distribution in Delta girders and together with the finite element simulation results, new design equations are proposed and assessed to determine the shear yielding capacity of Delta girders. The chapter also provides a comparison between the shear resistance of I-sections using FE results and current design equations in AISC (2016a) and EC3 (2005).

In Chapter 8, two design examples are provided to illustrate the use of the proposed equations as well as to compare the results with other design alternatives such as the use of a larger hot-rolled section or the addition of a compression flange cover plate. Finally, a succinct research summary and important conclusions are provided in Chapter 9 along with some suggestions for future work.

Chapter 2

Literature Review

2.1   <u>Introduction</u>

Experimental and numerical work has been conducted since 1961 on Delta girders to be used as an effective method to increase the stability and resistance of I-sections to out-of-plane bending and shear loads. This chapter starts with a summary of previous work done on Delta girders as well as a comparison between the advantages of longitudinal and delta stiffeners. In Section 2.4, a discussion of the limit state of lateral-torsional buckling (LTB) will be provided. This covers the available theoretical solutions for the elastic LTB and the equations to account for various boundary conditions and the effects of the load height. The section will end with a brief summary on work performed on inelastic LTB. The chapter will conclude with a review of some residual stress patterns and experimental measurements. The review covers the residual stresses in hot-rolled, welded and monosymmetric cross-sections.

2.2   <u>Delta Girders</u>

A Delta girder is formed by welding two inclined rectangular plates to the compression flange of and the compression portion of the web of a hot-rolled or welded I-section. A typical Delta girder cross-section is shown in Figure 2.1. The first and only available experimental test on Delta girders was performed by Hadley (1961) at the University of Washington. The main purpose of this exploratory test was to check whether the delta stiffeners could satisfactorily stiffen the web without the use of vertical stiffeners. The test results reinforced this hypothesis.

The test program consisted of the use of five full scale specimens. The main test girder was 18.6 m long and 95.3 cm deep, with a 61 cm wide top flange and 40.6 cm wide bottom flange. The junction point between the delta stiffeners and the web was set at $h/4$, where h represents the height of the web. This girder was later cut into three approximately equal length girders and four additional tests were performed. The cross-section dimensions of the tested Delta girders are shown in Figure 2.1. The author had indicated that the configuration used for the delta stiffeners was not necessarily an optimal one, and that other configurations could have produced better results (Hadley, 1961).
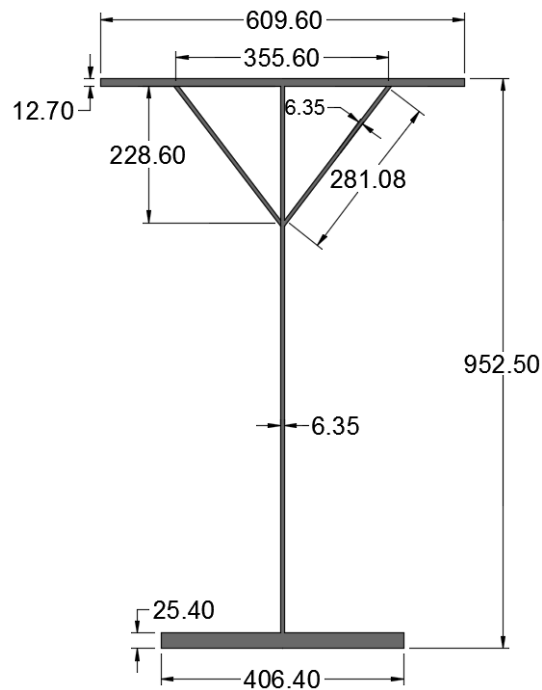
Figure 2.1 Cross-section dimensions in mm (Hadley, 1961)

Based on these successful and promising experimental results, two bridges that employed Delta girders were constructed in the U.S. Hadley (1964) summarized the cross-sectional dimensions and the erection procedures of the two bridges. The first was the Taylor Creek

12

Bridge in Cedar River watershed in Seattle. The span of this single lane simply-supported bridge is 23 m. The intersection point between the delta stiffeners and the web was set at $h/3.87$. The second constructed bridge was the Parker Bridge in Yakima, Washington. It is a two-lane continuous bridge on a vertical curve with three spans of 23, 73, and 23 m. Due to the presence of negative moment, the designer employed a double-Delta girder design near the abutments and used a regular Delta girder in the middle 36.5 m span. The double-Delta girders used for this bridge, as shown in Figure 2.2, vary in depth, web thickness, and top flange width. The junction point between the stiffeners and the web was set at $h/3$ in the span. The bridge received an AISC award for the most beautiful bridge of its class in the U.S. In both bridges, vertical stiffeners were provided only at the bearing and cross-frame locations (Hadley, 1964).
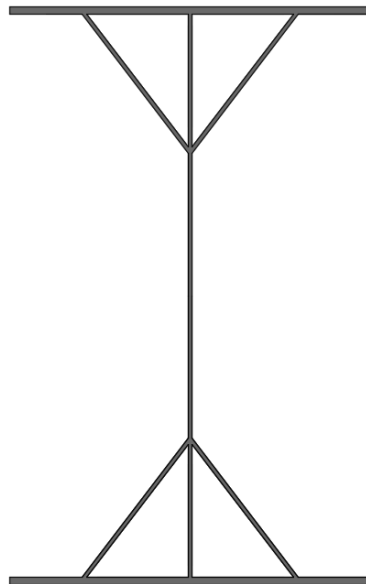
Figure 2.2 General shape of a double-Delta girder

Recently, and after five decades following Hadley's experiments, research has resumed on the behavior of Delta girders as an effective means to increase the lateral stiffness of I-girders. Arabzadeh and Varmazyari (2009) investigated the resistance of Delta girders to eccentric patch

loading using non-linear finite element (FE) modeling. The authors developed their own FE code to perform the analysis and calibrated their results against the experimental data of Hadley (1961). The study revealed that delta stiffeners are more effective than longitudinal stiffeners in general, and in the case of eccentric patch loading in particular. This effectiveness was demonstrated through a 95% increase in the critical eccentric patch loading of Delta girders in comparison to longitudinally stiffened I-girders. The authors also recommended using a thickness ratio of inclined stiffeners to web of 1.5 to avoid local buckling problems (Arabzadeh & Varmazyari, 2009).

The optimum configuration of delta stiffeners plays an important role in producing an economical and efficient design. Hatami and Esmaeili (2013) developed a simple elastic finite element model to obtain preliminary results on the optimum configuration of delta stiffeners. The results indicated that employing delta stiffeners can increase the buckling resistance of the girder by 250% in comparison to increasing the web thickness. The authors also concluded that an intersection point of $h/5$ between the delta stiffeners and the web provides optimum results (Hatami & Esmaeili, 2013). However, no description of the finite element model used in the study was provided. Another study on the optimum configuration of delta stiffeners from an economical standpoint was performed by Sahnehsaraei and Erfani (2014). The study employed an elastic finite element model and provided inconclusive results. Thus, the authors recommended an inelastic analysis to be performed in future research (Sahnehsaraei & Erfani, 2014).

The nonlinear inelastic behavior of Delta girders was investigated by Mohebkhah and Azandariani (2015) by means of FE modeling. The main purpose of the study was to investigate the moment gradient factor C_b. To this end, various unbraced lengths and load heights with

14

respect to the shear center under uniform moment and mid-span concentrated load were employed. The finite element model took into account the initial imperfections of the girders, but ignored the effect of residual stresses. Several simplifying assumptions, such as modeling the delta part of the girder as a single closed cell section and ignoring the effect of the web in the delta region were utilized to compute the torsional properties of the cross-section. Based on the results, the authors proposed a modified moment gradient equation for the inelastic beams and a straight line transition equation between the inelastic and elastic zones. Because of the limited number of beams studied, the findings of this study were not conclusive and the authors recommended that further work must be performed to validate the results (Mohebkhah & Azandariani, 2015).

2.3 Comparison between the Advantages of Longitudinal and Delta Stiffeners

Research on incorporating longitudinal stiffeners in the design and construction of plate girders is abundant in the literature. Zhao and Tonias (2012) summarized the advantages of using longitudinal stiffeners as follows: reducing the requirements for the web thickness, increasing out-of-plane stiffness, increasing the shear and moment resistances of the section, and reducing the buckling susceptibility of web plate. Despite the numerous advantages of this type of stiffeners, engineers and fabricators tend to replace the longitudinal stiffeners when needed by simply increasing the web thickness which provides higher shear and moment resistance. Additional reasons behind this replacement vary from simplifying the design and fabrication to providing an economical solution when the span length is below 61 m (200 ft) (Knight, 2003).

Delta stiffeners provide a much enhanced section when compared to a longitudinally stiffened section. This is due to the increase in torsional strength and lateral stiffness in the

15

compressive zone, which is the most vulnerable part of the girder, through forming two triangular closed cells between the web and the compression flange. As a result, the LTB resistance of the beam can be increased. In addition to the increase in lateral resistance, they increase the bending capacity of the beams due to the simple fact that more material and resistance area are present in the compressive zone (Hadley, 1961). Another advantage of utilizing the delta stiffeners over the traditional longitudinal stiffeners lies in providing an excellent support of the compression flange. This support will help reduce the possibility of local buckling of the (non-compact) compressive flange and tend to provide more flexibility in selecting the size of this flange.

Hadley (1961) reported that delta stiffeners can eliminate the need to use transverse stiffeners throughout the length of the girder except at locations where bearing stiffeners are usually required or at locations where cross-frames are used. This replacement, aside from improving the appearance of the girder, reduces the amount of welding needed for the transverse stiffeners, and more importantly reduces the stress induced on the steel web through the welding process. Note that machine welding can be performed on the delta stiffeners, leading to savings on fabrication time and labor work. One additional advantage that is attributed to delta girders lies in the relatively ease of transportation and erection due to the increased lateral stiffness (Hadley, 1961). This helps to reduce problems associated with transportation and erection due to the lack of lateral rigidity for slender girders that are prone to buckling or overturning under their self-weight or wind load (Durkee, 1961; Beckman & Mertz, 2005).

2.4   Lateral-Torsional Buckling

2.4.1   The limit state of lateral-torsional buckling

Lateral-torsional buckling (LTB) is a limit state for structural members wherein the final failure involves out-of-plane bending and twisting. Depending on the member characteristics, the failure pattern may be accompanied to some extent by yielding and local buckling. Flexural members like beams and girders are highly susceptible to lateral-torsional buckling during the construction phase when temporary cross-bracings are not installed, or are different from their permanent counterparts. Moreover, the problem of lateral-torsional buckling is of high importance in the design of crane runway and bridge beams because, in contrast to bridge girders, they often lack lateral supports. To prevent this type of failure, a designer is recommended to: (a) design and provide adequate lateral bracings such as cross-frames, diaphragms or triangulated lacing, (b) select a section of high torsional rigidity such as box girders, and (c) check that the LTB capacity is higher than the required design moment (Ziemian, 2010).

The LTB resistance curve in AISC (2016a) and AASHTO (2014) codes is divided into three segments or zones as illustrated in Figure 2.3 based on the unbraced length of the compression flange. For relatively short spans or closely spaced lateral bracings, the cross-section falls into the plastic zone or what is classified as the plateau region. The plastic zone resistance is the plastic moment for compact sections; the yield moment multiplied by the web plastification factor, R_{pc}, for other compact and non-compact web sections; and the yield moment multiplied by the bending strength reduction factor, R_{pg}, for slender web sections. As the span or distance between lateral bracings increases, the beam will fail at a lower moment by inelastic LTB. In inelastic buckling, the yield strain is reached in some part of the cross-section

as LTB occurs. The inelastic zone is obtained by a linear interpolation between the plastic and

the elastic zones. Further increase in the laterally unbraced length of the compression flange will

lead the beam to fall in the elastic zone and the beam will be designed for the theoretical elastic

LTB. In this zone, the cross-section will buckle elastically before the yield moment is reached.

To determine the zone under which a beam falls, the lateral unbraced length of the compression

flange, L_b, is compared against two limiting values L_p and L_r as shown in Figure 2.3, where L_p

and L_r are the limiting laterally unbraced lengths for the limit states of yielding and inelastic

lateral-torsional buckling, respectively (Subramanian & White, 2015).
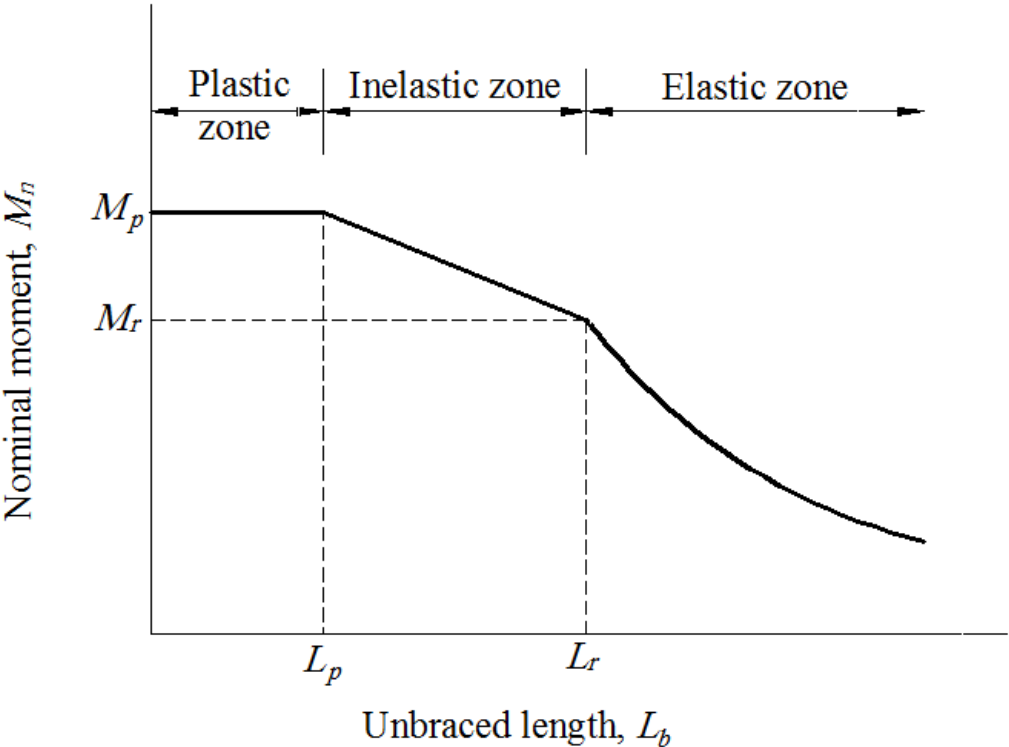
Figure 2.3 Nominal moment as function of unbraced length of compression flange

2.4.2   Elastic lateral-torsional buckling of monosymmetric beams

Research on the lateral-torsional buckling of doubly symmetric members is abundant in the literature and closed-form solutions are well established. For a prismatic simply-supported doubly symmetric I-section under uniform moment, the elastic critical buckling moment is obtained by solving the governing differential equations (Chen & Lui, 1987) as

$$M_{cr} = \frac{\pi}{L} \sqrt{EI_y GJ} \sqrt{1 + W^2} \qquad (2.1)$$

with

$$W = \frac{\pi}{L} \sqrt{\frac{EC_w}{GJ}} \qquad (2.2)$$

where L is the span length, E and G are the elastic and shear moduli, I_y is the minor axis moment of inertia, J is the torsion constant, and C_w is the warping constant.

In monosymmetric beams, i.e., beams with one axis of symmetry, the centroid C and the shear center S do not coincide and thus Eq. (2.1) is not applicable. Investigations on the behavior of monosymmetric sections are not as abundant as for doubly symmetric sections. Based on thin-walled open-section beam theory, closed-form solution for the governing differential equation of a monosymmetric simply-supported beam under uniform moment M_o was first obtained by Vlasov (1940) and Goodier (1942). For bending in the plane of symmetry, the elastic critical buckling moment is given by (Galambos T. V., 1968)

19

$$M_{cr} = \frac{\pi^2 EI_y}{L^2} \left\{ \frac{\beta_x}{2} \pm \sqrt{\left(\frac{\beta_x}{2}\right)^2 + \left[\frac{C_w}{I_y} + \frac{GJ}{EI_y}\frac{L^2}{\pi^2}\right]} \right\} \tag{2.3}$$

in which β_x, the coefficient of monosymmetry, the only term not defined in Eq. (2.1), is given by

$$\beta_x = \frac{1}{I_x} \int_A y(x^2 + y^2) \, dA - 2e_y \tag{2.4}$$

where I_x is the moment of inertia about the major axis, e_y is the distance from the centroid C to the shear center S of the cross-section, x and y are the coordinates with respect to the centroid C, and A is the cross-sectional area.

The term β_x emerges from the imbalance between the bending compressive and tensile stresses when the monosymmetric beam twists during lateral-torsional buckling, thereby giving rise to a resultant torque. This resultant torque leads to a change in the effective torsional stiffness in the governing differential equation from GJ to $(GJ + \beta_x M_o)$. This phenomenon is often referred to as the Wagner's effect (Wagner, 1936). For doubly symmetric cross-sections, β_x is equal to zero and hence Eq. (2.3) reduces to Eq. (2.1).

For practical design purposes, the following equation is proposed to determine the monosymmetry constant β_x for I-beams (Kitipornchai & Trahair, 1979)

$$\beta_x = 0.9h_o \left(\frac{2I_{yc}}{I_y} - 1\right)\left[1 - \left(\frac{I_y}{I_x}\right)^2\right] \tag{2.5}$$

where h_o is the distance between the flange centroids, I_{yc} is moment of inertia of the compression flange about the minor axis (axis of symmetry), I_y is the moment of inertia of the

full cross-section about the minor axis, and I_x is the moment of inertia of the full cross-section about the major axis.

The AISC (2016a) and the AASHTO (2014) specifications provide the following approximation for the critical elastic lateral-torsional buckling moment of singly symmetric I-section members bent about their major axis

$$M_{cr} = \frac{\pi^2 E \, S_{xc}}{\left(\frac{L_b}{r_t}\right)^2} \sqrt{1 + 0.078 \frac{J}{S_{xc} h_o} \left(\frac{L_b}{r_t}\right)^2} \tag{2.6}$$

with

$$r_t \approx \frac{b_c}{\sqrt{12 \left(1 + \frac{1}{6} \frac{h_c t_w}{b_c t_c}\right)}} \tag{2.7}$$

where L_b is the unbraced length of the beam, S_{xc} is the elastic section modulus with respect to the compression flange, b_c and t_c are the width and thickness of the compression flange respectively, t_w is the web thickness, and h_c is twice the distance from the centroid to the inside face of the compression flange.

Eq. (2.6) is a simplified equation that treats the monosymmetric section as a doubly symmetric one and is essentially equivalent to Eq. (2.1). It tends to provide conservative results when the compression flange is smaller than the tension flange, and unconservative results otherwise (AISC, 2016b). Studies have shown that the range of error of Eq. (2.6) for monosymmetric I-sections varies from 35% conservative to 9% unconservative depending on the relative sizes of the flanges (White & Jung, 2003).

In an actual application, beams may be subjected to different load patterns and various types of boundary conditions. This is accounted for by modifying Eqs. (2.3) and (2.6) as follows

$$M_{cr} = C_b \frac{\pi^2 E I_y}{(K_y L_b)^2} \left\{ \frac{\beta_x}{2} + \sqrt{\left(\frac{\beta_x}{2}\right)^2 + \left[\frac{C_w}{I_y}\left(\frac{K_y}{K_z}\right)^2 + \frac{GJ}{EI_y}\frac{(K_y L_b)^2}{\pi^2}\right]} \right\} \tag{2.8}$$

$$M_{cr} = C_b \frac{\pi^2 E \, S_{xc}}{\left(\frac{K_y L_b}{r_t}\right)^2} \sqrt{\left(\frac{K_y}{K_z}\right)^2 + 0.078\frac{J}{S_{xc}h_o}\left(\frac{K_y L_b}{r_t}\right)^2} \tag{2.9}$$

where C_b is the lateral-torsional buckling modification factor for non-uniform moment diagrams, K_y is the effective-length factor accounting for full cross-section lateral bending restraint at the ends of L_b, and K_z is the effective-length factor accounting for the warping restraint at the ends of L_b. A summary of the equations and the numerical approximations for C_b, K_y, and K_z is provided by Ziemian (2010).

In the derivation of the lateral-torsional buckling equations, it is assumed that the transverse loads are applied at the shear center. In an actual application, this assumption is not always satisfied and the height of the applied load with respect to the shear center affects the buckling moment. When the load is applied on the top flange, it will increase the out-of-plane bending and the twisting of the cross-section and thus decrease the critical buckling moment. The reverse is true when the load is applied the bottom flange. To account for the load height and the beam curvature effects, the following modification for the coefficient C_b in Eqs. (2.8) and (2.9) is recommended (Helwig, Frank, & Yura, 1997)

$$C_b^* = C_b\left(1.4^{2y_{lc}/h_o}\right)R_m \leq 3.0 \tag{2.10}$$

where y_{lc} is the distance between the location of the applied load and the mid-height of the cross-section (positive for loads acting below mid-height and negative otherwise), and R_m is parameter used to account for the beam curvature and is defined as follows

$$R_m = \begin{cases} 1.0 & \text{for unbraced lengths subjected to single curvature bending} \\ 0.5 + 2\left(\dfrac{I_{yc}}{I_y}\right)^2 & \text{for unbraced lengths subjected to double curvature bending} \end{cases} \quad (2.11)$$

where I_{yc} and I_y are the moments of inertia, of the top compression flange and the full cross-section respectively, about the weak axis.

Helwig et al. (1997) demonstrated that Eqs. (2.10) and (2.11) are not very accurate and can provide unsafe results with 30% error. However, no alternative solution is proposed for this problem and the load height is ignored in the AISC specifications (AISC, 2016a). The commentary part of the specifications acknowledges the effect of the load height and that Eq. (2.6) assumes the load to be applied along the beam centroidal axis. The commentary suggests that for unbraced compact sections with top flange loading, the square root in Eq. (2.6) may conservatively be set equal to unity (AISC, 2016b).

Clark and Hill (1960) derived the following general equation, often referred to as the 3-factor formula, for the elastic lateral-torsional buckling of monosymmetric beams

$$M_{cr} = C_1 \frac{\pi^2 E I_y}{(K_y L_b)^2} \left\{ \left(C_2 y_{ls} + C_3 \frac{\beta_x}{2} \right) \right.$$

$$\left. + \sqrt{\left(C_2 y_{ls} + C_3 \frac{\beta_x}{2} \right)^2 + \left[\frac{C_w}{I_y} \left(\frac{K_y}{K_z} \right)^2 + \frac{GJ}{E I_y} \frac{(K_y L_b)^2}{\pi^2} \right]} \right\} \quad (2.12)$$

where C_1, C_2, and C_3, provided in Figure 2.4, are coefficients to account for the various types of loadings and end-restraint conditions, and y_{ls} is the distance between the point of application of the transverse load and the shear center.
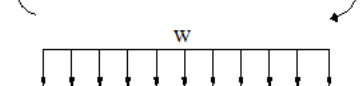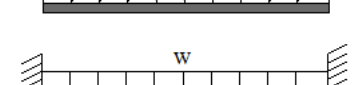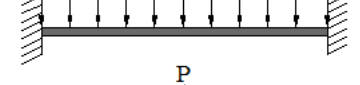
Case No.	Loading	Condition of Restraint Against Rotation about Vertical Axis at Ends	Values of Coefficients		
			C_1	C_2	C_3
Beams Restrained Against Lateral Displacement at Both Ends of Span					
1-	M ... M	Simple Support	1.0	--	1.0
		Fixed	1.0	--	1.0
2-	M ... M/2	Simple Support	1.31-1.32	--	
		Fixed	1.30-1.32	--	
3-	M	Simple Support	1.77-1.86	--	6.5
		Fixed	1.78-1.85	--	
4-	M ... M/2	Simple Support	2.33-2.62	--	
		Fixed	2.29-2.55	--	
5-	M ... M	Simple Support	2.56-2.74	--	
		Fixed	2.23-2.58	--	
6-	w	Simple Support	1.13	0.45	
		Fixed	0.97	0.29	
7-	w	Simple Support	1.30	1.55	
		Fixed	0.86	0.82	
8-	P	Simple Support	1.35	0.55	2.5
		Fixed	1.07	0.42	

Figure 2.4 Values of coefficients C_1, C_2, and C_3 (Clark & Hill, 1960)

Because of the general form of Eq. (2.12) and its applicability to both doubly symmetric and singly symmetric cross-sections, it was utilized in the development of Eurocode 3 "EC3" (EC3, 2005; Andrade, Camotim, & Providencia e Costa, 2007). The equation can also be used to obtain the buckling moment of box sections or shapes with multiple webs (Clark & Hill, 1960). Mohri, Brouki and Roth (2003) examined the coefficients C_1, C_2, and C_3 using FEM and

24

concluded that the values proposed for C_3, the coefficient that takes into account the Wagner's effect, by EC3 are very different from those numerically obtained. Andrade et al. (2007) extended the application of Eq. (2.12) to provide accurate results for cantilever beams. It is also worth noting that while the AISC specifications do not explicitly account for the effect of initial geometric imperfections for slender beams, the EC3 imposes a significant penalty for initial out-of-straightness (Ziemian, 2010).

The Japanese standard specifications for steel and composite structures employ the following equation to compute the elastic LTB of beams and it is very similar in form to Eq. (2.12) (JSCE, 2009)

$$M_{cr} = C_1 \frac{\pi^2 E I_y}{L_b{}^2} \left\{ \left(C_2 y_{ls} + C_3 \frac{\beta_x}{2} \right) + \sqrt{\left(C_2 y_{ls} + C_3 \frac{\beta_x}{2} \right)^2 + \frac{1}{\gamma_l} \frac{C_w}{I_y} \left(1 + \frac{GJ}{EC_w} \frac{L_b{}^2}{\pi^2} \right)} \right\} \quad (2.13)$$

with

$$\gamma_l = 1 - I_y/I_x \quad (2.14)$$

and the values of the coefficients C_1, C_2, and C_3 are provided in Figure 2.5.

Further studies on the elastic behavior of monosymmetric cross-sections include the work of Roberts and Burt (1985) who derived the elastic lateral-torsional buckling equations for I-beams and cantilevers using a general energy approach that takes into account the pre-buckling displacements. Sahraei, Wu and Mohareb (2015) derived a closed-form solution for the elastic LTB of simply-supported monosymmetric I-beams under uniform moment gradient taking into account shear deformation. For long spans, the results obtained using the derived equations agree well with FEM results. Other studies investigated the accuracy of the moment modification factor C_b and its application for both singly and doubly symmetric cross-sections (Kitipornchai,

25

Wang, & Trahair, 1986; Wang & Kitipornchai, 1986; Helwig, Frank, & Yura, 1997).

Conservatively, engineers may set C_b to unity, which corresponds to the case of uniform bending that provides the lowest critical buckling moment. However, a recent study reported a surprising result. For monosymmetric cross-sections, the lowest critical buckling moment does not necessarily correspond to the case of uniform bending and thus using a unity value for C_b may render the design unsafe (Camotim, Andrade, & Basaglia, 2012). Ioannidis and Kounadis (1994) studied the elastic post-buckling response of monosymmetric I-sections. Based on the examined model, the post-buckling path obtained is shallow and hence singly symmetric cross-sections exhibit limited elastic post-buckling strength.
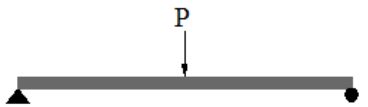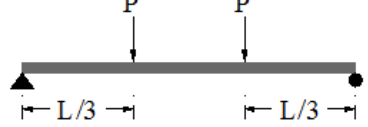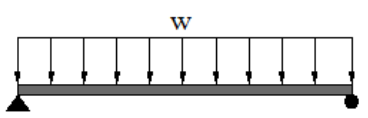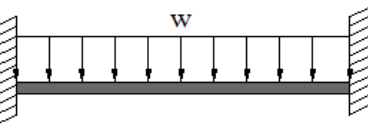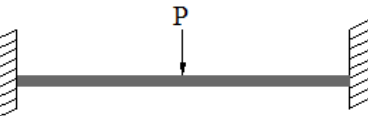
Case No.	Loading	Values of Coefficients		
		C_1	C_2	C_3
1-		1.365	0.533	0.406
2-		1.096	0.500	0.480
3-		1.040	0.422	0.570
4-		1.132	0.459	0.525
5-		1.286	1.563	0.782
6-		1.736	1.406	2.767

Figure 2.5 Values of coefficients C_1, C_2, and C_3 (JSCE, 2009)

26

2.4.3   Inelastic lateral-torsional buckling of monosymmetric beams

A good understanding of the LTB of slender beams in the elastic range is of high importance for practical applications such as crane runway and bridge beams or beam erection during the construction phase. It also serves as a base model for LTB in the inelastic range which occurs when the yield strain has been reached or exceeded in some portions of the beam. The yield progression in the cross-section results in a progressive reduction of its stiffness properties. The tangent-modulus theory has been shown to be a satisfactory model to account for this reduction. However, yielding level varies in different sections of a given beam under non-uniform bending, and the monosymmetry and stiffness properties also vary across the beam's length. Therefore, numerical methods become inevitable in an inelastic analysis (Galambos T. V., 1998).

Residual stresses and geometric imperfections play an important role in reducing the strength of beams in the inelastic range. Furthermore, the distribution and magnitude of residual stresses vary between hot-rolled and welded beams such as plate girders, and hence their effect on the inelastic LTB is different. In welded beams, compressive residual stresses at the tips of the flanges are generally less than those of hot-rolled beams and thus the start of the inelastic range is delayed. In addition, the yield spreading in the flanges of welded beams is fast due a nearly uniform distribution of residual stresses. This leads to almost uniform moment resistance of welded beams in the inelastic range, while hot-rolled beams exhibit almost linear increase in moment resistance in this range. The effects of residual stresses on the LTB behavior of both types of beams is illustrated in Figure 2.6 (Trahair, Bradford, Nethercot, & Gardner, 2008). Note that the most recent version of the AISC specifications (2016a) do not differentiate between hot-rolled and welded beams in computing their LTB resistance in the inelastic range (Ziemian, 2010).
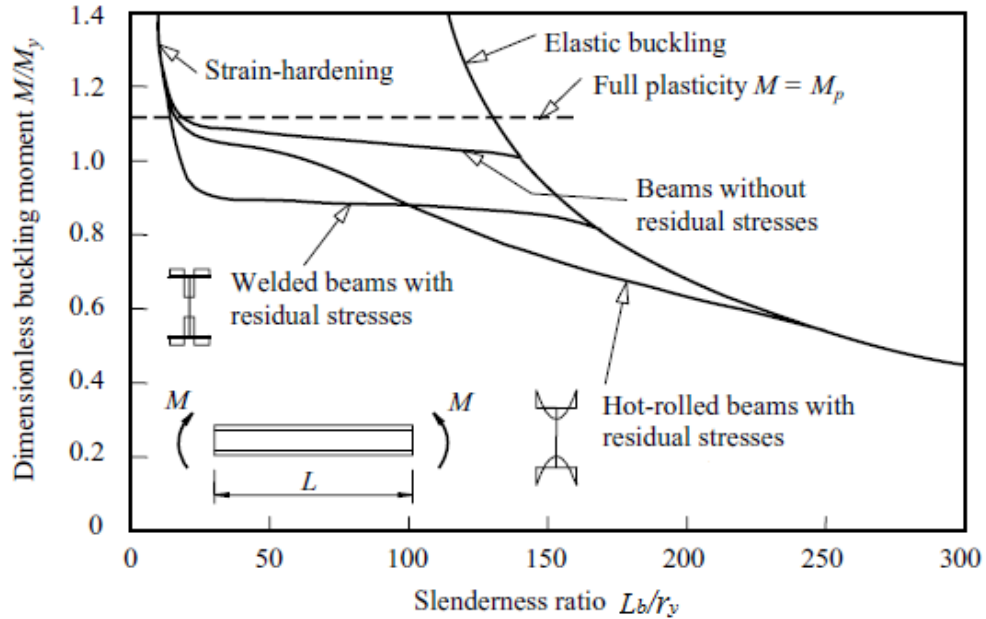
Figure 2.6 Effects of residual stresses on LTB resistance of beams (Trahair et al., 2008)

Early work on the inelastic LTB of monosymmetric beams under uniform bending includes the investigation performed by Nethercot (1973). The residual stresses were neglected in the study and the results showed that the inelastic buckling moments of monosymmetric cross-sections are substantially different from those of doubly symmetric cross-sections. Lindner (1976) investigated the inelastic LTB of monosymmetric beams by incorporating residual stresses of hot-rolled beams. The results indicated that monosymmetric cross-sections may have lower inelastic buckling moments than those of doubly symmetric cross-sections.

Very few experimental tests on monosymmetric welded I-girders are reported in the literature (Fukumoto & Itoh, 1981; O'hEachteirn & Nethercot, 1988a; 1988b). However, Kitipornchai and Wong-Chung (1987) studied the effects of the degree of beam monosymmetry and the distribution of the residual stresses on the inelastic behavior of monosymmetric beams. The analysis incorporated actual measured residual stresses in welded beams based on the work

28

of Cambridge University group (Dwight J. B., 1981; Dwight & Moxham, 1969; Young & Schulz, 1977). The study proposed a simple method to determine the inelastic critical buckling moment of welded monosymmetric beams. Trahair (2012) investigated the inelastic behavior of welded and hot-rolled monosymmetric I-beams. He proposed simple linear approximations that can be used for inelastic design of monosymmetric hot-rolled beams under uniform bending with good accuracy. Additionally, less accurate but conservative equations were proposed to determine the effect of moment gradient. EL-Mahdy and El-Saadawy (2015) developed a three-dimensional finite element model to study the elastic and inelastic behavior of monosymmetric I-beams and proposed a solution that provides optimal performance of the beams based on their degree of monosymmetry. However, the residual stresses were ignored in their study. Further work on monosymmetric beams includes the investigations of the inelastic behavior of tapered or stepped monosymmetric cross-sections (Bradford, 1989; Surla, Kang, & Park, 2015).

The limiting unbraced length for the limit state of inelastic lateral-torsional buckling, L_r, as discussed in Section 2.4.1 is given by AISC (2016a) specifications for both doubly and singly symmetric I-beams as

$$L_r = 1.95 r_t \frac{E}{F_L} \sqrt{\frac{J}{S_{xc}h_0} + \sqrt{\left(\frac{J}{S_{xc}h_0}\right)^2 + 6.76\left(\frac{F_L}{E}\right)^2}} \qquad (2.15)$$

in which F_L, defined as the magnitude of flexural stress in the compression flange at which LTB is influenced by yielding, is the only term not defined in Eqs. (2.6) & (2.7) and is given by

$$F_L = \begin{cases} 0.7F_y & when \dfrac{S_{xt}}{S_{xc}} \geq 0.7 \\ F_y \dfrac{S_{xt}}{S_{xc}} \geq 0.5F_y & when \dfrac{S_{xt}}{S_{xc}} < 0.7 \end{cases} \tag{2.16}$$

where S_{xt} and S_{xc} are the elastic section moduli with respect to the tension flange and the compressive flange, respectively, and F_y is yield stress of steel.

For monosymmetric beams, the AISC commentary (2016b) provides the following more accurate equation for L_r based on the work of White and Jung (2003)

$$L_r = \frac{1.38E\sqrt{I_y J}}{S_{xc}F_L} \sqrt{\frac{2.6\beta_x F_L S_{xc}}{EJ} + 1 + \sqrt{\left(\frac{2.6\beta_x F_L S_{xc}}{EJ} + 1\right)^2 + \frac{27.0C_w}{I_y}\left(\frac{F_L S_{xc}}{EJ}\right)^2}} \tag{2.17}$$

2.5 Residual Stresses in I-Sections

The importance of the effect of residual stresses on lateral-torsional buckling capacity of beams was discussed in Section 2.4.3. This section will review some previous work on residual stresses in I-sections. The manufacturing process plays an important role in the formation of residual stresses and hence the residual stress patterns are different for hot-rolled and welded I-sections. Clarin (2004) and Abambres and Quach (2016) provided in-depth reviews of a number of previous experimental and analytical work on residual stresses. The residual stresses in hot-rolled as well as welded doubly symmetric and in monosymmetric I-sections will be discussed hereafter. Note that residual stresses in high strength steel, cold-formed sections, and hot-rolled monosymmetric sections are not considered in this research.

2.5.1 Hot-rolled sections

Residual stresses in hot-rolled members are induced as a result of uneven cooling at the end of the rolling process. The main factors affecting the distribution and magnitude of residual stresses in hot-rolled members are the rolling temperature, the section geometry, the cooling conditions, the straightening procedures and the material properties (Beedle & Tall, 1960; Alpsten, 1968). Furthermore, heavy profiles tend to have higher residual stresses and a different distribution pattern due to different cooling behavior in thick plates (Alpsten & Tall, 1970). Thus, the following review is only valid for light to medium weight sections, i.e., sections with maximum web/flange thickness of 25 mm. On the other hand, cold straightening after the hot rolling process is known to reduce residual stresses in members. However, no detailed research has been done to determine the exact influence of cold straightening (Ziemian, 2010), and thus its beneficial effects are conservatively ignored.

Several researchers have investigated the residual stresses in hot-rolled I-sections, both experimentally and analytically. However, noticeable differences are reported in the published residual stress measurements and the proposed distribution patterns. This discrepancy could be attributed to different cooling conditions and cold-straightening techniques. Thus, a single residual stress pattern is not expected to be able to accurately predict the residual stresses in all members. Galambos and Ketter (G&K) (1959) proposed a bi-linear residual stress distribution for light to medium weight I-sections. This pattern is used the most often in North America for modeling residual stresses in compact I-sections and is depicted in Figure 2.7. Young (1975) proposed a parabolic distribution for residual stresses in hot-rolled I-section as shown in Figure 2.8 where the stresses were assumed to be independent of material properties and satisfy axial equilibrium as long as the yield stress is not exceeded.

31

$f_c=0.3F_y$

$f_t=f_cb_ft_f/(b_ft_f+t_w(d-2t_f))$
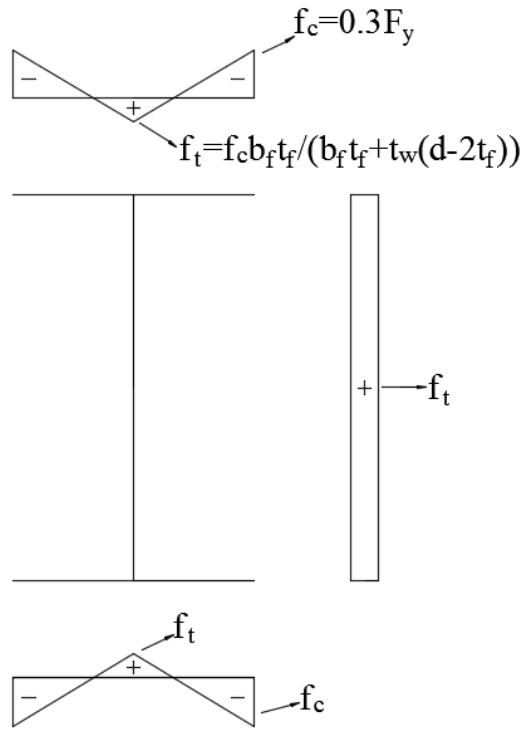
Figure 2.7 Residual stress pattern proposed by Galambos and Ketter (G&K) (1959)

$f_{cf}=165(1-ht_w/2.4b_ft_f)$

$f_t=100(0.7+ht_w/2b_ft_f)$

$f_{cw}=100(1.5+ht_w/2.4b_ft_f)$
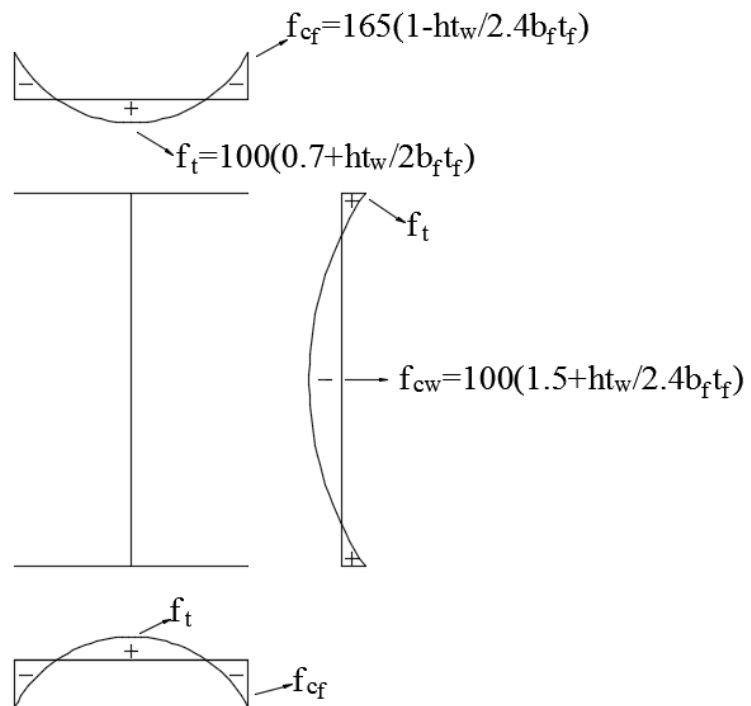
Figure 2.8 Residual stress pattern proposed by Young (1975)

32

The European Convention for Constructional Steelwork (ECCS) (1976) proposed a bi-linear residual stress pattern for hot-rolled I-sections where the maximum compressive and tensile stresses are equal. However, ECCS makes a distinction between the magnitude of residual stresses in I-sections and H-sections as shown in Figure 2.9. This proposed pattern is mostly used in Europe and was utilized in the development of the resistance curves in EC3 (2005). Subsequently, Fukomoto, Itoh and Kubo (1977) and Dux and Kitipornchai (D&K) (1983) performed experimental measurements of residual stresses in hot-rolled I-sections and representations of these residual stress patterns are provided in Figure 2.10. However, the authors did not propose a residual stress pattern to be used in analytical and numerical work. Recently proposed patterns include the work of Trahair (1993), who proposed residual stress distributions that are parabolic in the flanges and quartic in the web, and the work of Szalai and Papp (2005), who proposed a quartic distribution that satisfies all equilibrium conditions including torsion and warping effects. These two polynomial residual stress distributions require lengthy computations to obtain their patterns.
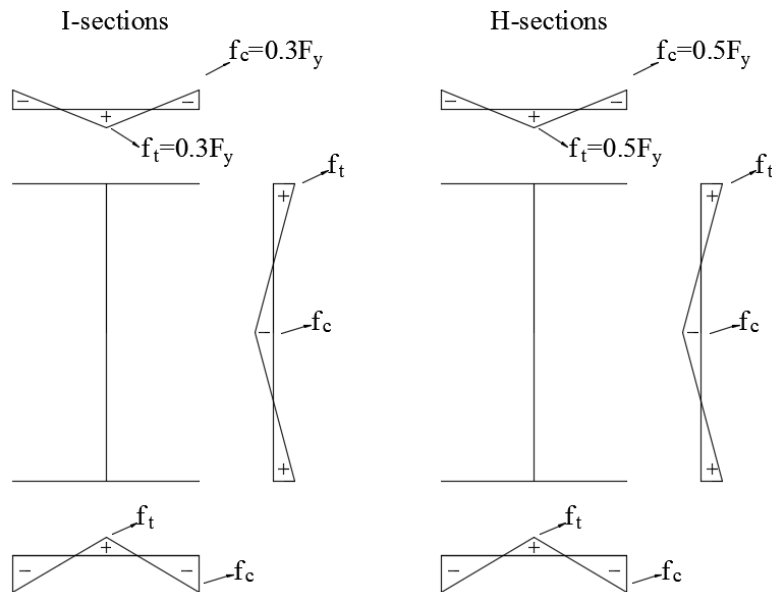
Figure 2.9 Residual stress pattern proposed in ECCS (1976)

33
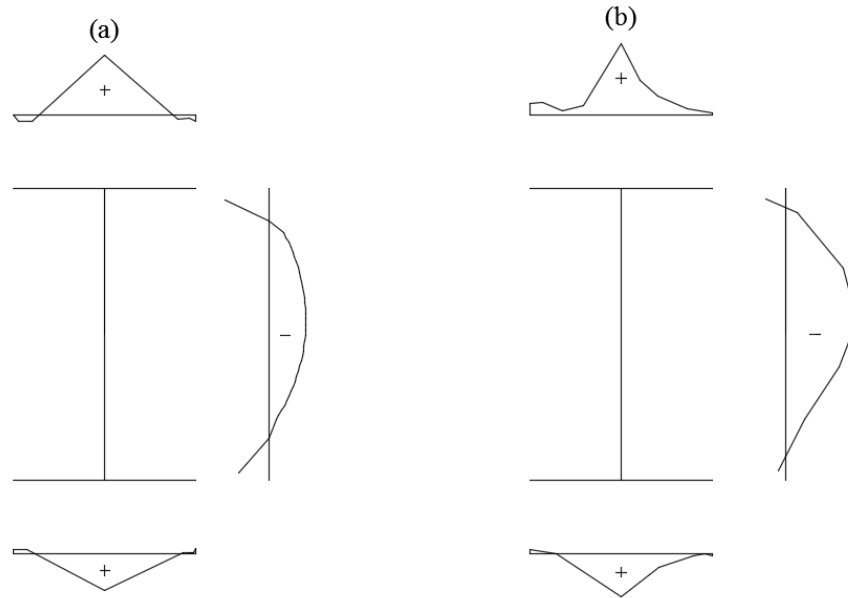
Figure 2.10 Experimental residual stress patterns measured by (a) Fukomoto et al. (1977) and (b)

Dux & Kitipornchai (1983)

Subramanian and White (2015, 2017) performed sensitivity studies in an attempt to

correlate finite element (FE) buckling results of beams with the AISC (2016a) LTB curves. The

comparison was made with respect to the AISC curves mainly because the unified flexural

resistance equations of the AISC specifications were built based on calibrations with large

experimental data. The study included studying various residual stress patterns and geometrical

imperfections represented by different flange sweep magnitudes. Seven different residual stress

patterns for hot-rolled I-sections were included in the study: G&K with full, half and one quarter

of its specified magnitudes, ECCS pattern, Szalai and Papp pattern, a pattern that represents Dux

& Kitipornchai (D&K) measurements and the case with zero residual stress. Figure 2.11

illustrates the results of one of the beams studied by Subramanian and White. The beam is a

W21x44 standard hot-rolled beam with various residual stress patterns and a flange sweep

magnitude of $L_b/2000$. As expected, the results showed that the highest effect of residual

stresses occurs in the inelastic LTB region of the buckling curve. The G&K residual stress pattern with full stress magnitudes provides the lowest resistance curve among the seven residual stress patterns used. Dux & Kitipornchai (D&K) residual stress pattern provides the highest resistance which is higher than the AISC curve in the inelastic region in some of the beams studied. It is interesting to observe (in Figure 2.11) that the case of zero residual stress combined with an initial imperfections magnitude of $L_b/2000$ provided the closest LTB resistance curve to the AISC curve. The authors concluded their study by proposing the use of one-half the G&K residual stress pattern along with $L_b/2000$ flange sweep for hot-rolled I-sections as this combination provided the most reasonable results in comparison with available experimental data while more severe combinations lead to a tangible and inconsistent difference in many cases.
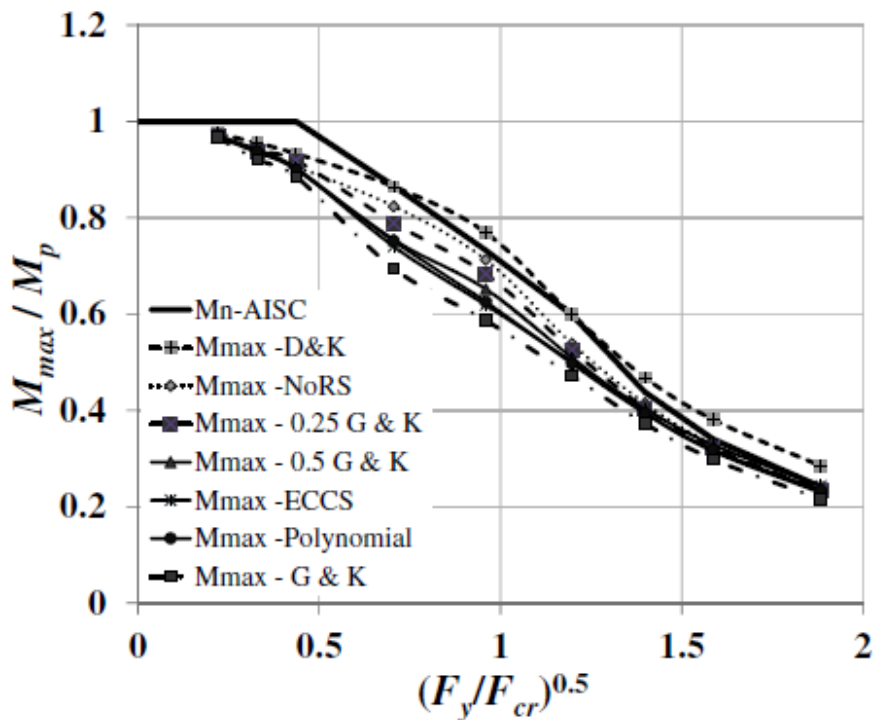
Figure 2.11 LTB curves for W21x44 with various residual stress patterns and $L_b/2000$ flange sweep (Subramanian & White, 2017)

35

2.5.2   Welded sections

The residual stress effects on the inelastic LTB capacity of hot-rolled and welded beams was shortly introduced in Section 2.4.3. Measurements of residual stresses in welded cross-sections (Beedle & Tall, 1960; Nagaraja Rao & Tall, 1964; McFalls & Tall, 1969; Young & Dwight, 1971) have clearly indicated a significant difference between both the magnitude and distribution pattern of these stresses in hot-rolled and welded I-sections as shown in Figure 2.12. Residual stresses in welded I-sections are mainly caused by locally concentrated heating which causes uneven cooling in the cross-section. The welding speed, heat input, number of passes and the technique used in cutting the plates (mechanically-cut or flame-cut technique) also affect the residual stress pattern and magnitude in welded sections (Abambres & Quach, 2016). The significant difference in residual stresses between flame-cut (oxygen cut) and mill-cut plates is observed at the flange tips. As opposed to mill-cut plates, the flame-cut plates have tension residual stresses at the flange tips, as illustrated in Figure 2.13, which was found to improve LTB capacity of the girder (Cherenko & Kennedy, 1991).
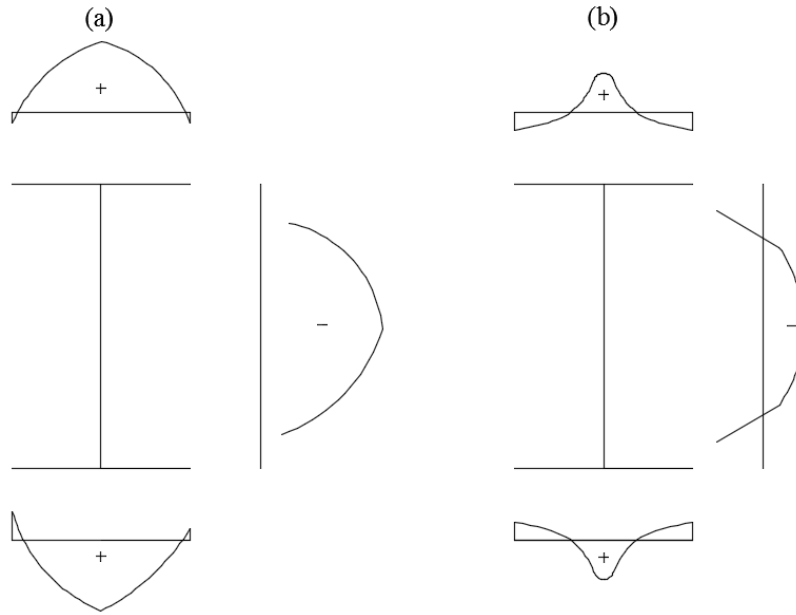
Figure 2.12 Pattern of measured residual stresses (not-to-scale) of: (a) hot-rolled $10\times5\,{}^{3}\!/_{4}$ UB

21 (Young & Dwight, 1971) and (b) universal mill plates welded 9×9 (Beedle & Tall, 1960)
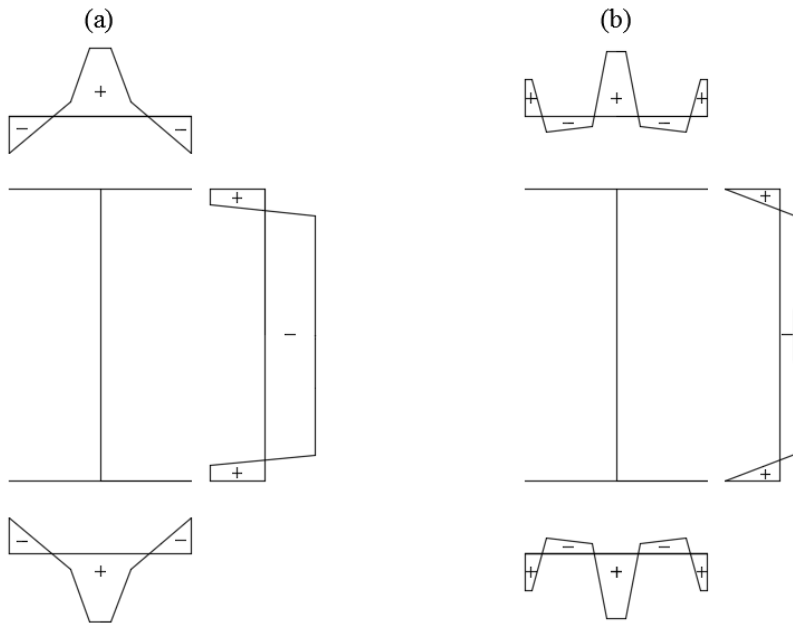
Figure 2.13 Representation of measured residual stresses in (a) welded and mill-cut plates and

(b) welded and flame-cut plates (Cherenko & Kennedy, 1991)

Other proposed residual stress patterns for welded beams include the work of Dwight and

Moxham (1969) at Cambridge, who proposed a rectangular tension block and related its width to

either the welding size or the heat input. This pattern was supported by the work of Young and

Dwight (1971). Yu and Tall (1971) at Lehigh, proposed a triangular tensile residual stress block

which leads, for very short spans, to higher buckling curves compared to those obtained using

the rectangular shape. Prawel, Morell and Lee (1974) proposed a bi-linear residual stress pattern

for welded I-section, shown in Figure 2.14(a), based on residual stress measurements of plates

with shear cut edges. Kim (2010) proposed the Best-Fit Prawel residual stress distribution,

shown in Figure 2.14(b), where the peak stress values were reduced to match the experimental

data from different sources. ECCS (1976) used a trapezoidal tensile stress block and a

rectangular compressive block in the flanges as shown in Figure 2.15. Other measurements of

residual stresses in welded beams have been reported by Fukumoto and Itoh (1981) and Dux and

Kitipornchai (1983).
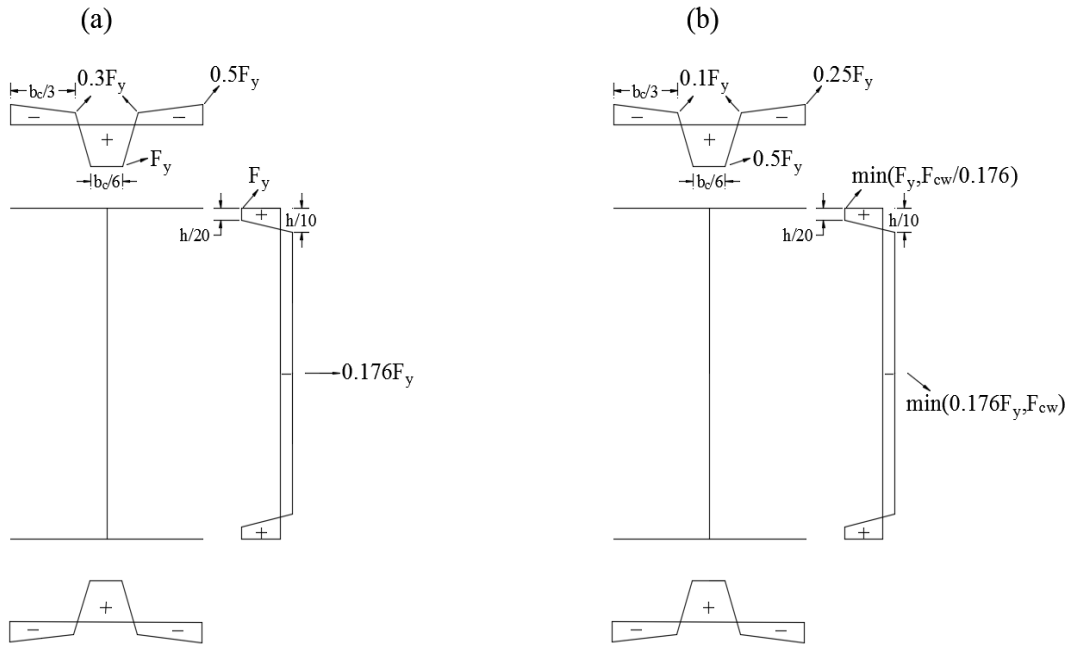
Figure 2.14 (a) Residual stress pattern reported by Prawel et al. (1976), (b) Best-Fit Prawel

residual stress pattern by Kim (2010)
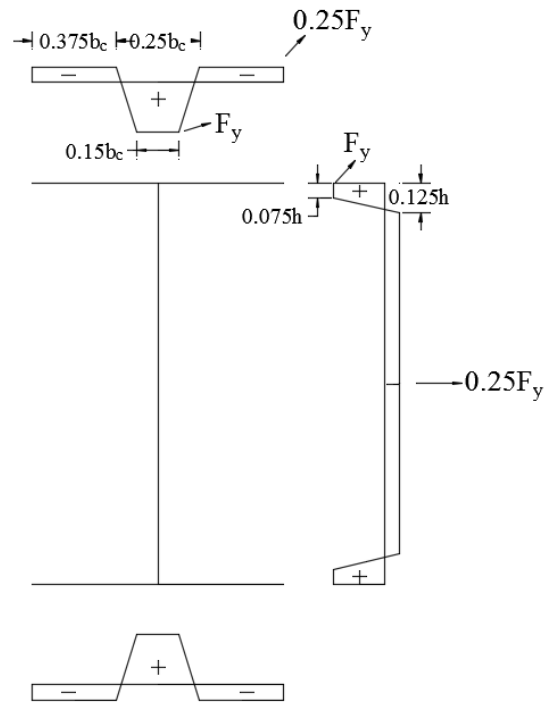
Figure 2.15 Residual stress pattern used in ECCS (1976)

Subramanian and White (2015, 2017) performed sensitivity studies on welded beams in a similar manner to the one described in Section 2.5.1 for hot-rolled beams. Three nominal residual stress patterns were used in their study: Best-Fit Prawel with full and half stress magnitudes and the case with zero residual stress. Figure 2.16 illustrates the results of one of the beams studied with various residual stress patterns and a flange sweep magnitude of $L_b/2000$. The study concluded that using the half Best-Fit Prawel along with flange sweep of $L_b/2000$ provides reasonable results in LTB FE simulation of welded beams. However, unlike the case for hot-rolled beams, Subramanian and White utilized very few residual stress patterns to study welded beams which indicates that more work is needed to attain better results.
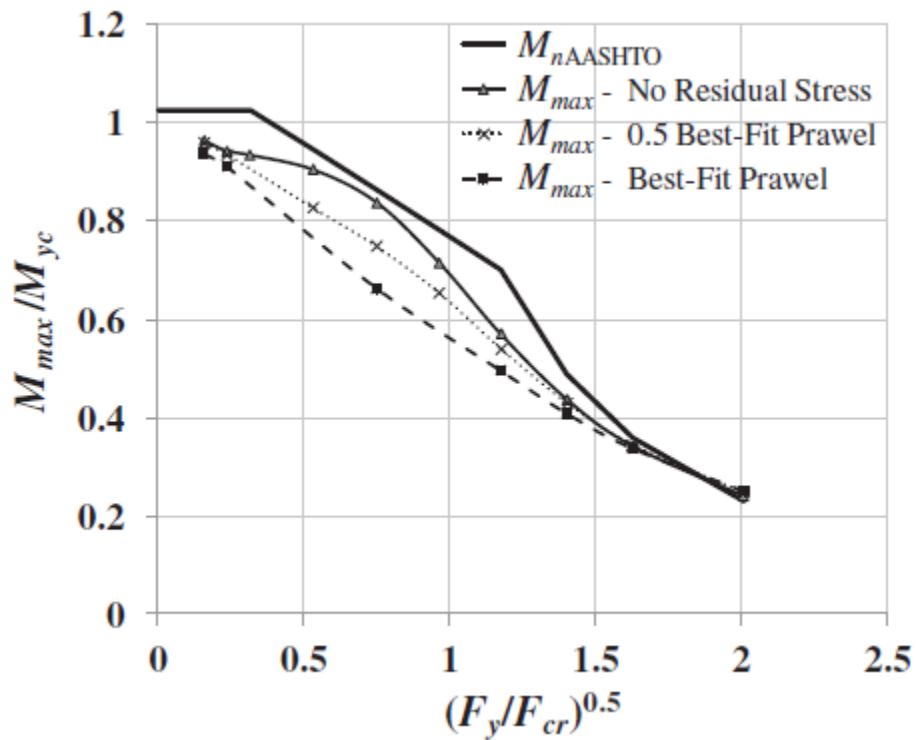
Figure 2.16 LTB curves for a welded beam with various residual stress patterns and $L_b/2000$ flange sweep (Subramanian & White, 2017)

2.5.3 Monosymmetric sections

Limited studies have been conducted to determine residual stresses in welded monosymmetric beams. Fukumoto (1982) provided measured residual stresses for four monosymmetric beams as shown in Figure 2.17. Kitipornchai and Wong-Chung (1987) suggested a residual stress pattern for welded monosymmetric beams. The pattern is shown in Figure 2.18 and is based on tendon force concept developed by White (1977a,b) at Cambridge. The tendon force F is given by

$$F = BA_{wel} \tag{2.18}$$

where B is the welding process constant and A_{wel} is the area of added weld metal. In Figure 2.18, the stresses f_{c1}, f_{c2} and the dimensions c_1, c_2 are functions of the tendon force F. This requires the area of the weld and the welding technique to be known in order to calculate the residual stresses in the cross-section. However, this information is rarely available and was not provided for Fukumoto's tests. This renders the proposed pattern by Kitipornchai and Wong-Chung to be impractical especially for comparison with previous measurements. Trahair (2012) proposed a simple residual stress pattern for welded monosymmetric beams as shown in Figure 2.19 where the compression residual stresses in the smaller flange were reduced. In addition, he ignored the residual stresses in the web because lateral-torsional buckling is only slightly affected by web yielding. This residual stress pattern was used in an analytical work to develop design equations for monosymmetric beams in the inelastic range. However, this proposed pattern was not verified against experimental data.
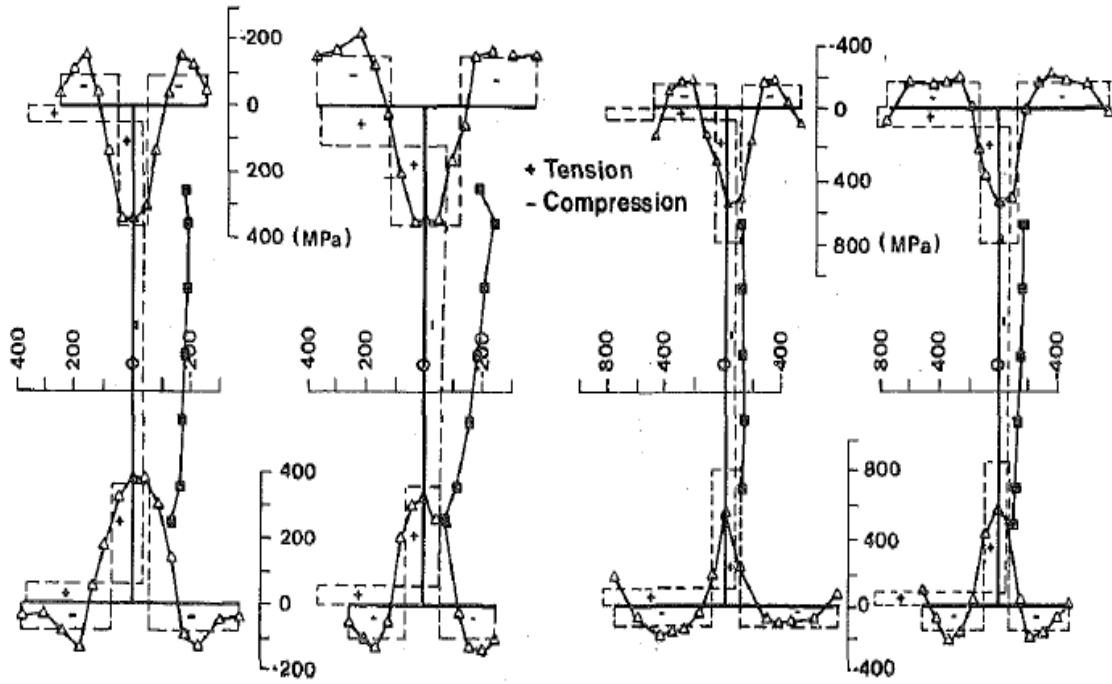
Figure 2.17 Residual stresses measured for welded monosymmetric beams (Fukomoto, 1982)
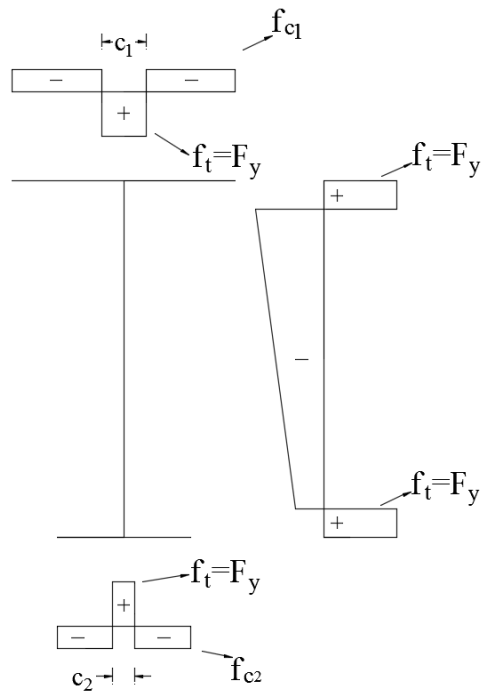
Figure 2.18 Residual stress pattern proposed for welded monosymmetric beams (Kitipornchai &

Wong-Chung, 1987)
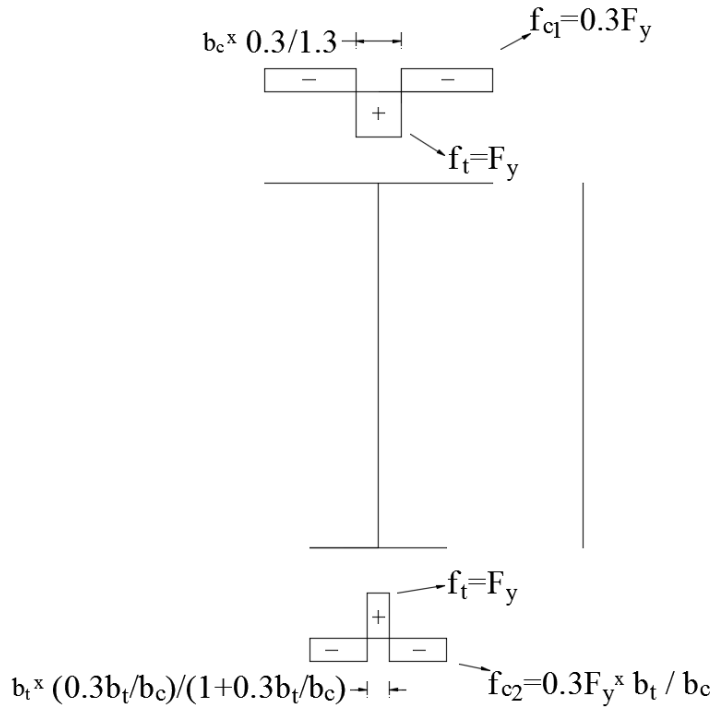
Figure 2.19 Residual stress pattern proposed for welded monosymmetric beams (Trahair, 2012)

2.6   <u>Summary</u>

Since 1961, several researchers have performed experimental and numerical work on Delta

girders to demonstrate their advantages. However, design equations for this type of girders have

not yet been developed. A survey of the available work shows that research has been done

primarily in the elastic range, while the only available nonlinear inelastic work ignores the effect

of imperfections despite its known importance in such type of analysis.

This chapter has provided a description of the limit state of lateral-torsional buckling

(LTB). Equations for the theoretical elastic LTB of monosymmetric beams were presented. It

should be noted that equations for doubly symmetric sections are used for monosymmetric

sections in the AISC (2016a) specifications. Furthermore, coefficients that account for boundary

conditions and load types were reviewed. Also, the effect of imperfections on the inelastic LTB

capacity of beams was discussed. The chapter concluded with a literature survey on some available residual stress patterns for hot-rolled and welded doubly symmetric I-sections as well as monosymmetric I-sections.

Chapter 3

Cross-section Properties of Delta Girders

3.1 <u>Introduction</u>

To determine the behavior of a structural element, the cross-section properties of that element must be known. In the case of lateral-torsional buckling (LTB) behavior of beams, the torsional properties of the cross-section are required in addition to the other geometrical properties. The two most important torsional properties are the torsional constant J and the warping constant C_w. The computation of C_w necessitates the determination of the location of the shear center. For commonly-used cross-sections, the equations for these torsion properties can be readily obtained from various handbooks. However, these equations are not available for Delta girders and hence they need to be derived. Although some finite element (FE) software is available to allow users to calculate torsional properties of any cross-sectional shapes, these software are not always at the disposal of every practicing engineer.

This chapter presents the cross-section properties of Delta girders; in particular, the derivation of the torsion properties' equations will be presented. The accuracy of these equations will be checked against numerical results obtained using a FE software. Since the Delta girder is a mixed cross-section, i.e., section composed of open profiles attached to a closed profile, the derivation of these torsional properties is not a very straight forward process. Thus, the aim of this chapter is to provide the engineers with a set of equations that can easily be incorporated in a runtime analysis and design of Delta girders.

3.2 <u>**Verification of the FE Solution**</u>

ShapeBuilder, a commercial FE software, will be used to calculate the cross-section properties of the Delta girder. The software determines approximate cross-section properties for plane areas based on its input geometry. Because the accuracy of the results is dependent on the selected mesh size, the mesh size needs to be adjusted until convergence is achieved. The exact methods that the software uses are not disclosed, but the developers state that the software computes torsional properties using a sophisticated numerical process. It is therefore necessary to check and verify the accuracy of the software output.

To verify the numerical results, various cross-sections are modeled using appropriate mesh size and the numerically calculated torsional and warping constants are compared with their analytical solutions. The software results will be verified for both open and closed cross-sections.

3.2.1   Monosymmetric I-shaped section

3.2.1.1   FE solution

The dimensions as well as the numerical torsional properties of the monosymmetric I-section are provided in Figure 3.1.
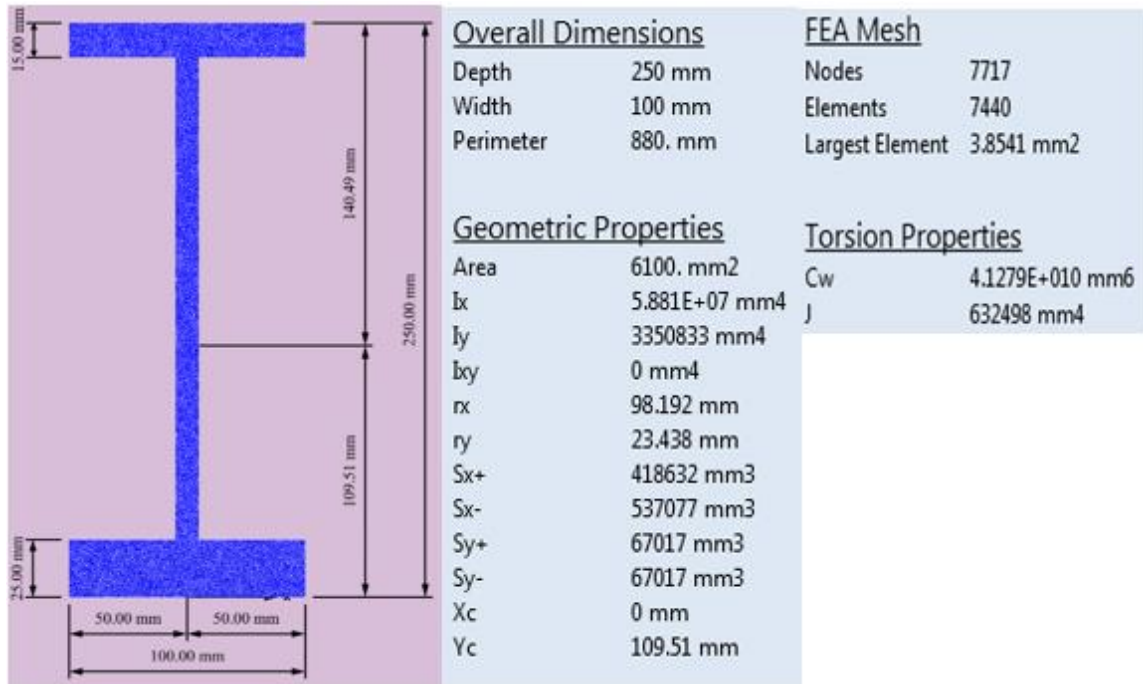
Figure 3.1 FE properties of I-shaped section

3.2.1.2 Analytical solution

The torsional constant of an I-section is computed using $J \approx \sum C_i b_i t_i^3$, where C_i is the aspect ratio

correction factor and b_i and t_i are the width and thickness of the component plate i, respectively.

$$J = (0.281{\times}100{\times}25^3 + 0.333{\times}210{\times}10^3 + 0.301{\times}100{\times}15^3) = 610{,}580 \text{ mm}^4$$

The warping constant of an I-section is computed using $C_w = \frac{h_o^2 I_c I_t}{I_c + I_t}$, where h_o is the distance

between the flange centroids, I_c and I_t are the moment of inertia for the compression and tension

flanges about the axis of symmetry, respectively.

$$C_w = \frac{230^2{\times}1{,}250{,}000{\times}2{,}083{,}333.3}{1{,}250{,}000 + 2{,}083{,}333.3} = 4.13{\times}10^{10} \text{ mm}^6$$

3.2.1.3 Comparison

The comparison between the numerical and analytical results is provided in Table 3.1.

Table 3.1 Comparison of I-shaped section results

Property	Numerical	Analytical	Error
$J\ (mm^4)$	632,498	610,580	-3.47 %
$C_w\ (mm^6)$	4.13×10^{10}	4.13×10^{10}	0 %

3.2.2   Hollow circular section

3.2.2.1 FE solution

The dimensions as well as the numerical torsional properties of the hollow circular section are provided in Figure 3.2.
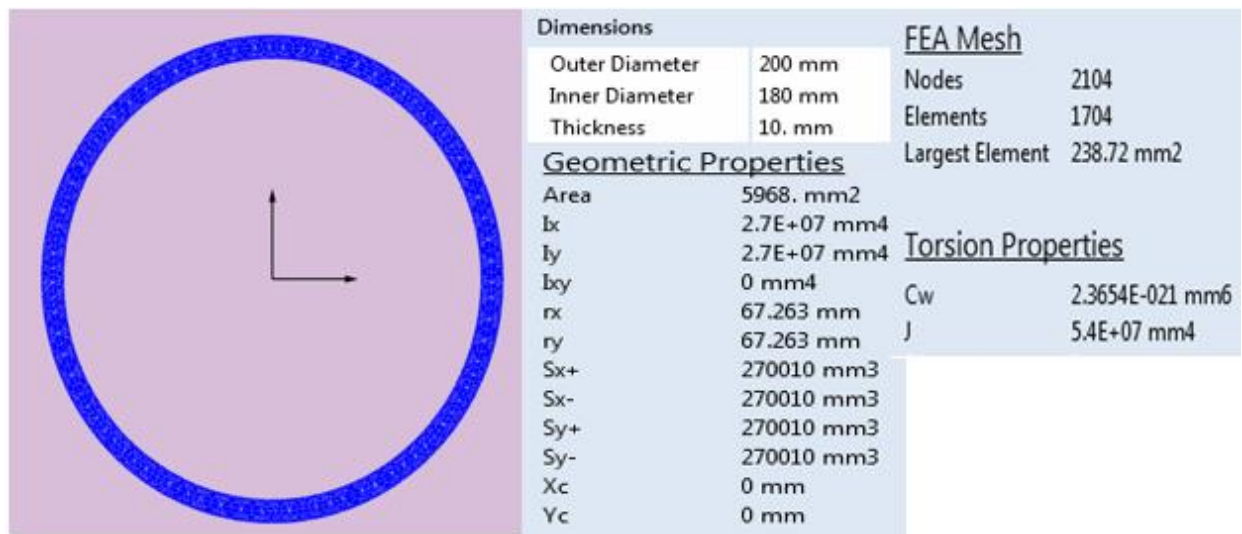
Figure 3.2 FE properties of hollow circular section

3.2.2.2 Analytical solution

The torsional constant of an I-section is computed using $J = \frac{\pi(r_o^4 - r_i^4)}{2}$, where r_i and r_o are the inner and outer radius, respectively.

$$J = \frac{\pi(100^4 - 90^4)}{2} = 5.4 \times 10^7 \text{ mm}^4$$

For axisymmetric cross-sections C_w is equal to zero.

3.2.2.3 Comparison

The comparison between the numerical and analytical results is provided in Table 3.2.

Table 3.2 Comparison of hollow circular section results

Property	Numerical	Analytical	Error
J (mm^4)	5.4×10^7	5.4×10^7	0 %
C_w (mm^6)	0	0	0 %

3.2.3   Rectangular tubular section

3.2.3.1 FE solution

The dimensions as well as the numerical torsional properties of the rectangular tubular section are provided in Figure 3.3. Note that the wall thickness t is uniform on all sides and is equal to 10.0 mm.
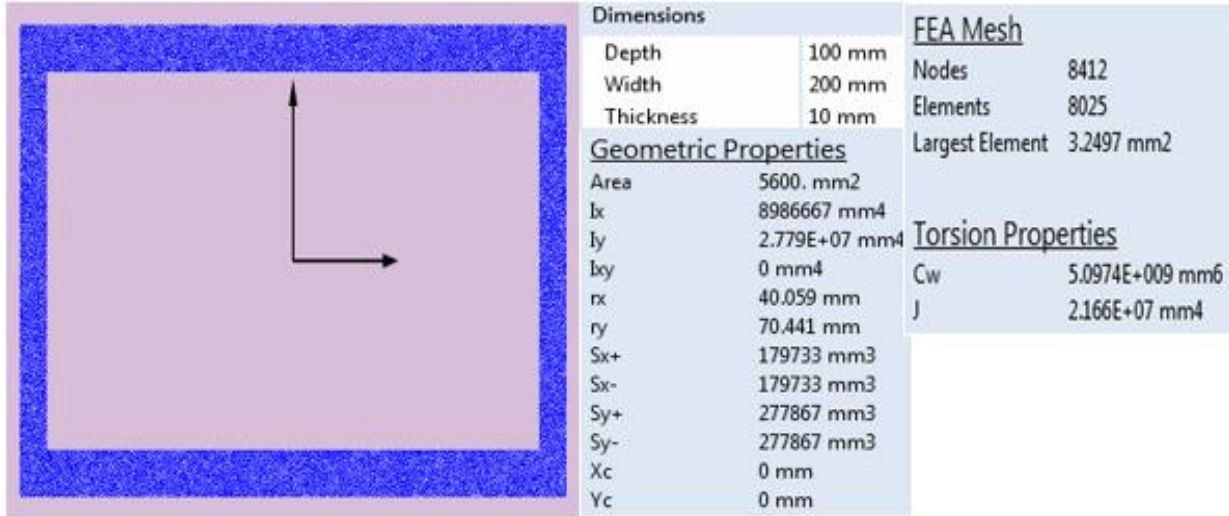
Figure 3.3 FE properties of rectangular tubular section

3.2.3.2 *Analytical solution*

The torsional constant of an I-section is computed using $J \approx \frac{2t^2(b_1-t)^2(b_2-t)^2}{b_1t+b_2t-2t^2}$, where t is the wall thickness and b_1 and b_2 are the total width and height of the cross-section, respectively.

$$J \approx \frac{2t^2(b_1-t)^2(b_2-t)^2}{b_1t+b_2t-2t^2} = 2.09 \times 10^7 \text{ mm}^4$$

C_w is calculated using the procedure of Section 3.3.2.3 and is equal to 4.91×10^9 mm^6.

3.2.3.3 *Comparison*

The comparison between the numerical and analytical results is provided in Table 3.3.

Table 3.3 Comparison of rectangular tubular results

Property	Numerical	Analytical	Comparison
$J\ (mm^4)$	2.17×10^7	2.09×10^7	-3.5 %
$C_w\ (mm^6)$	5.10×10^9	4.91×10^9	-3.7 %

50

3.2.4 Summary

Based on the above comparisons, the FE software can provide very accurate results for both the torsional constant J and the warping constant C_w. Thus, it will be used to compute the torsional properties of the Delta girder against which the analytical equations (derived in Section 3.3.2) will be checked.

3.3 Cross-Section Properties

3.3.1 Geometric properties

In this section, equations for some commonly-used geometric properties of the Delta girder are presented. The notations/dimensions used in the equations are depicted in Figure 3.4.
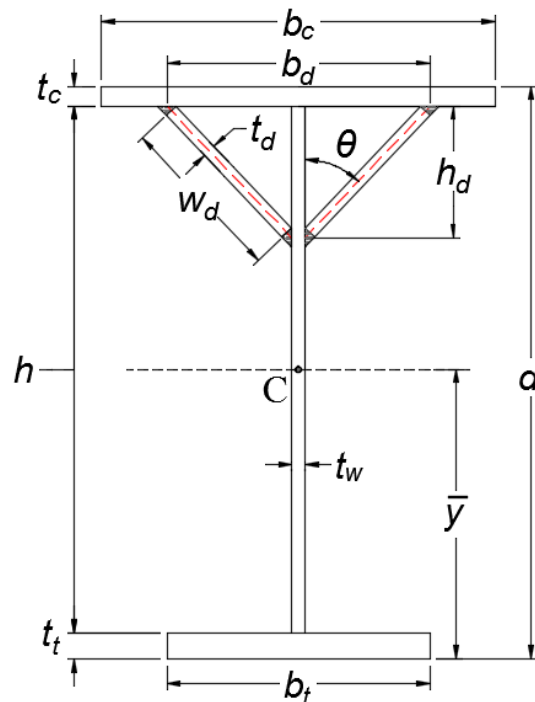
Figure 3.4 Notations of Delta girder dimensions

The area of the cross-section is

$$A = t_c b_c + t_t b_t + t_w h + 2 t_d \alpha \tag{3.1}$$

where

$$\alpha = \sqrt{\left(\frac{b_d - t_w}{2}\right)^2 + h_d^2} \tag{3.2}$$

The centroid location (distance from the bottom of the cross-section to the centroid) is

$$\bar{y} = \frac{\sum A_i y_i}{\sum A_i} \tag{3.3}$$

$$\bar{y} = \frac{1}{A}\left[t_c b_c\left(d - \frac{t_c}{2}\right) + \frac{t_t^2 b_t}{2} + t_w h\left(t_t + \frac{h}{2}\right) + 2 t_d \alpha\left(d - t_c - \frac{\alpha}{2}\cos\theta\right)\right] \tag{3.4}$$

where

$$\theta = \cos^{-1}\left(\frac{h_d}{\alpha}\right) \tag{3.5}$$

The moments of inertia of the delta stiffeners about their local coordinate axes are obtained by assuming that each stiffener is a rectangle having a width α and a thickness t_d as

$$I_{x',d} = \frac{\alpha\, t_d^3}{12} \tag{3.6}$$

$$I_{y',d} = \frac{t_d \alpha^3}{12} \tag{3.7}$$

The transformations of the delta stiffeners' moments of inertia to the global coordinate axes are

$$I_{x,d} = I_{x',d} \sin^2\theta + I_{y',d} \cos^2\theta \tag{3.8}$$

$$I_{y,d} = I_{x',d} \cos^2\theta + I_{y',d} \sin^2\theta \tag{3.9}$$

The moment of inertia of the Delta girder about the x-axis (nonsymmetric axis) is

$$I_x = \sum_i \left(I_{x,i} + A_i y_i^2\right)$$

(3.10)

$$I_x = \frac{b_t t_t^3}{12} + b_t t_t y_t^2 + \frac{b_c t_c^3}{12} + b_c t_c y_c^2 + \frac{t_w h^3}{12} + h t_w y_w^2$$

$$+ 2\left(I_{x,d} + \alpha t_d y_d^2\right)$$

(3.11)

where

$$y_d = d - \bar{y} - t_c - \frac{\alpha}{2}\cos\theta \ ; \ y_t = \bar{y} - \frac{t_t}{2}; \ y_c = d - \bar{y} - \frac{t_c}{2};$$

$$y_w = \frac{h}{2} + t_t - \bar{y}$$

(3.12)

The moment of inertia of the Delta girder about the y-axis (axis of symmetry) is

$$I_y = \sum_i \left(I_{y,i} + A_i x_i^2\right)$$

(3.13)

$$I_y = \frac{t_t b_t^3}{12} + \frac{t_c b_c^3}{12} + \frac{h t_w^3}{12} + 2\left(I_{y,d} + \alpha t_d x_d^2\right)$$

(3.14)

where

$$x_d = \frac{t_w}{2} + \frac{\alpha}{2}\sin\theta$$

(3.15)

The elastic section moduli about the x-axis are given by

$$S_{xc} = \frac{I_x}{d - \bar{y}}$$

(3.16)

$$S_{xt} = \frac{I_x}{\bar{y}}$$

(3.17)

where S_{xc} and S_{xt} are the section modulus with respect to the top and bottom fiber of the section.

3.3.2   Torsion properties

3.3.2.1   Torsion constant J

The torsional constant J, also called the pure torsional constant, of a hollow thin-wall member having multiple cells can be determined using the general procedure explained by Boresi and Schmidt (2003). The equations for the torque T and the angle of twist β per unit length are given by

$$T = 2 \sum_{i=1}^{N} \hat{A}_i q_i \tag{3.18}$$

and

$$\beta = \frac{1}{2G\hat{A}_i} \oint_{l_i} \frac{q_i - q'}{t} \, dl, \quad i = 1, 2, \ldots, N \tag{3.19}$$

where $\hat{A}_i$ is the area enclosed by the medial line of cell i, q_i is the shear flow of cell i, q' is the shear flow for the cell adjacent to the ith cell where dl is located, t is the thickness where dl is located, and l_i is the length of the mean perimeter of the ith cell.

For N cells, there are $N + 1$ unknowns to determine. They are the shear flow in each cell q_i (N values) and the angle of twist per unit length β. Eq. (3.19) provides a system of N equations relating β and q_i. Once q_i for each cell are obtained, they can be substituted back in Eq. (3.18). The torsional constant can then be computed from the following equation

$$J = \frac{T}{G\beta} \tag{3.20}$$

To illustrate the procedure, consider the two-cell delta cross-section shown in Figure 3.5, where the dotted red lines represent medial line for each cell. Using the dimensions shown in Figure 3.5, the area of each cell can be computed as follows

$$\widehat{A_1} = \widehat{A_2} = \frac{b_d}{2} \cdot \frac{t_c}{2} + \frac{h_d t_w}{2} + \frac{h_d}{2}\left(\frac{b_d - t_w}{2}\right) = \frac{b_d}{4}(t_c + h_d) + \frac{h_d t_w}{4} = \hat{A} \tag{3.21}$$
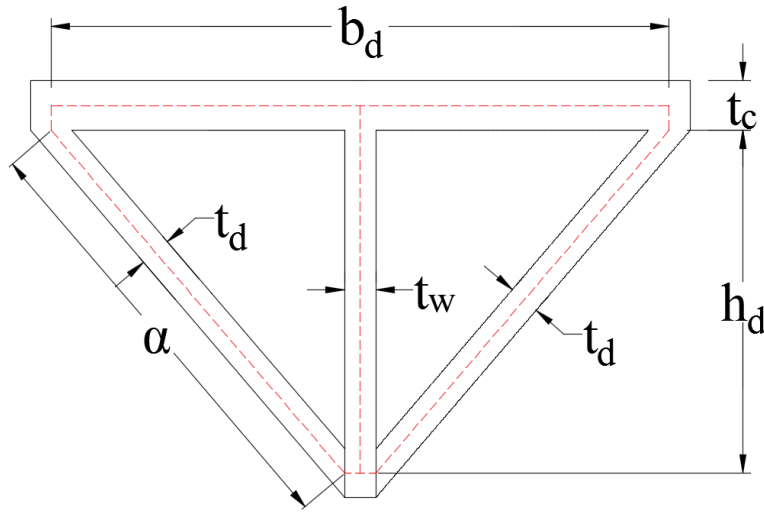
Figure 3.5 Delta section's notations

The torque is computed using Eq. (3.18) as

$$T = 2\sum_{i=1}^{N} \widehat{A_i} q_i = 2\hat{A}(q_1 + q_2) \tag{3.22a}$$

The angle of twist per unit length in each cell is obtained using Eq. (3.19) as

$$\beta = \frac{1}{2G\widehat{A_i}} \oint_{l_i} \frac{q_i - q'}{t} dl \tag{3.22b}$$

for $i = 1$: $\beta = \dfrac{1}{2G\hat{A}} \left[q_1 \left(\dfrac{b_d}{2t_c} + \dfrac{\alpha}{t_d} + \dfrac{t_w/2}{t_w} + \dfrac{t_c/2}{t_c} \right) + (q_1 - q_2) \left(\dfrac{h_d}{t_w} + \dfrac{t_c/2}{t_c} \right) \right]$ (3.23a)

for $i = 2$: $\beta = \dfrac{1}{2G\hat{A}} \left[q_2 \left(\dfrac{b_d}{2t_c} + \dfrac{\alpha}{t_d} + \dfrac{t_w/2}{t_w} + \dfrac{t_c/2}{t_c} \right) + (q_2 - q_1) \left(\dfrac{h_d}{t_w} + \dfrac{t_c/2}{t_c} \right) \right]$ (3.23b)

Solving Eqs. (3.23a) & (3.23b) for q_1 & q_2, we get

$$q_1 = q_2 = 4\hat{A}G\beta \left(\frac{t_c t_d}{b_d t_d + 2\alpha t_c + 2t_c t_d} \right)$$ (3.24)

Substitute Eq. (3.24) in Eq. (3.22a) to get the torque T as

$$T = G\beta \frac{t_c t_d (b_d h_d + b_d t_c + h_d t_w)^2}{b_d t_d + 2\alpha t_c + 2t_c t_d}$$ (3.25)

The torsional constant J is then obtained using Eq. (3.20) as

$$J = \frac{t_c t_d (b_d h_d + b_d t_c + h_d t_w)^2}{b_d t_d + 2\alpha t_c + 2t_c t_d}$$ (3.26)

In an actual application, the delta stiffeners are formed by welding two rectangular plates to the compression flange and the web of the I-girder. Thus, replacing the dimension α in Eq. (3.26) by the actual plate width w_d as shown in Figure 3.6, the torsional constant can be written as

$$J = \frac{(b_d h_d + b_d t_c + h_d t_w)^2}{\dfrac{b_d}{t_c} + 2\dfrac{w_d}{t_d} + 2}$$ (3.27)
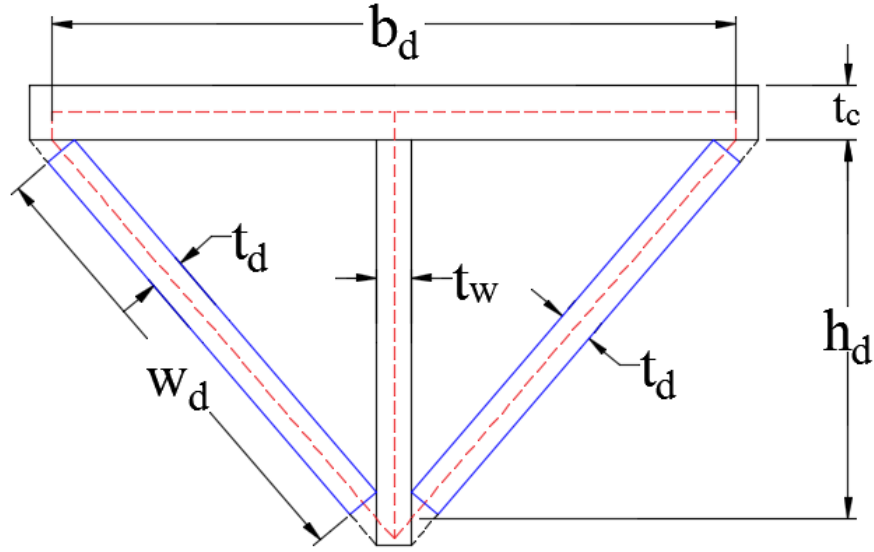
Figure 3.6 Actual dimensions of a Delta section

To check the accuracy of Eq. (3.27) with the numerical solution obtained using the FE software ShapeBuilder, 25 two-cell delta sections of practical dimensions are employed. The comparison between the analytical and the numerical results is provided in Table 3.4. It can be seen from Table 3.4 that for different configurations of a two-cell delta section, i.e., various b_d/h_d, t_d/t_w, t_c, and θ values, Eq. (3.27) provides results for J that are within 0.7% of the numerical solutions. This equation will now be extended to a full Delta section.

For the open profile without the delta part of the cross-section, the St. Venant torsional constant is given by

$$J = \sum_{i=1}^{n} C_i \frac{b_i t_i^{3}}{3} \tag{3.28}$$

where n is the number of elements, b_i is the width of element i, t_i is the thickness of element i, and C_i is the aspect ratio correction factor.

The torsional constant for the entire Delta section is the sum of the torsional constants of all the elements. Thus,

$$J = \sum_{i=1}^{n} C_i \frac{b_i t_i^3}{3} + J_\Delta \qquad (3.29)$$

Expanding Eq. (3.29), we obtain

$$J = \frac{1}{3}\left[(h - h_d)t_w^3 + b_t t_t^3\left(1 - 0.63\frac{t_t}{b_t}\right) + (b_c - b_d)t_c^3\left(1 - 0.63\frac{t_c}{b_c - b_d}\right)\right]$$

$$+ \frac{(b_d h_d + b_d t_c + h_d t_w)^2}{\frac{b_d}{t_c} + 2\frac{w_d}{t_d} + 2} \qquad (3.30)$$

The two bracketed terms of the form $(1 - 0.63\frac{t}{b})$ account for the aspect ratio correction factor of stocky flanges. These terms provide accurate results compared to solutions from elasticity theory (White & Jung, 2003). The accuracy of Eq. (3.30) will be evaluated in Section 3.4.

Table 3.4 Comparison between analytical and numerical results for Delta sections

Sec.	b_d (mm)	h_d (mm)	w_d (mm)	t_d (mm)	t_w (mm)	t_c (mm)	θ (deg.)	$J_{Num.}$ (mm^4)	$J_{Ana.}$ (mm^4)	Error
1	177.8	355.6	351.79	6.35	6.35	12.7	13.6	3.61E+07	3.62E+07	0.2%
2	228.6	355.6	361.44	6.35	6.35	12.7	17.4	5.58E+07	5.58E+07	0.1%
3	228.6	355.6	360.93	6.35	7.94	12.7	17.2	5.66E+07	5.67E+07	0.2%
4	304.8	355.6	376.69	6.35	6.35	12.7	22.8	9.07E+07	9.07E+07	0.0%
5	304.8	355.6	470.15	6.35	6.35	12.7	18.1	1.23E+08	1.23E+08	0.0%
6	254	254	264.92	12.7	12.7	31.8	25.4	1.15E+08	1.11E+08	-0.5%
7	254	254	264.92	12.7	12.7	25.4	25.4	1.02E+08	1.02E+08	-0.2%
8	342.9	304.8	331.47	12.7	12.7	31.8	28.4	2.20E+08	2.19E+08	-0.3%
9	342.9	304.8	337.06	7.94	12.7	31.8	28.4	1.47E+08	1.46E+08	-0.7%
10	342.9	304.8	327.66	15.88	12.7	31.8	28.4	2.64E+08	2.63E+08	-0.5%
11	605	600	654.16	12	12	40	26.3	1.24E+09	1.23E+09	-0.2%
12	605	600	654.16	12	12	22	26.3	1.06E+09	1.06E+09	-0.1%
13	807	600	706.69	12	12	40	33.5	1.96E+09	1.96E+09	-0.2%
14	807	600	706.69	12	12	22	33.5	1.66E+09	1.66E+09	-0.1%
15	807	700	791.02	12	12	40	29.6	2.38E+09	2.38E+09	-0.1%
16	200	300	297.31	10	10	20	17.6	6.27E+07	6.28E+07	0.2%
17	200	300	300.78	8	10	20	17.6	5.14E+07	5.15E+07	0.2%
18	250	300	308.61	10	10	20	21.8	9.04E+07	9.04E+07	0.0%
19	250	300	305.71	12	10	20	21.8	1.05E+08	1.05E+08	-0.1%
20	400	300	346.86	10	10	20	33.0	1.88E+08	1.88E+08	-0.2%
21	200	150	172.05	6	6	10	32.9	1.37E+07	1.36E+07	-0.4%
22	200	150	169.28	8	8	12	32.6	1.86E+07	1.85E+07	-0.5%
23	200	200	214.64	6	6	10	25.9	2.00E+07	1.99E+07	-0.2%
24	200	200	211.59	8	8	12	25.6	2.71E+07	2.71E+07	-0.3%
25	200	300	305.04	6	6	10	17.9	3.29E+07	3.29E+07	0.0%

To derive an equation for the warping constant C_w, the location of the shear center needs to be known. Hence, the location of the shear center of the Delta girder is to be determined in this section.

Two techniques are available to determine the location of the shear center of a general thin-walled cross-section. One employs the resultant shear flow and equilibrium, and the other entails the use of a numerical procedure. Both methods are essentially the same. The selection is often dictated by the complexity of the cross-section. These two techniques are well explained by Heins (1975). The numerical procedure will be adopted to compute the location of the shear center of the Delta girder.

The location of the shear center of a general cross-section with respect to its centroid is given by (Heins, 1975)

$$e_x = \frac{I_{xy}I_{wx} - I_y I_{wy}}{I_{xy}^2 - I_x I_y} \tag{3.31}$$

$$e_y = \frac{I_x I_{wx} - I_{xy}I_{wy}}{I_{xy}^2 - I_x I_y} \tag{3.32}$$

where I_x is the moment of inertia about the x-axis, I_y is the moment of inertia about the y-axis, I_{xy} is the product of inertia, $I_{wx} = \int xw\, dA$ and $I_{wy} = \int yw\, dA$ are the sectorial linear moments or the warping products of inertia in which w is the double sectorial area defined in Eq. (3.35).

Eqs. (3.31) & (3.32) require only the determination of the two quantities I_{wx} and I_{wy} through the numerical procedure. The Delta girder is a monosymmetric cross-section in which

the y-axis is the axis of symmetry, thus we readily have e_x and I_{xy} equal to zero, and so e_y will

reduce to

$$e_y = -\frac{I_{wx}}{I_y} \tag{3.33}$$

The expression I_{wx} is given by

$$I_{wx} = \frac{1}{3}\sum_{i=0}^{i=n}(w_i x_i + w_j x_j)t_{ij}L_{ij} + \frac{1}{6}\sum_{i=0}^{i=n}(w_i x_j + w_j x_i)t_{ij}L_{ij} \tag{3.34}$$

in which i and j represent the starting and ending points for each element, x_i and x_j are the

horizontal distances measured from the centroid of the cross-section to points i and j,

respectively; t_{ij} is the thickness of the element connecting points i and j, and L_{ij} is the length of

the element connecting points i and j.

For an open section, and for a given component element, the double sectorial area or the

unit warping with respect to the centroid w_i and w_j are given by

$$w_i = \rho_{ij}L_{ij}, \qquad w_j = w_i + \rho_{ij}L_{ij} \tag{3.35a,b}$$

where ρ_{ij} is the perpendicular distance from the centroid of the cross-section to the tangent line

joining points i and j. ρ_{ij} is considered positive if the cross-section's centroid is located to the

left of the directional line created from i to j.

For a closed cross-section, the effect of the torsional function $\tilde{q}$ should be taken into

account when evaluating w_i and w_j as follows

$$w_i = \rho_{ij}L_{ij} + \frac{\tilde{q}}{t_{ij}}L_{ij}, \qquad w_j = w_i + \rho_{ij}L_{ij} + \frac{\tilde{q}}{t_{ij}}L_{ij} \qquad (3.36a,b)$$

where $\tilde{q}$ for the Delta girder can be obtained as follows

$$\tilde{q} = \frac{2(2\hat{A})}{\oint \frac{ds}{t}} = \frac{b_d t_c + b_d h_d + h_d t_w}{\frac{b_d}{t_c} + \frac{2\alpha}{t_d} + \frac{t_c}{t_c} + \frac{t_w}{t_w}} \qquad (3.37)$$

By simplification, the torsional function for the Delta Girder can be written as

$$\tilde{q} = \frac{b_d(t_c + h_d) + h_d t_w}{\frac{b_d}{t_c} + 2\frac{\alpha}{t_d} + 2} \qquad (3.38)$$

The above method and equations will be used to determine the location of the shear center of the Delta girder as follows. Because the y-axis is an axis of symmetry, only one vertical half of the cross-section is needed to do the computations. The result will then be multiplied by two to obtain the complete solution. Figure 3.7 depicts the numbers of the starting and ending points for each element of the cross-section.

w_i and w_j are computed using Eqs. (35a,b) and (36a,b) as follows

$$w_0 = w_3 = w_4 = 0, \qquad w_1 = \frac{b_d}{2}\left(\frac{\tilde{q}}{t_c} - h_{cu}\right)$$

$$w_2 = \frac{b_d \tilde{q}}{2t_c} - \frac{b_c h_{cu}}{2}, \qquad w_5 = \frac{b_t h_{cl}}{2}$$

where

$$h_{cu} = d - \bar{y} - \frac{t_c}{2}, \qquad h_{cl} = \bar{y} - \frac{t_t}{2}$$

62

Figure 3.7 Delta girder numbering for shear center calculation

All the terms in Eq. (3.34) are presented in Table 3.5.

Table 3.5 Evaluation of terms in Eq. (3.34)

Element	w_i	w_j	x_i	x_j	t_{ij}	L_{ij}
0-1	w_0	w_1	0	$\dfrac{b_d}{2}$	t_c	$\dfrac{b_d}{2}$
1-2	w_1	w_2	$\dfrac{b_d}{2}$	$\dfrac{b_c}{2}$	t_c	$\dfrac{b_c - b_d}{2}$
1-3	w_1	w_3	$\dfrac{b_d}{2}$	0	t_d	$\alpha + t_w$
3-4	w_3	w_4	0	0	-	-
4-5	w_4	w_5	0	$\dfrac{b_t}{2}$	t_t	$\dfrac{b_t}{2}$

Substituting these terms into Eq. (3.34), I_{wx} can be obtained as

$$I_{wx} = 2\left\{\frac{1}{3}\left[\frac{w_1 t_c b_d{}^2}{4} + \frac{w_1 b_d t_c}{2}\left(\frac{b_c - b_d}{2}\right) + \frac{w_2 b_c t_c}{2}\left(\frac{b_c - b_d}{2}\right) + \frac{w_1 b_d t_d(\alpha + t_w)}{2} + \frac{w_5 b_t{}^2 t_t}{4}\right]\right.$$
$$\left. + \frac{1}{6}\left[\frac{w_1 b_c t_c}{2}\left(\frac{b_c - b_d}{2}\right) + \frac{w_2 b_d t_c}{2}\left(\frac{b_c - b_d}{2}\right)\right]\right\}$$

From Eq. (3.33), the location of the shear center S can be determined as

$$e_y = \frac{1}{24\, I_y}\left[(b_d{}^2 - 3b_c{}^2)b_d \tilde{q} + 2\left(h_{cu} t_c b_c{}^3 - h_{cl} t_t b_t{}^3\right) - 8\gamma t_d b_d(\alpha + t_w)\right] \qquad (3.39)$$

where

$$\gamma = \frac{b_d}{2}\left(\frac{\tilde{q}}{t_c} - h_{cu}\right)$$

3.3.2.3   Warping constant C_w

For a mixed cross-section, i.e., a section that consists of a closed profile with open profiles attached to it, the warping function ω is given by

$$\omega_i = \omega_{i-1} - \int_0^s r\, ds + \int_0^s \frac{\tilde{q}}{t}\, ds \qquad (3.40)$$

where i is the number of the component element, r is the perpendicular distance from the shear center S to the medial line of an infinitesimal element with length ds and width t, and $\tilde{q}$ is torsional function given by Eq. (3.38).

The integration of $\int r\, ds$ can be expressed in terms of Cartesian coordinates x and y as

$$\int r\, ds = \int x\, dy - \int y\, dx \qquad (3.41)$$

Thus, by applying Eq. (3.40) to each segment, the torsional warping constant C_w can be expressed as

$$C_w = \frac{1}{3} \sum_A (\omega_i{}^2 + \omega_i \omega_{i+1} + \omega_{i+1}{}^2) t_i L_i \qquad (3.42)$$

where $\sum_A$ is the sum of all component elements, t_i is the thickness of element i, and L_i is the length of element i.

The numerical process that will be used to compute C_w of the Delta girder is explained by Nakai and Yoo (1988). Figure 3.8 depicts the numbering of each component element and the selected orientation of the axes. Because of the symmetry, only one vertical half of the cross-section needs to be considered. Note that r is considered positive when the element proceeds in a counterclockwise rotation around the shear center S. Table 3.6 illustrates the calculation of the warping function ω using Eqs. (3.40) and (3.41).
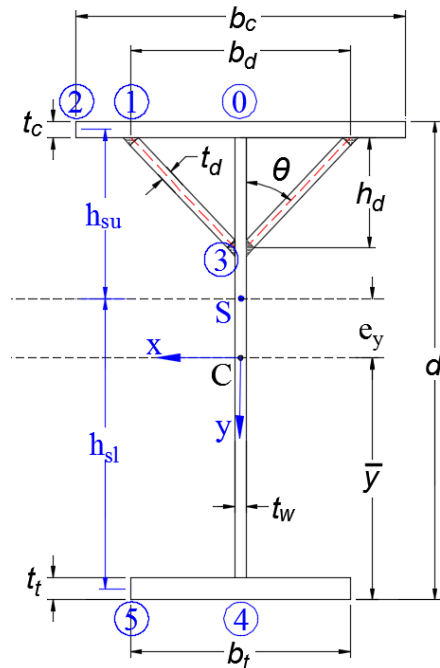
Figure 3.8 Delta girder numbering for warping constant calculation

Table 3.6 First step in computing the warping constant

Segment	$-x.\Delta_y$	$y.\Delta_x$	i	ω_i
$0-1$	0	$-h_{su}\dfrac{b_d}{2}$	1	$\dfrac{b_d}{2}\left(\dfrac{\tilde{q}}{t_c}-h_{su}\right)$
$1-2$	0	$-h_u\left(\dfrac{b_c-b_d}{2}\right)$	2	$\dfrac{b_d\tilde{q}}{2t_c}-\dfrac{b_ch_{su}}{2}$
$1-3$	$(-h_s\sin\theta\cos\theta)(-h_d)$	$(-h_s)(\sin^2\theta)\left(-\dfrac{b_d}{2}\right)$	3	$\begin{array}{l}b_d\left(\dfrac{\tilde{q}}{t_c}-h_{su}\right)\\+h_sh_d\sin\theta\cos\theta\\+\dfrac{h_sb_d}{2}\sin^2\theta+\left(\dfrac{\tilde{q}\alpha}{t_d}\right)=0\end{array}$
$3-4$	0	0	4	0
$4-5$	0	$h_{sl}\dfrac{b_t}{2}$	5	$h_{sl}\dfrac{b_t}{2}$

where $h_{su}=d-\bar{y}-e_y-\dfrac{t_c}{2}$, $h_{sl}=\bar{y}+e_y-\dfrac{t_c}{2}$, $h_s=d-\bar{y}-e_y-t_c-h_d$

and Table 3.7 shows the numerical process of obtaining C_w for the Delta girder.

Table 3.7 Second step in computing the warping constant

Segment			1	2	1×2
$i\sim i+1$	ω_i	ω_{i+1}	$\omega_i{}^2+\omega_i\omega_{i+1}+\omega_{i+1}{}^2$	t_iL_i	
$0-1$	0	ω_1	$\omega_1{}^2$	$t_c\dfrac{b_d}{2}$	$\omega_1{}^2t_c\dfrac{b_d}{2}$
$1-2$	ω_1	ω_2	$\omega_1{}^2+\omega_1\omega_2+\omega_2{}^2$	$t_c\left(\dfrac{b_c-b_d}{2}\right)$	$t_c\left(\dfrac{b_c-b_d}{2}\right)(\omega_1{}^2+\omega_1\omega_2+\omega_2{}^2)$
$1-3$	ω_1	0	$\omega_1{}^2$	$t_d(\alpha+\dfrac{t_w}{2})$	$t_d(\alpha+\dfrac{t_w}{2})\,\omega_1{}^2$
$3-4$	0	0	0	$-$	0
$4-5$	0	ω_5	$\omega_5{}^2$	$t_t\dfrac{b_t}{2}$	$t_t\dfrac{b_t}{2}\omega_5{}^2$
				$\sum=$	W

66

Thus, C_w can be computed from Eq. (3.42) as

$$C_w = \frac{1}{3}(2W) \tag{3.43}$$

Simplification of Eq. (3.43) provides the warping constant for Delta girders as

$$C_w = \frac{1}{3}[(t_c b_c + t_d t_w + 2t_d \alpha)\omega_1{}^2 + t_t b_t \omega_3{}^2 + t_c(b_c - b_d)(\omega_1 \omega_2 + \omega_2{}^2)] \tag{3.44}$$

where $\qquad \omega_1 = \frac{b_d}{2}\left(\frac{\tilde{q}}{t_c} - h_{su}\right), \qquad \omega_2 = \frac{b_d \tilde{q}}{2t_c} - \frac{b_c h_{su}}{2}, \qquad \omega_3 = h_{sl}\frac{b_t}{2} \tag{3.45}$

3.4   Comparison between Analytical and Numerical Results

In this section, the analytical and the finite element results of the geometric and torsion
properties of several Delta girders will be compared.

3.4.1   Hadley's cross-section

The first comparison will be made on the Delta girder used by Hadley (1961) in his experimental
research of this type of girder. The cross-section dimensions are depicted in Figure 3.9 where all
dimensions are in mm.

The cross-sectional dimensions are:

$b_c = 609.6$ mm; $\ b_d = 355.6$ mm; $\ b_t = 406.4$ mm; $\ d = 952.5$ mm; $h = 914.4$ mm;

$h_d = 228.6$ mm; $\ w_d = 281.08$ mm; $\ t_c = 12.7$ mm; $\ t_t = 25.4$ mm; $\ t_w = \ t_d = 6.35$ mm
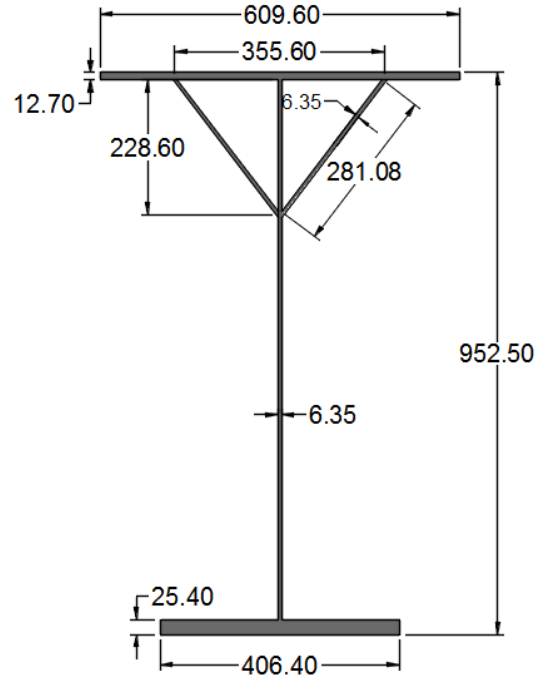
Figure 3.9 Cross-section dimension in mm (Hadley, 1961)

3.4.1.1 Cross-sectional properties calculated using the equations derived in section 3.3

Using Eq. (3.2): $\alpha = \sqrt{\left(\frac{355.6-6.35}{2}\right)^2 + 228.6^2} = 287.67$ mm

The area of the cross-section is obtained using Eq. (3.1):

$A = (12.7 \times 609.6) + (25.4 \times 406.4) + (914.4 \times 6.35) + 2(287.67 \times 6.35)$

$A = 27{,}524.33$ mm^2

The angle formed between the delta stiffener and the web is obtained from Eq. (3.5):

$\theta = \cos^{-1}\left(\frac{228.6}{287.67}\right) = 37.38°$

The centroid location is obtained using Eq. (3.4):

$$\bar{y} = \frac{1}{(27{,}524.33\,)}\left[(12.7\times609.6)\left(952.5 - \frac{12.7}{2}\right) + \frac{(406.4)(25.4)^2}{2}\right.$$

$$+ (914.4\times6.35)\left(25.4 + \frac{914.4}{2}\right)$$

$$\left. + 2(287.67\times6.35)\left(952.5 - 12.7 - \frac{287.67}{2}\cos 37.38\right)\right] = 482.27 \text{ mm}$$

The moments of inertia of the delta stiffeners about the global coordinate axis are calculated using Eqs. (3.6) to (3.9):

$$I_{x',d} = \frac{287.67\times6.35^3}{12} = 6{,}138.11 \text{ mm}^4$$

$$I_{y',d} = \frac{6.35\times287.67^3}{12} = 12{,}597{,}263.08 \text{ mm}^4$$

$$I_{x,d} = 6{,}138.11\ \cos^2(-52.62°) + 12{,}597{,}263.08\sin^2(-52.62°) = 7{,}956{,}569.92 \text{ mm}^4$$

$$I_{y,d} = 6{,}138.11\sin^2(-52.62°) + 12{,}597{,}263.08\cos^2(-52.62°) = 4{,}645{,}217.79 \text{ mm}^4$$

The moment of inertia of the Delta girder about the x-axis is obtained from Eq. (3.11):

$$I_x = \frac{406.4\times25.4^3}{12} + (406.4\times25.4)\left(482.27 - \frac{25.4}{2}\right)^2 + \frac{609.6\times12.7^3}{12}$$

$$+ (609.6\times12.7)\left(952.5 - 482.27 - \frac{12.7}{2}\right)^2 + \frac{6.35\times914.4^3}{12}$$

$$+ (914.4\times6.35)\left(\frac{914.4}{2} + 25.4 - 482.27\right)^2$$

$$+ 2[7{,}956{,}569.92 + (287.67\times6.35)(343.23)^2] = 4.79\times10^9 \text{ mm}^4$$

The moment of inertia of the Delta girder about the y-axis is obtained from Eq. (3.14):

$$I_y = \frac{25.4 \times 406.4^3}{12} + \frac{12.7 \times 609.6^3}{12} + \frac{914.4 \times 6.35^3}{12}$$

$$+ 2[4{,}645{,}217.79 + (287.67 \times 6.35)(90.50)^2] = 4.21 \times 10^8 \text{ mm}^4$$

The elastic section moduli about the x-axis are obtained from Eqs. (3.16) & (3.17):

$$S_{xc} = \frac{4.79 \times 10^9}{952.5 - 482.27} = 1.02 \times 10^7 \text{ mm}^3$$

$$S_{xt} = \frac{4.79 \times 10^9}{482.27} = 9.93 \times 10^6 \text{ mm}^3$$

The torsional constant can be obtained using Eq. (3.30):

$$J = \frac{1}{3}\left[(914.4 - 228.6)(6.35)^3 + 406.4 \times 25.4^3 \times \left(1 - 0.63 \times \frac{25.4}{406.4}\right)\right.$$

$$\left. + (609.6 - 355.6)(12.7)^3 \times (1 - 0.63 \times \frac{12.7}{609.6 - 355.6}\right]$$

$$+ \frac{(355.6 \times 228.6 + 355.6 \times 12.7 + 228.6 \times 6.35)^2}{\frac{355.6}{12.7} + \frac{2 \times 281.08}{6.35} + 1} = 6.66 \times 10^7 \text{ mm}^4$$

The location of the shear center is computed using Eq. (3.39) as follows:

$$h_{cu} = 463.88 \text{ mm}, \qquad h_{cl} = 469.57 \text{ mm}, \qquad \tilde{q} = 723.51 \text{ mm}^2$$

$$\gamma = \frac{355.6}{2}\left(\frac{723.51}{12.7} - 463.88\right) = -72{,}348.7 \text{ mm}^2$$

$$e_y = \frac{1}{24 \times 4.21 \times 10^8} [(355.6^2 - 3 \times 609.6^2)(355.6)(730.09)$$

$$+ \, 2(463.88 \times 12.7 \times 609.6^3 - 469.57 \times 25.4 \times 406.4^3)$$

$$- \, 8(-72{,}348.7\,)(6.35 \times 355.6 \times (287.67 + 6.35))]$$

$$e_y = 118.55 \text{ mm}$$

Finally, the warping constant is calculated based on Eqs. (3.44) & (3.45):

$$h_{su} = 952.5 - 482.27 - 118.55 - 0.5 \times 12.7 = 345.33 \text{ mm}$$

$$h_{sl} = 482.27 + 118.55 - 0.5 \times 12.7 = 594.47 \text{ mm}$$

$$\omega_1 = \frac{355.6}{2} \left(\frac{723.51}{12.7} - 345.66 \right) = -51{,}329.21 \text{ mm}^2$$

$$\omega_2 = \frac{355.6 \times 723.51}{2 \times 12.7} - \frac{609.6 \times 345.33}{2} = -95{,}127.44 \text{ mm}^2$$

$$\omega_3 = \frac{594.47 \times 406.4}{2} = 120{,}796.30 \text{ mm}^2$$

$$C_w = \frac{1}{3} [(12.7 \times 609.6 + 6.35 \times 12.7 + 2 \times 6.35 \times 287.67)(-51{,}329.21)^2$$

$$+ \, 25.4 \times 406.4 \times 120{,}796.3^2 + (12.7)(609.6 - 355.6)(41{,}329.21 \times 95{,}127.44$$

$$+ \, 95{,}127.44^2)]$$

$$C_w = 7.42 \times 10^{13} \text{ mm}^6$$

3.4.1.2   Cross-sectional properties computed by FE

Figure 3.10 depicts the model and the results obtained through finite element analysis. These

include the geometric and torsion properties along with the used FE mesh to obtain the results.
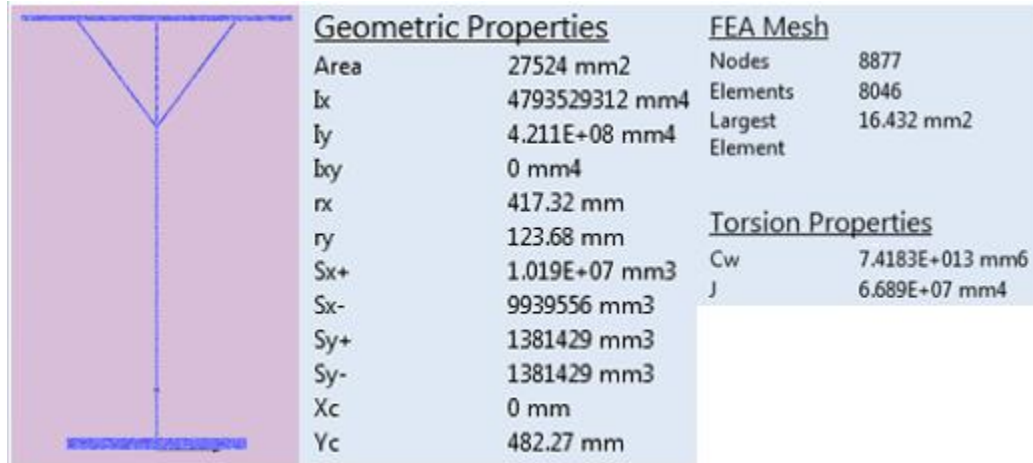
Figure 3.10 FE properties of Hadley's cross-section

3.4.1.3   Results Comparison

Table 3.8 summarizes the main cross-sectional properties that were obtained numerically and

from the equations derived in section 3.3. From the 4th column in the table that shows the percent

error, it can be seen that excellent results are obtained. For the torsion properties, the analytical

equations derived in section 3.3 provided excellent results for the shear center location e_y and

the warping constant C_w, while the torsional constant J was only 0.45 % lower than the FE

solution. These results indicate the accuracy of the analytical cross-sectional quantities derived

for the Delta girder.

    In order to better understand the effects of adding delta stiffeners on the cross-sectional

properties of a plate girder. The same girder, i.e., Hadley's girder, was numerically modeled

without the delta stiffeners. The results are provided in the 5th column of Table 3.8. A

comparison between the models with and without stiffeners was performed and the change in percentage due to the addition of stiffeners is presented in the 6th column. The most notable increase is in the torsional constant J. The creation of a partially closed cross-section has increased J by 2,434 %. On the other hand, the value of the warping constant C_w has decreased by 4.5% and the shear center is now closer to the centroid. Finally, the delta stiffeners increase the cross-sectional area by around 15%, i.e., the weight of the section will be increased by 15%. It remains to be verified that this weight increase due to the addition of inclined stiffeners will produce more effective results when compared with alternative solutions such as increasing the web thickness of the girder.

Table 3.8 Comparison of Hadley's cross-section results

Geometric properties	FE results	Analytical results	Error	Numerical results (w/o stiffeners)	Effect of the inclined stiffeners
A (mm^2)	27,524	27,524.33	0.0 %	23,871	+15.3 %
I_x (mm^4)	4.79×10^9	4.79×10^9	0.0 %	4.28×10^9	+11.9 %
I_y (mm^4)	4.21×10^8	4.21×10^8	0.0 %	3.82×10^8	+10.2 %
$S_{xc}(mm^3)$	1.02×10^7	1.02×10^7	0.0 %	9.96×10^6	+2.4 %
Torsion properties					
J (mm^4)	6.69×10^7	6.66×10^7	−0.45 %	2.64×10^6	2,434 %
e (mm)	118.51	118.55	0.0 %	169.07	−29.9 %
C_w (mm^6)	7.42×10^{13}	7.42×10^{13}	0.0 %	7.77×10^{13}	−4.5 %

3.4.2 Mohebkhah and Azandariani's (2015) cross-section

The Delta girder shown in Figure 3.11 is now used to make a comparison between the analytical

and the FE results for the geometrical and torsional properties.
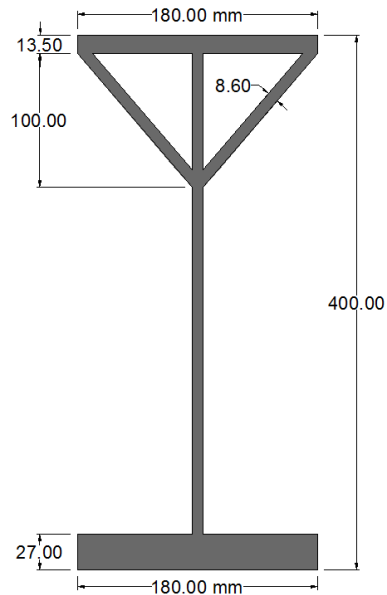
Figure 3.11 Cross-section dimension in mm (Mohebkhah & Azandariani, 2015)

The cross-sectional dimensions are:

$b_c = 180$ mm; $b_d = 168.67$ mm; $b_t = 180$ mm; $d = 400$ mm; $h = 359.5$ mm;

$h_d = 93.39$ mm; $w_d = 114.29$ mm; $t_c = 13.5$ mm; $t_t = 27$ mm; $t_w = t_d = 8.6$ mm

3.1.1. *Cross-sectional properties using the equations derived in section 3.3*

Using Eq. (3.2): $\alpha = 123$ mm

The area of the cross-section using Eq. (3.1): $A = 12{,}497.3$ mm^2

The angle formed between the delta stiffeners and the web from Eq. (3.5): $\theta = 40.6°$

The centroid location is obtained from Eq. (3.4): $\bar{y} = 190.38$ mm

The moments of inertia of the delta stiffeners about the global coordinate axis are calculated using Eq. (3.6) to Eq. (3.9):

$$I_{x,d} = 6{,}519.57 \; \cos^2(-49.4°) + 1{,}333{,}621.35 \sin^2(-49.4°) = 771{,}583.35 \text{ mm}^4$$

$$I_{y,d} = 6{,}519.57 \sin^2(-49.4°) + 1{,}333{,}621.35 \cos^2(-49.4°) = 568{,}556.57 \text{ mm}^4$$

The moment of inertia of the Delta girder about the x-axis is obtained from Eq. (3.11):

$$I_x = 335{,}297{,}305 \text{ mm}^4$$

The moment of inertia of the Delta girder about the y-axis is obtained from Eq. (3.14):

$$I_y = 24{,}994{,}762 \text{ mm}^4$$

The elastic section modulus about the x-axis are obtained from Eqs. (3.16) & (3.17):

$$S_{xc} = 1{,}599{,}548.25 \text{ mm}^3 \text{ and } S_{xt} = 1{,}761{,}200.26 \text{ mm}^3$$

The torsional constant can be obtained using Eq. (3.30):

$$J = 9.88{\times}10^6 \text{ mm}^4$$

The location of the shear center is computed using Eq. (3.39):

$$e_y = -11.5 \text{ mm}$$

Finally, the warping constant is calculated based on Eq.'s (3.44) & (3.45):

$$C_w = 7.52{\times}10^{11} \text{ mm}^6$$

The cross-sectional properties provided by Mohebkhah and Azandariani are summarized in

Table 3.9 given in Section 3.4.2.3. The equations they used to compute the torsional properties

are presented in this section.

To obtain the torsional constant J, Mohebkhah and Azandariani used the following

equation

$$J = \frac{1}{3} \sum_{i=1}^{m} b_i t_i^3 + J_\Delta \tag{3.46}$$

where J_Δ is the torsional constant of the delta part of the cross-section and is obtained by

$$J_\Delta = \frac{4A^2}{\oint \frac{ds}{t}} \tag{3.47}$$

By adopting this approach, the authors have ignored the web of the delta part of the

cross-section and consider it as a single closed cell. The percentage of error associated with this

technique is provided in Section 3.4.2.3.

To compute the warping constant C_w, the authors used the approximate equation that was

originally provided by Nakai and Yoo (1988) as

$$C_w \cong \sum_{i=1}^{m} (C_{w,i} + x_i^2 I_{\bar{x},i} + y_i^2 I_{\bar{y},i}) \tag{3.48}$$

However, this approximate equation was developed to compute the warping constant C_w for

multiple I- and/or box girders connected by rigid sways and lateral bracings. Thus, the use of this

equation for a Delta girder is not appropriate. The comparison of C_w obtained using these equations with the FE values is presented in Section 3.4.2.3.

3.4.2.2 Cross-sectional properties computed by FE

Figure 3.12 depicts the model and the results obtained through finite element analysis. These include the geometric and torsional properties along with the used finite element mesh to obtain the results.

Geometric Properties		FEA Mesh	
Area	12497 mm2	Nodes	8529
Ix	3.353E+08 mm4	Elements	8070
Iy	2.501E+07 mm4	Largest Element	7.2866 mm2
Ixy	0 mm4		
rx	163.79 mm	Torsion Properties	
ry	44.736 mm	J	9909658 mm4
Sx+	1599300 mm3	B1	30.194 mm
Sx-	1761076 mm3		
Sy+	277893 mm3		
Sy-	277893 mm3		
Xc	0 mm		
Yc	190.37 mm		
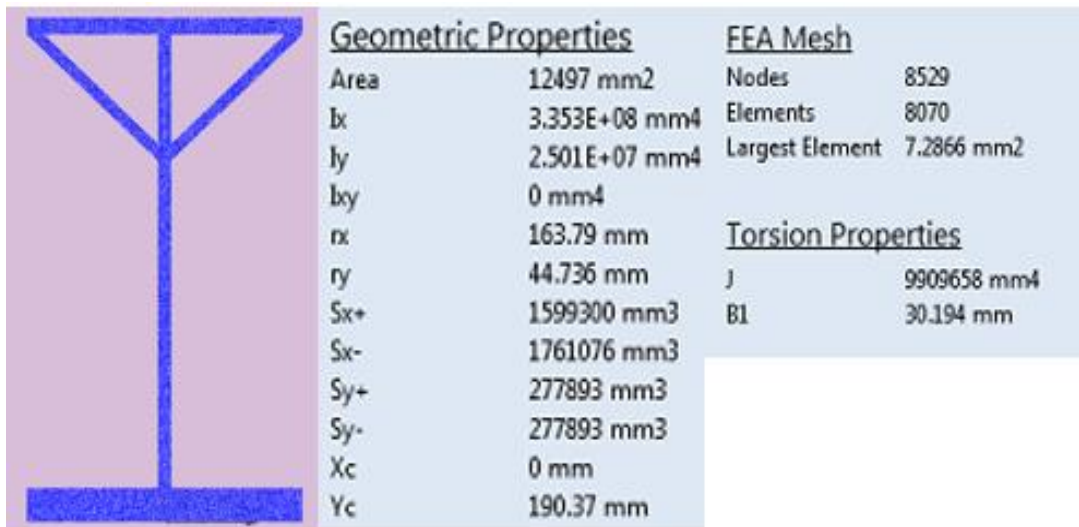
Figure 3.12 FE properties of Mohebkhah and Azandariani's cross-section

3.4.2.3 Results Comparison for Mohebkhah and Azandariani's Cross-section

The comparison between the results is provided in Table 3.9. It is clear that while excellent results are obtained for both the geometric properties and torsional properties using the derived equations, a noticeable difference is observed for the results obtained using the Mohebkhah and Azandariani's equations. This discrepancy for the geometric properties could be due to a slight

change in the angle θ used in their calculation, or due to the method used in obtaining these values.

The torsional constant J obtained by Mohebkhah and Azandariani is 14.2 % below the FE solution. The technique used by them, which ignores the web of the delta part, is explained in section 4.2.2. However, it is worth noting that while their results overestimate the moment of inertia about the nonsymmetry axis by 16.4 %, they underestimate the torsional constant by 14.2 %. Finally, the warping constant C_w obtained by them, based on the method described in section 4.2.2, is 15.2 % higher than the numerical solution. This difference was expected because of the approximate nature of the equation used to compute C_w.

Table 3.9 Comparison of Mohebkhah and Azandariani's cross-section results

Geometric properties	Numerical results	Analytical results as per section 3	Error	Mohebkhah & Azandariani results	Error
A (mm^2)	12,497	12,497.3	0 %	-	-
I_x (mm^4)	3.35×10^8	3.35×10^8	0 %	3.90×10^8	+16.4 %
I_y (mm^4)	2.50×10^7	2.50×10^7	0 %	2.59×10^7	+3.6 %
S_{xc}(mm^3)	1.60×10^6	1.60×10^6	0 %	-	-
Torsion properties					
J (mm^4)	9.91×10^6	9.88×10^6	−0.3 %	8.50×10^6	−14.2 %
C_w (mm^6)	7.58×10^{11}	7.52×10^{11}	−0.8 %	8.73×10^{11}	+15.2 %

3.4.3   Verification of the derived torsional properties' equations

To examine the accuracy of the derived equations for the torsional constant J, the shear center

location e_y, and the warping constant C_w, a list of 25 cross-sections were created and modeled

using the FE software. These 25 cross-sections were selected to cover a range of extreme

practical configurations for the delta stiffeners, and cases where the stiffeners have different

thickness in comparison with the web of the girder.

     The two extreme practical dimensions that are selected for the stiffeners height are $h_d =$

$\frac{h}{5}$ and $h_d = \frac{h}{3}$. The widths of the delta stiffeners are chosen as $b_d = \frac{b_c}{2}$ and $b_d = \frac{2}{3}b_c$. Therefore,

four combinations are created and will be tested for different thicknesses t_d as shown in Table

3.10.

<div align="center">

Table 3.10 Combinations used in forming the Delta section

</div>

Combination #	h_d	b_d
1	$\dfrac{h}{5}$	$\dfrac{b_C}{2}$
2	$\dfrac{h}{5}$	$\dfrac{2}{3}b_c$
3	$\dfrac{h}{3}$	$\dfrac{b_C}{2}$
4	$\dfrac{h}{3}$	$\dfrac{2}{3}b_c$

     Two sets of cross-sections are used, set A and set B. Set A contains 13 cross-sections and

is based on the dimensions of the girder used by Hadley. Section 1 dimensions are typical to

those used by Hadley and therefore it can be used as a source for comparison. Note that in

Hadley's cross-section, the thickness of the delta stiffeners t_d is equal to that of the web t_w which is 6.35 mm. Sections 2 to 13 employ four different combinations while changing t_d and keeping t_w unchanged. A summary of all combinations used is provided in Table 3.11. The following are some common dimensions for set A that are not provided in Table 3.11:

$b_c = 609.6$ mm, $b_t = 406.4$ mm, $d = 952.5$ mm, $h = 914.4$ mm, $t_c = 12.7$ mm,

$t_t = 25.4$ mm.

Set B consists of 12 cross-sections (sections 14 to 25) and employs the same techniques that were used in Set A in addition to changing the web thickness t_w. The 12 combinations used are summarized in Table 3.11. The following dimensions are common for set B:

$b_c = 300$ mm, $b_t = 300$ mm, $d = 600$ mm, $h = 576$ mm, $t_c = t_t = 12$ mm.

Table 3.12 presents the torsional properties for the 25 cross-sections and a comparison of the analytical results with respect to the FE results. Note that the percent of difference of the analytical solution from the FE solution is used in computing the percentage of error. The results of the torsional constant J, calculated using Eq. (3.30), are within 1.9 % of the FE results. The range of error is -1.9 % to 0.8 %. Furthermore, 19 out of 25 results have a percentage error within 1 %. It is also worth mentioning that Eq. (3.30) overestimates the torsional constant in only one cross-section. The comparison of the shear center location e_y indicates that Eq. (3.39) provides results with a maximum error of 1.6%. The results also indicate that in 16 cases (64 %), e_y was calculated to within 0.3 % error. Eq. (3.44) provides the warping constant C_w for the Delta girder with a maximum error of 0.3 %. It can be also seen that in 21 cases (84 %), C_w is obtained with a maximum error of 0.1 %.

These results demonstrate that the derived equations for the torsional properties of Delta girders provide very accurate results. This accuracy should facilitate the computation of the critical buckling moment equation M_{cr} of Delta girders in a later stage of this research. As a concluding remark, the maximum torsional constant for Hadley's cross-section was obtained using cross-section 13. The percentage of increase of J with respect to Hadley's original cross-section (number 1) is 141 %. This increase is associated with 12 % increase in cross-section weight.

3.5   <u>Summary</u>

The cross-section properties of a structural element are essential to study its behavior. In the case of Delta girders, these properties have not been derived yet and approximate equations have been used by previous researchers to determine the torsional properties. These approximate equations are shown to provide an error in the range of -14.2% (conservative) to 16.4% (unconservative) in comparison with the FE solution. In this chapter, equations for the geometric and torsional properties of Delta girders are presented. The accuracy of these equations was checked against results obtained from a finite element analysis software. The results of the comparison based on 25 tested cross-sections have shown that the torsional constant J can be obtained with a maximum error of 1.8 %, the shear center location e_y can be obtained with a maximum error of 1.6 %, and the warping constant C_w can be obtained with a maximum error of 0.3%. These equations can therefore be used to calculate cross-sectional properties for Delta girders with a high level of precision and can conveniently be used by design engineers.

For practical convenience, Tables 3.13 and 3.14 summarize the geometric and torsional properties of Delta girders. All equations are provided in a format that allows engineers to

directly implement them on a spreadsheet, similar to the one created by the author and shown in

Figure 3.13, and hence be able to obtain all these properties by simply inputting the cross-

sectional dimensions.

Cross-Sectional Properties of Delta Girders

Please input the following dimensions

b_c	300.00
b_d	200.00
b_t	300.00
d	500.00
h_d	100.00
t_c	12.00
t_t	12.00
t_w	10.00
t_d	10.00

(consistent set of units should be used)

Cross-sectional properties

Area

A | 1.47E+04 | $(unit^2)$

Width of the stiffeners

w_d | 127.92 | $(unit)$

Centroid location

$\bar{y}$ | 285.24 | $(unit)$

Location of the shear center

e_y | -19.29 | $(unit)$

Moment of inertia about the non-symmetry axis

I_x | 6.00E+08 | $(unit^4)$

Moment of inertia about the symmetry axis

I_y | 6.37E+07 | $(unit^4)$

Torsional constant

J | 1.27E+07 | $(unit^4)$

Warping constant

C_w | 3.15E+12 | $(unit^6)$

Plastic neutral axis (PNA)

$\bar{y}_p$ | 387.9 | $(unit)$

Plastic section modulus

Z_x | 2.652E+06 | $(unit^3)$

Figure 3.13 Spreadsheet developed by the author to obtain the necessary cross-section properties

by simply inputting the cross-sectional dimensions

Table 3.11 Stiffeners dimensions for Sets A and B

Set	Section	b_d (mm)	h_d (mm)	t_w (mm)	t_d (mm)	w_d (mm)	θ (deg.)
A	1	355.6	228.6	6.35	6.35	281.08	37.38
	2	304.8	182.9	6.35	6.35	229.57	39.21
	3	406.4	182.9	6.35	6.35	264.66	47.56
	4	304.8	304.8	6.35	6.35	331.33	26.09
	5	406.4	304.8	6.35	6.35	357.65	33.27
	6	304.8	182.9	6.35	3.175	232.81	39.21
	7	406.4	182.9	6.35	3.175	267.85	47.56
	8	304.8	304.8	6.35	3.175	335.35	26.09
	9	406.4	304.8	6.35	3.175	361.11	33.27
	10	304.8	182.9	6.35	9.525	226.33	39.21
	11	406.4	182.9	6.35	9.525	261.48	47.56
	12	304.8	304.8	6.35	9.525	327.54	26.09
	13	406.4	304.8	6.35	9.525	354.19	33.27
B	14	150	115.2	8	6	128.61	31.65
	15	200	115.2	8	6	143.86	39.81
	16	150	192	8	6	195.49	20.29
	17	200	192	8	6	207.16	26.57
	18	150	115.2	10	8	125.79	31.28
	19	200	115.2	10	8	141.17	39.51
	20	150	192	10	8	191.93	20.03
	21	200	192	10	8	204.15	26.33
	22	150	115.2	8	10	124.13	31.65
	23	200	115.2	8	10	139.79	39.81
	24	150	192	8	10	189.34	20.29
	25	200	192	8	10	202.16	26.57

Table 3.12 Comparison between analytical and numerical results

Sec.	J_{Num} (mm^4)	J_{Ana} (mm^4)	Comp.	$e_{y\,Num}$ (mm)	$e_{y\,Ana}$ (mm)	Comp.	$C_{w\,Num}$ (mm^6)	$C_{w\,Ana}$ (mm^6)	Comp.
1	6.69E+07	6.66E+07	-0.5%	118.5	118.6	0.0%	7.42E+13	7.41E+13	-0.1%
2	4.02E+07	4.00E+07	-0.6%	120.5	120.6	0.1%	7.47E+13	7.47E+13	0.0%
3	5.81E+07	5.78E+07	-0.6%	124.3	124.3	0.0%	7.49E+13	7.48E+13	-0.1%
4	7.73E+07	7.71E+07	-0.2%	114.7	114.8	0.1%	7.42E+13	7.43E+13	0.1%
5	1.20E+08	1.19E+08	-0.3%	119.7	119.7	0.0%	7.38E+13	7.37E+13	-0.1%
6	2.40E+07	2.38E+07	-0.6%	142.6	142.6	0.0%	7.59E+13	7.59E+13	-0.1%
7	3.46E+07	3.44E+07	-0.6%	144.3	144.3	0.0%	7.60E+13	7.59E+13	-0.1%
8	4.36E+07	4.35E+07	-0.3%	139.6	139.5	-0.1%	7.58E+13	7.58E+13	0.0%
9	6.81E+07	6.79E+07	-0.2%	142.5	142.3	-0.1%	7.56E+13	7.55E+13	-0.1%
10	5.32E+07	5.26E+07	-1.1%	101.8	102.1	0.3%	7.38E+13	7.38E+13	0.0%
11	7.63E+07	7.56E+07	-1.1%	107.6	107.8	0.1%	7.42E+13	7.42E+13	-0.1%
12	1.04E+08	1.05E+08	0.8%	94.6	93.9	-0.7%	7.29E+13	7.30E+13	0.0%
13	1.62E+08	1.61E+08	-0.6%	100.1	100.3	0.2%	7.22E+13	7.22E+13	0.0%
14	7.37E+06	7.30E+06	-0.9%	-22.0	-21.9	-0.3%	4.60E+12	4.59E+12	-0.1%
15	1.08E+07	1.07E+07	-0.9%	-15.3	-15.2	-0.3%	4.68E+12	4.67E+12	-0.2%
16	1.33E+07	1.33E+07	-0.3%	-22.0	-21.9	-0.3%	4.64E+12	4.64E+12	0.0%
17	2.08E+07	2.07E+07	-0.3%	-12.6	-12.6	0.1%	4.72E+12	4.71E+12	-0.1%
18	9.42E+06	9.31E+06	-1.1%	-24.9	-24.7	-0.7%	4.58E+12	4.58E+12	-0.1%
19	1.36E+07	1.35E+07	-1.2%	-16.0	-15.8	-1.0%	4.69E+12	4.67E+12	-0.2%
20	1.74E+07	1.73E+07	-0.4%	-24.6	-24.4	-0.9%	4.62E+12	4.63E+12	0.1%
21	2.67E+07	2.65E+07	-0.6%	-13.1	-13.0	-1.2%	4.71E+12	4.70E+12	-0.1%
22	1.07E+07	1.05E+07	-1.8%	-32.8	-32.5	-0.9%	4.58E+12	4.58E+12	0.0%
23	1.55E+07	1.52E+07	-1.9%	-22.4	-22.2	-0.8%	4.71E+12	4.70E+12	-0.2%
24	2.02E+07	2.00E+07	-0.9%	-32.7	-32.2	-1.6%	4.61E+12	4.63E+12	0.3%
25	3.09E+07	3.06E+07	-1.0%	-19.6	-19.3	-1.6%	4.71E+12	4.71E+12	0.1%

Table 3.13 Summary of geometric properties of Delta girders

Geometrical Cross-Sectional Properties of Delta Girders	
	Dimensions $$y_c = d - \bar{y} - \frac{t_c}{2}$$ $$y_t = \bar{y} - \frac{t_t}{2}$$ $$y_w = \frac{h}{2} + t_t - \bar{y}$$ $$y_d = d - \bar{y} - t_c - \frac{\alpha}{2}\cos\theta$$ $$x_d = \frac{t_w}{2} + \frac{\alpha}{2}\sin\theta$$ $$\alpha = \sqrt{\left(\frac{b_d - t_w}{2}\right)^2 + h_d^2}$$

Inclination of stiffeners

$$\theta = \cos^{-1}\left(\frac{h_d}{\alpha}\right)$$

Area

$$A = t_c b_c + t_t b_t + t_w h + 2t_d \alpha$$

Centroid location

$$\bar{y} = \frac{1}{A}\left[t_c b_c\left(d - \frac{t_c}{2}\right) + \frac{t_t^2 b_t}{2} + t_w h\left(t_t + \frac{h}{2}\right) + 2t_d\alpha\left(d - t_c - \frac{\alpha}{2}\cos\theta\right)\right]$$

Moments of inertia

$$I_x = \frac{b_t t_t^3}{12} + b_t t_t y_t^2 + \frac{b_c t_c^3}{12} + b_c t_c y_c^2 + \frac{t_w h^3}{12} + h t_w y_w^2 + 2\left(I_{x,d} + \alpha t_d y_d^2\right)$$

$$I_y = \frac{t_t b_t^3}{12} + \frac{t_c b_c^3}{12} + \frac{h t_w^3}{12} + 2\left(I_{y,d} + \alpha t_d x_d^2\right)$$

where

$$I_{x,d} = \frac{\alpha t_d^3}{12}\sin^2\theta + \frac{t_d \alpha^3}{12}\cos^2\theta$$

$$I_{y,d} = \frac{\alpha t_d^3}{12}\cos^2\theta + \frac{t_d \alpha^3}{12}\sin^2\theta$$

85

Table 3.14 Summary of torsional properties of Delta girders

Torsional Cross-Sectional Properties of Delta Girders	
	Dimensions $$h_{cu} = d - \bar{y} - \frac{t_c}{2}$$ $$h_{cl} = \bar{y} - \frac{t_t}{2}$$ $$h_{su} = d - \bar{y} - e_y - \frac{t_c}{2}$$ $$h_{sl} = \bar{y} + e_y - \frac{t_c}{2}$$ **Parameters** $$\alpha = \sqrt{\left(\frac{b_d - t_w}{2}\right)^2 + h_d{}^2}$$ $$\gamma = \frac{b_d}{2}\left(\frac{\tilde{q}}{t_c} - h_{cu}\right)$$

Torsional constant

$$J = \frac{1}{3}\left[(h - h_d)t_w{}^3 + b_t t_t{}^3\left(1 - 0.63\frac{t_t}{b_t}\right) + (b_c - b_d)t_c{}^3\left(1 - 0.63\frac{t_c}{b_c - b_d}\right)\right] + \frac{(b_d h_d + b_d t_c + h_d t_w)^2}{\frac{b_d}{t_c} + 2\frac{w_d}{t_d} + 2}$$

Shear center

$$e_y = \frac{1}{24\,I_y}\left[(b_d{}^2 - 3b_c{}^2)b_d\tilde{q} + 2(h_{cu}t_c b_c{}^3 - h_{cl}t_t b_t{}^3) - 8\gamma t_d b_d(\alpha + t_w)\right]$$

Warping constant

$$C_w = \frac{1}{3}\left[(t_c b_c + t_d t_w + 2t_d\alpha)\omega_1{}^2 + t_t b_t\omega_3{}^2 + t_c(b_c - b_d)(\omega_1\omega_2 + \omega_2{}^2)\right]$$

Torsional function

$$\tilde{q} = \frac{b_d(t_c + h_d) + h_d t_w}{\frac{b_d}{t_c} + 2\frac{\alpha}{t_d} + 2}$$

Warping functions

$$\omega_1 = \frac{b_d}{2}\left(\frac{\tilde{q}}{t_c} - h_{su}\right), \qquad \omega_2 = \frac{b_d\tilde{q}}{2t_c} - \frac{b_c h_{su}}{2}, \qquad \omega_3 = h_{sl}\frac{b_t}{2}$$

Others are symmetrical with respect to centerline of the cross-section

Chapter 4

Elastic Lateral-Torsional Buckling Capacity

4.1 <u>Introduction</u>

The elastic lateral torsional buckling (LTB) equation that can be used to determine the flexural capacity of monosymmetric beams is provided in Section 2.4.2 by Eq. (2.3). Although this equation is generally applicable for open cross-sections, it will be shown that it can also be used for Delta girders provided that the proper cross-section properties are used and the coefficient of monosymmetry is addressed. In Chapter 3, the cross-section properties of the Delta girders were derived. This chapter will verify that Eq. (2.3) is capable of predicting the LTB capacity of Delta girders given that the cross-section properties are obtained in accordance with the equations given in Chapter 3. The verification will be performed by comparing the LTB capacities of Delta girders using Eq. (2.3) with results obtained from developed finite element analysis.

The chapter will start with an analytical derivation that explains the presence of β_x in the LTB equation of monosymmetric beams. This will be followed by a description of the FE model and a verification of the analytical equation. Afterwards, linear elastic buckling analysis results of simply-supported Delta girders under uniform moment are obtained using the eigenvalue buckling analysis option in the general purpose commercial finite element software Abaqus. These results are then investigated and compared to those of I-girders and an alternative solution. Finally, a parametric study is performed to investigate several parameters that affect the LTB capacity of Delta girders.

4.2   <u>Theoretical Solution</u>

The governing differential equations of a simply-supported monosymmetric beam under uniform

bending are given by (Galambos T. V., 1968)

$$EI_x \frac{d^2v}{dz^2} + M_o = 0 \tag{4.1}$$

$$EI_y \frac{d^2u}{dz^2} + \gamma_t M_o = 0 \tag{4.2}$$

$$EC_w \frac{d^3\gamma_t}{dz^3} - (GJ + M_o\beta_x)\frac{d\gamma_t}{dz} + M_o \frac{du}{dz} = 0 \tag{4.3}$$

Eq. (4.1) involves only the vertical deflection v and is independent of the other two equations.

Eqs. (4.2) and (4.3) involve the lateral deflection u of the shear center and the angle of twist γ_t

and they are correlated and provide us with important information about the buckling behavior of

the beam. These two equations can be combined into a single equation and the solution to the

resulting equation is provided in Eq. (2.3) with β_x given in Eq. (2.4). While the process of

solving the differential equation of monosymmetric beams can be found in a number of articles

and textbooks, the presence of the β_x term in the differential equation (4.3) is seldom explained

and thus will be discussed next.
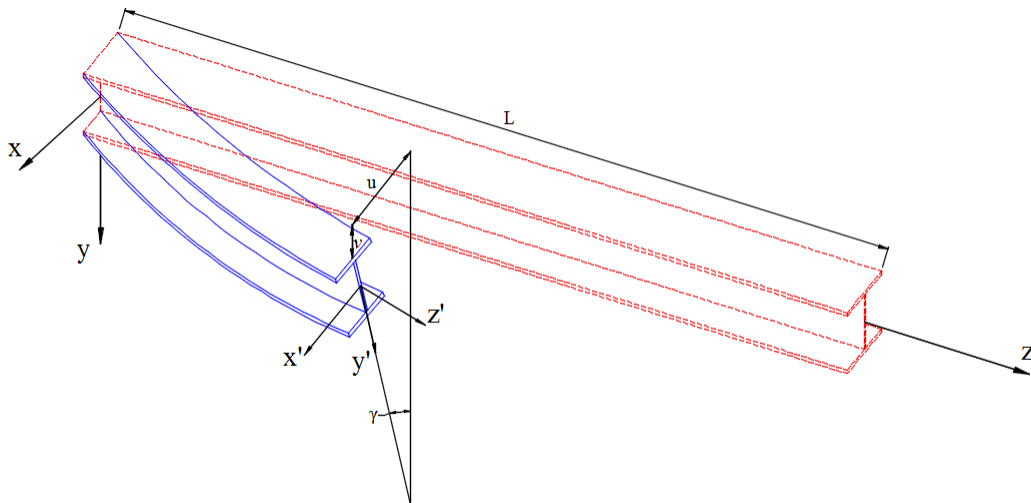
Figure 4.1 Oriented axis of a cross-section after deformation

After deformation of the beam occurs, the axes of the rotated and deflected cross-section are now represented by $x'y'z'$ as shown in Figure 4.1. The moment about the z' axis is a twisting moment which is the sum of two components

$$M_{z'} = M_{z_1'} + M_{z_2'} \tag{4.4}$$

where

$$M_{z_1'} = M_o \frac{du}{dz} \tag{4.5}$$

and $M_{z_2'}$ is caused by relative warping of two cross-sections dz' apart. Due to this warping, a stress element σdA is hence inclined with respect to the z' axis by an angle $a_\sigma \left(\frac{d\gamma_t}{dz'} \right)$, where σ is the stress anywhere in the cross-section and a_σ is the distance between the shear center and the point where σ acts. Thus, $\sigma dA \left(a_\sigma \frac{d\gamma_t}{dz'} \right)$ is the component of this stress element and it creates a twist about the shear center equal to

$$dM_{z_2'} = -a_\sigma (\sigma dA) \left(a_\sigma \frac{d\gamma_t}{dz'} \right) \tag{4.6}$$

Integrating Eq. (4.6) over the whole cross-section gives

$$M_{z_2'} = -\frac{d\gamma_t}{dz'} \int_A \sigma a^2 \, dA \tag{4.7}$$

By setting $\int_A \sigma a_\sigma^2 \, dA = K$ and noting that $dz' \cong dz$ when small displacements are assumed and higher order terms are neglected, we obtain

$$M_{z_2'} = -K \frac{d\gamma_t}{dz} \tag{4.8}$$
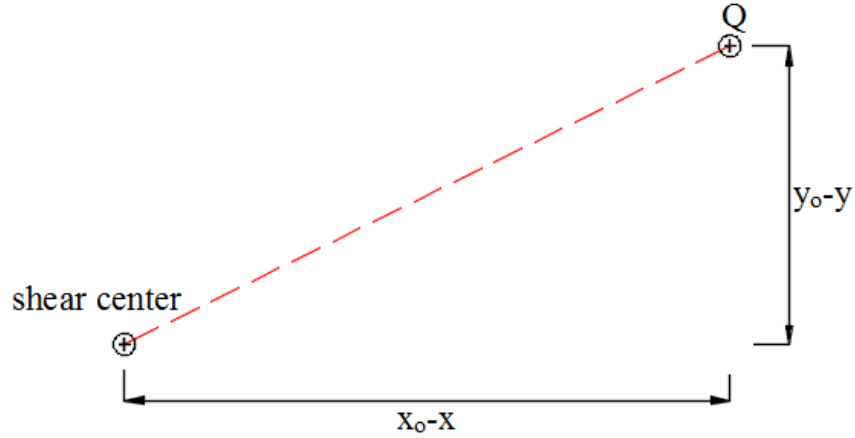
Figure 4.2 Displacement of a point Q in a cross-section

From Figure 4.2, the term a_σ can be expressed as

$$a_\sigma{}^2 = (x_o - x)^2 + (y_o - y)^2 \tag{4.9}$$

Expanding Eq. (4.9), we have

$$a_\sigma{}^2 = x_o^2 + x^2 - 2xx_o + y_o^2 + y^2 - 2yy_o \tag{4.10}$$

Using Eq. (4.10) and the general stress equation $\sigma = \frac{M_o y}{I_x}$, the term K can be expressed as

$$K = \frac{M_o}{I_x}\left(x_o^2 \int_A y \, dA + \int_A x^2 y \, dA - 2x_o \int_A xy \, dA + y_o^2 + y^2 - 2yy_o\right) \tag{4.11}$$

If we define a cross-section property β_x as

$$\beta_x = \frac{1}{I_x}\int_A y(x^2 + y^2) \, dA - 2e_y \tag{4.12}$$

and substitute Eq. (4.12) and the following relationships from elementary strength of materials to Eq. (4.11)

$$\int_A y \, dA = \int_A x \, dA = \int_A xy \, dA = 0 \tag{4.13}$$

$$\int_A dA = A; \quad \int_A x^2 \, dA = I_y; \quad \int_A y^2 \, dA = I_x \tag{4.14}$$

90

we obtain

$$K = M_o \beta_x \qquad\qquad (4.15)$$

and thus explains the presence of the coefficient of monosymmetry β_x in Eq. (4.3).

4.3   Description of the FE Model

4.3.1   Geometry and element type

A three-dimensional (3D) finite element model was developed to perform elastic eigenvalue

buckling analysis for prismatic Delta girders using the general purpose commercial finite

element software Abaqus version 6.14-2. Figure 4.3 depicts the 3D geometry of a typical Delta

girder model. All the girder's elements were modeled using shell elements. Shell elements are

typically used when one dimension, the thickness, is very small compared to the other two

dimensions and can be used for all types of cross-sections: compact, noncompact and slender

sections. The member web, flanges and delta stiffeners were each modeled using the

conventional S4R shell element which is defined as a 4-node general-purpose shell element with

reduced integration and finite membrane strains. A conventional shell element has six degrees of

freedom per node. A general-purpose shell element allows for shear deformation. It employs

thick shell theory as the shell thickness increases and discrete Kirchhoff thin shell elements as

the thickness decreases; thus, when the shell thickness decreases the transverse shear

deformation becomes insignificant. Reduced integration shell elements employ reduced

integration (lower-order) to form the element stiffness. However, the mass matrix and distributed

loadings are fully integrated. This technique reduces the simulation time significantly and

provides more accurate results as long as the elements are neither distorted nor loaded to cause

in-plane bending. Figure 4.4 illustrates the difference between a full and a reduced integration 4-node shell elements. S4R shell elements account for finite membrane strains and large rotations which make them appropriate for large-strain analysis (Simulia, 2014). This type of shell elements is widely used in finite element modeling of buckling problems of steel cross-sections.
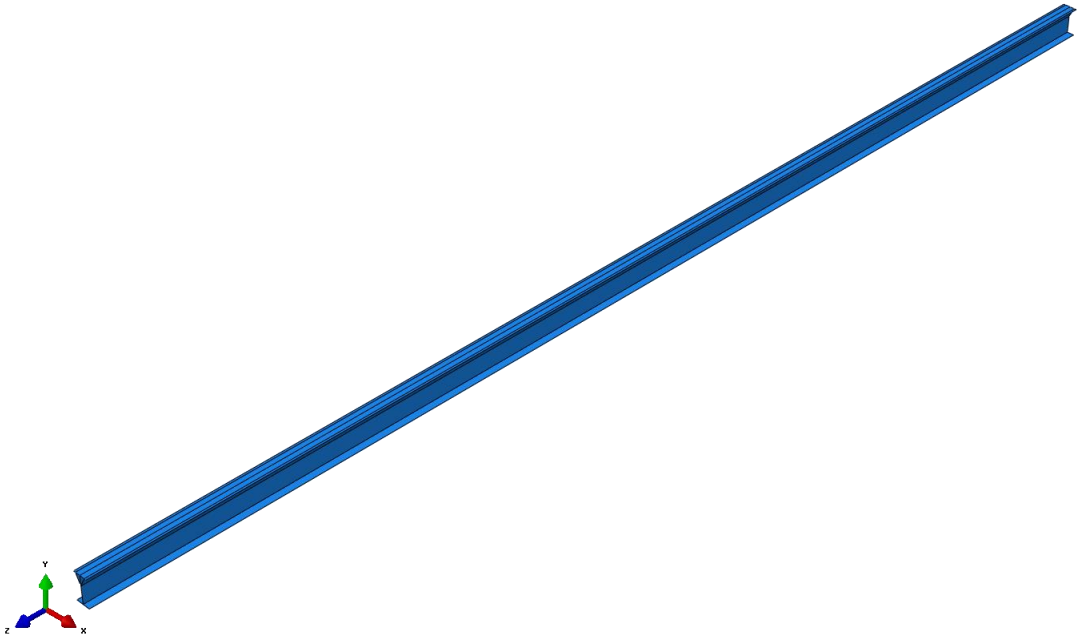
Figure 4.3 3D geometry of a typical SDG model
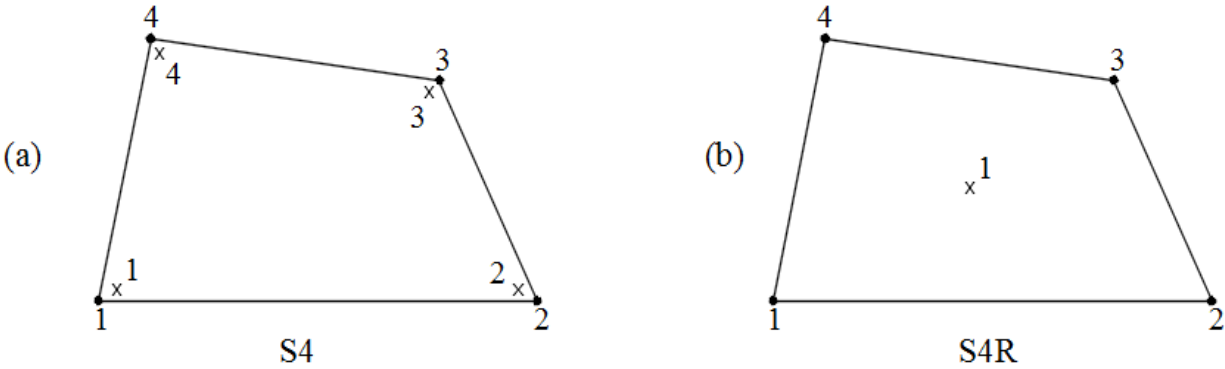
Figure 4.4 Full (a) and reduced (b) integration of a 4-node shell element

4.3.2 Mesh sizes and material properties

In the present analysis, steel is modeled as a linear elastic isotropic material with a modulus of elasticity of 200 GPa and a shear modulus of 75 GPa (i.e., $\nu = 0.333$). The mesh size in this type of elastic analysis does not have a significant effect on the run time or accuracy of the results. However, a convergence study was performed to reinforce the preceding statement. Three Delta girders, described in Section 4.3.5, were modeled using various mesh sizes and the theoretical critical buckling moment M_{cr} was compared to the FE solution. Tables 4.1, 4.2 and 4.3 provide the dimensions and number of elements used in the convergence study along with the calculated percentage of error.

Table 4.1 Convergence study of M_{cr} of Delta girder 6

Approximate global size of elements (cm)	Number of elements			Error (%)
	Flange (F)	Web (W)	Delta stiffener (S)	
1.5	14	35	9	5.3
2	10	26	7	4.5
2.5	8	21	6	4.5
3	8	18	5	4.3
3.5	6	15	4	4.6
4	6	14	4	4.5
4.5	6 (top) / 4 (bottom)	12	3	4.1
5	6 (top) / 4 (bottom)	10	3	4.1
5 (W&S), 1.5 (F)	14	10	3	4.0
5 (W&S), 2 (F)	10	10	3	3.5
5 (W&S), 3 (F)	8	10	3	3.7

Table 4.2 Convergence study of M_{cr} of Delta girder 11

Approximate global size of element (cm)	Number of elements			Error (%)
	Flange (F)	Web (W)	Delta stiffener (S)	
1.5	20	25	11	3.5
2	14 (top) / 16 (bottom)	18	8	3.3
2.5	12	14	6	3.3
3	10	13	5	3.7
3.5	8	11	5	3.9
4	8	9	4	3.8
4.5	8 (top) / 6 (bottom)	9	4	4.4
5	6	8	3	3.4
5 (W&S), 2 (F)	14 (top) / 16 (bottom)	8	3	3.0
5 (W&S), 3 (F)	10	8	3	3.5
5 (W), 2 (F&S)	14 (top) / 16 (bottom)	8	8	3.0

Table 4.3 Convergence study of M_{cr} of Delta girder 16

Approximate global size of element (cm)	Number of elements			Error (%)
	Flange (F)	Web (W)	Delta stiffener (S)	
1.5	20	38	15	5.2
2	14 (top) / 16 (bottom)	28	12	5.2
2.5	12	23	9	5.3
3	10	19	8	4.3
3.5	8	16	7	4.4
4	8	14	6	4.4
4.5	6	13	5	4.6
5	6	11	5	4.6
5 (W&S), 2 (F)	14 (top) / 16 (bottom)	11	5	4.7
5 (W&S), 3 (F)	10	11	5	4.1
5 (W), 2 (F&S)	14 (top) / 16 (bottom)	11	12	4.8

The convergence study performed herein has shown that the FE solution has converged and that the percent error between a coarse and fine mesh is less than 1.5%. Based on the results, an approximate element size of 5 cm was found to be sufficient to model the Delta girders and to provide accurate results without consuming large disk space and long run time. Both flanges, the web and the delta stiffeners will consequently have different number of elements depending on their relative dimensions. The longitudinal aspect ratio of the shell elements was set to 1.0. Figure 4.5 depicts the mesh of girder 16 where the flanges were modeled using 6 elements each, the delta stiffeners using 5 elements and the web using 11 elements. This 24-m long girder was modeled using a total of 15,840 linear quadrilateral S4R shell elements.
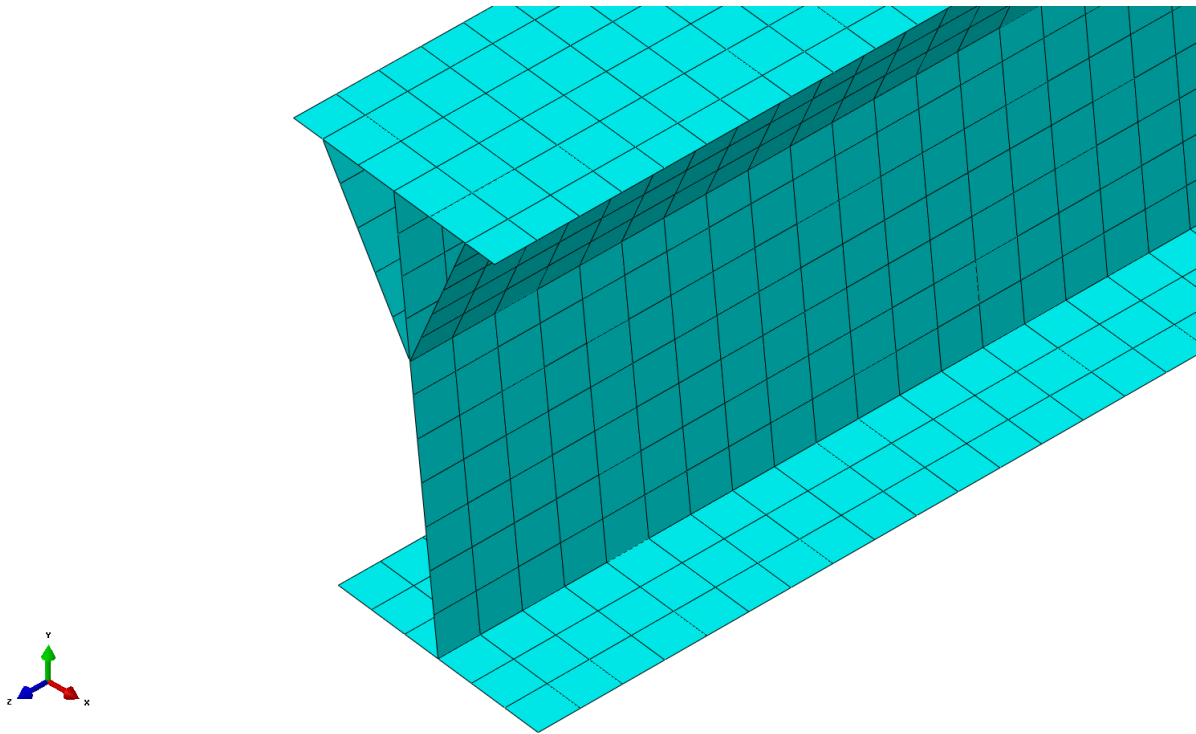
Figure 4.5 Mesh of Delta girder 16

4.3.3 Loads and boundary conditions

The loads and boundary conditions applied to the finite element model must match those of the theoretical solution in order to obtain accurate results. Applying concentrated moments directly at the girder ends results in stress concentration and local buckling problems. These problems are frequently encountered when concentrated forces or moments are applied directly to the nodes of shell elements. To avoid these problems, equal and opposite concentrated moments are applied to reference points located at a distance from the girder ends. A surface-based kinematic coupling is used to couple the motion of the reference points to the entire cross-section at the ends of the girder as illustrated in Figure 4.6. The coupling nodes on the surface will be automatically selected. Note that only the rotational degrees of freedom need to be constrained due to the nature of the applied load. This technique of load application allows the moment to be correctly applied to the cross-section at the supports.
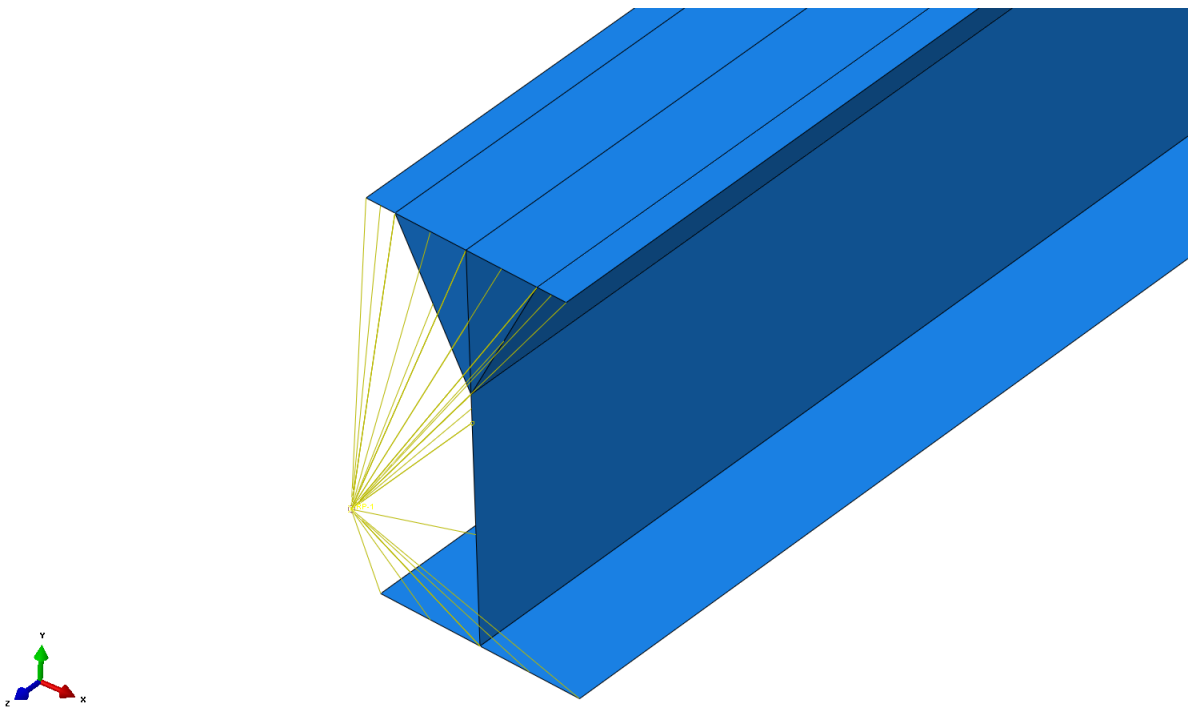
Figure 4.6 Technique used to apply a concentrated moment

Simply-supported boundary conditions are modeled by restraining the nodes at the centroid location at the ends of the girder. At one end, the three translational degrees of freedom are restrained as well as the rotational degree of freedom around the longitudinal axis. At the other end, the same restraints are applied except for the longitudinal translational degree of freedom. The theoretical solution assumes the ends to be torsionally simply-supported or what is known as the fork boundary condition, i.e., the girder ends are free to warp. To simulate this boundary condition in the finite element model, the four corners of the two flanges at each end are constrained against out-of-plane translation. Figure 4.7 depicts the boundary conditions at one of the ends.
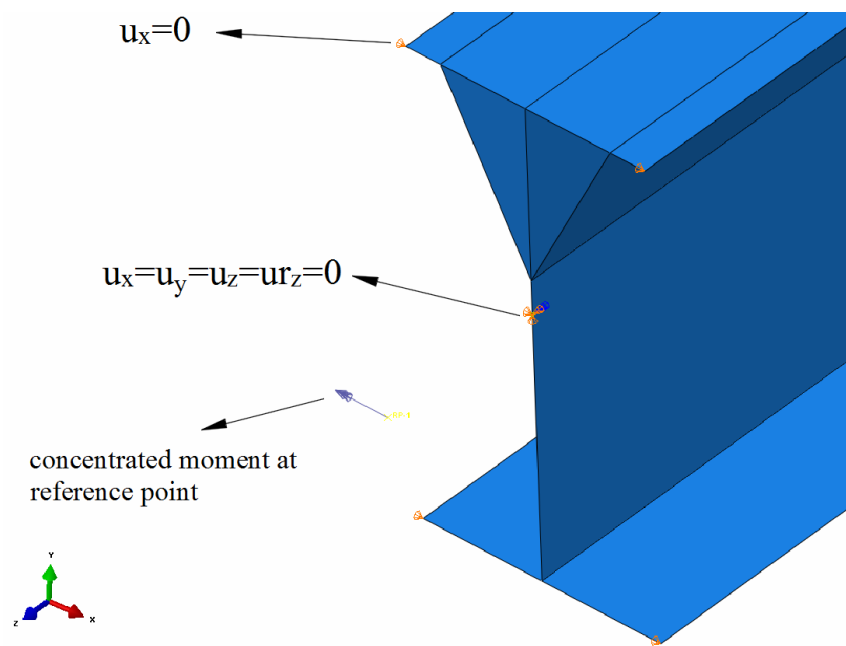
Figure 4.7 Boundary conditions

4.3.4   Analysis procedure

Two main analysis procedures or steps are available in Abaqus and in most general-purpose finite element software: general analysis procedure and linear perturbation procedure. While a general analysis step can be used to analyze both linear and nonlinear responses, the linear perturbation step considers linear problems exclusively. To determine the elastic critical buckling load of Delta girders, an eigenvalue buckling analysis is utilized. This type of analysis is a linear perturbation procedure. In an eigenvalue buckling problem, the buckling load is determined when the modal stiffness matrix becomes singular so that Eq. (4.16) has non trivial solutions (Simulia, 2014)

$$K^{MN} v^M = 0 \tag{4.16}$$

where K^{MN} is the tangent stiffness matrix when the loads are applied and v^M are the nontrivial displacement solutions.

An eigenvalue buckling analysis also predicts the buckling mode shapes (eigenvectors). For the Delta girder problem, the second buckling mode is desired since the first one corresponds to a negative eigenvalue as can be predicted by inspecting the theoretical solution in Eq. (2.3).

4.3.5   Model and theoretical solution verifications

To verify the FE results, 16 cross-sections were created and modeled using Abaqus and their elastic critical buckling moments were compared with their respective theoretical solutions obtained from Eq. (2.3). These cross-sections are selected to cover a range of extreme practical configurations of the girder dimensions and the delta stiffener configurations. The girder dimensions are based on the following standard European steel H- and I-sections: IPE 360, IPE

550, HEA 400 and HEA 600. For each of these sections, four extreme practical configurations of delta stiffeners are added using the same technique described in Section 3.4.3 and Table 3.10. The full dimensions of the resulting 16 Delta girders are provided in Table 4.4.

Table 4.4 Dimensions of Delta girders

Section	b_f(mm)	b_d(mm)	d(mm)	h_d(mm)	w_d(mm)	t_f(mm)	t_w(mm)	t_d(mm)
1	170	85	360	66.92	68.0	12.7	8	8
2	170	113.3	360	66.92	76.9	12.7	8	8
3	170	85	360	111.5	105.0	12.7	8	8
4	170	113.3	360	111.5	113.0	12.7	8	8
5	210	105	550	103.1	97.4	17.2	11	12
6	210	140	550	103.1	108.3	17.2	11	12
7	210	105	550	171.9	154.6	17.2	11	12
8	210	140	550	171.9	165.3	17.2	11	12
9	300	150	390	70.4	86.9	19	11	12
10	300	200	390	70.4	105.3	19	11	12
11	300	150	390	117.3	122.7	19	11	12
12	300	200	390	117.3	138.4	19	11	12
13	300	150	590	108	112.4	25	13	14
14	300	200	590	108	128.7	25	13	14
15	300	150	590	180	171.5	25	13	14
16	300	200	590	180	185.7	25	13	14

The buckling mode of one of the Delta girders is depicted in Figure 4.8. Table 4.5 presents a comparison between the theoretical and the numerical elastic critical buckling moments of the 16 Delta girders under investigation. L_r, the limiting laterally unbraced length for the limit state of inelastic lateral-torsional buckling, was computed using Eq. (2.17). L_b, the

lateral unbraced length of the compression flange, was selected to be larger than L_r. The theoretical buckling moment was obtained using Eq. (2.3). The results show that the FE model is capable of predicting the buckling moment with an average error of 4.3% with respect to the theoretical solution. The range of error is 0.8% to 8.0%.

Table 4.5 Comparison between theoretical and numerical buckling moments

Section	L_r (m)	L_b (m)	$M_{cr,theo}$ (kN-m)	$M_{cr,Num}$ (kN-m)	Error (%)
1	7.8	13.0	152.7	146.6	4.1%
2	9.3	13.0	187.4	179.0	4.5%
3	10.0	13.0	204.2	192.0	6.0%
4	12.5	13.0	260.4	244.8	6.0%
5	8.7	15.0	414.8	394.3	4.9%
6	10.5	15.0	516.0	494.9	4.1%
7	11.1	15.0	558.3	516.5	7.5%
8	14.1	15.0	722.0	663.9	8.0%
9	17.7	29.0	389.1	381.3	2.0%
10	20.4	29.0	463.9	460.8	0.7%
11	23.5	29.0	523.6	505.9	3.4%
12	28.5	29.0	646.7	635.4	1.8%
13	14.8	24.0	827.3	802.1	3.0%
14	17.6	24.0	1003.8	978.6	2.5%
15	18.8	24.0	1087.0	1031.1	5.1%
16	23.3	24.0	1372.1	1308.9	4.6%

Undeformed shape
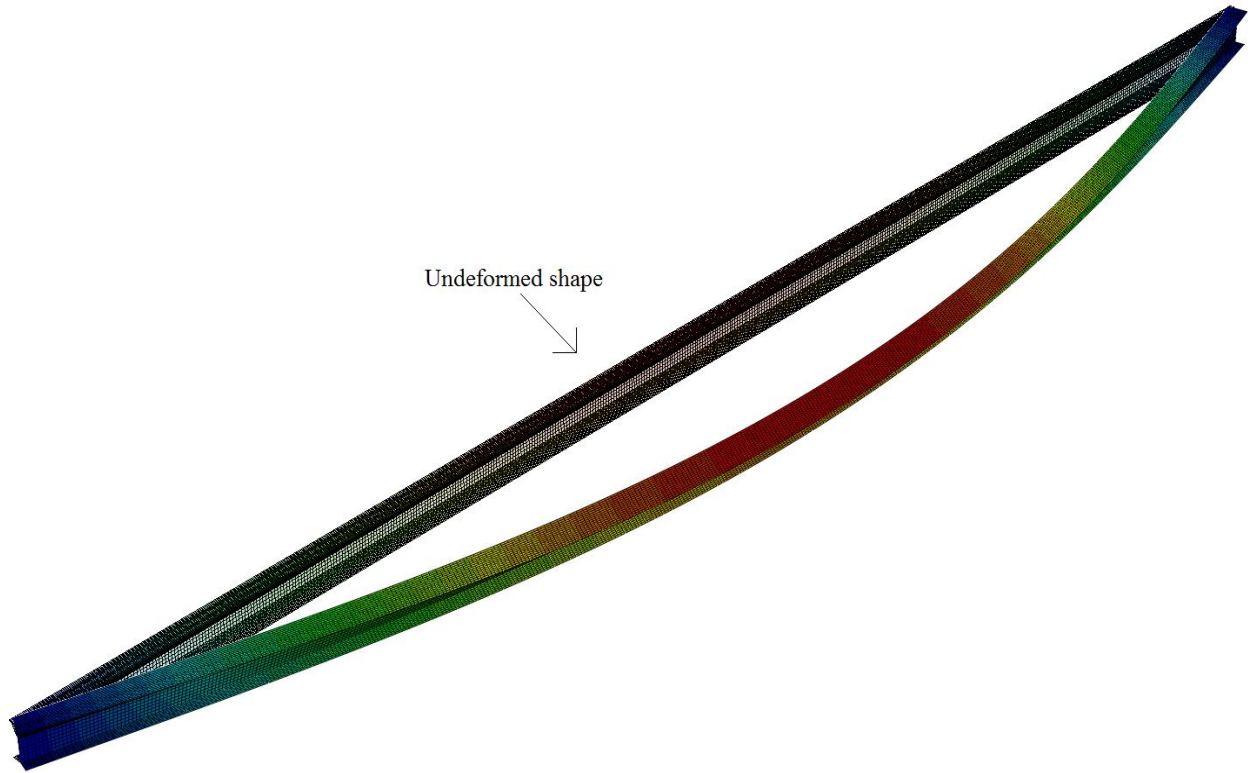
Figure 4.8 Lateral-torsional buckling of a Delta girder

4.4   Sensitivity Study of the Elastic LTB of Delta Girders

4.4.1   The coefficient of monosymmetry β_x

The first step to determine the critical buckling moments of Delta girders is the calculation of

their cross-section properties. The equations for these properties are summarized in Section 3.5.

Of the various terms in these equations, the only term that remains to be investigated is the

coefficient of monosymmetry β_x, which is given in Eq. (2.5) as an approximation for I-sections,

while the general form is provided in Eq. (2.4). The accuracy of utilizing Eq. (2.5) for Delta

girders is examined through computing the critical buckling moments for the 25 Delta girders

listed in Table 3.11 using Eq. (2.3). The analytical cross-section properties from Table 3.12 were

101

used. The addition of the delta stiffeners makes the closed-form solution for β_x very lengthy and thus the integral was evaluated numerically. Table 4.6 provides the values of β_x using both techniques as well as the percent error as a result of using Eq. (2.5). Note that the moment of inertia of the delta stiffeners about the weak axis was added to the I_{yc} term in Eq. (2.5). The critical buckling moment, under uniform bending and simply-supported conditions, was then obtained and compared for the two values of β_x. The following dimensions and material properties were used in the computations:

$$L_{b,Set\ A} = 18.288 \text{ m}, \qquad L_{b,Set\ B} = 12.0 \text{ m}, \qquad E = 200 \text{ GPa}, \qquad G = 75 \text{ GPa}$$

The comparison between the values of the monosymmetry coefficient β_x, provided in Table 4.6, shows that the approximate equation given in Eq. (2.5) for I-shaped members can result in large errors. Because the errors for Set B are much larger than those for Set A, this indicates that β_x is sensitive to cross-section dimensions. However, the error in β_x does not appear to have a noticeable effect on the critical buckling moment. Although the errors for β_x range from -2.3 % to 107.9%, the errors for M_{cr} range only from -0.3 % to 1.5 %. Thus, the approximate equation for β_x given by Eq. (2.5) can be used to determine the critical buckling moments of Delta girders with a relative high degree of accuracy, provided that the I_{yc} term is appropriately accounted for in this equation.

Table 4.6 Comparison between the exact and the approximate solutions for Delta girders

Set	Section	$\beta_{x,Exact}$(mm)	$\beta_{x,Approx}$(mm)	Error	$M_{cr,Exact}$ (kN-m)	$M_{cr,Approx}$ (kN-m)	Error
A	1	252.02	270.97	7.52%	4016	4044	0.7%
	2	241.10	249.58	3.52%	3189	3201	0.4%
	3	260.21	282.58	8.60%	3844	3878	0.9%
	4	253.99	264.09	3.98%	4247	4262	0.3%
	5	269.71	302.88	12.30%	5355	5406	0.9%
	6	236.50	231.92	-1.94%	2589	2582	-0.3%
	7	246.58	249.94	1.36%	3024	3029	0.2%
	8	245.36	239.71	-2.30%	3274	3266	-0.2%
	9	254.67	261.55	2.70%	4020	4030	0.2%
	10	246.72	266.24	7.91%	3621	3649	0.8%
	11	273.69	311.74	13.90%	4445	4506	1.4%
	12	260.29	286.54	10.09%	4971	5009	0.8%
	13	280.90	338.56	20.53%	6363	6456	1.5%
B	14	15.33	29.39	91.73%	699	704	0.8%
	15	33.54	54.38	62.14%	862	871	1.0%
	16	60.60	43.33	41.60%	938	943	0.6%
	17	51.47	74.58	44.89%	1205	1215	0.9%
	18	18.63	38.73	107.89%	788	797	1.1%
	19	41.59	70.35	69.16%	978	991	1.3%
	20	36.11	56.77	57.21%	1079	1088	0.8%
	21	61.18	95.50	56.09%	1393	1409	1.2%
	22	25.50	47.45	86.09%	843	852	1.1%
	23	53.04	84.96	60.18%	1056	1071	1.4%
	24	44.89	68.72	53.09%	1175	1185	0.9%
	25	73.53	113.72	54.66%	1530	1550	1.3%

4.4.2   Elastic LTB comparison between I-girders and Delta girders

The elastic critical buckling moment is now computed for the same 25 cross-sections without the delta stiffeners. This reduces Set A to a single cross-section and Set B to two cross-sections with two different web thicknesses. Note that the cross-sections of Set B become doubly symmetric without the inclined stiffeners and thus β_x vanishes. The results are shown in Table 4.7 where it can be seen that Eq. (2.5) produces an 8.9% error for the monosymmetric I-shaped section of Set A. This error leads to a 2.1% error (conservative) in the computation of the LTB moment, which is larger than the error obtained for the LTB of Delta girders.

Table 4.7 Comparison between the exact and the approximate solutions for I-girders

Set	Section	$\beta_{x,Exact}$(mm)	$\beta_{x,Approx}$(mm)	Error	$M_{cr,Exact}$ (kN-m)	$M_{cr,Approx}$ (kN-m)	Error
A	1-13	233.87	213.15	-8.9%	1541	1508	-2.1%
B	14-17 22-25	0	-	-	268	-	-
	18-21	0	-	-	278	-	-

To better understand the effects of the delta stiffeners on the elastic lateral-torsional buckling capacity of slender beams, the critical buckling moments of the 25 I-girders and Delta girders are compared in Table 4.8. The table also includes a comparison of cross-section areas. In the table, A^* and M_{cr}^* are defined as follows

$$A^* = \frac{A_D - A_I}{A_I} \times 100\% \tag{4.17}$$

$$M_{cr}^* = \frac{M_{crD} - M_{crI}}{M_{crI}} \times 100\% \tag{4.18}$$

Table 4.8 Comparison between the buckling moment of Delta girders and I-girders

	I-Girder vs. Delta Girder					
Section	A_I (mm^2)	A_D (mm^2)	A^*	M_{crI} (kN-m)	M_{crD} (kN-m)	M_{cr}^*
1	23871	27524	15.3%	1541	4016	160.6%
2	23871	26869	12.6%	1541	3189	107.0%
3	23871	27313	14.4%	1541	3844	149.5%
4	23871	28181	18.1%	1541	4247	175.6%
5	23871	28501	19.4%	1541	5355	247.1%
6	23871	25370	6.3%	1541	2589	68.0%
7	23871	25592	7.2%	1541	3024	96.3%
8	23871	26026	9.0%	1541	3274	112.4%
9	23871	26186	9.7%	1541	4020	160.9%
10	23871	28368	18.8%	1541	3621	135.0%
11	23871	29034	21.6%	1541	4445	188.5%
12	23871	30336	27.1%	1541	4971	222.6%
13	23871	30816	29.1%	1541	6363	312.9%
14	11808	13432	13.8%	268	699	160.7%
15	11808	13608	15.2%	268	862	221.2%
16	11808	14264	20.8%	268	938	249.5%
17	11808	14384	21.8%	268	1205	349.1%
18	12960	15117	16.6%	278	788	183.8%
19	12960	15349	18.4%	278	978	251.9%
20	12960	16230	25.2%	278	1079	288.4%
21	12960	16387	26.5%	278	1393	401.3%
22	11808	14514	22.2%	268	843	214.2%
23	11808	14807	25.4%	268	1056	293.6%
24	11808	15902	34.7%	268	1175	337.9%
25	11808	16101	36.4%	268	1530	470.1%

Where A_D, A_I, M_{crD} and M_{crI} are the cross-section areas and LTB moment capacities of the

Delta and I-girders, respectively. Eqs. (4.17) and (4.18) represent the percent increase in cross-

section area and LTB capacity. From Table 4.8, it can be seen that the increase in LTB capacity

ranges from 68% to an impressive 470% with an average of 222%. This improvement in the

LTB strength is associated with a cross-sectional area (or weight) increase from 6% to 36% with

an average of 19%. Thus, the effect of the delta stiffeners on the critical buckling moment is

quite noticeable.

4.4.3   Comparison with an alternative solution

Zhao and Tonias (2012) have suggested that increasing the thickness of the web is a practical,

simple, and economical way to increase the lateral stiffness of I-girders that span less than 61

meters. Thus, the beneficial effect of the Delta girders needs to be validated against this

alternative solution. The thickness of the webs of the I-girders of Section 4.4.2 was increased

until the cross-sectional areas were approximately equal to those of the Delta girders. The web

thickness increments take into consideration the actual available increments in the market, which

are 3.175 mm (1/8 in.) for Set A (US market) and 2 mm for Set B (European market). The

comparison of the cross-section areas and the exact elastic critical buckling moments are given in

Table 4.9. In the table, A_{MI} and M_{crMI} denote the cross-section area and LTB moment capacity

of the modified I-girder, and A^* and $M_{cr}{}^*$ are computed using Eqs. (4.17) and (4.18) with A_I and

M_{crI} replaced by A_{MI} and M_{crMI}, respectively. The increase in LTB capacity of the Delta girders

(M_{crD}) when compared to the modified I-girders (M_{crMI}) ranges from 66% to 359% with an

average of 196%. These results demonstrate the effectiveness of the Delta girders in enhancing

the LTB capacity against the commonly used practice of increasing the web thickness.

A comparison between the critical buckling moments of the I-girders and the modified I-girders shows that increasing the web thickness has little effect on increasing the LTB capacity of the girders. The range of increase in LTB capacity is from 1% to 24% and in cross-section area is from 12% to 39%. However, it should be noted that increasing the web thickness decreases the web slenderness and hence help with increasing the shear resistance as well as the web yielding and web crippling strengths of the cross-section.

Table 4.9 Comparison with an alternative solution

Section	A_{MI} (mm^2)	A_D (mm^2)	A^*	M_{crMI} (kN-m)	M_{crD} (kN-m)	M_{cr}^*
			Modified I-Girder vs. Delta Girder			
1	26774	27524	2.8%	1559	4016	157.6%
2	26774	26869	0.4%	1559	3189	104.6%
3	26774	27313	2.0%	1559	3844	146.6%
4	26774	28181	5.3%	1559	4247	172.4%
5	26774	28501	6.5%	1559	5355	243.5%
6	26774	25370	-5.2%	1559	2589	66.1%
7	26774	25592	-4.4%	1559	3024	94.0%
8	26774	26026	-2.8%	1559	3274	110.0%
9	26774	26186	-2.2%	1559	4020	157.8%
10	29677	28368	-4.4%	1565	3621	131.4%
11	29677	29034	-2.2%	1565	4445	184.0%
12	29677	30336	2.2%	1565	4971	217.6%
13	29677	30816	3.8%	1565	6363	306.6%
14	14112	13432	-4.8%	292	699	139.3%
15	14112	13608	-3.6%	292	862	195.1%
16	14112	14265	1.1%	292	938	221.1%
17	14112	14384	1.9%	292	1205	312.6%
18	15264	15117	-1.0%	310	788	154.3%
19	15264	15349	0.6%	310	978	215.4%
20	16416	16230	-1.1%	333	1079	224.1%
21	16416	16388	-0.2%	333	1393	318.2%
22	15264	14514	-4.9%	310	843	171.9%
23	15264	14807	-3.0%	310	1056	240.6%
24	16416	15902	-3.1%	333	1175	252.8%
25	16416	16101	-1.9%	333	1530	359.3%

4.5   Parametric Study

The previous section provided an initial overview of the LTB capacity of Delta girders. However, the parameters affecting the strength of Delta girders have not been systematically examined. In this section, a parametric study is conducted to gain a better understanding of the LTB behavior of prismatic Delta girders. The elastic LTB capacities under uniform bending and simply-supported boundary conditions are calculated using Eqs. (2.3) and (2.5). For each Delta girder, a corresponding I-section is created for the purpose of comparing their LTB capacities. The study includes the following key design parameters:

1) A clear web depth h of 40, 60, 80 and 100 cm

2) Variable flange width ratio with a doubly symmetric initial I-section where $b_c = b_t$ and a monosymmetric initial I-section where $b_c = 1.5\ b_t$

3) Variable delta stiffener depths of $h_d = h/5, h/4, h/3\ and\ 2h/5$

4) Variable delta stiffener widths of $b_d = 2b_c/5, b_c/2, 2b_c/3\ and\ 3b_c/4$

5) Variable delta stiffener thicknesses of $t_d = t_w\ and\ t_W + 2$ mm

6) Variable Delta girder lengths of $L_b = L_r\ and\ 1.2\ L_r$.

The following assumptions and parameters are included in the study:

- The section aspect ratio h/b_c is kept below the suggested limit of 7 as recommended by the AISC (2016a)

- The web slenderness ratio h/t_w is selected to provide a compact web for all I-sections, i.e., $h/t_w \leq 3.76\sqrt{E/F_y}$

- The flange thickness ratio t_c/t_t is equal to 1 for all girders

- The length of the Delta girders L_b is equal to L_r, the limiting laterally unbraced length for the limit states of inelastic LTB, which is calculated using Eq. (2.17)

- The length of each I-section L_b is set to the length of its corresponding Delta girder for a meaningful comparison, and because L_r of a Delta girder is larger than L_r of its corresponding I-section

- The modulus of elasticity and the yield strength of steel are 200 GPa and 345 MPa, respectively

- The thickness of the delta stiffeners is at least equal to the web thickness to avoid the possibility of local buckling

- The cross-section dimensions associated with each web depth h are provided in Table 4.10.

Table 4.10 Selected main dimensions for the parametric study

			Case 1	Case 2	
h (cm)	t_W (cm)	t_f (cm)	b_f (cm)	b_c (cm)	b_t (cm)
40	0.6	1.2	18	27	18
60	0.8	1.2	22	33	22
80	1.0	1.4	28	42	28
100	1.2	1.4	32	48	32

After generating a comprehensive set of possible configurations from the previously listed cross-sectional parameters, 1,024 girders were created and equally divided between Delta girders and I-girders. The percent increase in elastic LTB capacity M_{cr} after adding the delta stiffeners to an I-section was then computed. However, a comparison of the increase in buckling capacity alone is not a sufficient indicator of the effectiveness of the delta stiffeners as different

configurations yield different cross-section areas and hence higher material cost and an increase

self-weight. For this reason, a term "κ" is introduced. This term represents the ratio of the

percent increase in buckling moment capacity $M_{cr}{}^{*}$ to the percent increase of cross-section area

A^{*} when delta stiffeners are added to the I-section. In other words, a κ value of 10 means that a 1

% increase in cross-section weight (cost) is associated with a 10% increase in LTB capacity of

the cross-section. This term κ will thus be used to examine the various parameters under

investigation. From this parametric study, a number of key observations can be made on the LTB

behavior of Delta girders as follows:

a) Overall observation: By comparing the 512 Delta girders with the corresponding I-

   girders, the maximum increase in LTB capacity is 1294.2% with a 52.6% increase in the

   cross-section area and a κ value of 24.6. The highest value of κ obtained is 25.5, which

   corresponds to a 1152.5% increase in LTB capacity and a 45.1% increase in cross-section

   area. The average increase in LTB capacity is 422.5% while the average κ value obtained

   is 12.6. The average, maximum and minimum values of this study are provided in Table

   4.11. Note that the values in each column are independent of the others, i.e., the

   maximum values of κ and $M_{cr}{}^{*}$ for instance do not necessarily correspond to the same

   cross-section.

Table 4.11 Summary of the parametric study results

	A^{*}	$M_{cr}{}^{*}$	κ
Average	32.6%	422.5%	12.6
Maximum	55.6%	1294.2%	25.5
Minimum	9.6%	78.3%	4.6

b) Cross-section effects: It can be seen from Table 4.12 that the maximum value of κ increased by 18% from $h = 40$ cm to $h = 100$ cm while the average value of κ obtained is within 4%. The maximum percent increase in LTB capacity becomes more pronounced as the cross-section size increases (an increase of 542% from $h = 40$ cm to $h = 100$ cm), but this occurs with an increase in cross-section area. Figure 4.9 compares the percent increase in critical moment for each value of h. It can be concluded that delta stiffeners are slightly more effective for larger cross-sections.

Table 4.12 Effects of cross-section dimensions on M_{cr}^{*} and κ

	$h = 40$ cm		$h = 60$ cm		$h = 80$ cm		$h = 100$ cm	
	M_{cr}^{*}	κ	M_{cr}^{*}	κ	M_{cr}^{*}	κ	M_{cr}^{*}	κ
Average	326.9%	12.2	423.7%	12.6	445.6%	12.8	493.8%	12.7
Maximum	752.7%	21.6	1046.8%	23.8	1121.2%	24.7	1294.2%	25.5
Minimum	78.3%	5.9	107.6%	5.1	125.4%	4.9	112.9%	4.6
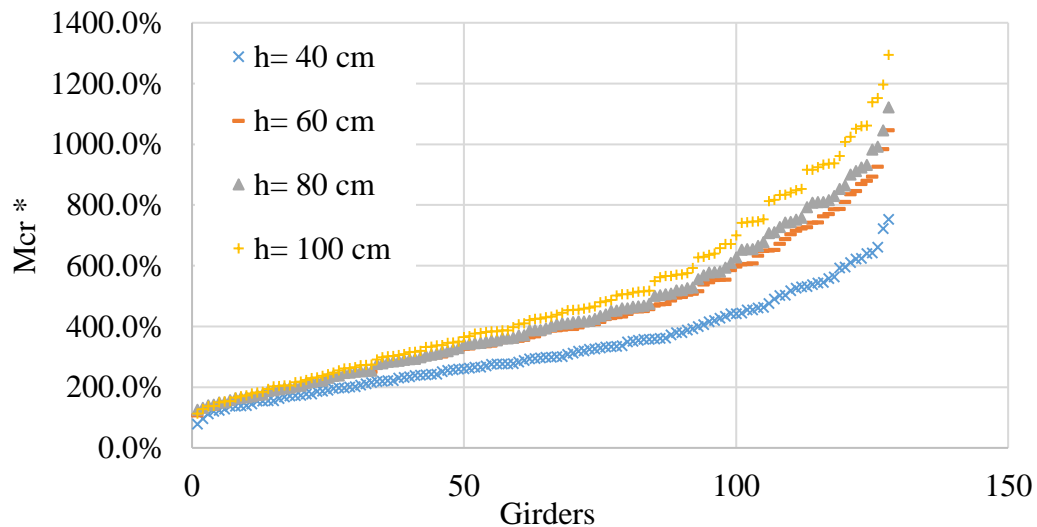
Figure 4.9 Comparison of critical moment increase (ascending order) for h

112

c) Length effect: It can be seen from Table 4.13 and Figure 4.10 that adding the delta stiffeners provides a slight advantage when the girder becomes longer. The maximum and average values of both M_{cr}^* and κ are under 10% for both cases. On the other hand, it is interesting to note that for one section ($h = 40$ cm, $b_C = b_t$, $h_d = h/5$, $b_d = 2b_c/5$ and $t_d = t_w$) the percent increase in the LTB capacity decreases when the length of the girder increases.

Table 4.13 Effects of girder length on M_{cr}^* and κ

	$L_b = L_r$		$L_b = 1.2\,L_r$	
	M_{cr}^*	κ	M_{cr}^*	κ
Average	401.9%	11.9	443.0%	13.2
Maximum	1196.9%	23.5	1294.2%	25.5
Minimum	96.5%	4.6	78.3%	5.5
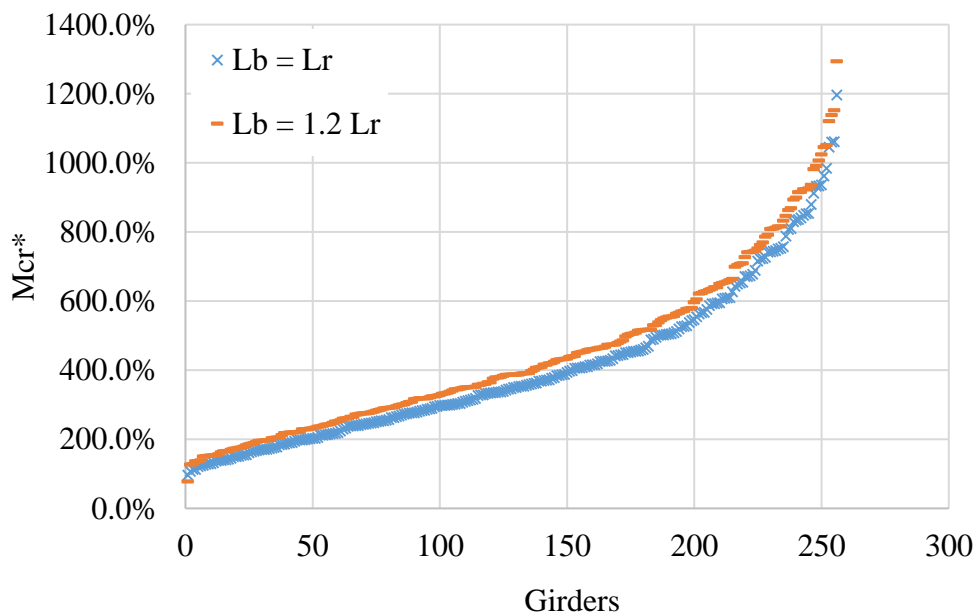
Figure 4.10 Comparison of critical moment increase (ascending order) for L_b

113

d) Compression flange size effect: The difference in the compression flange width with respect to the tension flange width is used to study the effects of adding delta stiffeners to initially doubly symmetric or monosymmetric I-sections. The results show that increasing the value of b_c by 50% increases the average value of κ by 17% and the maximum value by 20%. The average and maximum percent increase in M_{cr} are increased by 12% and 14% respectively. These results are illustrated in Table 4.14 and Figure 4.11. This demonstrates that the delta stiffeners provide better results when they are added to monosymmetric I-sections.

Table 4.14 Effects of the compression flange size on $M_{cr}{}^*$ and κ

	$b_c = b_t$		$b_c = 1.5\, b_t$	
	$M_{cr}{}^*$	κ	$M_{cr}{}^*$	κ
Average	397.3%	11.6	443.0%	13.6
Maximum	1138.6%	21.2	1294.2%	25.5
Minimum	78.3%	4.6	78.3%	5.8
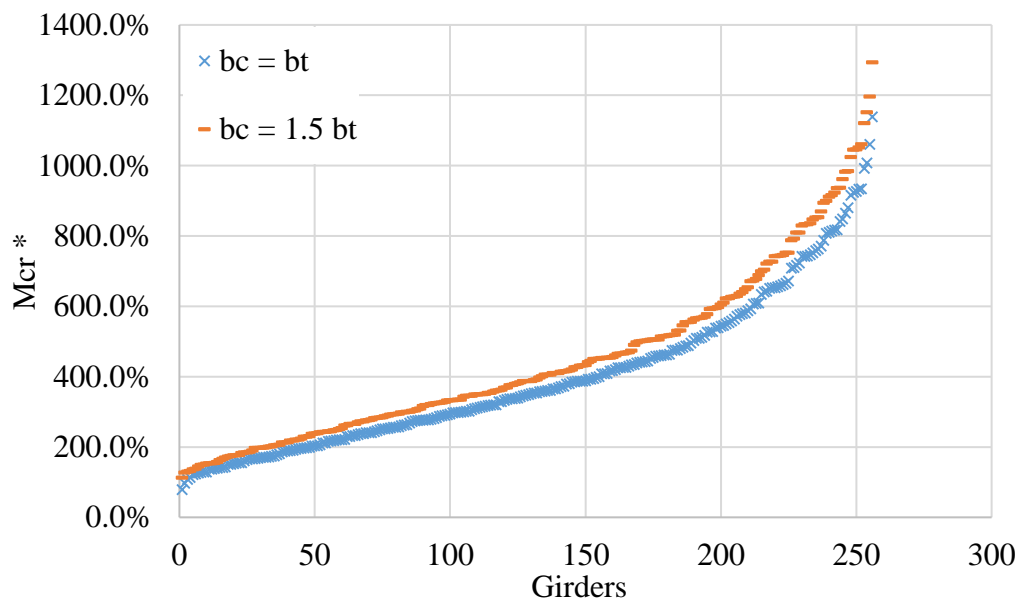
Figure 4.11 Comparison of critical moment increase (ascending order) for b_c

e) Delta stiffener thickness effect: Table 4.15 and Figure 4.12 show that the percent increase of M_{cr} is more pronounced when the thickness of the stiffeners increases. However, the maximum, minimum and average values of κ decrease. Therefore, increasing the stiffener thickness is not an effective method to increase the LTB capacity of the section and changing the stiffener configurations may be more desirable. Note that decreasing the stiffener thickness below the web was not attempted in this parametric study to avoid possible problems with local buckling.

Table 4.15 Effects of the delta stiffeners thickness on $M_{cr}{}^{*}$ and κ

	$t_d = t_w$		$t_d = t_W + 2$ mm	
	$M_{cr}{}^{*}$	κ	$M_{cr}{}^{*}$	κ
Average	391.5%	13.0	453.5%	12.2
Maximum	1152.5%	25.5	1294.2%	24.6
Minimum	78.3%	4.7	121.0%	4.6
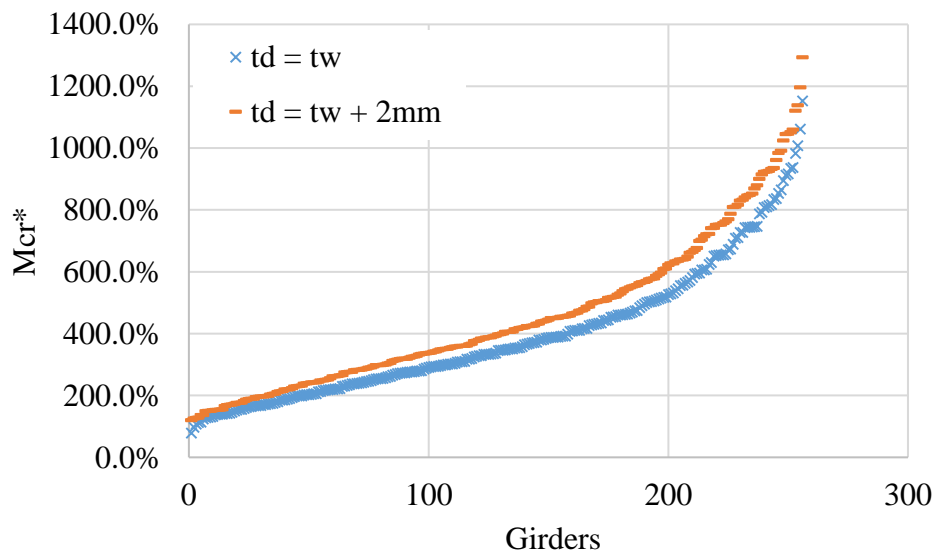
Figure 4.12 Comparison of critical moment increase (ascending order) for t_d

115

f) Effect of the stiffener configuration: The last parameter to be investigated is the positioning (configuration) of the delta stiffeners. This was also done through a comparison of the κ value for all girder combinations. The results are presented in Table 4.16 which show that for the range of girders used in the present study, the combination of $h_d = \frac{2h}{5}$ and $b_d = \frac{3b_c}{4}$ gives the best result with an average κ value of 20.5 and average percent increase in M_{cr} of 896%. The combination that provides the second best result is $h_d = \frac{h}{3}$ and $b_d = \frac{3b_c}{4}$ with an average κ value of 19.3. It can also be deducted from the results that, in general, the larger values of h_d and b_d, the better the results due to the larger size of the closed delta section. Another important observation from the current analysis is the effect of b_d on the results. It can be seen from Table 4.16 that b_d of $\frac{2b_c}{5}$ and $\frac{b_c}{2}$ provide a maximum κ value of 11 for all h_d values. On the other hand, b_d of $\frac{2b_c}{3}$ and $\frac{3b_c}{4}$ provide an average κ value between 12.8 and 20.5 for all h_d values. Thus, the general conclusion is that for delta stiffeners design, the value of b_d is as important as the value of h_d in determining the LTB capacity of Delta girders.

On a final note, it is important to state that the delta stiffener configurations comparison presented herein is only concerned with the increase in the elastic LTB capacity. In an actual design, other limit states such as compression or tension flange yielding could very well control the design. Thus, the designer should select the configuration that provides the most optimum design. Additional recommendations in this regard are provided in Chapter 6.

Table 4.16 Effects of the delta stiffeners configuration on $M_{cr}{}^{*}$ and κ

	$h_d = \dfrac{h}{5}; b_d = \dfrac{2b_c}{5}$		$h_d = \dfrac{h}{5}; b_d = \dfrac{b_c}{2}$		$h_d = \dfrac{h}{5}; b_d = \dfrac{2b_c}{3}$		$h_d = \dfrac{h}{5}; b_d = \dfrac{3b_c}{4}$	
	$M_{cr}{}^{*}$	κ	$M_{cr}{}^{*}$	κ	$M_{cr}{}^{*}$	κ	$M_{cr}{}^{*}$	κ
Average	139.6%	6.5	198.8%	8.8	317.3%	12.8	385.1%	14.8
Maximum	183.3%	8.8	261.9%	10.9	421.0%	14.7	515.4%	17.0
Minimum	78.3%	4.6	138.6%	6.8	216.0%	11.2	257.1%	12.6
	$h_d = \dfrac{h}{4}; b_d = \dfrac{2b_c}{5}$		$h_d = \dfrac{h}{4}; b_d = \dfrac{b_c}{2}$		$h_d = \dfrac{h}{4}; b_d = \dfrac{2b_c}{3}$		$h_d = \dfrac{h}{4}; b_d = \dfrac{3b_c}{4}$	
	$M_{cr}{}^{*}$	κ	$M_{cr}{}^{*}$	κ	$M_{cr}{}^{*}$	κ	$M_{cr}{}^{*}$	κ
Average	180.9%	6.9	261.8%	9.7	420.8%	14.5	511.2%	17.0
Maximum	242.4%	9.4	350.7%	12.1	570.4%	17.0	699.8%	20.0
Minimum	123.4%	5.0	177.7%	7.5	276.8%	12.3	329.1%	14.1
	$h_d = \dfrac{h}{3}; b_d = \dfrac{2b_c}{5}$		$h_d = \dfrac{h}{3}; b_d = \dfrac{b_c}{2}$		$h_d = \dfrac{h}{3}; b_d = \dfrac{2b_c}{3}$		$h_d = \dfrac{h}{3}; b_d = \dfrac{3b_c}{4}$	
	$M_{cr}{}^{*}$	κ	$M_{cr}{}^{*}$	κ	$M_{cr}{}^{*}$	κ	$M_{cr}{}^{*}$	κ
Average	253.4%	7.5	368.9%	10.6	596.0%	16.3	724.7%	19.3
Maximum	345.7%	10.0	506.3%	13.1	833.4%	19.6	1024.9%	23.6
Minimum	167.6%	5.5	240.3%	8.4	372.3%	13.2	442.0%	15.2
	$h_d = \dfrac{2h}{5}; b_d = \dfrac{2b_c}{5}$		$h_d = \dfrac{2h}{5}; b_d = \dfrac{b_c}{2}$		$h_d = \dfrac{2h}{5}; b_d = \dfrac{2b_c}{3}$		$h_d = \dfrac{2h}{5}; b_d = \dfrac{3b_c}{4}$	
	$M_{cr}{}^{*}$	κ	$M_{cr}{}^{*}$	κ	$M_{cr}{}^{*}$	κ	$M_{cr}{}^{*}$	κ
Average	312.8%	7.7	455.8%	11.0	736.8%	17.2	896.0%	20.5
Maximum	432.3%	10.1	636.0%	13.5	1051.6%	21.1	1294.2%	25.5
Minimum	202.2%	5.9	288.3%	9.0	444.1%	13.4	526.7%	15.6

4.6 Summary

This chapter covered the elastic lateral-torsional buckling capacity of Delta girders. The analytical buckling equation was explored and the analytical results were compared against FE results. A detailed description of the FE model was also presented. The main conclusions of this chapter can be summarized as follows:

- The elastic lateral-torsional buckling equation (Eq. 2.3) of a monosymmetric simply-supported beam under uniform moment, which is typically used for open cross-sections, is capable of predicting the lateral-torsional buckling capacity of Delta girders.

- The FE model presented herein can be used to predict the buckling loads of Delta girders, using the eigenvalue buckling analysis option in Abaqus, with high accuracy.

- The monosymmetry coefficient β_x for Delta girders, obtained through the approximation given in Eq. (2.5), incurs a large error when compared with the exact solution. However, this error does not seem to have an appreciable effect on the elastic LTB buckling capacity.

- For a small group of 25 Delta girders, the addition of delta stiffeners increases the LTB capacity of the initial I-girders by an average of 222% associated with 19% average increase in cross-section weight. On the other hand, the alternative solution of increasing the web thickness provides a maximum increase in the elastic LTB capacity of only 24% and is accompanied by a 39% increase in the cross-section weight.

- A parametric study that included a total of 1,024 sections provided the following results: the maximum increase in the LTB capacity is 1294.2% associated with a 52.6% increase in cross-section weight; delta stiffeners are slightly more effective for larger cross-

sections; delta stiffeners provide a minor advantage when the girder length increases, and

better results are obtained when they are added to an initially monosymmetric I-section;

increasing the stiffener thickness above the web thickness is not an effective method to

increase the LTB capacity of the girder; the combination of $h_d = \frac{2h}{5}$ and $b_d = \frac{3b_c}{4}$

provides the maximum increase in LTB capacity; and finally, the value of b_d is as

important as h_d in affecting the LTB capacity of Delta girders.

Chapter 5

Nonlinear Finite Element Modeling

5.1   <u>Introduction</u>

All numerical simulations presented in this research are based on a 3D nonlinear FE model created using the commercial FE software Abaqus (Simulia, 2014). In this chapter, a comprehensive description of the nonlinear FE model will be presented. Details of the FE model including geometry, element type, mesh size, material properties, analysis procedure, loads and boundary conditions will be discussed. The description will also cover the shape and magnitude of initial geometrical imperfections used in the analysis, and a proposed residual stress pattern for Delta girders developed based on the available residual stress patterns reported for welded monosymmetric I-sections and rectangular steel plates. The FE procedure presented herein will be used in Chapters 6 and 7 unless otherwise noted.

In the second part of this chapter, the developed FE analysis procedure and modeling techniques will be validated by comparing the numerical result with experimental result of a test girder. The last part of the chapter will include an assessment of the nonlinear FE model. The third part of this chapter contains a sensitivity study of the effects of initial geometrical imperfections and residual stress magnitudes on the lateral-torsional buckling (LTB) capacity of Delta girders. This study will emphasize the importance of including imperfections and residual stresses in inelastic LTB simulations.

5.2　Description of the Nonlinear LTB FE Model

5.2.1　Geometry, loads, and boundary conditions

The geometry, loads, and boundary conditions of the nonlinear FE model are similar to those
described in Section 4.2 for the elastic eigenvalue buckling model. The flanges, web, delta and
vertical stiffeners are all modeled using S4R shell element which is a 4-node shell element with
reduced integration. Fork boundary conditions (torsionally simply-supported) are used and
concentrated equal and opposite moments are applied at distant reference as shown in the
structural model of Figure 5.1. Preliminary analyses have shown that high stress concentrations
and web yielding could occur near the ends of the girder; thus, to avoid these problems
transverse (vertical) stiffeners as shown in Figure 5.2 are provided at those locations. The
transverse stiffeners are assumed to have the same thickness as the delta stiffeners and are
connected to the delta girder using the tie constraint option in Abaqus.
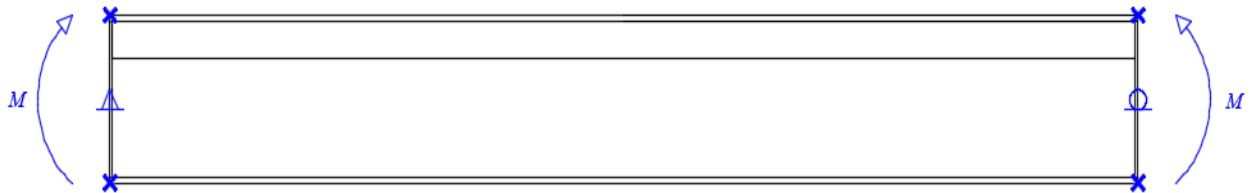
Figure 5.1 Structural model used in FE simulations
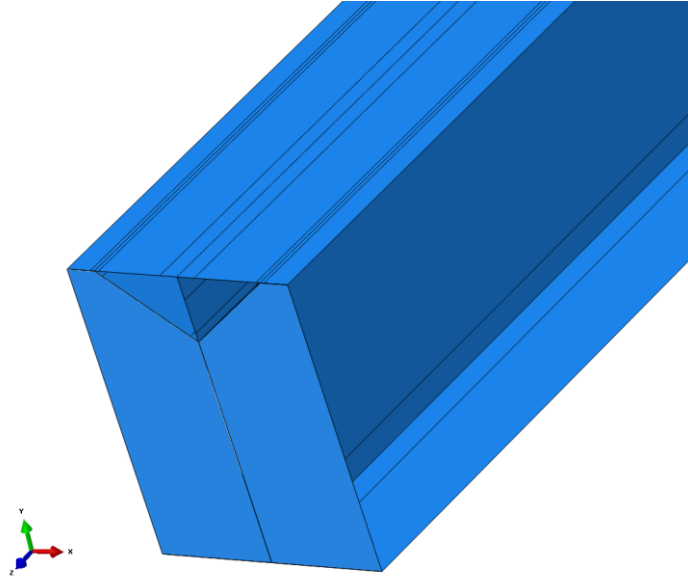
Figure 5.2 Transverse stiffeners at the ends of the girder

5.2.2 Material properties

In this research, all plate components of the Delta girder are modeled using A572 Grade 50 material (equivalent to S355 European structural steel). The yield stress F_y is 345 MPa (50 ksi) and the ultimate strength F_u is 450 MPa (65 ksi). The modulus of elasticity is 200 GPa (29000 ksi) and the Poisson's ratio is 0.333. The following assumptions are used to develop the engineering stress-strain curve:

- The yield strain ε_y is equal to (345/200000) 0.001725 m/m

- The stress is constant in the yield plateau region

- The strain at the onset of strain hardening ε_{sh1} is ten times the yield strain

- The stress at the end of the initial strain hardening region F_{sh2} is obtained using the following equation:

$$F_{sh2} = F_y + \frac{2}{3}\left(F_u - F_y\right) = 415 \text{ MPa} \tag{5.1}$$

- The strain hardening modulus E_{sh} is equal to 5 GPa (700 Ksi)

- After the initial strain hardening region, the stress increases linearly until it reaches F_u at an ultimate strain ε_u equals to seventy times the yield strain, i.e.,

$$\varepsilon_u = 70 \times \varepsilon_y = 0.12075 \text{ m/m} \tag{5.2}$$

- Beyond the ultimate strain, the stress remains constant and equals to F_u. This simplification is justified because the maximum stress reached in all the simulations is much less than the ultimate stress F_u.

Several researchers, e.g., Kim (2010), have used a similar stress-strain curve in FE simulations. Abaqus documentation (Simulia, 2014) requires the engineering (nominal) stress-strain for a uniaxial test to be converted to true stress-strain in FE simulations. The true stress-strain curve is obtained using the following equations:

$$\sigma_{true} = \sigma_{eng}(1 + \varepsilon_{eng}) \tag{5.3}$$

$$\varepsilon_{true} = \ln(1 + \varepsilon_{eng}) \tag{5.4}$$

where σ_{true} and ε_{true} are the true stress and strain, respectively, and σ_{eng} and ε_{eng} are the engineering stress and strain, respectively. Both the engineering and the true stress-strain curves for A572 Grade 50 steel are plotted in Figure 5.3.
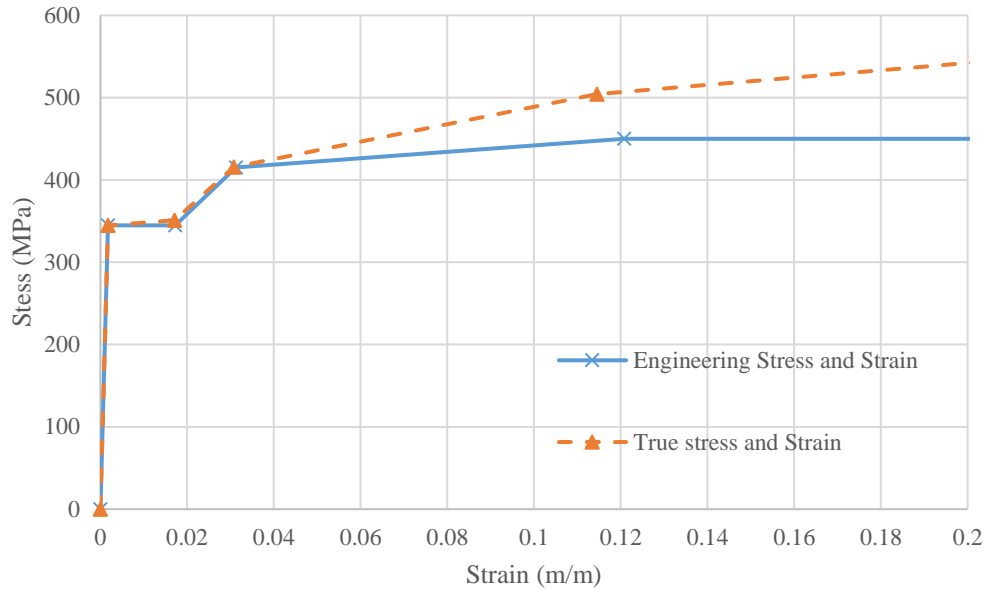
Figure 5.3 Engineering and true stress-strain curves

5.2.3   Proposed residual stress pattern for Delta girders

A review of the available residual stress patterns has been provided in Section 2.5. The addition

of delta stiffeners to an I-section will affect the existing residual stresses in the girder due to the

welding process. Since experimental data of residual stress measurements for Delta girders are

not available, a residual stress pattern is to be deduced from existing patterns. This will be

achieved by superimposing the residual stresses of rectangular steel plates to those of

monosymmetric welded I-sections and enforcing axial or longitudinal equilibrium over the cross-

section. Three different types of plates are used in welded sections: as-rolled, flame-cut, and

mechanically-cut steel plates. The residual stress distributions vary among the three types of

plates. The mechanically-cut steel plate refers to a shear cutting technique that does not include

heat input in the process. On the other hand, flame-cut steel plates are produced by oxy-fuel

cutting, laser or plasma cutting, and few other technologies that introduce intense heat input to

124

the edges of the steel plate. This process will create high tensile stresses in the heat affected zone that often reach the yield stress of the material F_y. The penetration depth of the tensile stresses depends on various factors such as the thickness of the plate, the welding method, the number of passes, etc. Consequently, the compressive residual stresses are to be calculated so they will satisfy longitudinal equilibrium. Welding of mechanically-cut steel plates will result in a residual stress pattern similar to that of flame-cut steel plates. Thus, ECCS (1976) proposes a simplified residual stress pattern shown in Figure 5.4 for use in steel plates that are flame-cut at both edges, or in mechanically-cut steel plates that are welded at both edges.
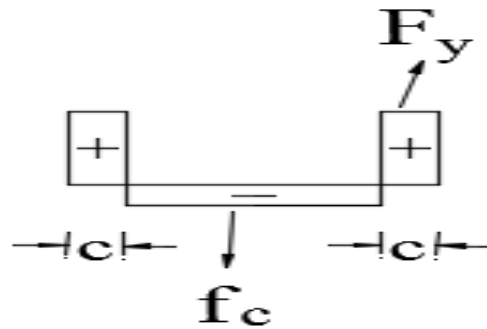
Figure 5.4 Residual stresses in flame-cut plates at both edges or in mechanically-cut plates welded at both edges (ECCS, 1976)

ECCS (1976) recommends the width of the tension block zone c, and the compressive residual stress f_c, to be calculated using the following equations

$$c = \frac{1100\sqrt{t}}{F_y} \tag{5.5}$$

$$f_c = F_y \frac{2c}{b - 2c} \tag{5.6}$$

125

where c is the width of each tension zone in mm, t is the plate thickness in mm, F_y is the steel yield stress in MPa, f_c is the compressive residual stress, and b is the total width of the steel plate.

In monosymmetric I-sections, the compressive residual stress in each flange is dependent on its relative dimensions. Two residual stress patterns for monosymmetric welded I-sections are available in the literature and are reviewed in Section 2.5.3. The first one is proposed by Kitipornchai and Wong-Chung (1987) and requires prior knowledge of the welding area and welding technique; thus, it is not very practical. The second pattern is proposed by Trahair (2012) and will be used as the base pattern for Delta girders. A Uniform compressive web residual stress equals to $0.3F_y$ is added to Trahair's pattern. The width of the two tension blocks where yielding occurs in the material due to welding is obtained from longitudinal equilibrium. To superimpose the residual stress patterns of the delta stiffeners (rectangular steel plates) and the monosymmetric I-section, the following assumptions are made:

- The material yields at the locations of the welds. This is a conservative approach and is adopted in a number of proposed residual stress patterns for welded sections as discussed in Section 2.5.
- At the point of intersection between the delta stiffeners and the top flange, equal tension block width c_2 is assumed for both components as shown in Figure 5.5.
- At the point of intersection between the delta stiffeners and the web, the width of the web tension block c_4 is twice that of the delta stiffeners tension block c_2 due to having one line of weld on each side of the web.

- Once the residual stresses of the delta stiffeners are added, the widths of the compression blocks in the top flange and the web, c_1 and c_3, are obtained from longitudinal equilibrium.

The proposed residual stress pattern for Delta girders is shown in Figure 5.5. This simple model satisfies longitudinal equilibrium and is easy to incorporate in a FE simulation. The same pattern will be used regardless of whether the initial section is a hot-rolled or a welded I-section. The compressive residual stress values and the dimensions shown in Figure 5.5 are calculated using the following equations

$$f_{c1} = 0.3 F_y \tag{5.7}$$

$$f_{c2} = \begin{cases} 0.3 F_y & \text{(equal flange size)} \\ 0.3 F_y \dfrac{b_t}{b_c} & \text{(unequal flange size)} \end{cases} \tag{5.8}$$

$$f_{c3} = F_y \frac{2 c_2}{w_d - 2 c_2} \tag{5.9}$$

$$c_1 = \frac{0.3}{1.3} b_c - 2 c_2 \tag{5.10}$$

$$c_2 = 1100 \frac{\sqrt{t_d}}{F_y} \tag{5.11}$$

$$c_3 = \frac{0.3}{2.6} h - c_2 \tag{5.12}$$

$$c_4 = 2200 \frac{\sqrt{t_d}}{F_y} \tag{5.13}$$

127

$$c_5 = \begin{cases} \dfrac{0.3}{1.3}b_t & \text{(equal flange size)} \\[2ex] b_t \dfrac{0.3b_t/b_c}{1 + (0.3b_t/b_c)} & \text{(unequal flange size)} \end{cases} \qquad (5.15)$$

where c_2 is in mm, t_d is in mm, and F_y is in MPa. The cross-section dimensions used in these equations are provided in Table 3.13.
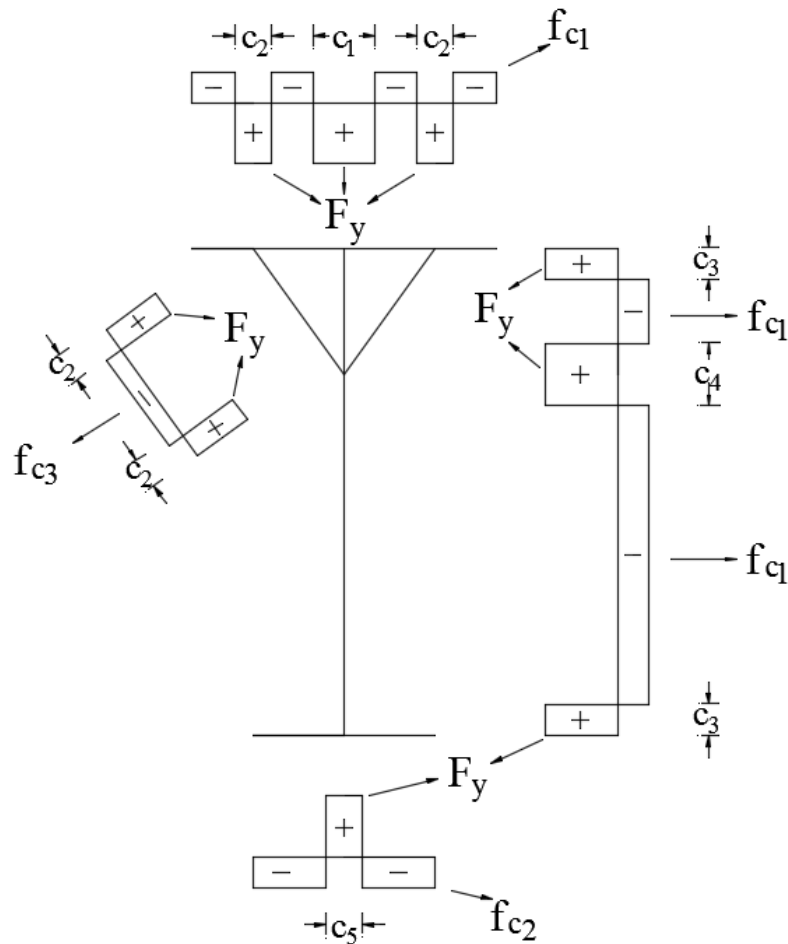
Figure 5.5 Proposed residual stress pattern for Delta girders

The S4R shell element used in this research employs a one point Gauss integration rule. Hence, the FE model of the Delta girder is partitioned at the ends of each dimension c to model

the residual stresses in the relatively narrow tension stress blocks. Thereafter, the residual

stresses are introduced in the initial analysis step using the predefined initial stress option in

Abaqus as shown in Figure 5.6.
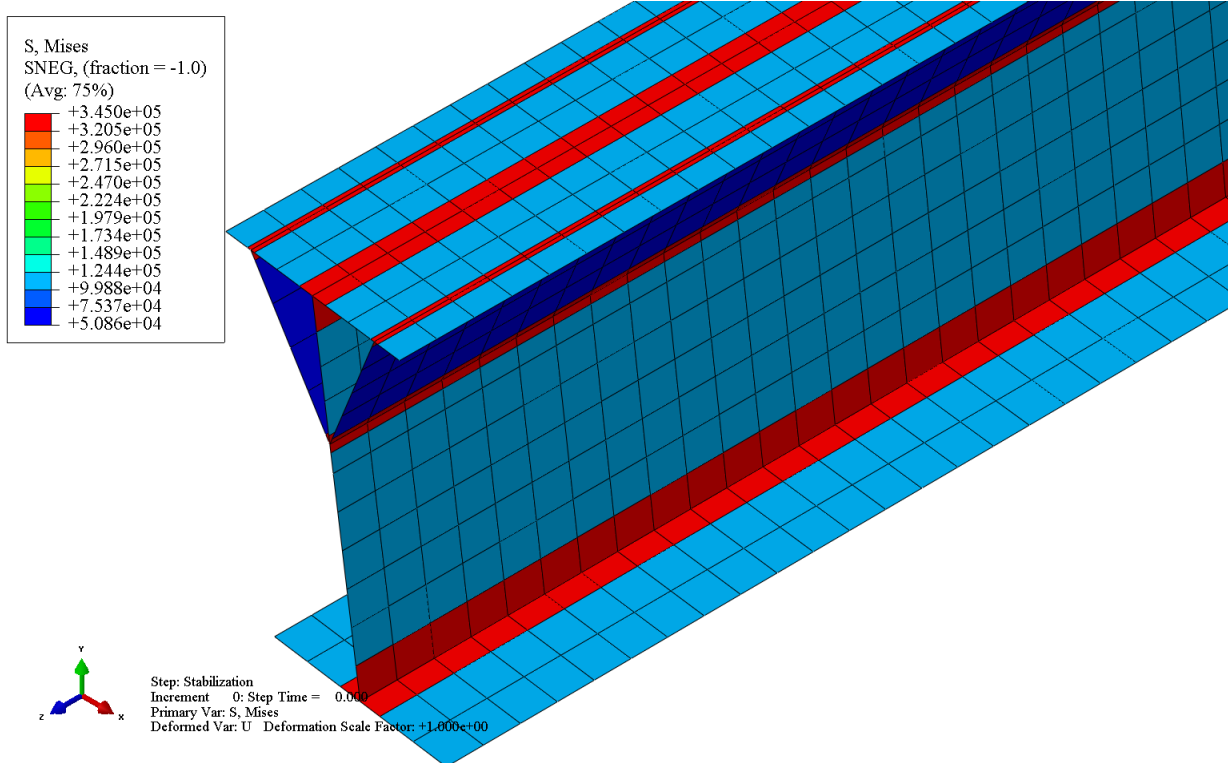
Figure 5.6 Residual stresses in Delta girder 16

5.2.4 Initial geometric imperfections

Several techniques exist for modeling initial geometrical imperfections. The most common

technique is to model the beam's out-of-straightness as the lowest positive buckling mode with a

maximum value of $L_b/1000$ as permitted by the AISC COSP (2010), where L_b is the unbraced

length of the beam. Boissonnade and Somja (2012) compared the different available techniques

for the modeling of initial geometrical imperfections and concluded that using the lowest poitive

buckling mode with a maximum value of $L_b/1000$ is suitable for modeling imperfections.

Thus, for each Delta girder, an eigenvalue analysis is first performed and the nodal displacements of the lowest positive buckling mode (the second mode for monosymmetric beams) are scaled to a maximum value of $L_b/1000$ and introduced to the inelastic FE model. Figure 5.7 illustrates the out-of-straightness in one of the tested Delta girders before the load application.

Step: Stabilization
Increment   0: Step Time =   0.000
Deformed Var: U   Deformation Scale Factor: +1.000e+00
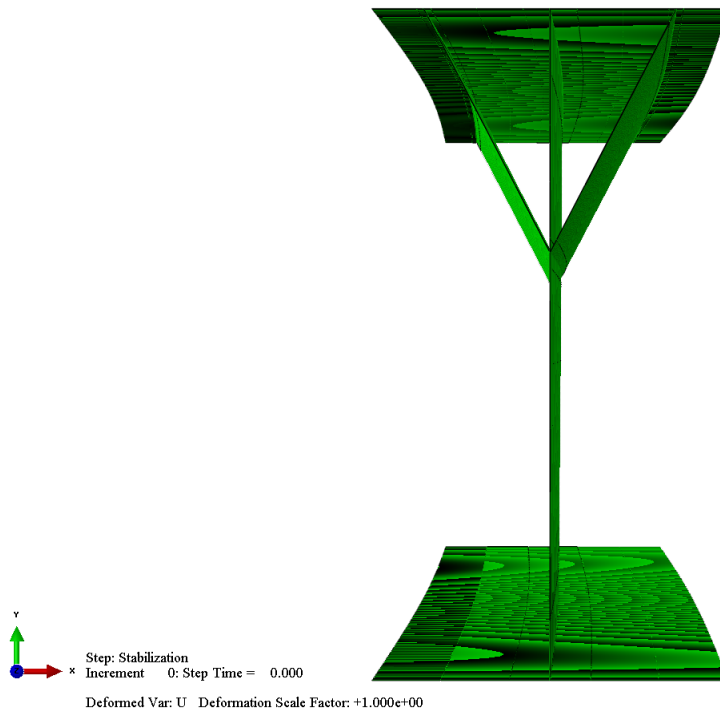
Figure 5.7 Initial imperfections in Delta girder 16 (scale factor = 1)

5.2.5   Mesh size

The mesh size is selected in a similar manner as that described in Section 4.2.2 for the elastic model with an approximate maximum element size of 5 cm. However, the partitions at the ends of the tension residual stress blocks require the use of smaller element sizes so the residual stress pattern can be modeled more accurately as shown in Figure 5.8. In cases where the width of the

flange is equal to or less than 12 cm, the approximate maximum element size used is 3 cm. The

number of elements in each component of the Delta girder is dependent on the component's

width. A convergence study has shown that the selected element dimensions are adequate to

produce a good solution.
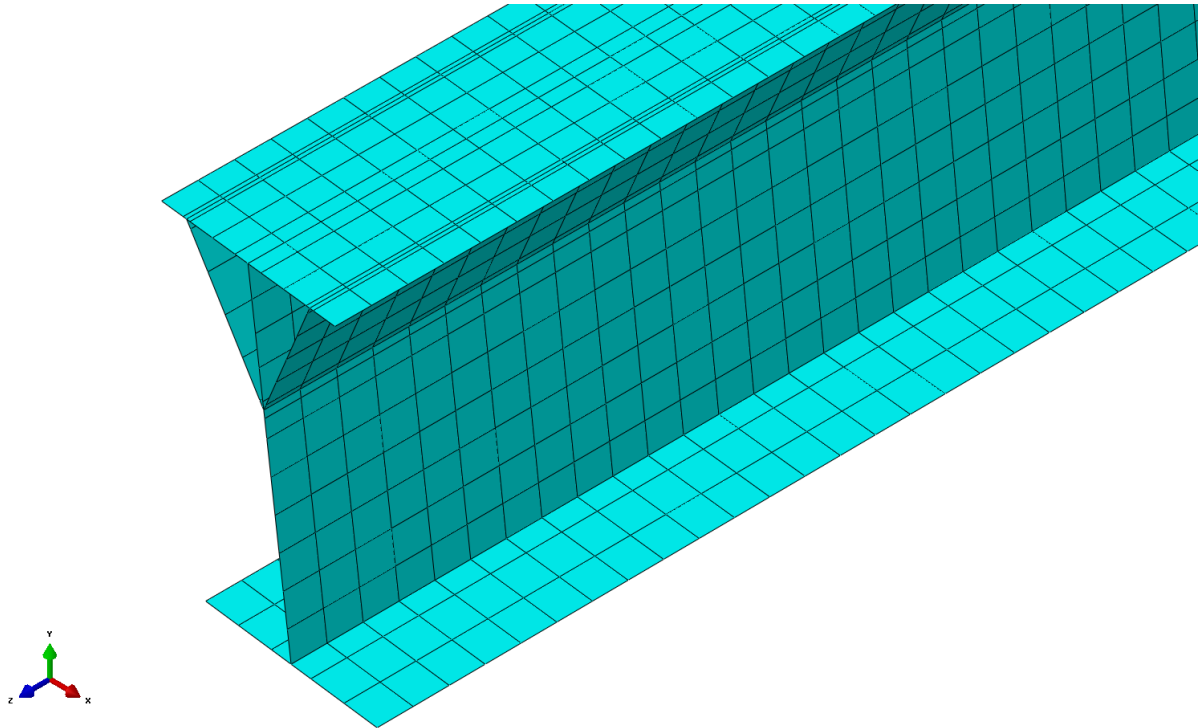
Figure 5.8 Typical mesh of a Delta girder

5.2.6   Analysis procedure

The residual stresses are in a self-equilibrating condition when the beam is perfectly straight.

However, when these stresses are applied in conjunction with initial geometrical imperfections, a

general static stabilization step needs to be implemented to ensure that these stresses reach a state

of equilibrium before any external loads are to be applied. The NLGEOM option in Abaqus is

turned on to allow large displacements (geometric nonlinearity). In the second step, the Riks

buckling method is used to perform the nonlinear inelastic bucking analysis of the beam under uniform moment. The Riks method solves for loads and displacements simultaneously, using the load magnitude as an additional unknown. Thus, an additional quantity is needed to measure the solution's progress. To do this, Abaqus uses the static equilibrium path in a load-displacement space along with the arc length. This method is known as the Modified Riks algorithm and solutions will be obtained regardless of whether the response is stable or unstable (Simulia, 2014). The buckling load is then obtained as the maximum load proportionality factor. Figure 5.9 shows a plot of the buckling moment versus the arc length for Delta girder 6 with L_b = 10.0 m, while Figure 5.10 depicts the buckling failure of the girder.
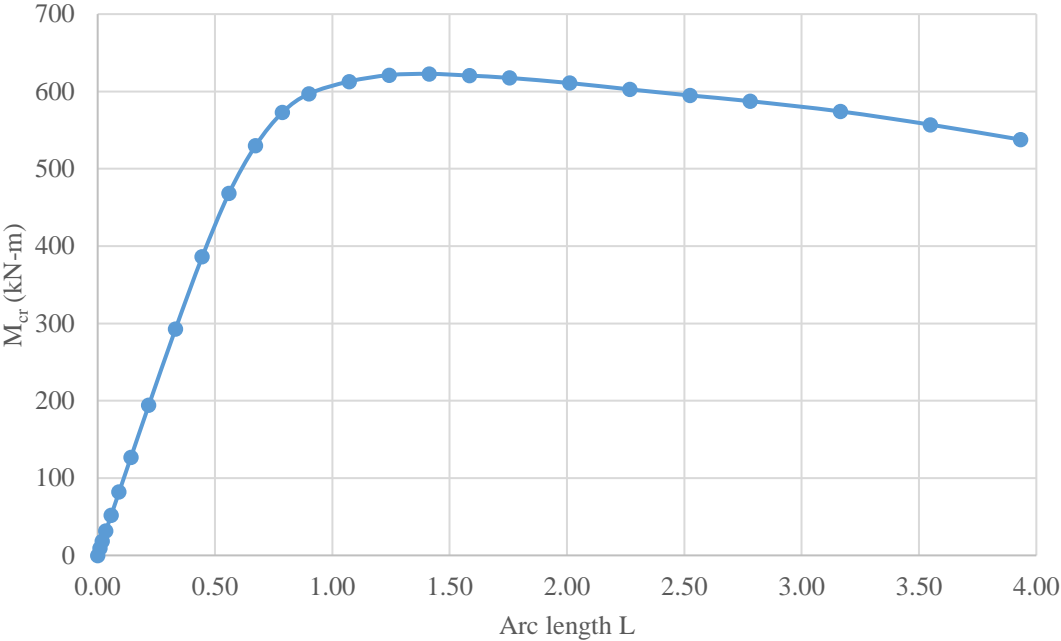
Figure 5.9 Buckling moment vs. arc length for Delta girder 6

S, Mises
SNEG, (fraction = -1.0)
(Avg: 75%)

+4.300e+05
+3.952e+05
+3.604e+05
+3.255e+05
+2.907e+05
+2.559e+05
+2.210e+05
+1.862e+05
+1.514e+05
+1.165e+05
+8.171e+04
+4.688e+04
+1.205e+04

Step: InelasticBuckling
Increment   25: Arc Length =   3.934
Primary Var: S, Mises
Deformed Var: U   Deformation Scale Factor: +1.000e+00
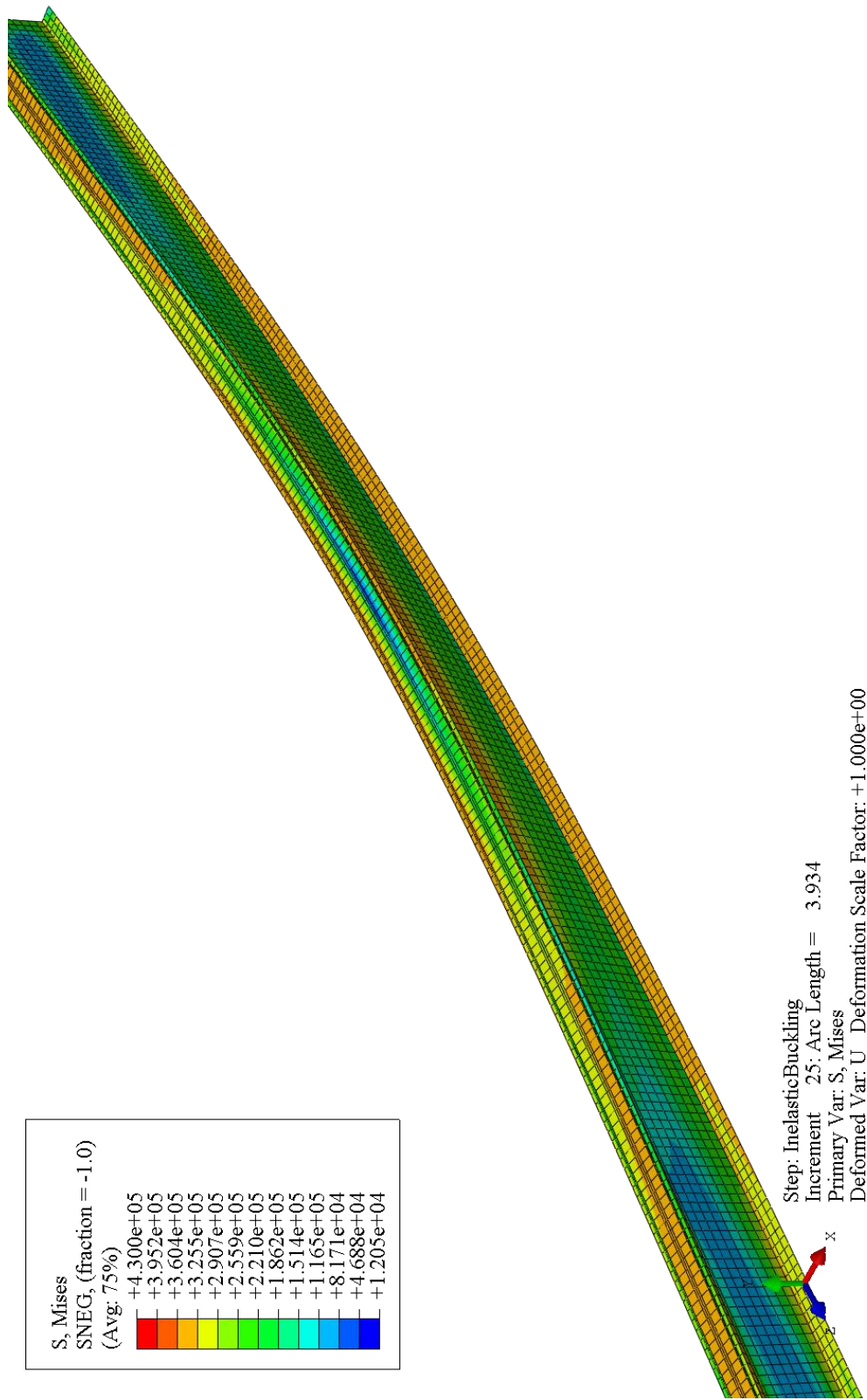
Figure 5.10 Buckling shape of Delta girder 6 (Stresses in kPa)

133

5.3   FE Model Validation

5.3.1   Description of test beam

The findings of what follows in this chapter as well as the following two chapters are mainly based on nonlinear FE simulations using Abaqus; therefore, it is imperative to verify the results of the FE model. Analytical closed-form equations for the inelastic LTB of monosymmetric beams are not available. Hence, the results of the FE model need to be verified against experimental work. The only available experimental testing on Delta girders, described in Section 2.2, was performed by Hadley (1961). The main objective of these tests was to determine whether the delta stiffeners could satisfactorily stiffen the web to replace the vertical stiffeners. Consequently, none of the tested girders failed by LTB and can be used in the FE model verification. In addition, multiple tests were performed on the same Delta girder.

To verify the FE model, a comparison is performed between the experimental and FE simulation results of LTB tests conducted by Dux and Kitipornchai (1983). In these tests, nine simply-supported beams were tested and they all failed by inelastic LTB under three different loading patterns, i.e., three different moment gradients. Figure 5.11 shows the three-point bending test setup used for FE verification. The tested beam, designated "No. 2" in the experimental work, is a hot-rolled universal 250UB37 I-section with a total span L of 9 m. The measured dimensions of this compact cross-section are provided in Table 5.1. The load was applied on the top flange of the beam by a bearing plate that allows minor axis rotation during the load application. The test load was applied in increments starting from 10 kN and decreasing to 0.5 kN towards the expected buckling load of the beam. Knife edge bracings over the full web depth from both sides are provided at the support locations and under the point of load

134

application as shown in Figure 5.11. The measured initial imperfections, residual stresses and material properties will be provided in the following section.

Table 5.1 Measured c ross-section dimensions (Dux & Kitipornchai, 1983)

Designation in test	b_c (mm)	b_t (mm)	d (mm)	t_c (mm)	t_t (mm)	t_w (mm)	L (m)	L_b (m)
No. 2	147.43	147.85	256.35	10.77	10.57	6.82	9	4.5
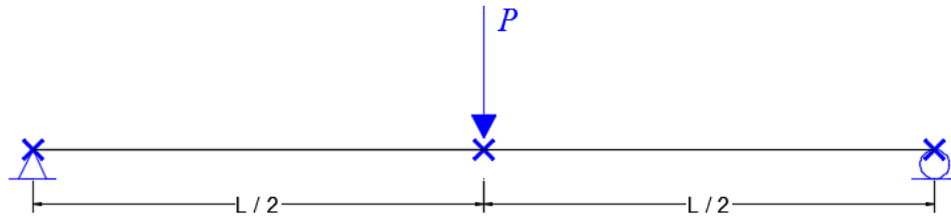
Figure 5.11 Test configuration for FE verification

5.3.2 FE modeling of the test girder

An FE model is developed using all the measurements, imperfections and material properties provided by Dux and Kitipornchai. The same analysis procedure, element type and mesh size used to model the Delta girders and described in Section 5.2 are applied to the test girder. The load is applied at midspan as a concentrated downward force on the top flange. Simply-supported boundary conditions are applied as a line boundary condition across the width of the bottom flange at each end. The full depth of the web is constrained against lateral displacement at the three locations marked x as shown in Figure 5.11 to simulate the knife edge lateral bracing used in the experiment. Vertical stiffeners are not incorporated in this FE model.

Dux and Kitipornchai (1983) performed tension coupon test on 25 specimens (17 from flanges and 8 from webs) to measure the material yield stress. The mean yield stress F_y obtained for the flange and web are 285 MPa and 321 MPa, respectively. An engineering stress-strain curve is generated for each yield stress and transformed to true stress-strain curve using the same procedure described in Section 5.2.2. Figures 5.12 and 5.13 show the engineering and true stress-strain curves, where the latter was used in the FE simulations. Based on the results of 12 tests, the mean Young's modulus, E, is 209.9 GPa. The maximum measured initial geometrical imperfection for the test beam is $L_b/3300$. The imperfection is applied to the FE model using the same procedure described in Section 5.2.4. The maximum deflection of the lowest positive buckling mode, under the same load and boundary conditions, is scaled down to $L_b/3300$ and inserted as an initial geometry in the initial step. The lowest positive buckling mode of the test girder is shown in Figure 5.14.

Sectioning method was used to measure six sets of residual strains and these strains are transformed to residual stresses using a Young's modulus of 209.9 GPa. The mean values and ranges of the measured residual stresses are provided in Figure 5.15. The results show that the residual stresses in the flanges are mainly in tension, which is attributed to roller straightening. The mean values are introduced to the FE model in the initial step using the initial stress option in Abaqus as shown in Figure 5.16.
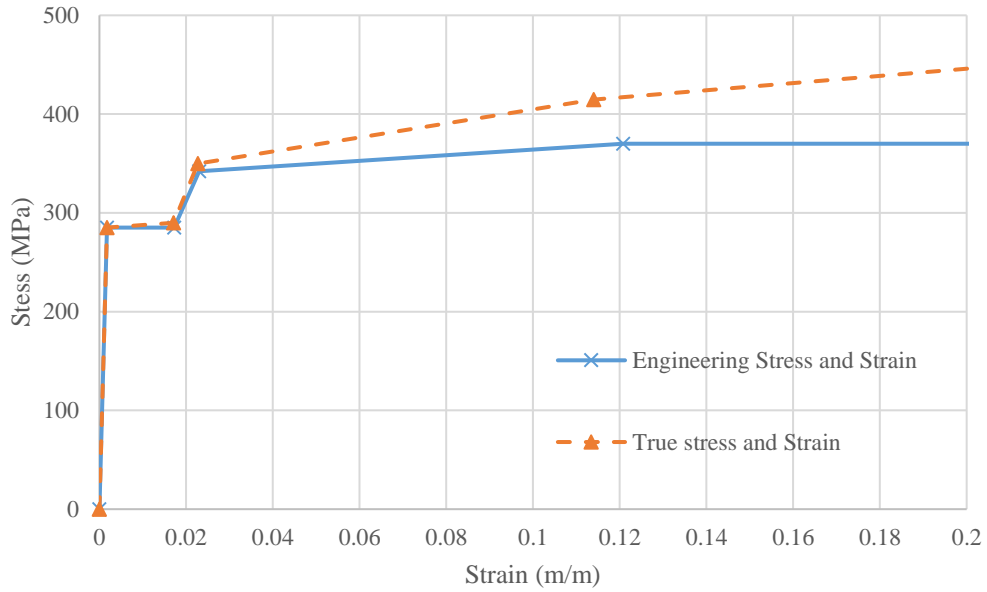
Figure 5.12 Stress-strain curves of the flanges on the test beam
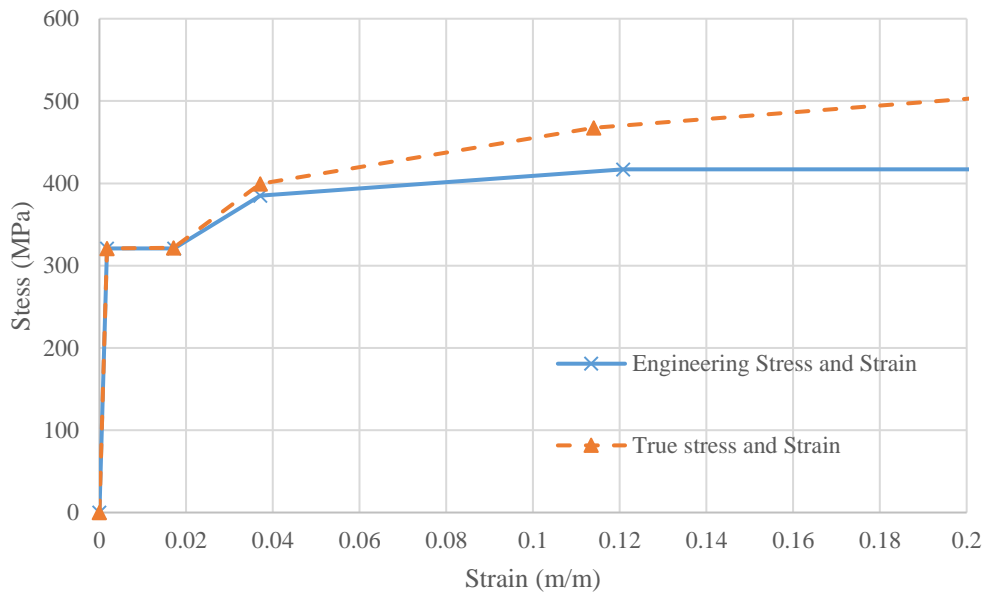
Figure 5.13 Stress-strain curves of the web on the test beam

Figure 5.14 Imperfection shape used in the FE simulation of the test beam

Figure 5.15 Residual stress measurements (Dux & Kitipornchai, 1983)

138

S, Mises
SNEG, (fraction = -1.0)
(Avg: 75%)
+1.763e+05
+1.617e+05
+1.471e+05
+1.324e+05
+1.178e+05
+1.032e+05
+8.855e+04
+7.393e+04
+5.930e+04
+4.468e+04
+3.005e+04
+1.543e+04
+8.000e+02

Step: Stabilization
Increment   0: Step Time =   0.000
Primary Var: S, Mises
Deformed Var: U   Deformation Scale Factor: +1.000e+00

Figure 5.16 Implementation of measured residual stresses in model verification

5.3.3   Assessment of the FE model results

Dux and Kitipornchai (1983) reported the buckling load of the test beam to be 62.6 kN ($\pm$ 0.25 kN error margin). The buckling load obtained in the FE simulation is 60.0 kN. The difference between the experimental test and the FE simulation is 4.15%. However, because the fillet areas at the junction points of the web and flanges (1% of the total area for 250UB37 section) are neglected in the FE modeling, a slightly lower buckling load than the experimental one is expected. Moreover, the use of mean values for material properties and residual stresses in the FE simulation could also lead to small errors in the comparison. This result shows that the nonlinear FE model and the modeling techniques described in Section 5.2 can provide accurate

results for studying the inelastic LTB behavior. The following two points provide additional justifications for the FE model:

- It is shown in Section 4.2.5 that the FE model can predict the elastic critical buckling moment of Delta girders with an average error of 4.3% with respect to the theoretical elastic LTB solution.

- It is also shown in Section 6.4.2 that for short beams, the FE models can attain the plastic moment capacity for all simulated Delta girders with a maximum difference of 2%. The plastic moment capacity is the maximum theoretical moment that can be achieved for a given cross-section.

5.4   Imperfections Sensitivity Study

This section will investigate the sensitivity of LTB curves to geometrical imperfections and residual stresses. Experimental data have shown that the measured residual stresses could be well below the recommended values in nominal residual stress patterns (Dux & Kitipornchai, 1983). This can be attributed to the effects of various cold straightening techniques. In addition, Dux and Kitipornchai (1983) and Essa and Kennedy (1993) reported maximum initial imperfections of L_b/3300 and L_b/2000, respectively, in their experimental studies. On the other hand, residual stresses are sometimes completely neglected in FE analysis of LTB behavior (Hassanein, Kharoob, & El Hadidy, 2013; Mohebkhah & Azandariani, 2015).

In this study, five Delta girders from Section 4.4 are selected and their LTB curves are obtained under various initial imperfection and residual stresses magnitudes using FE simulations. The cross-section dimensions of the selected Delta girders are provided in Table 5.1.

All the FE simulations are run under simply-supported boundary conditions and uniform moments as detailed in Section 4.2.3. For each Delta girder, three magnitudes of maximum initial imperfections are considered: $L_b/1000$, $L_b/2000$ and $L_b/4000$; and two magnitudes of residual stress pattern as specified in Section 5.2.3 are used: full and half of its specified magnitude. This results in a total of six LTB curves for each Delta girder which are presented in Figure 5.17 to 5.21.

Table 5.2 Dimensions of Delta girders used in imperfections sensitivity study (in mm)

Section	$b_{c,t}$	b_d	d	h_d	w_d	$t_{c,t}$	t_w	t_d
3	170	85	360	111.5	105.2	12.7	8	8
6	210	140	550	103.1	108.3	17.2	11	12
9	300	150	390	70.4	86.9	19	11	12
12	300	200	390	117.3	138.4	19	11	12
16	300	200	590	180	1485.7	25	13	14
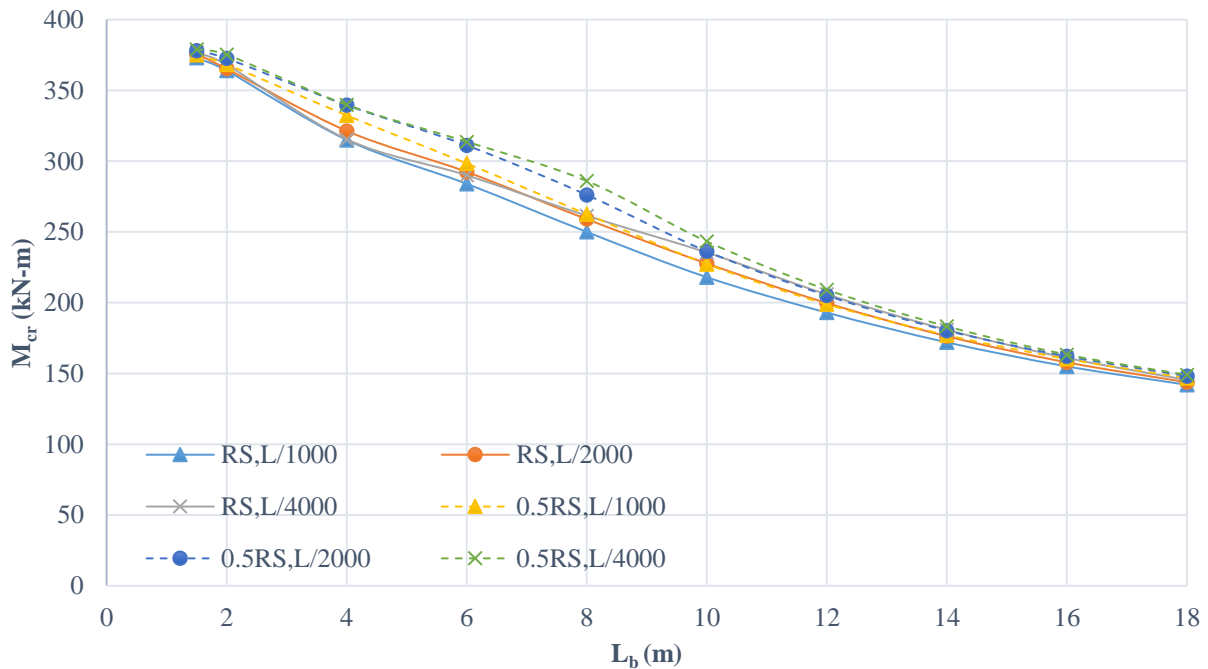
Figure 5.17 LTB curves for Delta girder 3 with various imperfections

141
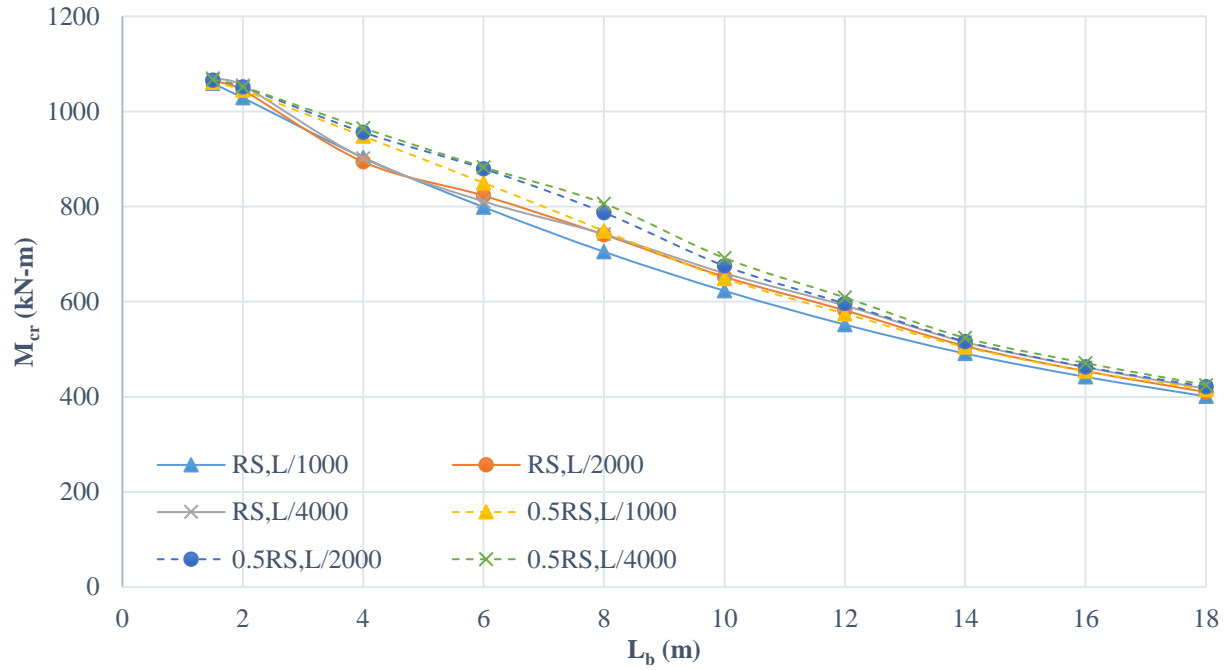
Figure 5.18 LTB curves for Delta girder 6 with various imperfections
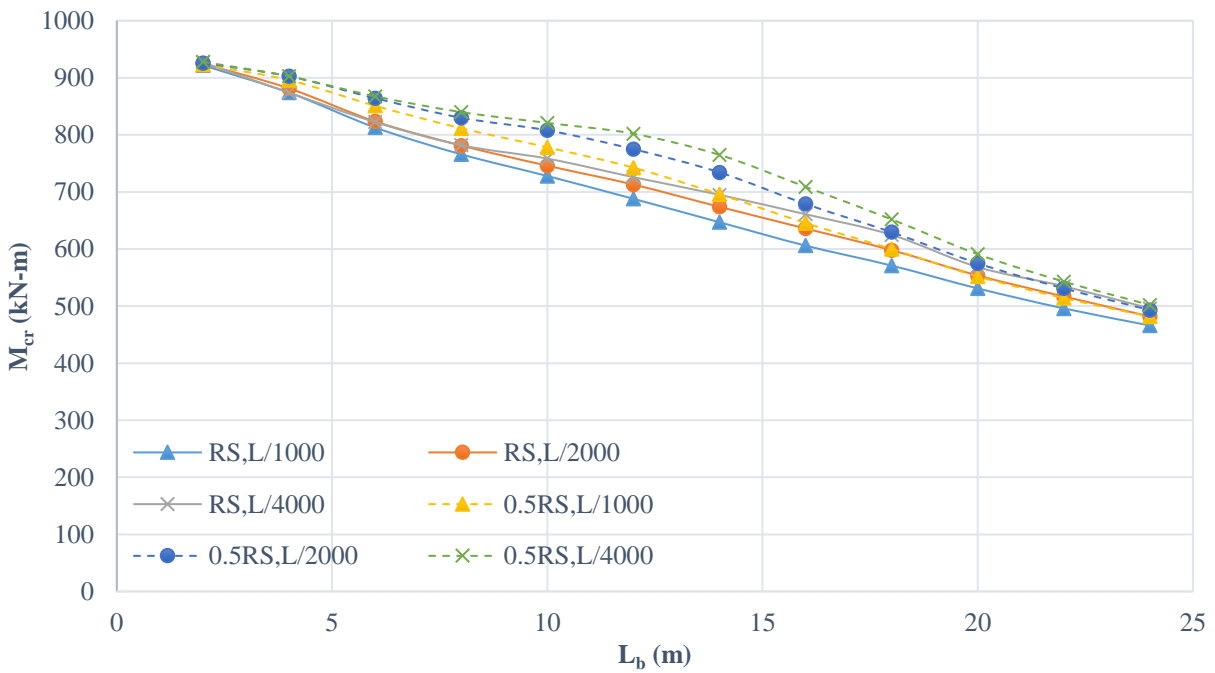
Figure 5.19 LTB curves for Delta girder 9 with various imperfections
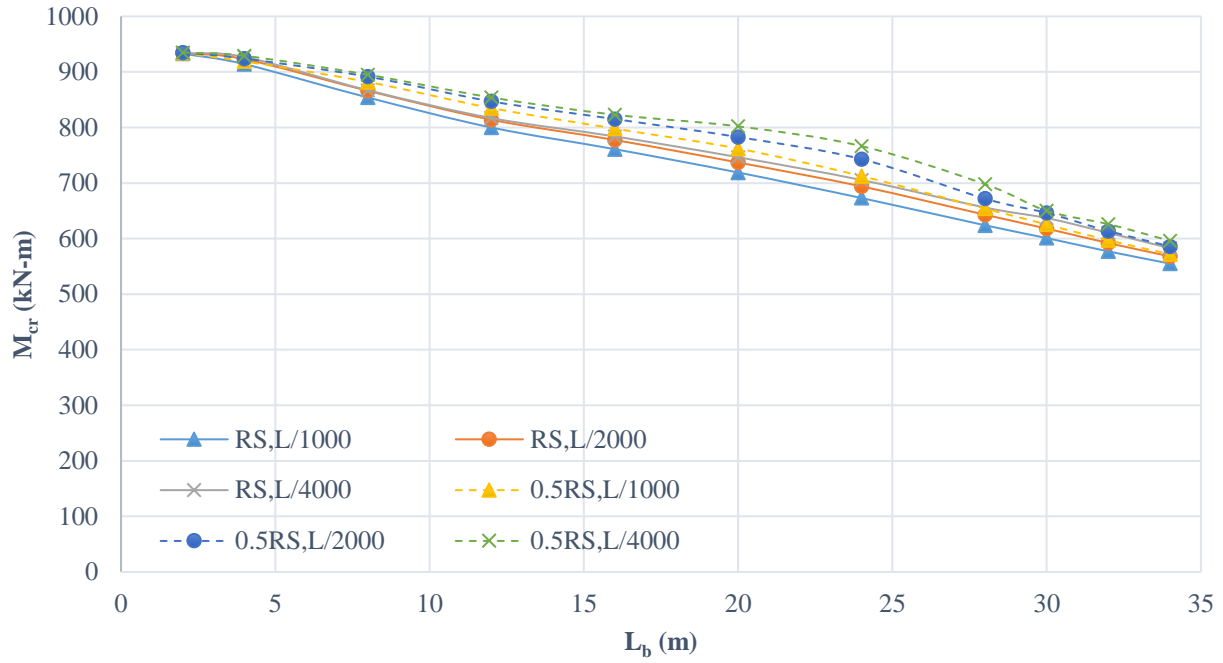
Figure 5.20 LTB curves for Delta girder 12 with various imperfections
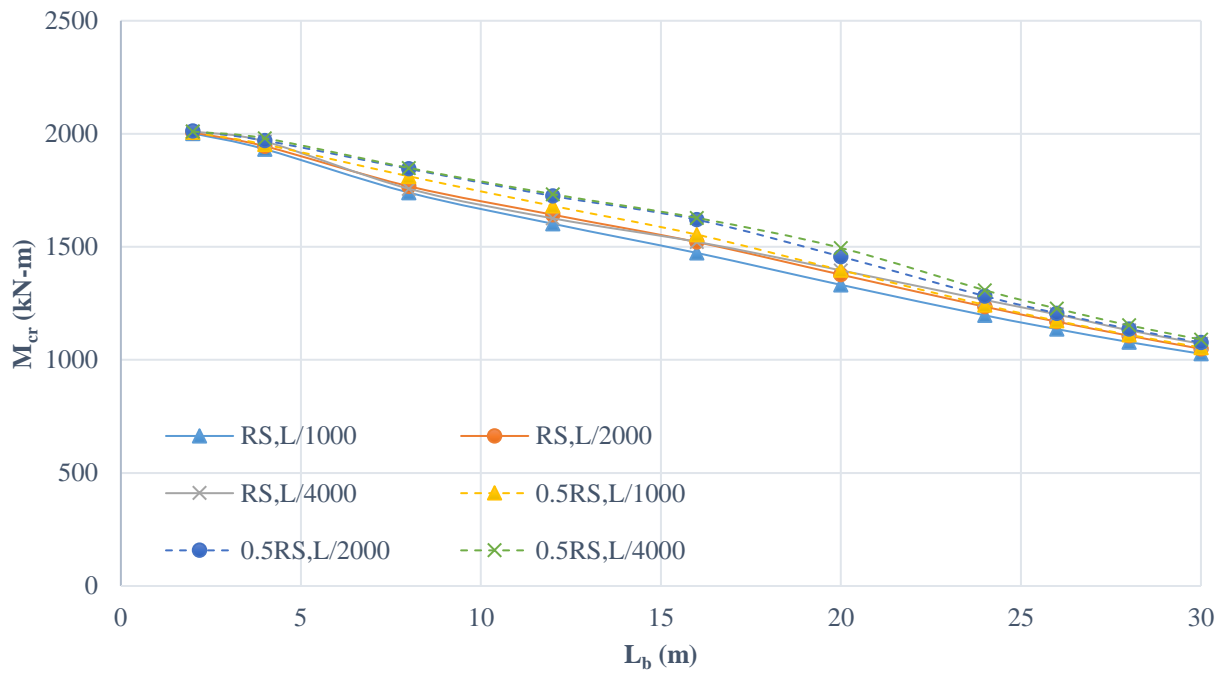
Figure 5.21 LTB curves for Delta girder 16 with various imperfections

The results of the study show that the magnitude of residual stresses and initial imperfections affect the moment capacity as well as the shape of the LTB curve. It is observed that the nonlinearity of the buckling curves increases when the magnitudes of residual stresses and initial imperfections decrease. In addition, the buckling curve changes from an upward concave shape to a downward concave shape. The maximum difference between the buckling curves is generally obtained in the middle of the inelastic range, which is the region limited in AISC (2016a) specifications by L_p and L_r as shown in Figure 2.3. As expected, the buckling curves converge at the full plastic moment capacity and when the length of the beam increases towards the elastic range. Moreover, the buckling capacity of the beam increases when the magnitudes of residual stresses and imperfections decrease. The maximum difference in moment capacity for all girders in this study is obtained between the case of full magnitude residual stress along with an imperfection of $L_b/1000$ and the case of half magnitude residual stress along with an imperfection of $L_b/4000$. This maximum difference ranges from 12.2% to 18.2% in Delta girders 16 and 9, respectively. These results show the sensitivity of the LTB curves to the magnitudes of imperfections and the necessity to include residual stresses in inelastic LTB studies. Otherwise, the FE simulations will overestimate the buckling capacity of the girders.

Altough experimental measurements have shown that the maximum geometrical imperfections can be below $L_b/1000$, this does not preclude the possibility that other manufactured beams may reach the maximum allowable tolerance as per AISC COSP (2010). Thus, to be conservative residual stresses with full magnitude and a maximum initial imperfection of $L_b/1000$ will be used throughout in all subsequent analyses.

5.5   <u>Summary</u>

This chapter started with a description of the nonlinear FE model that included the geometry, loads, boundary conditions, mesh size, material properties and analysis procedure. Furthermore, a modeling technique to account for imperfections in the FE model was presented. A simple residual stress pattern for Delta girders, based on available patterns of welded monosymmetric I-sections and rectangular steel plates, was proposed.

The second part of this chapter provided a validation of the FE model and the modeling techniques. This was done by simulating a test beam and comparing the experimental inelastic buckling load to the one obtained numerically. The comparison yielded a 4.15% difference in the buckling loads.

The effects of the magnitudes of initial geometrical imperfections and residual stresses were then investigated. The sensitivity study included three magnitudes of initial imperfections, L_b/1000, L_b/2000 and L_b/4000, as well as full and half the magnitudes of the proposed residual stress values. The study included five Delta girders and the results have shown that using reduced imperfection magnitudes increases the buckling capacity by up to 18.2%. Reducing the magnitudes of the imperfections also affect the shape of the buckling curve, particularly in the inelastic range. Hence, it was concluded that residual stresses should be included in inelastic LTB FE simulations.

Chapter 6

Flexural Resistance of Delta Girders Subject to Uniform Bending

6.1 <u>Introduction</u>

The lateral-torsional buckling (LTB) curve of a given cross-section provides the moment resistance of the cross-section at various unbraced lengths L_b. The curve takes into account the effects of residual stresses and initial geometrical imperfections. Since different techniques were used to develop of the LTB curves in AISC (2016a) and EC3 (2005), noticeable differences in the LTB capacity are obtained. The main distinctions between the two codes are that EC3 (2005) explicitly differentiate between hot-rolled and welded sections, and between sections with different depth over compression flange width ratio (d/b_c).

This chapter starts with an overview and comparison between the LTB design provisions for beams in AISC (2016a) and EC3 (2005). Equations derived for the plastic neutral axis and plastic section modulus of Delta girders are then presented. Afterwards, results of LTB FE simulations of various Delta girders are compared to the LTB curves of AISC (2016a) and EC3 (2005). Based on these results, design equations that can be used to assess the flexural resistance of Class 1 (compact) Delta girders are recommended. These equations are then assessed at various critical d/b_c ratios. At the end of the chapter, design guidelines are provided to assist the design engineers in selecting effective delta stiffener configurations.

6.2   Overview of the AISC (2016a) and EC3 (2005) LTB Resistance Curves

6.2.1   AISC (2016a) lateral-torsional buckling equation

The lateral-torsional buckling capacity of monosymmetric I-beams with compact or noncompact webs is provided in Section F4.2 of the AISC (2016a) specifications. The AISC buckling curve is divided into three regions based on the unbraced length L_b of the compression flange as explained in Section 2.4.1 and illustrated in Figure 2.3. In the elastic region, i.e., when $L_b > L_r$, the nominal buckling capacity M_n is taken as the theoretical elastic buckling capacity M_{cr} of a doubly symmetric beam under uniform bending using Eqs. (2.6) and (2.7). The limiting length L_r is computed using Eqs. (2.15) and (2.16). For a more accurate solution, the AISC (2016b) commentary recommends using Eqs. (2.3) and (2.17) to compute M_{cr} and L_r, respectively. In the inelastic region, i.e., when $L_p < L_b \leq L_r$, the nominal flexural resistance is assumed to be a linear function between L_p to L_r given by

$$M_n = C_b \left[R_{pc}M_{yc} - \left(R_{pc}M_{yc} - F_L S_{xc}\right) \left(\frac{L_b - L_p}{L_r - L_p}\right) \right] \leq R_{pc}M_{yc} \qquad (6.1)$$

in which M_{yc}, the only term not defined in Section 2.4, is the moment that corresponds to yielding of the extreme compression fiber given by

$$M_{yc} = F_y S_{xc} \qquad (6.2)$$

The web plastification factor R_{pc} is determined using one of the following equations

i) When $I_{yc}/I_y > 0.23$

    a) For $h_c/t_w \leq \lambda_{pw}$

$$R_{pc} = \frac{M_p}{M_{yc}} \tag{6.3}$$

b) For $h_c/t_w > \lambda_{pw}$

$$R_{pc} = \left[\frac{M_p}{M_{yc}} - \left(\frac{M_p}{M_{yc}} - 1 \right) \left(\frac{\lambda - \lambda_{pw}}{\lambda_{rw} - \lambda_{pw}} \right) \right] \leq \frac{M_p}{M_{yc}} \tag{6.4}$$

ii) When $I_{yc}/I_y \leq 0.23$

$$R_{pc} = 1 \tag{6.5}$$

where M_p is is the plastic bending moment, λ is a slenderness parameter given by h_c/t_w, λ_{pw} and λ_{rw} are the limiting slenderness for compact and noncompact webs respectively, h_c is defined as twice the distance from the centroid to the inside face of the compression flange less the fillet for rolled sections, to the inside face of the compression flange for welded sections and to the nearest line of fasteners for built-up sections.

The web limiting slenderness equations for monosymmetric sections subject to flexure are given in Table B4.1b of the AISC specifications as

$$\lambda_{pw} = \frac{\frac{h_c}{h_p} \sqrt{\frac{E}{F_y}}}{\left(0.54 \frac{M_p}{M_y} - 0.009 \right)^2} \leq \lambda_{rw} \tag{6.6}$$

$$\lambda_{rw} = 5.70 \sqrt{\frac{E}{F_y}} \tag{6.7}$$

where h_p is defined as twice the distance from the plastic neutral axis to the inside face of the compression flange when welds are used or to the nearest line of fasteners.

148

When the beam falls into the plastic region, i.e., $L_b \leq L_p$, the limit state of lateral-torsional buckling does not apply and the nominal moment is equal to the full plastic bending moment capacity of the cross-section M_p, i.e.,

$$M_n = M_p = F_y Z_x \leq 1.6 F_y S_{xc}$$
(6.8)

where Z_x is the plastic section modulus about the x-axis (strong axis of bending)

From the aforementioned discussion, it can be seen that manual calculations of the lateral-torsional buckling capacity of monosymmetric cross-sections according to AISC specifications can be a lengthy procedure. Moreover, the AISC specifications do not differentiate between hot-rolled and welded sections, and ignore the effect of the depth to compression flange width ratio d/b_c, which can affect the buckling capacity of the cross-section as will be discussed in Sections 6.2.2 and 6.4.2.

6.2.2 EC3 (2005) lateral-torsional buckling equations

The lateral-torsional buckling capacity curves in EC3 (2005) are based on numerical calibrations of finite element simulations (Rebelo, Lopes, Simoes da Silva, Nethercot, & Vila Real, 2009). The buckling capacity of a laterally unrestrained beam in EC3 is computed using the following equation

$$M_{b,Rd} = \chi_{LT} W_y \frac{f_y}{\gamma_{M1}}$$
(6.9)

where $M_{b,Rd}$ is the design buckling resistance moment, χ_{LT} is a reduction factor for lateral-torsional buckling, f_y is the yield stress of steel, γ_{M1} is a partial safety factor for resistance of the

member to instability assessed by member checks, and W_y is the appropriate section modulus about the y-axis, which is defined as the strong axis in EC3, as:

- $W_y = W_{pl.y}$ for Class 1 or 2 cross-sections

- $W_y = W_{el.y}$ for Class 3 cross-sections

- $W_y = W_{eff.y}$ for Class 4 cross-sections

in which

- $W_{pl.y}$ is the plastic section modulus about the y-axis

- $W_{el.y}$ is the elastic section modulus about the y-axis

- $W_{eff.y}$ is the effective section modulus about the y-axis

- Class 1 cross-sections are sections that form plastic hinge with the required rotation capacity for plastic analysis without reduction in resistance

- Class 2 cross-sections are sections that can develop plastic moment resistance but have limited rotation capacity due to local buckling

- Class 3 cross-sections are sections that can reach the yield strength at the extreme compression fiber assuming elastic distribution of stresses, but plastic moment will not develop due to local buckling

- Class 4 cross-sections are sections that experience local buckling before yielding starts in any part of the cross-section.

EC3 defines two cases for the lateral-torsional buckling resistance of beams:

- General case (section 6.3.2.2 in EC3)

- Rolled sections or equivalent welded sections (section 6.3.2.3 in EC3)

While the second case applies to standard hot-rolled sections or equivalent welded sections, the general case can be applied to all common cross-sections, i.e., hot-rolled sections, welded sections of dimensions larger than standard hot-rolled sections, castellated and cellular beams, etc. In the general case, the LTB reduction factor is computed as follows

$$\chi_{LT} = \frac{1}{\Phi_{LT} + \sqrt{\Phi_{LT}^2 - \bar{\lambda}_{LT}^{\,2}}} \leq 1.0 \tag{6.10}$$

in which

$$\Phi_{LT} = 0.5\left[1 + \alpha_{LT}\left(\bar{\lambda}_{LT} - 0.2\right) + \bar{\lambda}_{LT}^{\,2}\right] \tag{6.11}$$

and

$$\bar{\lambda}_{LT} = \sqrt{\frac{W_y f_y}{M_{cr}}} \tag{6.12}$$

is the non-dimensional slenderness, where:

α_{LT} is the imperfection factor provided in Table 6.1

$\bar{\lambda}_{LT}$ is the non-dimensional slenderness for lateral-torsional buckling

M_{cr} is the theoretical elastic LTB moment.

The equation for M_{cr} is not given in EC3. Users are expected to use the appropriate equation from available references (Nethercot & Gardner, 2005).

Table 6.1 Recommended values of LTB imperfection factors (EC3, 2005)

Buckling curve	a	b	c	d
Imperfection factor α_{LT}	0.21	0.34	0.49	0.76

The imperfection factor α_{LT} takes into account the effects of initial geometrical imperfections and residual stresses. EC3 (2005) provides four buckling curves that distinguishes between different cross-section types and the height to width ratios d/b_c (the total cross-section depth is designated by the letter h in EC3). Figure 6.1 shows the four buckling curves as a function of the reduction factor χ_{LT} and the non-dimensional slenderness $\bar{\lambda}_{LT}$. This figure can also be used to quickly determine the values of χ_{LT} for the appropriate non-dimensional slenderness $\bar{\lambda}_{LT}$ for each buckling curve. Table 6.2 shows the recommended LTB curves for the general case.
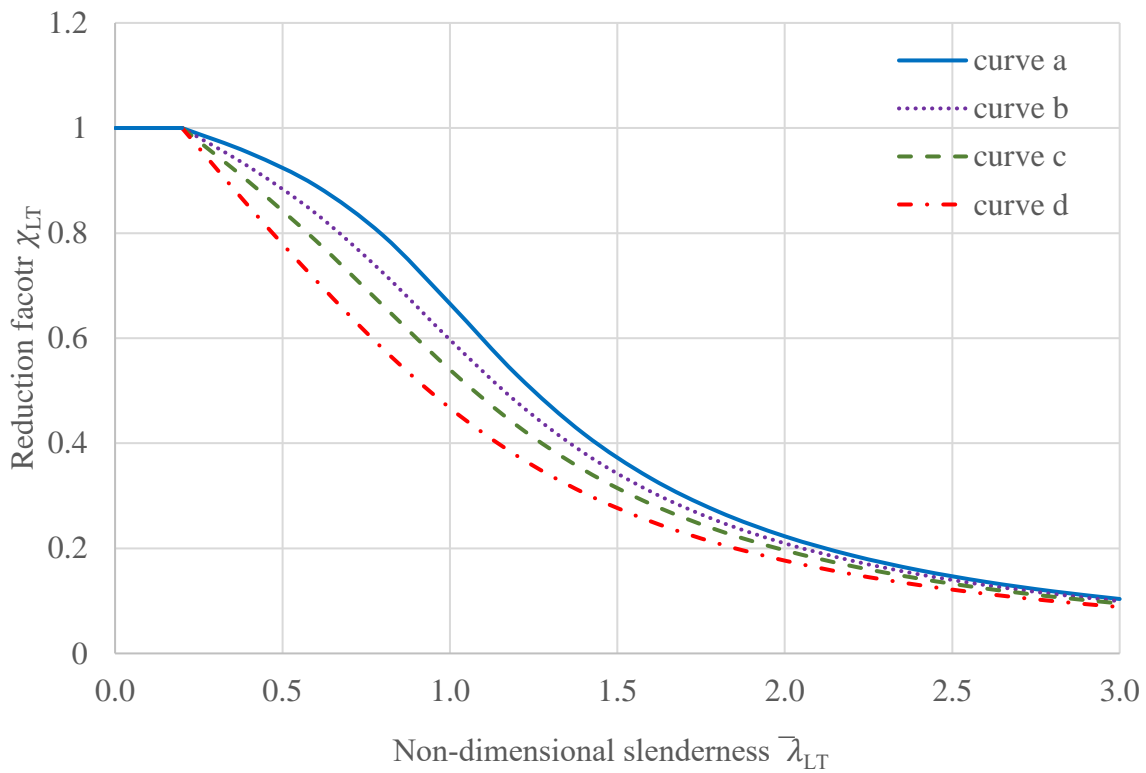
Figure 6.1 LTB buckling curves in EC3 (2005)

Table 6.2 Recommended LTB curves for the general case

Cross-section	Limits	Buckling curve
Rolled I-sections	$d/b_c \leq 2$	a
	$d/b_c > 2$	b
Welded I-sections	$d/b_c \leq 2$	c
	$d/b_c > 2$	d
Other cross-sections	-	d

For the rolled sections or equivalent welded sections case, the reduction factor is computed using the following expression

$$\chi_{LT} = \frac{1}{\Phi_{LT} + \sqrt{\Phi_{LT}^2 - \beta\bar{\lambda}_{LT}^2}} \leq \begin{cases} 1.0 \\ 1/\bar{\lambda}_{LT}^2 \end{cases} \tag{6.13}$$

in which

$$\Phi_{LT} = 0.5\left[1 + \alpha_{LT}(\bar{\lambda}_{LT} - \bar{\lambda}_{LT,0}) + \beta\bar{\lambda}_{LT}^2\right] \tag{6.14}$$

where the recommended values of the parameters $\bar{\lambda}_{LT,0}$ and β are 0.4 (maximum value) and 0.75 (minimum value), respectively. EC3 notes that other values for these parameters in addition to the d/b_c ratio can be validated and included in the National Annex. The National Annex is prepared by Eurocodes Committee and is nationally used in conjunction with EC3.

The recommended LTB curves for rolled sections and equivalent welded sections are provided in Table 6.3. For slenderness $\bar{\lambda}_{LT} \leq \bar{\lambda}_{LT,0}$, the section should be designed for its full plastic moment M_p. Figure 6.2 compares the buckling curves of the general and the rolled or equivalent welded sections cases using buckling curve "b". As can be seen, the buckling curve for rolled sections or equivalent welded sections provides higher buckling capacity. Additionally,

the case for rolled sections or equivalent welded sections provides a longer plateau region and savings in calculation efforts (Nethercot & Gardner, 2005). The main differences between the two LTB cases in EC3 can be summarized as follows:

- The general case has a higher reduction factor α_{LT} and hence lower buckling resistance curves

- The general case provides a shorter plateau region with $\bar{\lambda}_{LT,0}$ value of 0.2 as can be seen in Figure 6.2

- The general case provides the option of "other cross-section" which can be used for beams that are not rolled or welded I-sections.

Table 6.3 Recommended LTB curves for rolled sections and equivalent welded sections case (EC3, 2005)

Cross-section	Limits	Buckling curve
Rolled I-sections	$d/b_c \leq 2$	b
	$d/b_c > 2$	c
Welded I-sections	$d/b_c \leq 2$	c
	$d/b_c > 2$	d
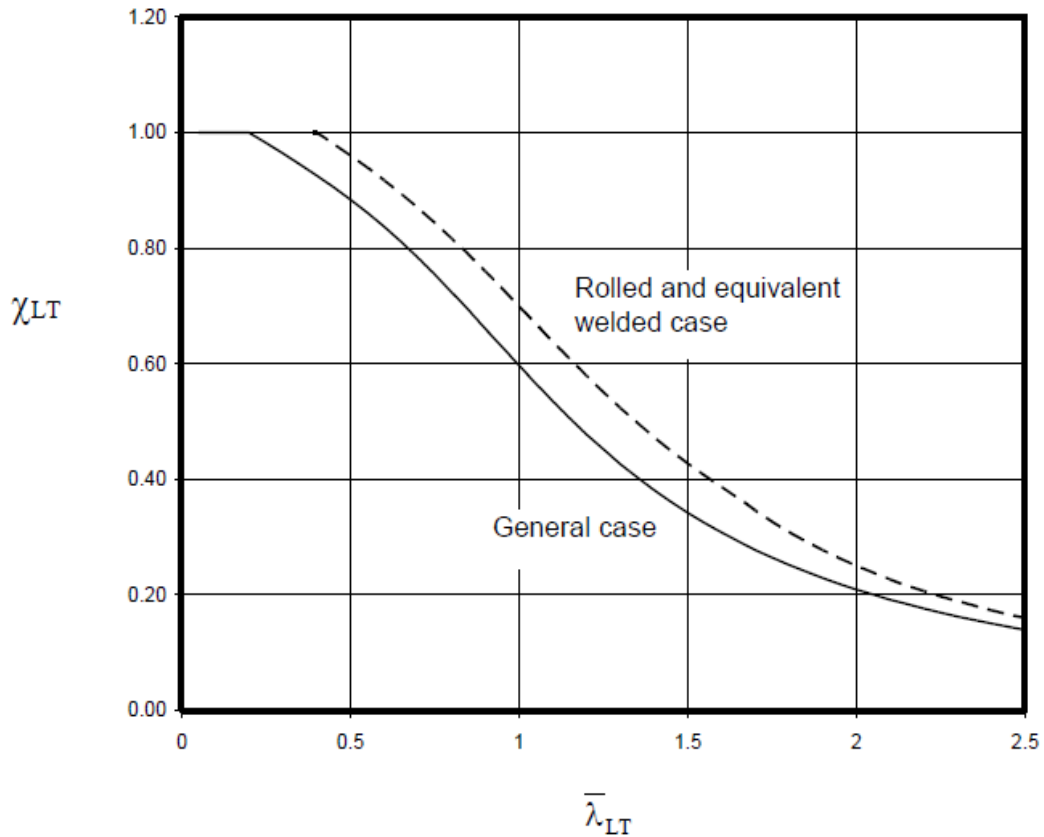
Figure 6.2 Comparison between LTB curves of general case and rolled or equivalent welded

sections (Nethercot & Gardner, 2005)

6.2.3   Comparison between AISC and EC3 LTB curves

From the aforementioned discussions, the main differences between the AISC and EC3

flexural resistance curves for beams under uniform moment are:

- After the plastic moment or plateau region, the AISC buckling curve continues into a

  linear inelastic and a nonlinear elastic LTB regions. On the other hand, EC3 provides one

  buckling curve for both inelastic and elastic LTB.

- EC3 provides four buckling curves based on different cross-section types (rolled or welded) and d/b_c ratios. These distinctions are absent in the AISC specifications and their effects on capturing the LTB behavior of beams will be shown in Section 6.4.

- The theoretical elastic buckling moment M_{cr} for monosymmetric beams is calculated in the AISC specifications using the theoretical equation for doubly symmetric beams, while the exact theoretical equation is provided in the AISC (2016b) commentary. However, EC3 does not provide an equation for M_{cr} and expects the user to determine the appropriate equation to use.

- The effect of initial imperfections is not implicitly considered in the AISC specifications but it is explicitly considered in EC3.

- For any given beam under uniform bending, AISC provides larger LTB nominal resistance than EC3. However, this does not show the full picture. Because each standard is calibrated with its corresponding building code and load factors, an additional factor that affects the nominal resistance in each standard is the targeted reliability level and whether it varies with the beam slenderness (Ziemian, 2010).

6.3   The Plastic Section Modulus of Delta Girders

The plastic section modulus about the major x-axis Z_x is required to determine the plastic moment M_p, the inelastic LTB moment in AISC (2016a), and the buckling resistance moment $M_{b.Rd}$ in EC3 (2005). For homogeneous sections, the plastic neutral axis divides the cross-section in such a way that the tension force is equal to the compression force. The plastic section modulus is the first moment of area about the plastic neutral axis (PNA). The Delta girder is assumed to be homogenous, i.e., the entire cross-section has the same yield stress; therefore, the

area above and below the PNA should be equal. The PNA needs to be located before M_p can be

calculated, it is also required to determine the value of h_p in Eq. (6.6) of Section 6.2.1. The

derived equations in this section have been verified using the finite element software

ShapeBuilder. The plastic neutral axis $\bar{y}_p$ of a Delta girder should be computed as $\bar{y}_{p1}$ or $\bar{y}_{p2}$ as

follows

$$\bar{y}_{p1} = \frac{1}{2}\left[(d - t_c + t_t) + \frac{1}{t_w}(b_c t_c - b_t t_t + 2\alpha t_d)\right] \tag{6.15}$$

and if $\bar{y}_{p1} > (d - t_c - h_d)$, the PNA is located within the delta part of the section and should be

computed using the following equation

$$\bar{y}_{p2} = \frac{1}{2t_w \cos\theta + 4t_d}[t_w \cos\theta\,(d - t_c + t_t) + t_d(4d - 2h_d - 4t_c)] \tag{6.16}$$

Once the PNA is located, the plastic section modus Z_x of a Delta girder can be obtained using

the following equation

$$Z_x = (b_t t_t)\left(\bar{y}_p - \frac{t_t}{2}\right) + \frac{t_w}{2}(\bar{y}_p - t_t)^2 + \frac{t_w}{2}(d - \bar{y}_p - t_c)^2$$

$$+ (b_c t_c)\left(d - \bar{y}_p - \frac{t_c}{2}\right) + (2\alpha t_d)\left(d - \bar{y}_p - t_c - \frac{h_d}{2}\right) \tag{6.17}$$

where $\bar{y}_p$ is the controlling value obtained from Eq. (6.15) or (6.17), and all the remaining

notations can be found in Table 3.13.

6.4   Finite Element Analysis Results

6.4.1   Girder configurations and variables

To determine the LTB capacity curves of Delta girders, a series of FE simulations were

conducted using the procedure described in Section 5.2. The proposed residual stress pattern

presented in Section 5.2.3 with full magnitude and maximum initial geometrical imperfections of

$L_b/1000$ were included in all the FE models. Ten Delta girders were selected from Section 4.2.5

to cover a range of d/b_c ratios and four practical configurations for delta stiffeners. The initial I-

sections, on which the delta stiffeners are welded, were assumed to be welded sections with

dimensions based on European standard H- or I-sections. These sections are classified as

compact sections or Class 1 sections as defined in Section 6.2.2. To avoid local buckling, the

thickness of the delta stiffeners for each Delta girder was selected to be greater than or equal to

the web thickness. The dimensions and the d/b_c ratios for the ten sections are provided in Table

6.4. Furthermore, the following variables are considered in this study:

- Each Delta girder is modeled with 8 to 12 different unbraced lengths in order to obtain

  the full flexural resistance curve. The lengths are selected to cover the plastic moment

  region, the inelastic LTB and the elastic LTB regions in accordance with AISC (2016a)

  definitions of these three regions as explained in Section 6.2.1.

- For Delta girders 5 to 12, two base sections (IPE 550 and HEA 400) are modeled with

  four different delta stiffener configurations to evaluate whether the configuration affects

  the buckling curve.

- Five of the selected Delta girders have a d/b_c ratio smaller than 2 and five have a ratio

  larger than 2 to assess the effect of this ratio as per EC3 (2005).

Table 6.4 Dimensions of Delta girders used in FE analysis

Delta girder no.	Base section	d/b_c	b_d	h_d	t_d (mm)
3	IPE 360	2.12	$b_c/2$	$h/3$	8
5	IPE 550	2.62	$b_c/2$	$h/5$	12
6	IPE 550	2.62	$2b_c/3$	$h/5$	12
7	IPE 550	2.62	$b_c/2$	$h/3$	12
8	IPE 550	2.62	$2b_c/3$	$h/3$	12
9	HEA 400	1.3	$b_c/2$	$h/5$	12
10	HEA 400	1.3	$2b_c/3$	$h/5$	12
11	HEA 400	1.3	$b_c/2$	$h/3$	12
12	HEA 400	1.3	$2b_c/3$	$h/3$	12
16	HEA 600	1.97	$2b_c/3$	$h/3$	14

6.4.2   FE simulation results

Figure 6.3 to 6.12 show the FE analysis results for the ten Delta girders. The small triangles

represent the data pints at the various unbraced lengths. Also shown in these figures are five

flexural resistance curves. One of the flexural resistance curves is based on the AISC (2016a)

specifications and is obtained using the equations of Section 6.2.1. The remaining four flexural

resistance curves represent the four EC3 (2005) curves for rolled sections or equivalent welded

sections as discussed in Section 6.2.2. For all curves, the theoretical elastic LTB moments are

computed using Eqs. (2.3) and (2.5). The EC3 general case is not computed as it provides

conservative results in comparison with the rolled sections or equivalent sections case. Table 6.5

to 6.14 show the statistics when the FE simulation results are compared to the nominal flexural

resistance calculated based on AISC (2016a) and EC3 (2005). The comparison is made based on

the ratio of the FE simulation flexural capacity M_{FEM} over the nominal flexural capacity M_n at each unbraced length. The statistics include the mean, standard deviation (STD), coefficient of variation (COV), maximum (Max) and minimum (Min) values of M_{FEM}/M_n for all computed L_b values for each Delta girder.

Based on these results, the following observations are made:

- The AISC (2016a) nominal resistance curve in the LTB region overestimates the flexural capacity of all Delta girders in both the inelastic and elastic ranges. The results show a larger error for cases where d/b_c is larger than 2.

- The maximum difference between the AISC (2016a) and FE simulation flexural resistance curves is obtained at an unbraced length equal to L_r. Moreover, it can be seen that the elastic LTB curve overestimates the buckling capacity in the elastic range and hence the current L_r equation in AISC (2016a) is unconservative for the design of Delta girders.

- The shape of the FE flexural resistance curves and that of EC3 (2005) seems to be in good agreement. This is mainly because the EC3 resistance curves are numerically calibrated.

- The EC3 (2005) curves "a" and "b" corresponding to rolled sections or equivalent welded sections case appear to represent the buckling curves of all tested Delta girders well.

- For short Delta girders inside the plateau region, the FE simulation results are within 2% of the plastic moment M_p for all sections analyzed.

- The widths of the plateau region obtained using AISC (2016a) and EC3 (2005) are very close to each other. The FE simulation results show good agreement with

recommendations provided in both codes. Exceptions do exist for three Delta girders (5, 6, 9) where both codes slightly overestimate the extent of the plateau region.

- A comparison between the AISC (2016a) and EC3 (2005) curves and the FE simulation results for all analyzed Delta girders is provided in Table 6.15. On average, AISC overestimates the buckling capacity by 9%. The maximum and minimum differences are 21% (unconservative) and 2% (conservative), respectively. On the other hand, EC3 curves "c" and "d" predict the buckling moment with averages of 10% (conservative) and 23% (conservative), respectively. Buckling curves "a" and "b" provide the best results with average values of 6% (unconservative) and 2% (conservative), respectively.
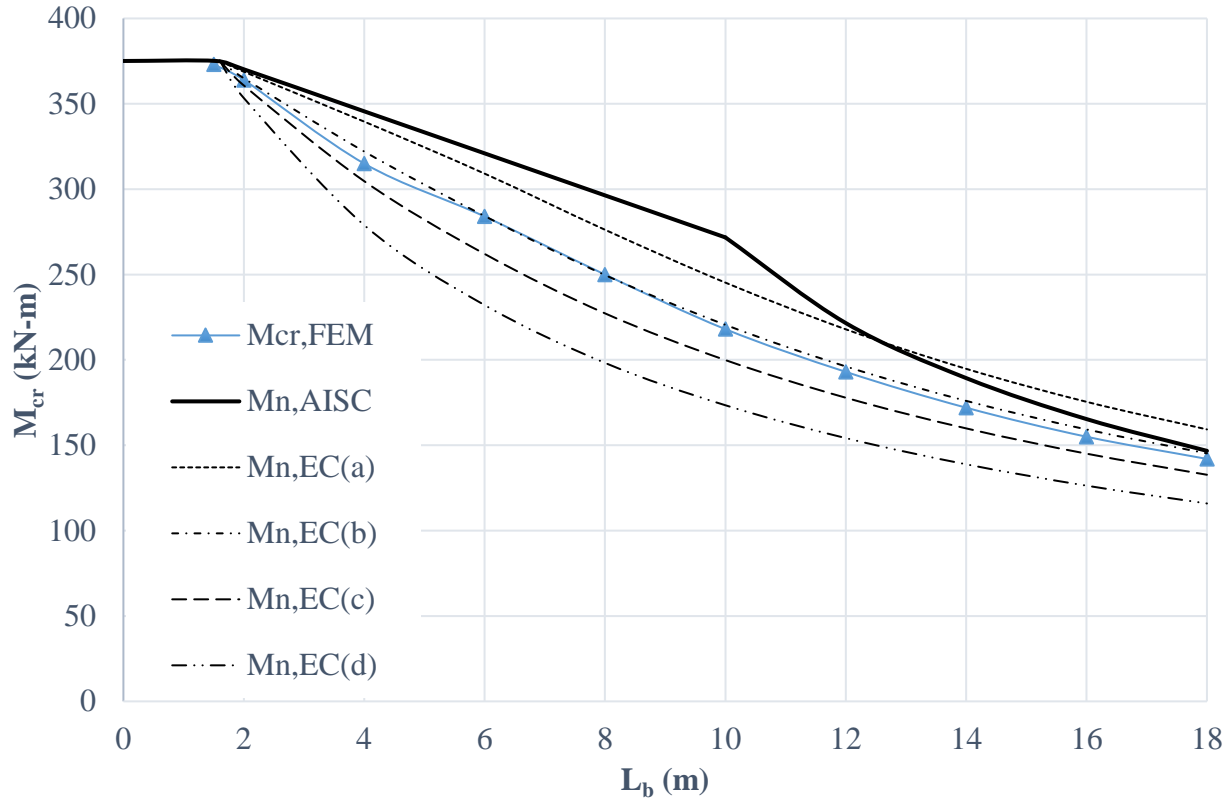
Figure 6.3 Comparison between FE simulations, AISC (2016a) and EC3 (2005) flexural

resistance curves for Delta girder 3

Table 6.5 Statistics for LTB capacity comparison for Delta girder 3

Statistics	$M_{FEM}/M_{EC(a)}$	$M_{FEM}/M_{EC(b)}$	$M_{FEM}/M_{EC(c)}$	$M_{FEM}/M_{EC(d)}$	M_{FEM}/M_{AISC}
Mean	0.91	0.99	1.07	1.20	0.90
STD	0.03	0.01	0.03	0.07	0.05
COV	0.04	0.01	0.03	0.06	0.06
Max	0.99	1.00	1.10	1.26	0.98
Min	0.88	0.97	1.01	1.03	0.80
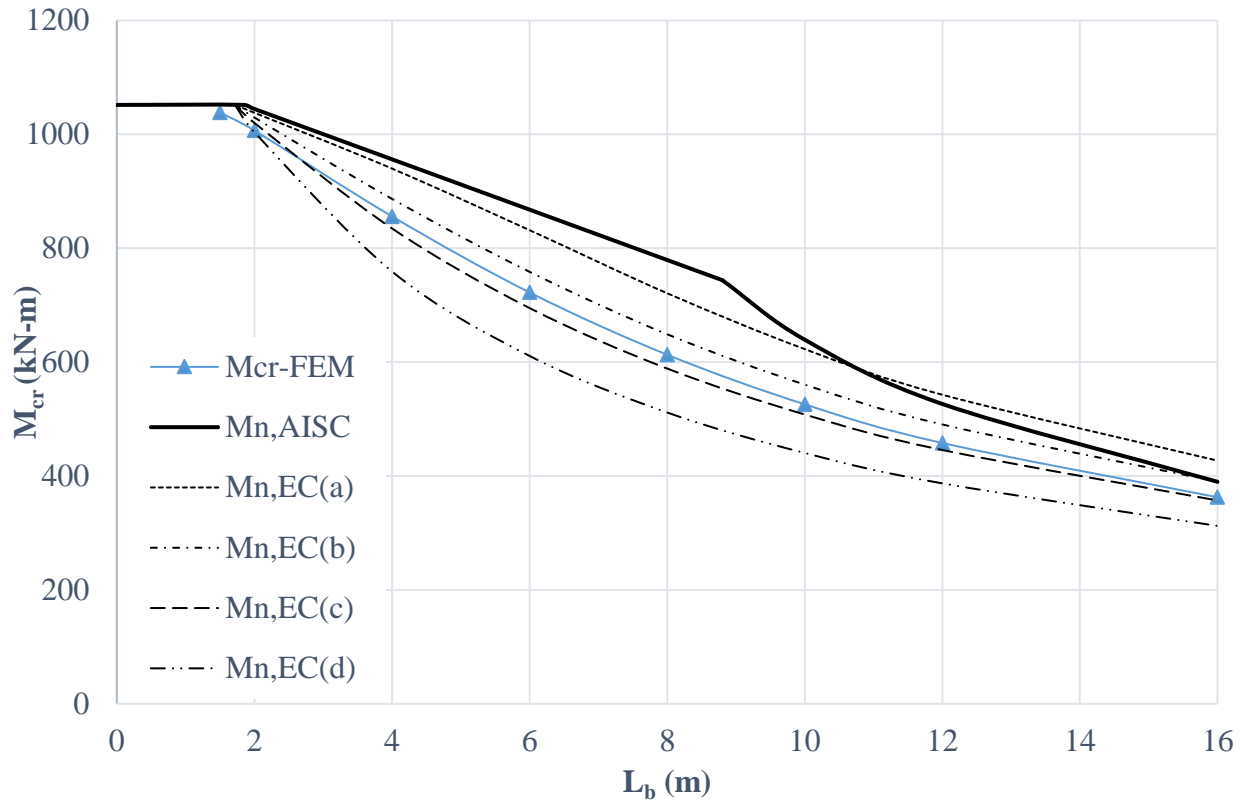
Figure 6.4 Comparison between FE simulations, AISC (2016a) and EC3 (2005) flexural

resistance curves for Delta girder 5

Table 6.6 Statistics for LTB capacity comparison for Delta girder 5

Statistics	$M_{FEM}/M_{EC(a)}$	$M_{FEM}/M_{EC(b)}$	$M_{FEM}/M_{EC(c)}$	$M_{FEM}/M_{EC(d)}$	M_{FEM}/M_{AISC}
Mean	0.88	0.95	1.02	1.15	0.87
STD	0.04	0.02	0.02	0.06	0.06
COV	0.05	0.02	0.02	0.06	0.07
Max	0.97	0.98	1.04	1.20	0.96
Min	0.84	0.93	0.99	1.00	0.79

Figure 6.5 Comparison between FE simulations, AISC (2016a) and EC3 (2005) flexural

resistance curves for Delta girder 6

Table 6.7 Statistics for LTB capacity comparison for Delta girder 6

Statistics	$M_{FEM}/M_{EC(a)}$	$M_{FEM}/M_{EC(b)}$	$M_{FEM}/M_{EC(c)}$	$M_{FEM}/M_{EC(d)}$	M_{FEM}/M_{AISC}
Mean	0.89	0.97	1.05	1.18	0.89
STD	0.03	0.01	0.03	0.08	0.05
COV	0.04	0.01	0.03	0.07	0.06
Max	0.98	0.98	1.08	1.24	0.98
Min	0.87	0.95	0.98	0.99	0.80

Figure 6.6 Comparison between FE simulations, AISC (2016a) and EC3 (2005) flexural

resistance curves for Delta girder 7

Table 6.8 Statistics for LTB capacity comparison for Delta girder 7

Statistics	$M_{FEM}/M_{EC(a)}$	$M_{FEM}/M_{EC(b)}$	$M_{FEM}/M_{EC(c)}$	$M_{FEM}/M_{EC(d)}$	M_{FEM}/M_{AISC}
Mean	0.92	0.99	1.06	1.18	0.89
STD	0.04	0.01	0.03	0.08	0.06
COV	0.05	0.01	0.03	0.07	0.07
Max	1.00	1.00	1.09	1.24	1.00
Min	0.87	0.96	1.00	1.00	0.81

Figure 6.7 Comparison between FE simulations, AISC (2016a) and EC3 (2005) flexural

resistance curves for Delta girder 8

Table 6.9 Statistics for LTB capacity comparison for Delta girder 8

Statistics	$M_{FEM}/M_{EC(a)}$	$M_{FEM}/M_{EC(b)}$	$M_{FEM}/M_{EC(c)}$	$M_{FEM}/M_{EC(d)}$	M_{FEM}/M_{AISC}
Mean	0.95	1.01	1.08	1.19	0.92
STD	0.04	0.01	0.04	0.09	0.06
COV	0.04	0.01	0.03	0.08	0.07
Max	1.01	1.02	1.11	1.28	1.01
Min	0.90	1.00	1.01	1.01	0.82

Figure 6.8 Comparison between FE simulations, AISC (2016a) and EC3 (2005) flexural

resistance curves for Delta girder 9

Table 6.10 Statistics for LTB capacity comparison for Delta girder 9

Statistics	$M_{FEM}/M_{EC(a)}$	$M_{FEM}/M_{EC(b)}$	$M_{FEM}/M_{EC(c)}$	$M_{FEM}/M_{EC(d)}$	M_{FEM}/M_{AISC}
Mean	0.96	1.04	1.13	1.28	0.89
STD	0.01	0.03	0.06	0.11	0.06
COV	0.01	0.03	0.05	0.08	0.07
Max	0.98	1.08	1.19	1.37	0.99
Min	0.95	1.00	1.02	1.05	0.80
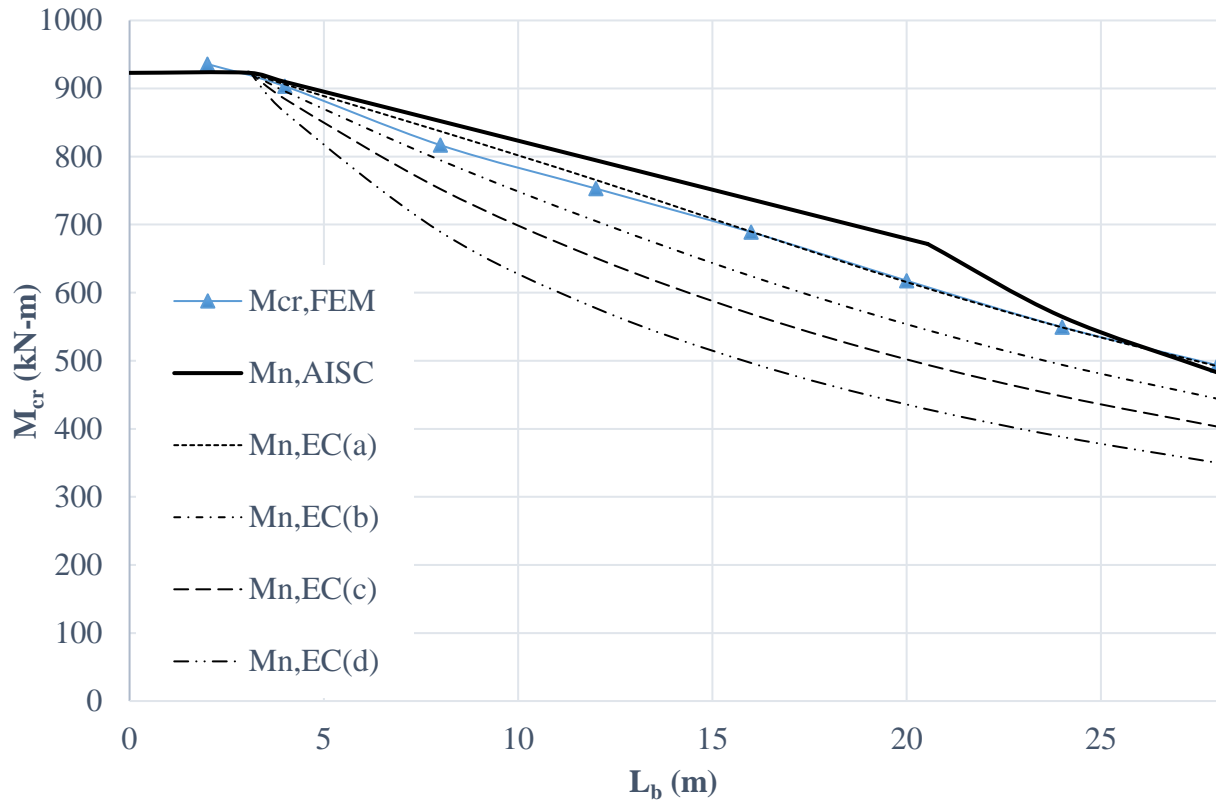
Figure 6.9 Comparison between FE simulations, AISC (2016a) and EC3 (2005) flexural

resistance curves for Delta girder 10

Table 6.11 Statistics for LTB capacity comparison for Delta girder 10

Statistics	$M_{FEM}/M_{EC(a)}$	$M_{FEM}/M_{EC(b)}$	$M_{FEM}/M_{EC(c)}$	$M_{FEM}/M_{EC(d)}$	M_{FEM}/M_{AISC}
Mean	0.99	1.08	1.17	1.31	0.96
STD	0.01	0.04	0.08	0.13	0.03
COV	0.01	0.04	0.07	0.10	0.04
Max	1.00	1.12	1.23	1.42	1.02
Min	0.98	1.01	1.02	1.04	0.91
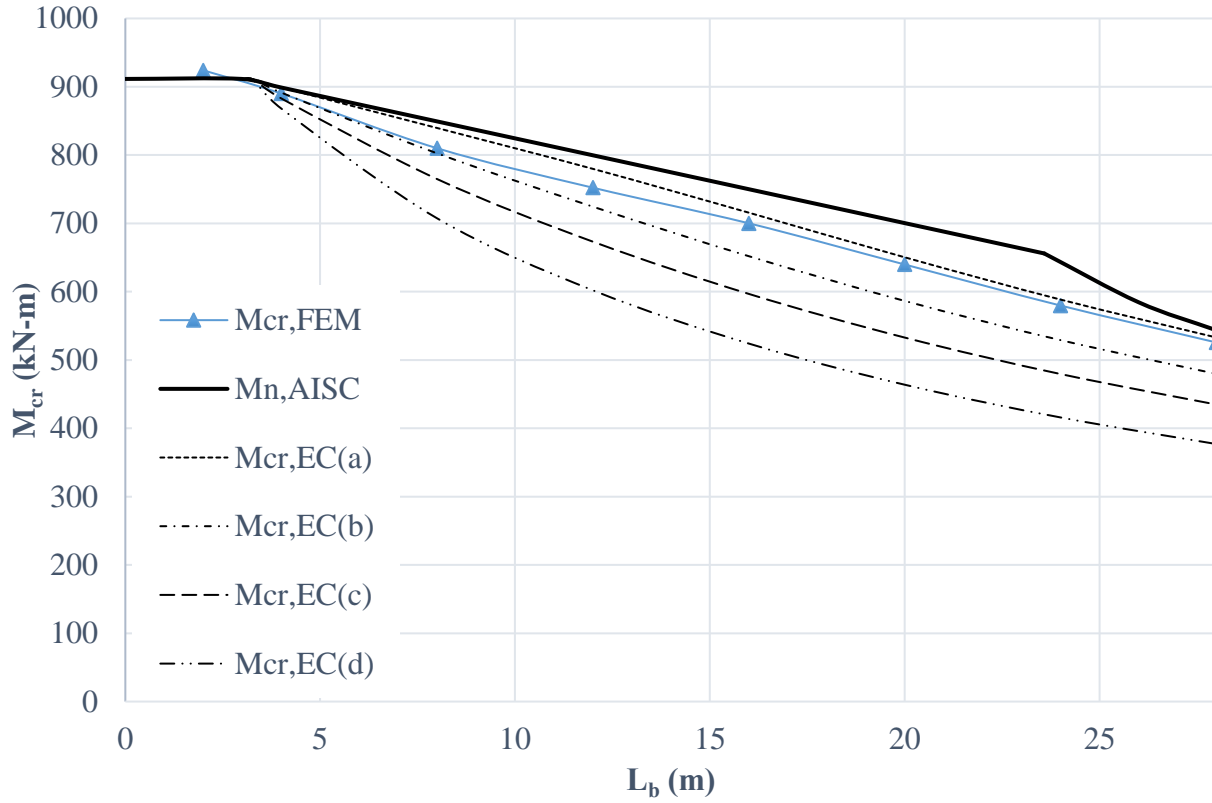
Figure 6.10 Comparison between FE simulations, AISC (2016a) and EC3 (2005) flexural

resistance curves for Delta girder 11

Table 6.12 Statistics for LTB capacity comparison for Delta girder 11

Statistics	$M_{FEM}/M_{EC(a)}$	$M_{FEM}/M_{EC(b)}$	$M_{FEM}/M_{EC(c)}$	$M_{FEM}/M_{EC(d)}$	M_{FEM}/M_{AISC}
Mean	0.98	1.06	1.14	1.27	0.94
STD	0.01	0.04	0.07	0.13	0.03
COV	0.01	0.04	0.07	0.10	0.03
Max	0.99	1.10	1.21	1.39	0.99
Min	0.96	1.00	1.01	1.03	0.91
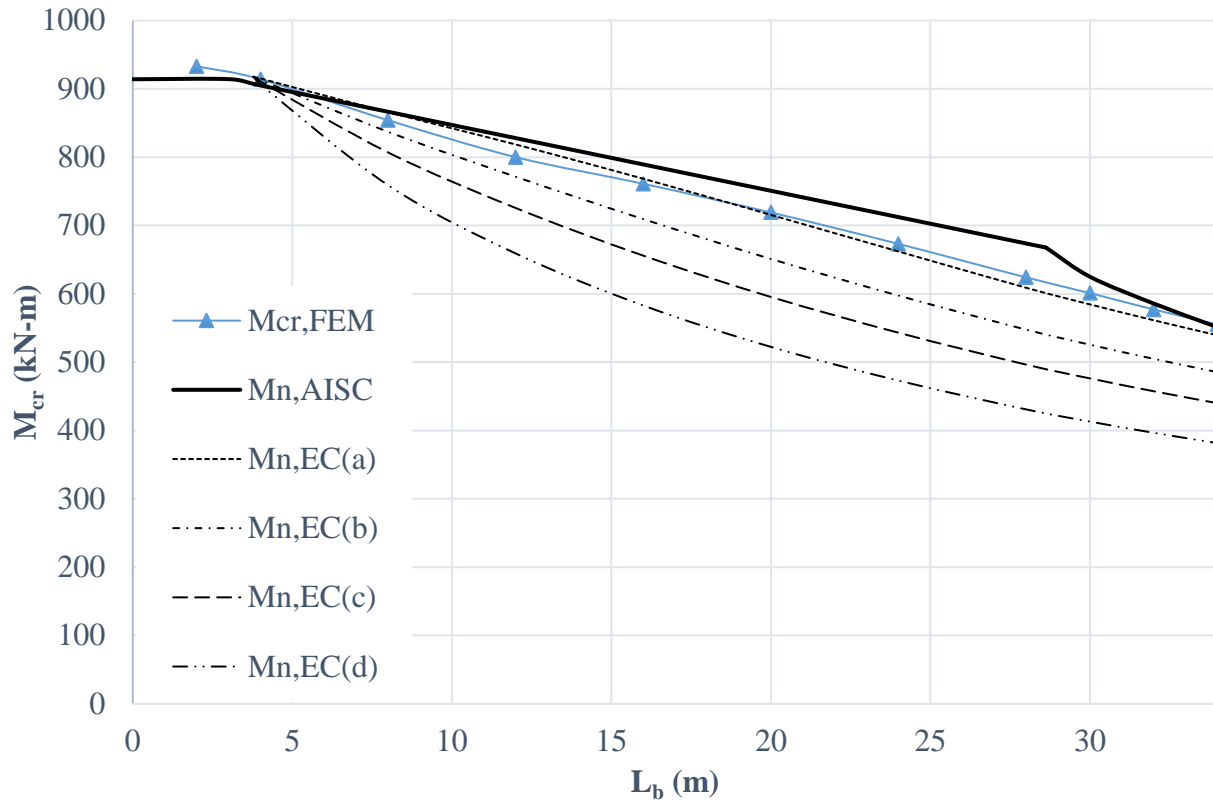
Figure 6.11 Comparison between FE simulations, AISC (2016a) and EC3 (2005) flexural

resistance curves for Delta girder 12

Table 6.13 Statistics for LTB capacity comparison for Delta girder 12

Statistics	$M_{FEM}/M_{EC(a)}$	$M_{FEM}/M_{EC(b)}$	$M_{FEM}/M_{EC(c)}$	$M_{FEM}/M_{EC(d)}$	M_{FEM}/M_{AISC}
Mean	1.01	1.09	1.18	1.33	0.97
STD	0.02	0.05	0.09	0.15	0.03
COV	0.02	0.05	0.08	0.11	0.03
Max	1.03	1.14	1.26	1.46	1.01
Min	0.98	1.00	1.00	1.01	0.93
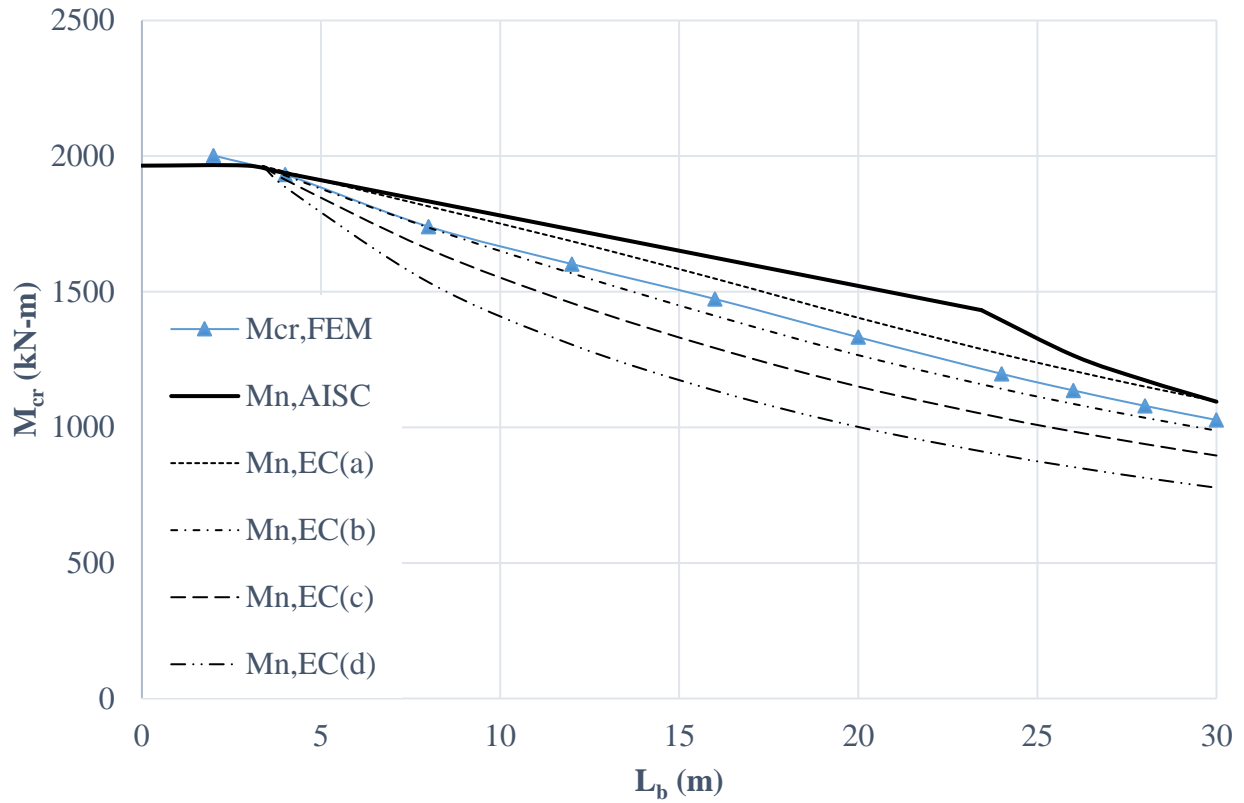
Figure 6.12 Comparison between FE simulations, AISC (2016a) and EC3 (2005) flexural

resistance curves for Delta girder 16

Table 6.14 Statistics for LTB capacity comparison for Delta girder 16

Statistics	$M_{FEM}/M_{EC(a)}$	$M_{FEM}/M_{EC(b)}$	$M_{FEM}/M_{EC(c)}$	$M_{FEM}/M_{EC(d)}$	M_{FEM}/M_{AISC}
Mean	0.95	1.03	1.12	1.26	0.92
STD	0.02	0.02	0.05	0.10	0.04
COV	0.02	0.02	0.05	0.08	0.04
Max	0.99	1.05	1.16	1.33	1.00
Min	0.94	1.00	1.01	1.02	0.87

Table 6.15 Summary comparison between FE simulations, AISC (2016a) and EC3 (2005) LTB

capacity for Delta girders

Statistics	$M_{FEM}/M_{EC(a)}$	$M_{FEM}/M_{EC(b)}$	$M_{FEM}/M_{EC(c)}$	$M_{FEM}/M_{EC(d)}$	M_{FEM}/M_{AISC}
Mean	0.94	1.02	1.10	1.23	0.91
Max	1.03	1.14	1.26	1.46	1.02
Min	0.84	0.93	0.98	0.99	0.79

6.5   Recommended Design Equations for the Flexural Capacity of Delta Girders

White (2008) has discussed the development of the AISC (2016a) flexural resistance curves

through calibrations to experimental data. However, recent studies have shown some

discrepancies between the experimental results and the AISC curves (Righman, 2005) as well as

those results obtained using FE simulations (Subramanian & White, 2015). The discrepancies

manifest themsleves in the inelastic LTB region. Kim (2010) and Subramanian and White (2016,

2017) have attempted to resolve this problem by recommending the following:

- Decreasing the width of the plateau region by reducing L_p.

- Decreasing the value of F_L to a value below $0.7F_y$. This will lead to a reduction in the

  inelastic LTB capacity and an increase in the value of L_r.

- Decreasing the magnitude of initial geometrical imperfections and residual stresses used

  in FE simulations in conjunction with the first two recommendations.

However, the results of Section 6.4.2 have shown that the EC3 (2005) flexural resistance

curves can provide a better fit for the FE simulation results of Delta girders. Therefore, the EC3

flexural resistance curves will be used to represent the flexural capacity of Delta girders. Tables

172

6.16 and 6.17 show a comparison between the EC3 (2005) and AISC (2010a) flexural resistance curves and the FE simulation results based on the indicated d/b_c ratio. Based on these results, it is recommended to use the rolled sections or equivalent welded sections case in EC3 with buckling curve "a" for Class 1 (compact) Delta girders with $d/b_c \leq 2$ and buckling curve "b" for $d/b_c > 2$. These recommendations are summarized in Table 6.18. Both curves predict the LTB capacity of Delta girders with an average error of only 2% (unconservative) when compared with the FE simulation results. The maximum differences are 6% (unconservative) for $d/b_c \leq 2$ and 7% (unconservative) for $d/b_c > 2$. These maximum errors are reached at the largest L_b value used for each Delta girder, i.e., in the elastic range. It is also suggested to use the EC3 recommended values for the parameters $\bar{\lambda}_{LT,0}$ and β since the FE results show good agreement with the plateau region width as discussed in Section 6.4.2. In addition, the results of Delta girders 5 to 12 show that the delta stiffener configurations do not affect the LTB curve selection. Finally, it is worth mentioning that although AISC (2016a) predicts the LTB capacity for Delta girders with $d/b_c \leq 2$ with an average error of 6% (unconservative), the maximum error is 20% (unconservative) in the inelastic LTB region.

Table 6.16 Comparison between FE simulations, AISC (2016a) and EC3 (2005) LTB curves for Delta girders with $d/b_c \leq 2$

Statistics	$M_{FEM}/M_{EC(a)}$	$M_{FEM}/M_{EC(b)}$	$M_{FEM}/M_{EC(c)}$	$M_{FEM}/M_{EC(d)}$	M_{FEM}/M_{AISC}
Mean	0.98	1.06	1.15	1.29	0.94
Max	1.03	1.14	1.26	1.46	1.02
Min	0.94	1.00	1.00	1.01	0.80

Table 6.17 Comparison between FE simulations, AISC (2016a) and EC3 (2005) LTB curves for

Delta girders with $d/b_c > 2$

Statistics	$M_{FEM}/M_{EC(a)}$	$M_{FEM}/M_{EC(b)}$	$M_{FEM}/M_{EC(c)}$	$M_{FEM}/M_{EC(d)}$	M_{FEM}/M_{AISC}
Mean	0.91	0.98	1.06	1.18	0.89
Max	1.01	1.02	1.11	1.28	1.01
Min	0.84	0.93	0.98	0.99	0.79

Table 6.18 Recommendation for using rolled sections or equivalent welded sections case in EC3

(2005) for Delta girders

Cross-section	Limits	Buckling curve
Delta girders	$d/b_c \leq 2$	a
	$d/b_c > 2$	b

6.6   Assessment of the Proposed Equations

The distinction between the recommended flexural resistance curves for Delta girders in Section

6.5 is based on the d/b_c ratio. The Delta girders used in the FE analysis cover a wide range of

d/b_c ratios as shown in Table 6.4. However, it is important to examine the performance of the

recommended flexural resistance curves for cases when d/b_c equals to 2 and for the lowest d/b_c

ratio available in the standard European sections. To do so, the four Delta girders in Table 6.19

were modeled and the comparison curves are presented in Figure 6.13 to 6.16. Table 6.20 to 6.23

show the statistics for the comparison. As per Table 6.18, EC3 buckling curve "a" is

recommended for Delta girders with $d/b_c \leq 2$. The results show that the average difference

between the FE simulation results and buckling curve "a" ranges from 1% (conservative) to 2%

(unconservative). The maximum difference obtained is 5% (unconservative) and 5%

(conservative) for Delta girders 17 and 31, respectively. The results are in good agreement with those of Section 6.4.2. Thus, it is concluded that a value of 2 for the limiting ratio d/b_c works well for Delta girders as well as for I-girders. It is worth noting that the average difference between the AISC LTB curves and the FE simulation results is 4% (unconservative) for these four Delta girders with a maximum difference of 12% (unconservative). This is also in line with the results of Section 6.4.2 where it has been shown that the AISC flexural resistance curve improves as the d/b_c ratio decreases.

Table 6.19 Dimensions of Delta girders used in assessment of proposed model

| Delta girder no.	Base section	d/b	b_d	h_d	t_d (mm)
17	HEA 280	0.96	$b_c/2$	$h/5$	8
24	IPE 240	2.00	$2b_c/3$	$h/3$	8
28	IPE 300	2.00	$2b_c/3$	$h/3$	8
31	HEA 220	0.95	$b_c/2$	$h/3$	8
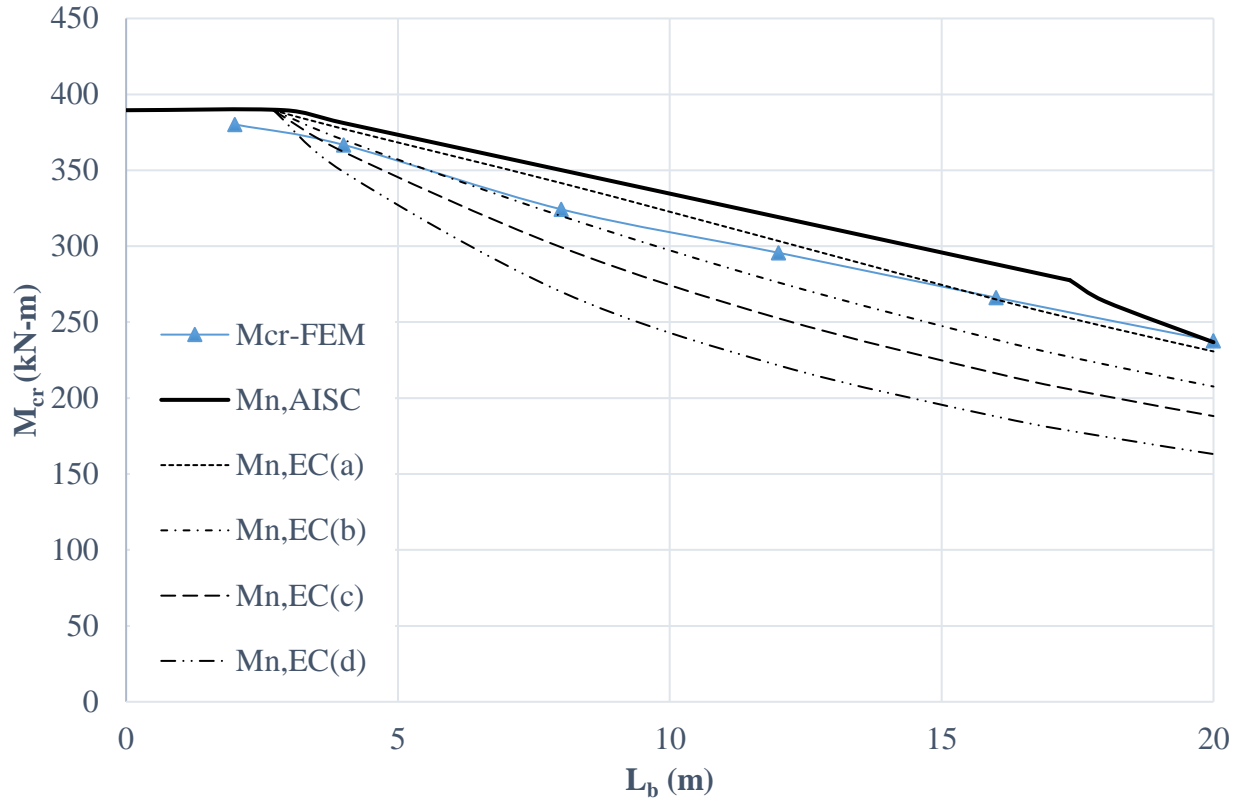
Figure 6.13 Comparison between FE simulations, AISC (2016a) and EC3 (2005) flexural

resistance curves for Delta girder 17

Table 6.20 Statistics for LTB capacity comparison for Delta girder 17

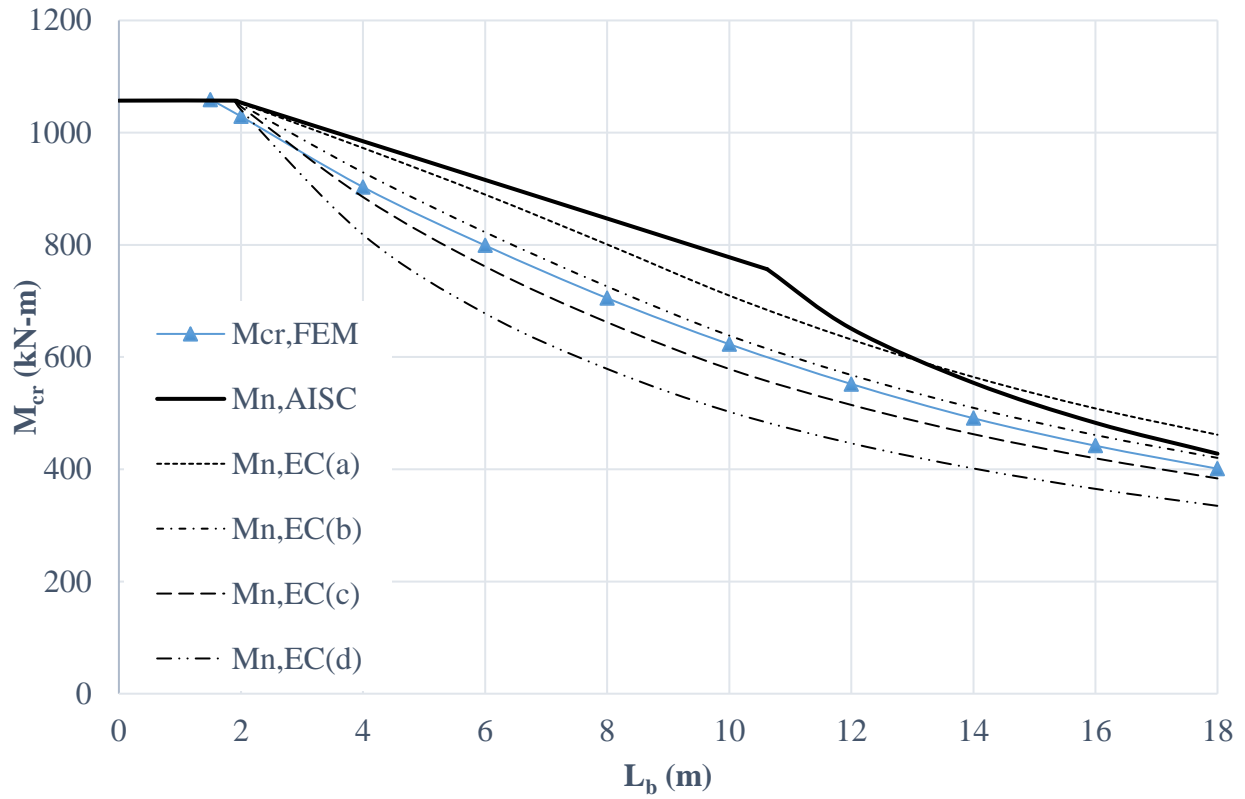| Statistics	$M_{FEM}/M_{EC(a)}$	$M_{FEM}/M_{EC(b)}$	$M_{FEM}/M_{EC(c)}$	$M_{FEM}/M_{EC(d)}$	M_{FEM}/M_{AISC}
Mean	0.99	1.07	1.15	1.29	0.95
STD	0.03	0.06	0.09	0.15	0.03
COV	0.03	0.05	0.08	0.12	0.03
Max	1.03	1.14	1.26	1.46	1.00
Min	0.95	0.99	1.01	1.05	0.92
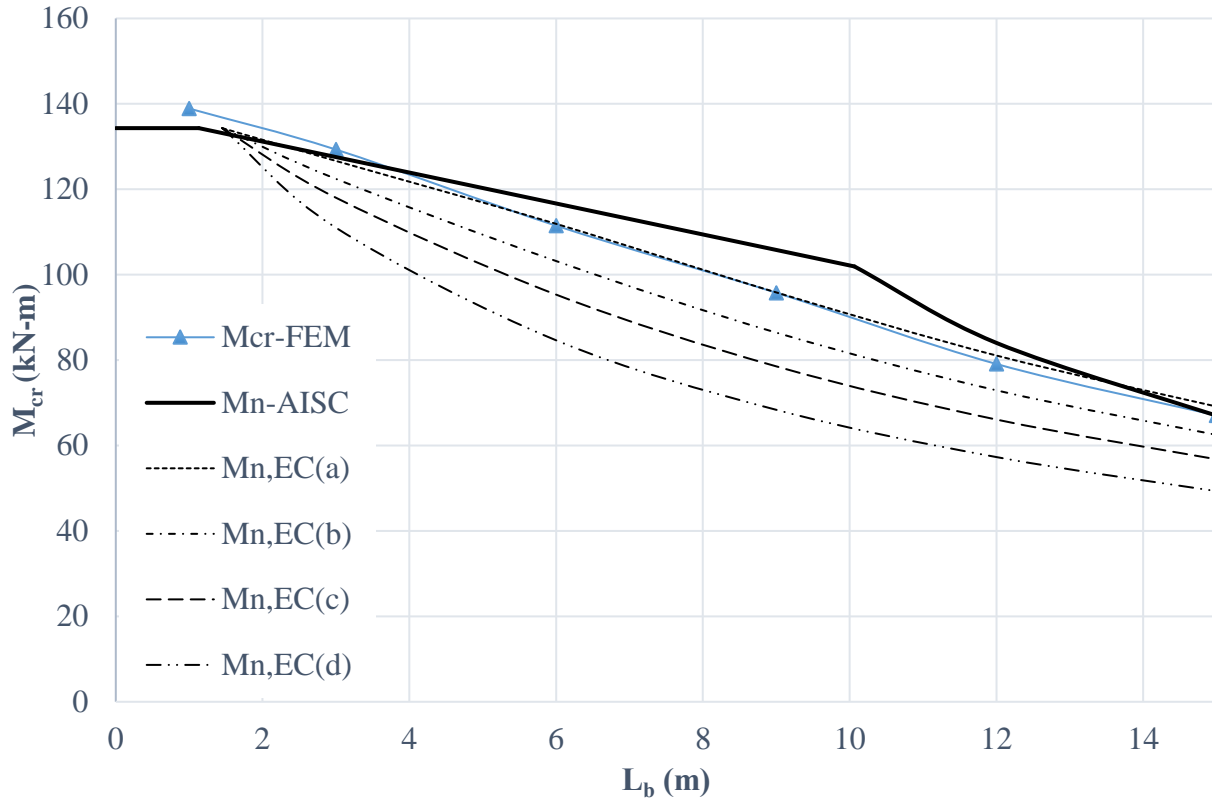
Figure 6.14 Comparison between FE simulations, AISC (2016a) and EC3 (2005) flexural

resistance curves for Delta girder 24

Table 6.21 Statistics for LTB capacity comparison for Delta girder 24

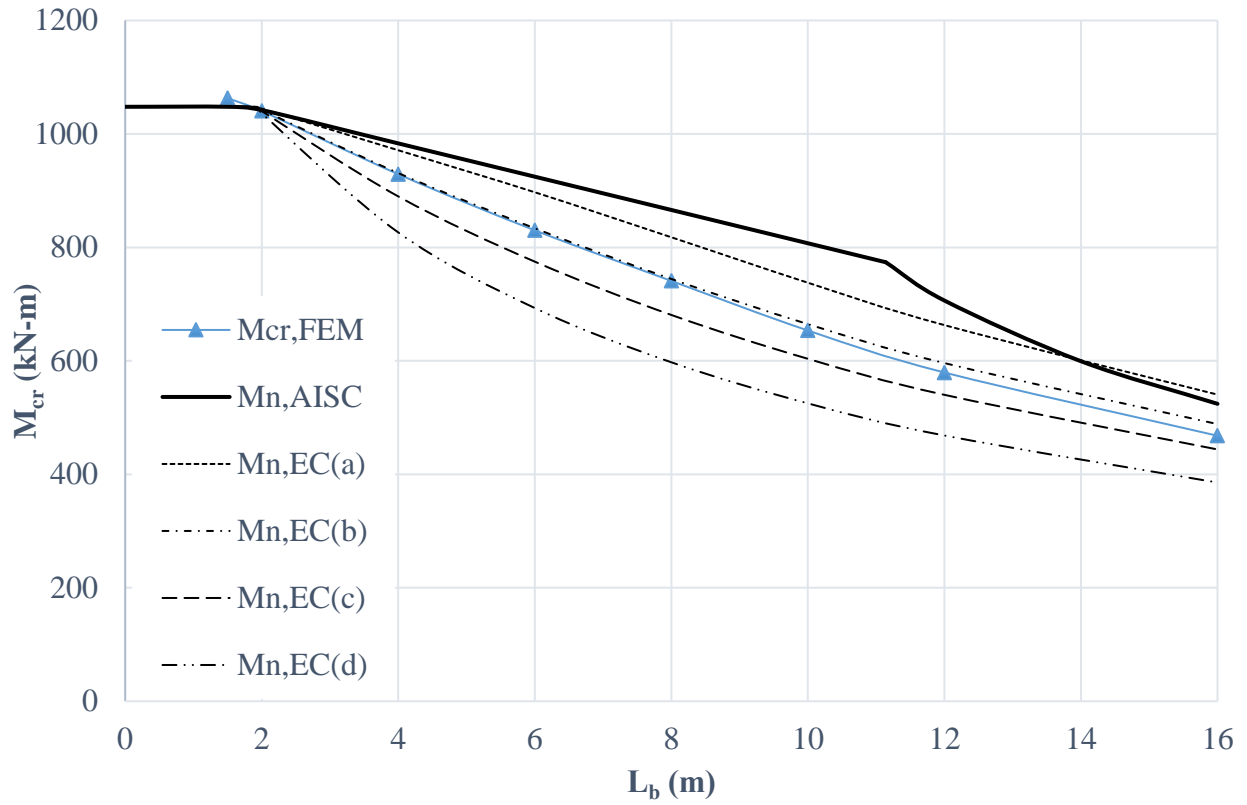| Statistics	$M_{FEM}/M_{EC(a)}$	$M_{FEM}/M_{EC(b)}$	$M_{FEM}/M_{EC(c)}$	$M_{FEM}/M_{EC(d)}$	M_{FEM}/M_{AISC}
Mean	0.99	1.08	1.17	1.32	0.96
STD	0.02	0.02	0.04	0.08	0.04
COV	0.02	0.02	0.04	0.06	0.04
Max	1.02	1.11	1.22	1.40	1.01
Min	0.97	1.06	1.10	1.16	0.91
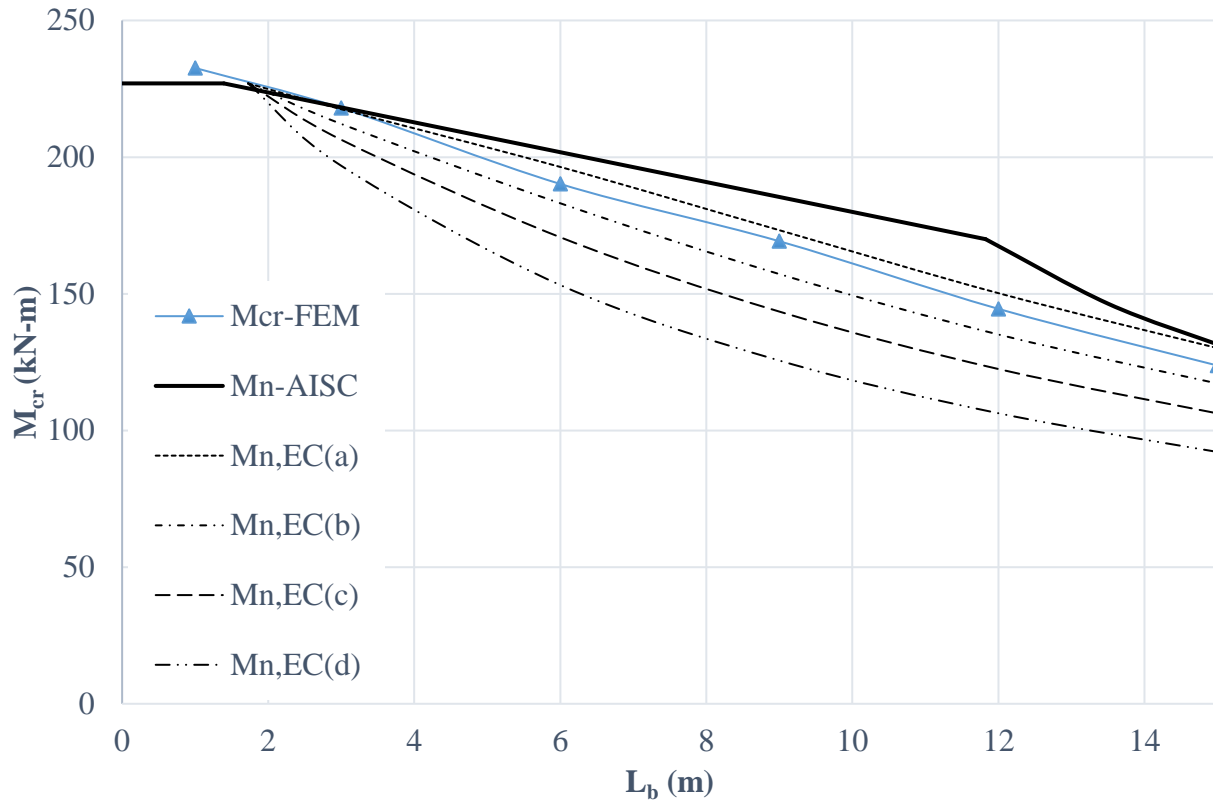
Figure 6.15 Comparison between FE simulations, AISC (2016a) and EC3 (2005) flexural

resistance curves for Delta girder 28

Table 6.22 Statistics for LTB capacity comparison for Delta girder 28

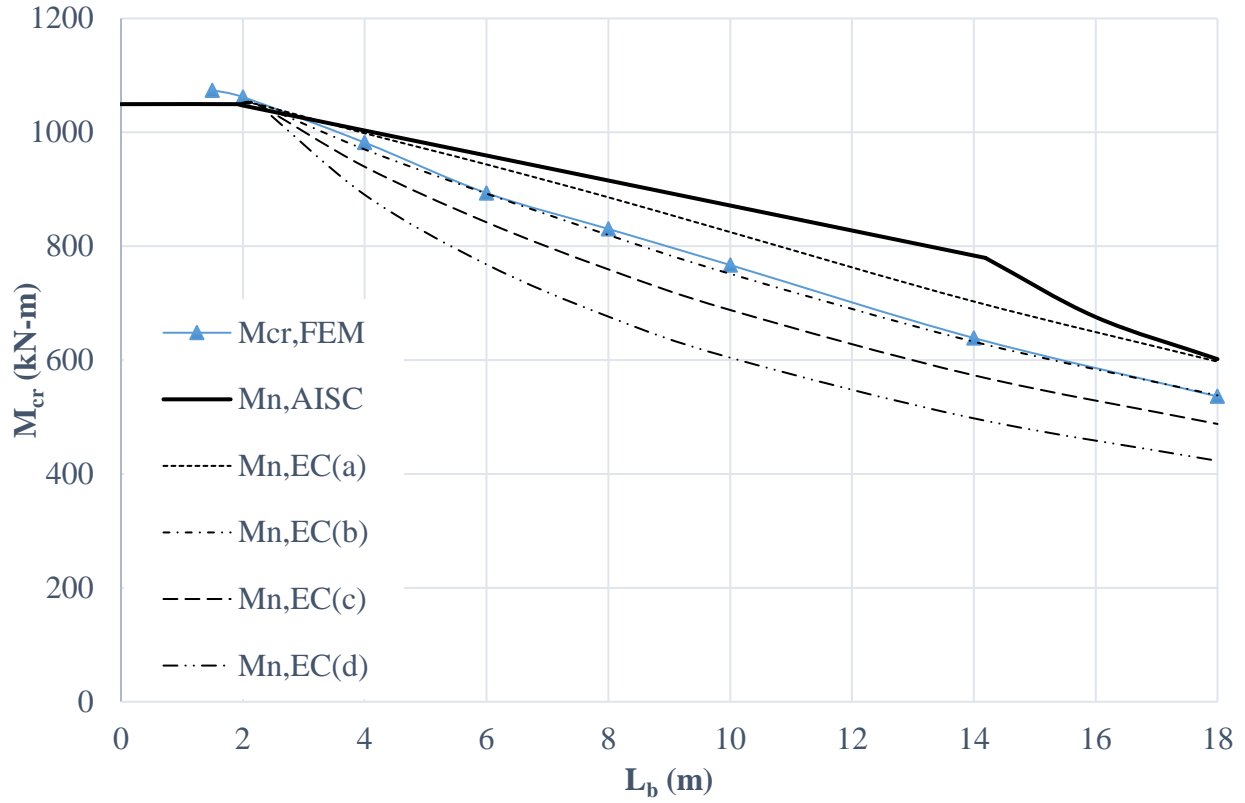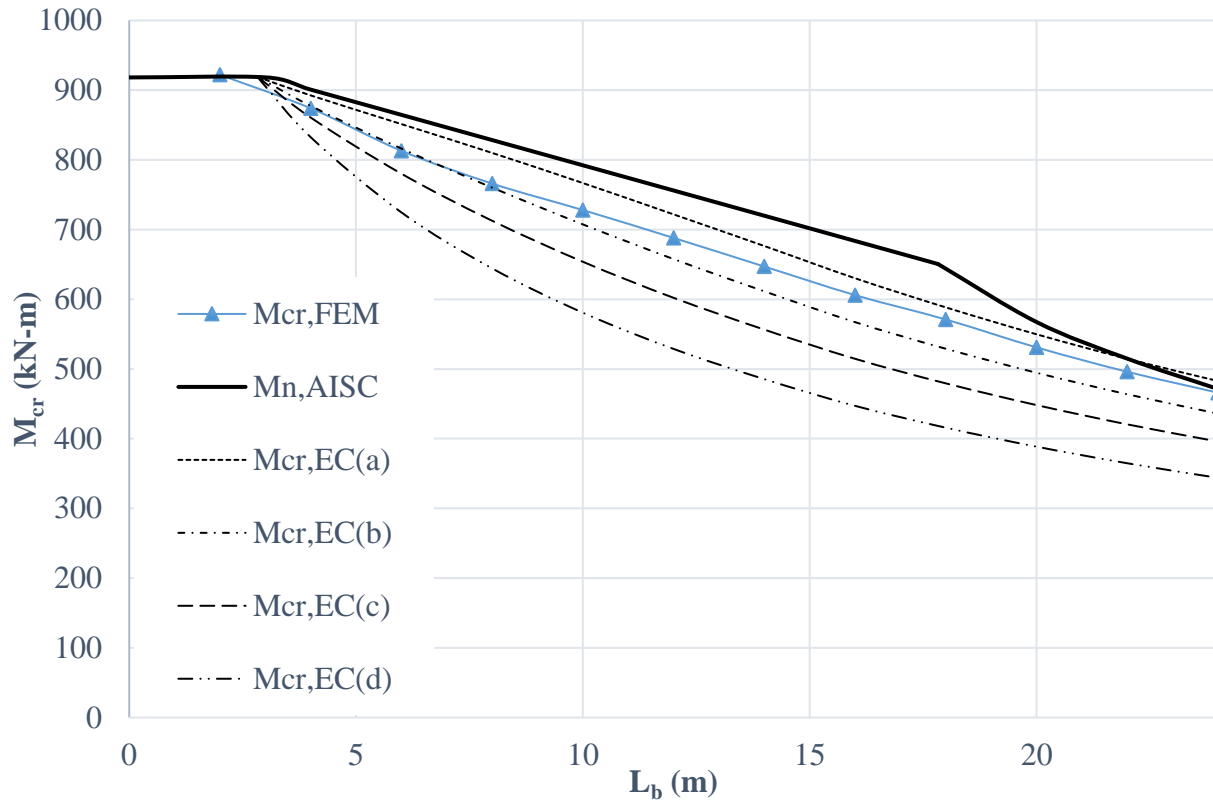| Statistics	$M_{FEM}/M_{EC(a)}$	$M_{FEM}/M_{EC(b)}$	$M_{FEM}/M_{EC(c)}$	$M_{FEM}/M_{EC(d)}$	M_{FEM}/M_{AISC}
Mean	0.98	1.06	1.14	1.29	0.94
STD	0.01	0.02	0.05	0.10	0.04
COV	0.01	0.02	0.04	0.08	0.04
Max	1.00	1.08	1.19	1.37	1.00
Min	0.96	1.03	1.06	1.11	0.88
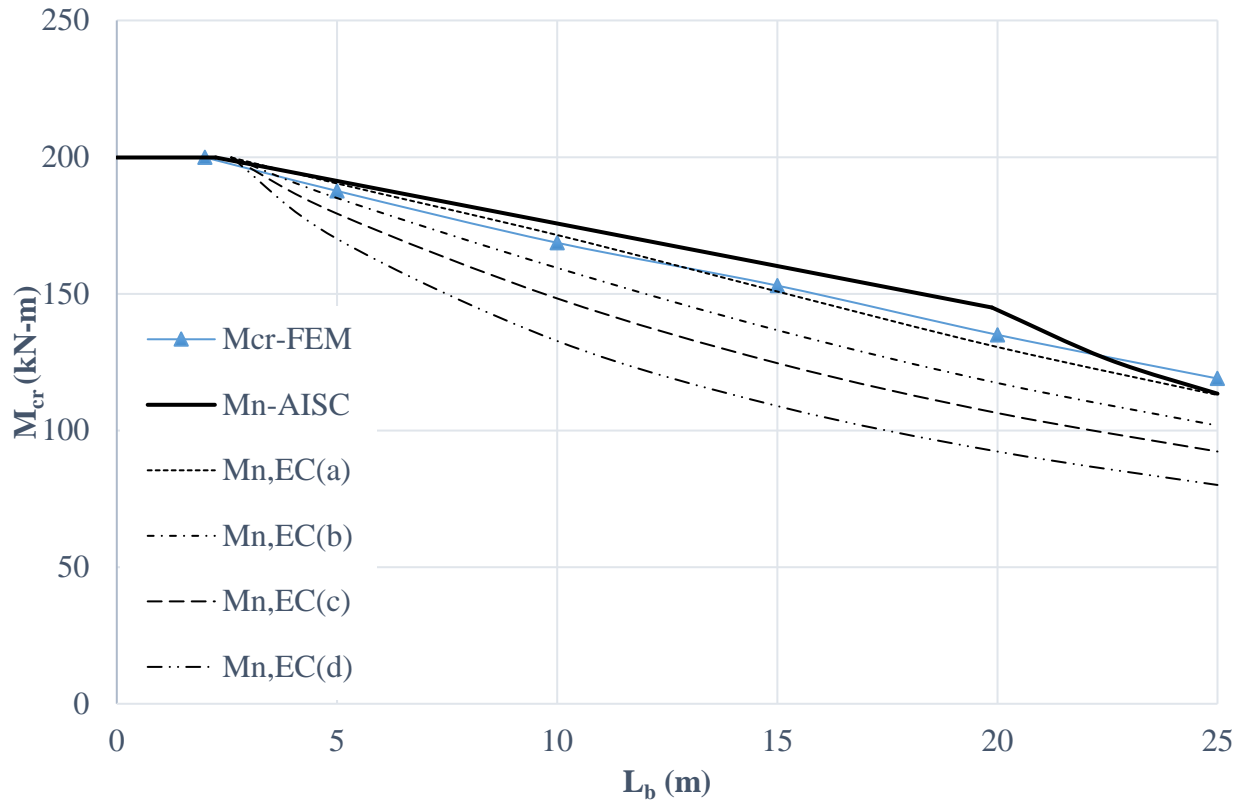
Figure 6.16 Comparison between FE simulations, AISC (2016a) and EC3 (2005) flexural

resistance curves for Delta girder 31

Table 6.23 Statistics for LTB capacity comparison for Delta girder 31

Statistics	$M_{FEM}/M_{EC(a)}$	$M_{FEM}/M_{EC(b)}$	$M_{FEM}/M_{EC(c)}$	$M_{FEM}/M_{EC(d)}$	M_{FEM}/M_{AISC}
Mean	1.01	1.10	1.19	1.35	0.98
STD	0.03	0.06	0.09	0.14	0.04
COV	0.03	0.05	0.08	0.11	0.04
Max	1.05	1.17	1.29	1.49	1.05
Min	0.98	1.01	1.05	1.10	0.95

6.7   Comparison between the Flexural Resistance Curves of Delta Girders and I-girders

The LTB effect of adding delta stiffeners to I-sections will be examined in this section by comparing the LTB capacity of the 16 Delta girders presented in Tables 4.4 and 6.4 with their corresponding welded I-sections. This results in a four standard-size I-sections whereby each one is compared to four Delta girders with different delta stiffener configurations. The buckling curves to represent the flexural capacity of Delta girders are obtained using the recommendations of Section 6.5. On the other hand, the buckling curves for the I-sections are obtained using welded I-sections curves for rolled sections or equivalent welded sections case in EC3 (2005). For a better comparison with the Delta girder, the cross-section type for the I-sections is selected to be equivalent welded sections of standard hot-rolled sections. This is because welded residual stresses are assumed for all sections. The LTB flexural capacity curves are shown in Figure 6.17 to 6.20. Table 6.23 to 6.26 show A^* for each Delta girder as well as M_{cr}^* and κ at different unbraced length L_b. A^* and M_{cr}^* represent the percent increase in cross-section area and LTB capacity, respectively, and are given by Eqs. (4.17) and (4.18). The term "κ" was introduced in Section 4.4 and represents the ratio of M_{cr}^* to A^*. When comparing the LTB capacities of an I-girder to Delta girders with different stiffener configurations, the comparison should be made based on κ values when the most effective design is desired since κ takes into account the increase of the cross-section weight (cost). On the contrary, the comparison should be made based on M_{cr}^* values when maximum increase in LTB capacity of a given section is desired.

The results of the comparison for each I-section are summarized as follows:

- Welded IPE 360: It can be observed that M_{cr}^* increases with an increase of A^* as well as an increase of the unbraced length L_b. The maximum increase in M_{cr}^* is 370% for Delta

180

girder 4 at L_b= 20 m. The delta stiffener configuration of Delta girder 4 $(2b_c/3, h/3)$ provides a 28.2% increase in the cross-section area of the I-section. However, the highest values of κ at every L_b value are reached in Delta girder 2 $(2b_c/3, h/5)$. The highest value of κ is 13.5, which corresponds to M_{cr}^* and A^* values of 262% and 19.5%, respectively.

- Welded IPE 550: The maximum value of M_{cr}^* is 394%, which is obtained for Delta girder 8 at L_b= 20 m. Delta girder 8 $(2b_c/3, h/3)$ increases the cross-section area of IPE 550 by 34.2%. The highest values of κ at every L_b value are reached in Delta girder 6 $(2b_c/3, h/5)$ in a similar way as welded IPE 360. The highest value of κ is 12.5 which corresponds to M_{cr}^* and A^* values of 283% and 22.6%, respectively.

- Welded HEA 400: The maximum values of M_{cr}^* and κ are 255% and 10.8, respectively. Both values are reached for Delta girder 12 at L_b= 25 m. The delta stiffener configuration of Delta girder 12 $(2b_c/3, h/3)$ provides a 23.7% increase in cross-section area of the I-section. However, unlike the IPE sections, the highest values of κ at different unbraced lengths corresponds to different Delta girders. For L_b between 2.5 m and 15 m, the highest values of κ are reached in Delta girder 9 $(b_c/2, h/5)$. For L_b= 20 m, the highest value of κ is reached in Delta girder 10 $(2b_c/3, h/5)$. At L_b= 25 m, the highest value of κ is reached in Delta girder 12 $(2b_c/3, h/3)$.

- Welded HEA 600: The maximum value of M_{cr}^* is 278% for Delta girder 16 and the maximum value of κ is 11.3 for Delta girder 14 $(2b_c/3, h/5)$. Both values are reached at L_b= 25 m. The maximum values of κ at L_b= 2.4 and 5 m are reached in Delta girder 13 $(b_c/2, h/5)$. For the remaining unbraced lengths, the maximum values of κ are reached in Delta girder 14 $(2b_c/3, h/5)$.

- Overall observations: For each I-section, the maximum increase in M_{cr}^* occurs in the Delta girder that provides the highest A^*. Additionally, M_{cr}^* increases as L_b increases. However, the largest values of κ are not obtained for Delta girders that provide the largest values of M_{cr}^* and A^*. It is also observed that for the two I-sections with $d/b_c > 2$ (IPE 360 and IPE 550), the highest values of κ at different L_b values are all obtained in the same Delta girder (Delta girders 2 and 6). On the other hand, for the two I-sections with $d/b_c \leq 2$ (HEA 400 and HEA 600), different Delta girders (i.e., different delta stiffener configurations) provide the highest values of κ at different L_b values. This is particularly noticeable in short to medium length girders. The inconsistencies in the highest values of κ can be attributed to the nonlinearity of the EC3 (2005) curves. When delta stiffeners are added to a section with $d/b_c \leq 2$, the EC3 buckling curve shifts from "c" to "a" as discussed in Section 6.5. Figure 6.2 shows the difference in shapes for curves "a" and "c". The main difference between the two curves is observed when the non-dimensional slenderness λ_{LT} is below 1. In this region, curve "a" concaves downward while curve "c" is almost linear. On the contrary, less difference is observed between the shapes of curves "b" and "d" which leads to more consistent results when $d/b_c > 2$.

Based on the results of this section, some useful information can be recommended. When maximum increase in M_{cr}^* is required, delta stiffeners should be configured to provide maximum A^*. When the most effective design is required, a comparison should be made between different delta stiffener configurations to obtain the highest value of κ. Note that the configurations may change for different L_b when $d/b_c \leq 2$. A more detailed investigated of effective delta stiffener configurations is provided in the following section.
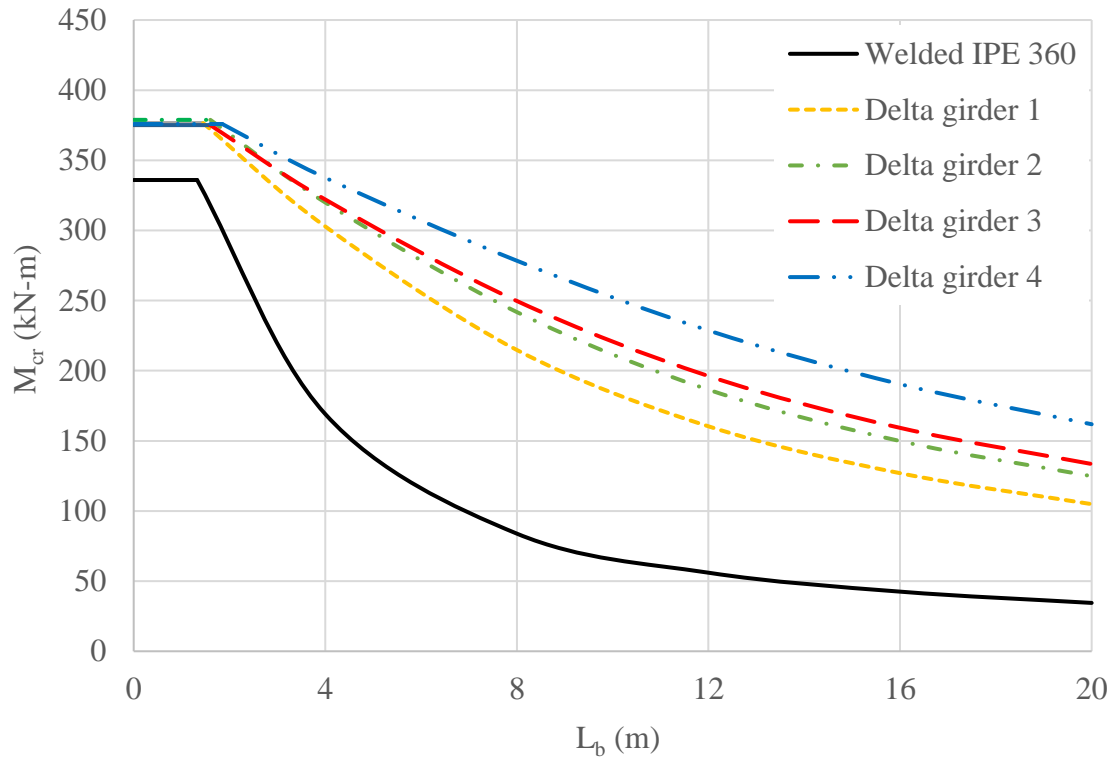
Figure 6.17 Comparison between flexural resistance curves for welded IPE 360 and Delta girders

1, 2, 3 and 4

Table 6.24 Results of the comparison (welded IPE 360 versus Delta girders 1, 2, 3 and 4)

	Delta Girder 1 ($A^* =17.7\%$)		Delta Girder 2 ($A^* =19.5\%$)		Delta Girder 3 ($A^* =27.0\%$)		Delta Girder 4 ($A^* =28.2\%$)	
L_b (m)	M_{cr}^*	κ	M_{cr}^*	κ	M_{cr}^*	κ	M_{cr}^*	κ
1.325	12.1%	0.68	12.8%	0.66	11.7%	0.43	11.9%	0.42
4	79.1%	4.48	89.2%	4.58	90.5%	3.35	99.6%	3.53
8	156.1%	8.84	188.3%	9.67	197.8%	7.33	232.0%	8.22
12	186.4%	10.55	233.0%	11.96	250.4%	9.28	308.4%	10.93
16	198.7%	11.25	252.6%	12.97	274.8%	10.18	348.1%	12.34
20	204.4%	11.58	262.2%	13.46	287.5%	10.65	369.7%	13.10
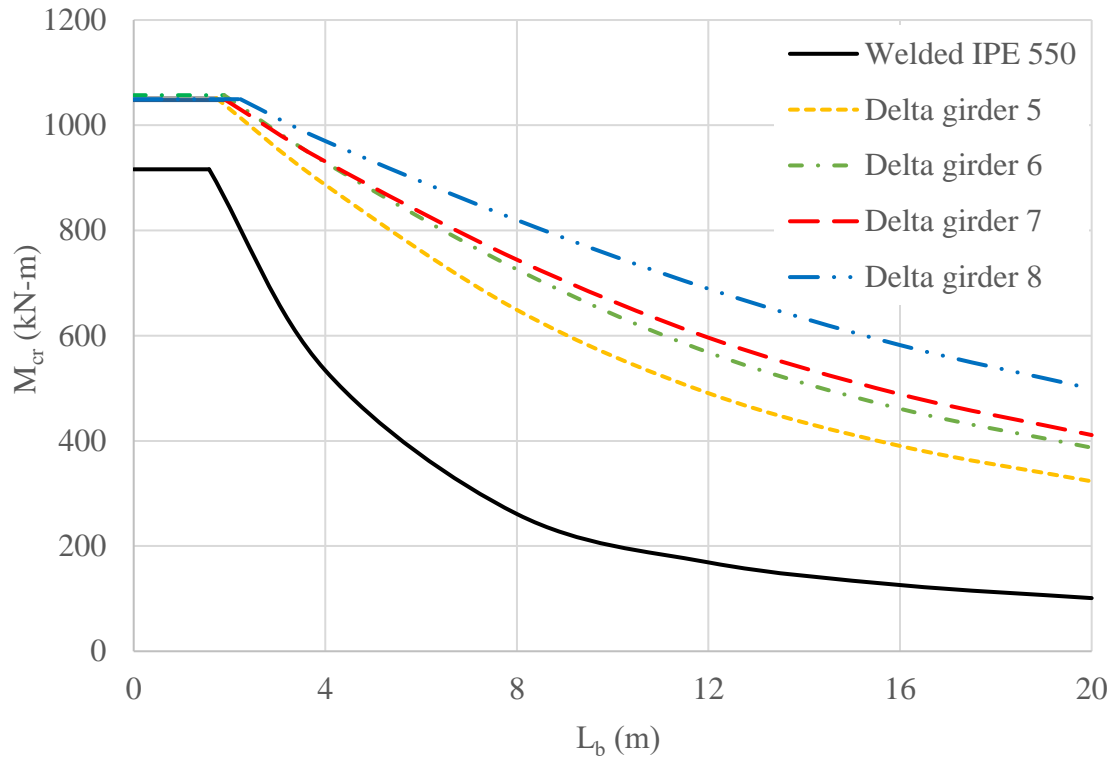
Figure 6.18 Comparison between flexural resistance curves for welded IPE 550 and Delta girders

5, 6, 7 and 8

Table 6.25 Results of the comparison (welded IPE 550 versus Delta girders 5, 6, 7 and 8)

	Delta Girder 5 ($A^* =21.1\%$)		Delta Girder 6 ($A^* =22.6\%$)		Delta Girder 7 ($A^* =33.2\%$)		Delta Girder 8 ($A^* =34.2\%$)	
L_b (m)	M_{cr}^*	κ	M_{cr}^*	κ	M_{cr}^*	κ	M_{cr}^*	κ
1.575	14.8%	0.70	15.4%	0.68	14.4%	0.43	14.6%	0.43
4	66.1%	3.13	74.0%	3.27	74.4%	2.24	81.7%	2.39
8	148.7%	7.05	178.1%	7.87	185.2%	5.59	214.1%	6.27
12	190.5%	9.03	236.3%	10.44	252.9%	7.63	308.0%	9.01
16	210.0%	9.96	266.2%	11.76	288.1%	8.69	362.4%	10.61
20	219.8%	10.42	283.1%	12.51	306.9%	9.25	394.0%	11.53
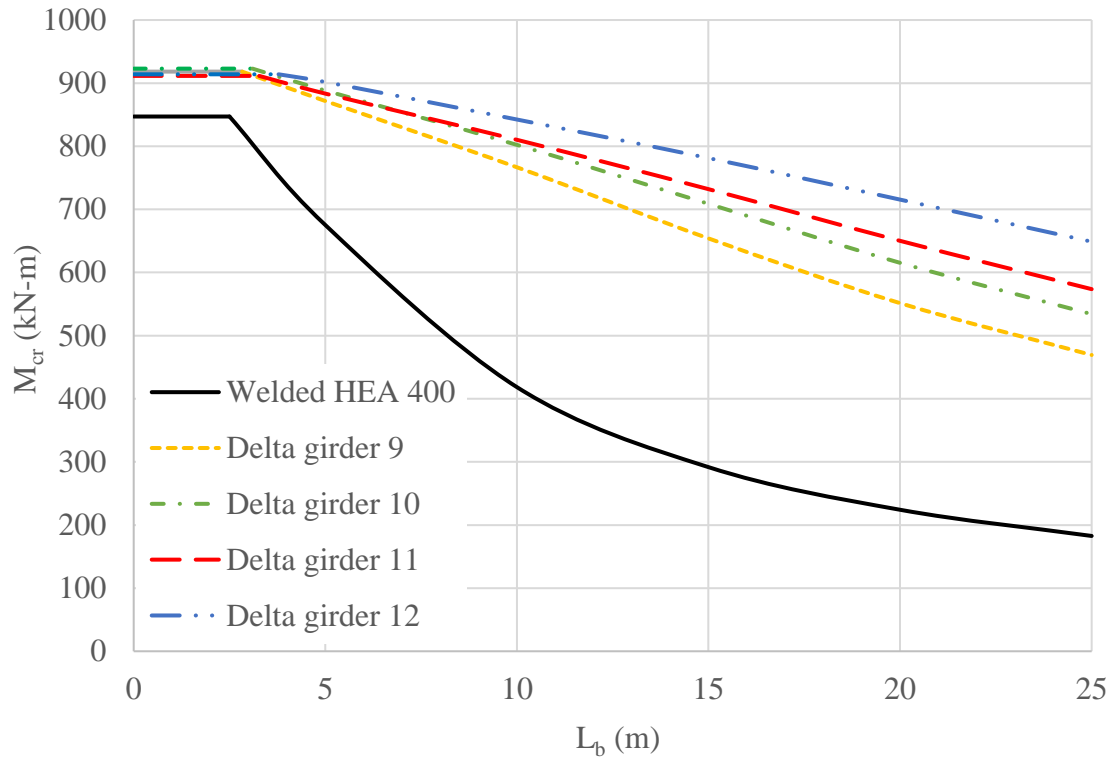
Figure 6.19 Comparison between flexural resistance curves for welded HEA 400 and Delta

girders 9, 10, 11 and 12

Table 6.26 Results of the comparison (welded HEA 400 versus Delta girders 9, 10, 11 and 12)

L_b (m)	Delta Girder 9 (A^* =15.5%)		Delta Girder 10 (A^* =18.5%)		Delta Girder 11 (A^* =21.4%)		Delta Girder 12 (A^* =23.7%)	
	M_{cr}^*	κ	M_{cr}^*	κ	M_{cr}^*	κ	M_{cr}^*	κ
2.5	8.4%	0.54	9.0%	0.49	7.6%	0.35	7.9%	0.33
5	29.1%	1.87	31.5%	1.70	30.8%	1.44	33.5%	1.39
10	83.2%	5.35	91.7%	4.95	93.6%	4.37	101.3%	4.24
15	124.2%	7.99	143.0%	7.72	151.0%	7.04	167.9%	7.05
20	146.0%	9.39	174.5%	9.43	190.1%	8.87	219.2%	9.22
25	157.0%	10.10	192.4%	10.38	214.1%	10.00	255.2%	10.74

185
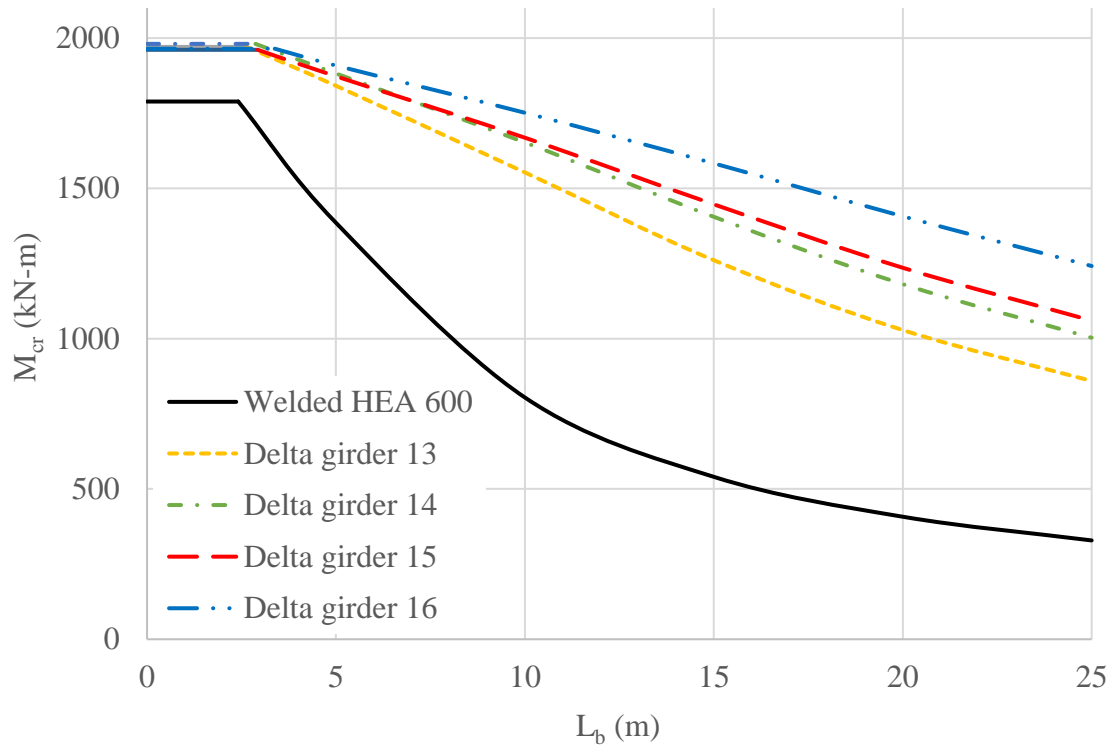
Figure 6.20 Comparison between flexural resistance curves for welded HEA 600 and Delta

girders 13, 14, 15 and 16

Table 6.27 Results of the comparison (welded HEA 600 versus Delta girders 13, 14, 15 and 16)

	Delta Girder 13 ($A^* =16.3\%$)		Delta Girder 14 ($A^* =18.2\%$)		Delta Girder 15 ($A^* =24.5\%$)		Delta Girder 16 ($A^* =25.8\%$)	
L_b (m)	M_{cr}^*	κ	M_{cr}^*	κ	M_{cr}^*	κ	M_{cr}^*	κ
2.415	10.2%	0.62	10.7%	0.59	9.6%	0.39	9.8%	0.38
5	32.9%	2.02	35.8%	1.97	35.2%	1.44	37.7%	1.46
10	93.1%	5.72	105.5%	5.81	107.4%	4.39	117.7%	4.57
15	133.4%	8.20	160.1%	8.81	167.8%	6.85	193.0%	7.48
20	152.3%	9.37	189.8%	10.45	203.2%	8.30	245.2%	9.51
25	161.4%	9.93	205.1%	11.29	222.4%	9.08	277.7%	10.77

186

6.8   Guidelines for Delta Stiffener Configurations

To provide some guidelines that will be useful for determining effective configurations of the delta stiffeners, the κ factor will be examined and compared for standard welded H- and I-sections with 16 different delta stiffener configurations. The selected sections cover a comprehensive range of d/b_c ratio. Table 6.28 shows the selected H- and I-section along with their d/b_c ratio and the thickness of the added delta stiffeners. The unbraced lengths L_b selected to perform the comparisons are based on L_r values of the Delta girders and the corresponding I-sections denoted by L_{rD} and L_{rI}, respectively. The comparisons are made at L_p (plastic moment capacity), L_{rI}, L_{rD}, selected lengths between L_p and L_{rI}, and selected lengths higher than L_{rI} and L_{rD}. The computed κ values are shown in Table 6.29 to 6.84. Note that in the table where $L_b = L_{rD}$, e.g. Table 6.35, the critical buckling moment of the corresponding I-section is computed at L_{rD}, which varies for each delta stiffener configuration.

Based on the results, the most effective delta stiffener configurations are seen to vary between sections with $d/b_c \leq 1$, $1 < d/b_c < 2$, and $d/b_c \geq 2$. For Delta girders with $1 < d/b_c < 2$, the results show that the highest values of κ correspond to different delta stiffener configurations at different unbraced lengths. However, it is noticed that smaller b_d and h_d values are more effective at shorter lengths and vice versa. On the other hand, the results are consistent for Delta girders with $d/b_c \leq 1$ and $d/b_c \geq 2$ at various unbraced lengths where the configuration with the smallest h_d and largest b_d is the most effective for girders with $d/b_c \geq 2$ and the configuration with the smallest h_d and b_d is the most effective for girders with $d/b_c \leq 1$. This is mainly because girders with $d/b_c \geq 2$ have a relatively smaller flange width in comparison to girders with $d/b_c < 2$. The only exception is at $L_b = L_p$ when the cross-section

187

can develop the full plastic moment M_p before lateral-torsional buckling occurs. Since the main purpose of delta stiffeners is to increase the LTB capacity of an I-section and LTB is ignored at $L_b \leq L_p$ or $\bar{\lambda}_{LT} \leq \bar{\lambda}_{LT,0}$, low values of κ are obtained at M_p and other alternative solutions, e.g., a cover plate, may provide more effective results. The results also show that delta stiffeners become more effective (higher κ values) when the length of the beam increases and that the height of delta stiffeners h_d of $h/5$ or $h/4$ always provide more effective results than $h/3$ and $2h/5$. Furthermore, it is worth noting that the results of this section do not contradict with the results of the parametric study in Section 4.5. The results of the previous parametric study were based on theoretical elastic LTB moments obtained at L_{rD}, i.e., comparisons between each delta stiffener configuration and the corresponding I-section were made at the corresponding L_{rD}. Similar comparisons are made herein in tables where $L_b = L_{rD}$ and results consistent with those of Section 4.5 are obtained. To gain some information from these comparisons on the effectiveness of delta stiffeners on increasing the LTB capacity of H- and I-sections, the highest κ factors for the examined Delta girders at $L_b = L_{rI}$ are examined. The average value of κ for these eight H- and I-sections is 5.43. This means that each 10% increase in the cross-section weight due to adding delta stiffeners is associated with a 54% increase in the LTB capacity of the initial girder.

In light of the aforementioned discussions and results, Table 6.85 presents some recommendations for the selection of delta stiffener configurations. The recommendations are based on the d/b_c ratio and unbraced length of the Delta girder in comparison to the L_r value of the base I-section. The recommendations for h_d and b_d are given in a range format so that the designer can select the appropriate configuration based on other design needs. For example, lateral deflection is an important aspect in the design of crane runway beams; thus, a larger b_d

value would provide higher moment of inertia about the axis of symmetry and hence better resistance to lateral deflection. These recommendations can also be used as a start point for designing Delta girders. Moreover, the following width-to-thickness ratio, based on EC3 (2005) Class 1 cross-sections, should be checked to avoid local buckling in the delta stiffeners

$$\frac{w_d}{t_d} \leq 72 \sqrt{\frac{235}{F_y}} \qquad (6.18)$$

where F_y is the yield stress of the delta stiffeners in MPa, and w_d and t_d are the width and thickness of the delta stiffener plate, respectively.

Table 6.28 H- and I- sections used to create Delta girders

Base section	d/b_c	t_d (mm)
HEA 240	0.96	8.0
HEA 280	0.96	8.0
HEA 400	1.30	12.0
HEA 600	1.97	14.0
IPE 300	2.00	8.0
IPE 360	2.12	8.0
IPE 450	2.37	10.0
IPE 550	2.62	12.0

Table 6.29 κ values of Delta girders (welded HEA 240 at $L_b = L_p$)

h_d \ b_d	$2b_c/5$	$b_c/2$	$2b_c/3$	$3b_c/4$
$h/5$	<u>0.52</u>	0.47	0.41	0.38
$h/4$	0.44	0.41	0.36	0.34
$h/3$	0.34	0.33	0.30	0.28
$2h/5$	0.29	0.28	0.26	0.24

Table 6.30 κ values of Delta girders (welded HEA 240 at L_b= 5.0 m)

h_d \ b_d	$2b_c/5$	$b_c/2$	$2b_c/3$	$3b_c/4$
$h/5$	<u>2.74</u>	2.52	2.18	2.04
$h/4$	2.53	2.38	2.11	1.99
$h/3$	2.20	2.12	1.95	1.86
$2h/5$	1.96	1.92	1.81	1.74

Table 6.31 κ values of Delta girders (welded HEA 240 at L_b = 7.0 m)

h_d \ b_d	$2b_c/5$	$b_c/2$	$2b_c/3$	$3b_c/4$
$h/5$	<u>4.54</u>	4.20	3.66	3.42
$h/4$	4.26	4.03	3.58	3.37
$h/3$	3.75	3.63	3.33	3.18
$2h/5$	3.37	3.31	3.10	2.98

Table 6.32 κ values of Delta girders (welded HEA 240 at $L_b = L_{rI} = 8.5$ m)

h_d \ b_d	$2b_c/5$	$b_c/2$	$2b_c/3$	$3b_c/4$
$h/5$	<u>5.79</u>	5.42	4.76	4.47
$h/4$	5.51	5.25	4.70	4.43
$h/3$	4.91	4.79	4.41	4.21
$2h/5$	4.44	4.38	4.12	3.97

Table 6.33 κ values of Delta girders (welded HEA 240 at L_b= 12.0 m)

h_d \ b_d	$2b_c/5$	$b_c/2$	$2b_c/3$	$3b_c/4$
$h/5$	<u>7.96</u>	7.66	6.96	6.61
$h/4$	7.84	7.66	7.04	6.70
$h/3$	7.24	7.21	6.78	6.50
$2h/5$	6.67	6.70	6.40	6.18

Table 6.34 κ values of Delta girders (welded HEA 240 at L_b= 16.0 m)

h_d \ b_d	$2b_c/5$	$b_c/2$	$2b_c/3$	$3b_c/4$
$h/5$	9.28	9.18	8.65	8.33
$h/4$	9.42	<u>9.48</u>	9.03	8.70
$h/3$	9.05	9.27	8.98	8.70
$2h/5$	8.53	8.80	8.63	8.40

Table 6.35 κ values of Delta girders (welded HEA 240 at $L_b = L_{rD}$)

h_d \ b_d	$2b_c/5$	$b_c/2$	$2b_c/3$	$3b_c/4$
$h/5$	8.81	9.06	9.13	9.12
$h/4$	4.29	8.55	10.47	10.58
$h/3$	9.84	10.96	12.09	12.45
$2h/5$	9.90	6.40	10.2	<u>13.50</u>

Table 6.36 κ values of Delta girders (welded HEA 280 at $L_b = L_p$)

h_d \ b_d	$2b_c/5$	$b_c/2$	$2b_c/3$	$3b_c/4$
$h/5$	<u>0.54</u>	0.50	0.43	0.40
$h/4$	0.46	0.43	0.38	0.36
$h/3$	0.36	0.34	0.31	0.30
$2h/5$	0.30	0.29	0.27	0.25

Table 6.37 κ values of Delta girders (welded HEA 280 at L_b= 5.0 m)

h_d \ b_d	$2b_c/5$	$b_c/2$	$2b_c/3$	$3b_c/4$
$h/5$	<u>2.32</u>	2.14	1.87	1.75
$h/4$	2.14	2.01	1.80	1.70
$h/3$	1.84	1.79	1.65	1.58
$2h/5$	1.64	1.62	1.53	1.48

Table 6.38 κ values of Delta girders (welded HEA 280 at L_b = 7.0 m)

h_d \ b_d	$2b_c/5$	$b_c/2$	$2b_c/3$	$3b_c/4$
$h/5$	<u>4.05</u>	3.74	3.26	3.05
$h/4$	3.77	3.56	3.17	2.99
$h/3$	3.30	3.20	2.94	2.81
$2h/5$	2.96	2.91	2.73	2.63

Table 6.39 κ values of Delta girders (welded HEA 240 at $L_b = L_{rl} = 9.4$ m)

h_d \ b_d	$2b_c/5$	$b_c/2$	$2b_c/3$	$3b_c/4$
$h/5$	<u>6.15</u>	5.77	5.08	4.77
$h/4$	5.85	5.58	5.01	4.73
$h/3$	5.21	5.09	4.70	4.49
$2h/5$	4.71	4.66	4.39	4.22

Table 6.40 κ values of Delta girders (welded HEA 280 at L_b= 12.0 m)

h_d \ b_d	$2b_c/5$	$b_c/2$	$2b_c/3$	$3b_c/4$
$h/5$	<u>7.92</u>	7.57	6.81	6.44
$h/4$	7.71	7.48	6.82	6.47
$h/3$	7.02	6.95	6.50	6.22
$2h/5$	6.42	6.42	6.11	5.89

Table 6.41 κ values of Delta girders (welded HEA 280 at L_b= 16.0 m)

h_d \ b_d	$2b_c/5$	$b_c/2$	$2b_c/3$	$3b_c/4$
$h/5$	9.69	9.53	8.87	8.50
$h/4$	<u>9.74</u>	9.72	9.14	8.77
$h/3$	9.21	9.35	8.96	8.65
$2h/5$	8.59	8.79	8.54	8.29

Table 6.42 κ values of Delta girders (welded HEA 280 at $L_b = L_{rD}$)

h_d \ b_d	$2b_c/5$	$b_c/2$	$2b_c/3$	$3b_c/4$
$h/5$	9.63	9.98	10.12	10.12
$h/4$	10.33	11.10	11.67	11.80
$h/3$	10.85	12.17	13.50	13.93
$2h/5$	10.92	12.56	14.43	<u>15.10</u>

Table 6.43 κ values of Delta girders (welded HEA 400 at $L_b = L_p$)

h_d \\ b_d	$2b_c/5$	$b_c/2$	$2b_c/3$	$3b_c/4$
$h/5$	0.39	<u>0.54</u>	0.49	0.46
$h/4$	0.48	0.46	0.42	0.40
$h/3$	0.37	0.35	0.33	0.32
$2h/5$	0.30	0.29	0.28	0.27

Table 6.44 κ values of Delta girders (welded HEA 400 at L_b= 5.0 m)

h_d \\ b_d	$2b_c/5$	$b_c/2$	$2b_c/3$	$3b_c/4$
$h/5$	<u>1.96</u>	1.87	1.70	1.62
$h/4$	1.74	1.69	1.59	1.53
$h/3$	1.44	1.44	1.39	1.36
$2h/5$	1.25	1.27	1.25	1.23

Table 6.45 κ values of Delta girders (welded HEA 400 at $L_b = L_{rI} = 10.0$ m)

h_d \\ b_d	$2b_c/5$	$b_c/2$	$2b_c/3$	$3b_c/4$
$h/5$	<u>5.47</u>	5.35	4.95	4.73
$h/4$	5.03	5.00	4.73	4.55
$h/3$	4.32	4.37	4.24	4.13
$2h/5$	3.83	3.91	3.85	3.78

Table 6.46 κ values of Delta girders (welded HEA 400 at L_b= 15.0 m)

h_d \\ b_d	$2b_c/5$	$b_c/2$	$2b_c/3$	$3b_c/4$
$h/5$	7.85	<u>7.99</u>	7.72	7.49
$h/4$	7.52	7.76	7.62	7.42
$h/3$	6.75	7.04	7.05	6.93
$2h/5$	6.13	6.42	6.49	6.42

Table 6.47 κ values of Delta girders (welded HEA 400 at L_b= 20.0 m)

h_d \ b_d	$2b_c/5$	$b_c/2$	$2b_c/3$	$3b_c/4$
$h/5$	8.99	9.39	9.43	9.30
$h/4$	8.83	9.40	<u>9.61</u>	9.51
$h/3$	8.22	8.87	9.22	9.18
$2h/5$	7.65	8.27	8.65	8.65

Table 6.48 κ values of Delta girders (welded HEA 400 at L_b= 25.0 m)

h_d \ b_d	$2b_c/5$	$b_c/2$	$2b_c/3$	$3b_c/4$
$h/5$	9.51	10.10	10.38	10.36
$h/4$	9.50	10.30	10.84	<u>10.87</u>
$h/3$	9.04	10.00	10.74	10.84
$2h/5$	8.55	9.49	10.28	10.40

Table 6.49 κ values of Delta girders (welded HEA 400 at $L_b = L_{rD}$)

h_d \ b_d	$2b_c/5$	$b_c/2$	$2b_c/3$	$3b_c/4$
$h/5$	8.13	8.90	9.56	9.76
$h/4$	8.36	9.42	10.56	10.95
$h/3$	8.31	9.73	11.53	12.22
$2h/5$	8.15	9.72	11.88	<u>12.78</u>

Table 6.50 κ values of Delta girders (welded HEA 600 at $L_b = L_p$)

h_d \ b_d	$2b_c/5$	$b_c/2$	$2b_c/3$	$3b_c/4$
$h/5$	<u>0.64</u>	0.62	0.59	0.57
$h/4$	0.53	0.52	0.50	0.48
$h/3$	0.40	0.39	0.38	0.40
$2h/5$	0.32	0.32	0.31	0.31

Table 6.51 κ values of Delta girders (welded HEA 600 at L_b= 4.0 m)

h_d \ b_d	$2b_c/5$	$b_c/2$	$2b_c/3$	$3b_c/4$
$h/5$	<u>1.42</u>	<u>1.42</u>	1.38	1.36
$h/4$	1.21	1.23	1.22	1.21
$h/3$	0.96	0.99	1.01	1.01
$2h/5$	0.82	0.85	0.88	0.88

Table 6.52 κ values of Delta girders (welded HEA 600 at L_b = 7.0 m)

h_d \ b_d	$2b_c/5$	$b_c/2$	$2b_c/3$	$3b_c/4$
$h/5$	3.42	<u>3.49</u>	3.43	3.36
$h/4$	2.99	3.08	3.09	3.06
$h/3$	2.45	2.54	2.60	2.60
$2h/5$	2.12	2.21	2.28	2.29

Table 6.53 κ values of Delta girders (welded HEA 600 at L_b= L_{rI} = 9.1 m)

h_d \ b_d	$2b_c/5$	$b_c/2$	$2b_c/3$	$3b_c/4$
$h/5$	4.92	5.12	5.15	5.07
$h/4$	4.39	4.61	<u>5.57</u>	4.66
$h/3$	3.67	3.87	4.00	4.00
$2h/5$	3.22	3.40	3.53	3.55

Table 6.54 κ values of Delta girders (welded HEA 600 at L_b= 15.0 m)

h_d \ b_d	$2b_c/5$	$b_c/2$	$2b_c/3$	$3b_c/4$
$h/5$	7.44	8.20	8.81	8.90
$h/4$	6.96	7.74	<u>10.59</u>	8.53
$h/3$	6.16	6.85	7.48	7.62
$2h/5$	5.59	6.19	6.75	6.88

Table 6.55 κ values of Delta girders (welded HEA 600 at L_b= 20.0 m)

h_d \ b_d	$2b_c/5$	$b_c/2$	$2b_c/3$	$3b_c/4$
$h/5$	8.30	9.37	10.45	<u>10.74</u>
$h/4$	7.91	9.05	10.28	10.63
$h/3$	7.20	8.30	9.51	9.86
$2h/5$	6.68	7.67	8.77	9.09

Table 6.56 κ values of Delta girders (welded HEA 600 at $L_b = L_{rD}$)

h_d \ b_d	$2b_c/5$	$b_c/2$	$2b_c/3$	$3b_c/4$
$h/5$	6.93	8.16	9.79	10.43
$h/4$	6.77	8.21	10.24	11.09
$h/3$	6.46	8.03	10.44	9.11
$2h/5$	6.23	7.83	10.37	<u>11.58</u>

Table 6.57 κ values of Delta girders (welded IPE 300 at $L_b = L_p$)

h_d \ b_d	$2b_c/5$	$b_c/2$	$2b_c/3$	$3b_c/4$
$h/5$	<u>0.56</u>	0.55	0.53	0.51
$h/4$	0.54	0.53	0.51	0.49
$h/3$	0.41	0.40	0.39	0.38
$2h/5$	0.33	0.33	0.32	0.32

Table 6.58 κ values of Delta girders (welded IPE 300 at $L_b = 3.0$ m)

h_d \ b_d	$2b_c/5$	$b_c/2$	$2b_c/3$	$3b_c/4$
$h/5$	2.86	2.96	<u>3.00</u>	2.99
$h/4$	2.79	2.89	2.94	2.93
$h/3$	2.29	2.40	2.49	2.50
$2h/5$	2.00	2.10	2.19	2.21

Table 6.59 κ values of Delta girders (welded IPE 300 at $L_b = L_{rI} = 4.3$ m)

h_d \ b_d	$2b_c/5$	$b_c/2$	$2b_c/3$	$3b_c/4$
$h/5$	4.56	4.81	<u>4.97</u>	<u>4.97</u>
$h/4$	4.46	4.72	4.89	4.89
$h/3$	3.76	3.99	4.19	4.23
$2h/5$	3.32	3.52	3.72	3.76

Table 6.60 κ values of Delta girders (welded IPE 300 at $L_b = 7.0$ m)

h_d \ b_d	$2b_c/5$	$b_c/2$	$2b_c/3$	$3b_c/4$
$h/5$	7.08	7.79	8.44	<u>8.59</u>
$h/4$	6.97	7.68	8.35	8.50
$h/3$	6.15	6.79	7.44	7.61
$2h/5$	5.57	6.14	6.73	6.90

Table 6.61 κ values of Delta girders (welded IPE 300 at L_b= 10.0 m)

h_d \ b_d	$2b_c/5$	$b_c/2$	$2b_c/3$	$3b_c/4$
$h/5$	8.36	9.44	10.63	<u>11.00</u>
$h/4$	8.27	9.35	10.57	10.95
$h/3$	7.15	8.55	9.78	10.18
$2h/5$	6.94	7.90	9.04	9.43

Table 6.62 κ values of Delta girders (welded IPE 300 at L_b= 12.0 m)

h_d \ b_d	$2b_c/5$	$b_c/2$	$2b_c/3$	$3b_c/4$
$h/5$	8.80	10.3	11.48	<u>11.98</u>
$h/4$	8.72	9.96	11.44	11.95
$h/3$	8.00	9.23	10.78	11.34
$2h/5$	7.46	8.62	10.10	10.63

Table 6.63 κ values of Delta girders (welded IPE 300 at $L_b = L_{rD}$)

h_d \ b_d	$2b_c/5$	$b_c/2$	$2b_c/3$	$3b_c/4$
$h/5$	7.03	8.44	10.43	11.28
$h/4$	7.01	8.44	10.50	11.38
$h/3$	6.74	8.30	10.72	11.84
$2h/5$	6.52	8.11	10.67	<u>11.90</u>

Table 6.64 κ values of Delta girders (welded IPE 360 at $L_b = L_p$)

h_d \ b_d	$2b_c/5$	$b_c/2$	$2b_c/3$	$3b_c/4$
$h/5$	<u>0.70</u>	0.68	0.65	0.64
$h/4$	0.58	0.57	0.55	0.54
$h/3$	0.44	0.43	0.42	0.41
$2h/5$	0.35	0.35	0.35	0.34

Table 6.65 κ values of Delta girders (welded IPE 360 at L_b= 3.0 m)

h_d \ b_d	$2b_c/5$	$b_c/2$	$2b_c/3$	$3b_c/4$
$h/5$	2.87	2.95	<u>2.97</u>	2.95
$h/4$	2.50	2.60	2.67	2.67
$h/3$	2.04	2.14	2.24	2.26
$2h/5$	1.77	1.87	1.97	2.00

Table 6.66 κ values of Delta girders (welded IPE 360 at L_b= L_{rI} = 4.8 m)

h_d \ b_d	$2b_c/5$	$b_c/2$	$2b_c/3$	$3b_c/4$
$h/5$	5.30	5.63	5.83	<u>5.84</u>
$h/4$	4.76	5.09	5.35	5.39
$h/3$	4.01	4.31	4.58	4.65
$2h/5$	3.55	3.81	4.07	4.13

Table 6.67 κ values of Delta girders (welded IPE 360 at L_b= 7.0 m)

h_d \ b_d	$2b_c/5$	$b_c/2$	$2b_c/3$	$3b_c/4$
$h/5$	7.37	8.08	8.71	<u>8.84</u>
$h/4$	6.80	7.52	8.21	8.38
$h/3$	5.93	6.57	7.24	7.42
$2h/5$	5.35	5.92	6.51	6.69

Table 6.68 κ values of Delta girders (welded IPE 360 at L_b= 10.0 m)

h_d \ b_d	$2b_c/5$	$b_c/2$	$2b_c/3$	$3b_c/4$
$h/5$	8.81	9.90	11.06	_11.40_
$h/4$	8.29	9.43	10.73	11.14
$h/3$	7.45	8.53	9.80	10.22
$2h/5$	6.86	7.84	9.00	9.40

Table 6.69 κ values of Delta girders (welded IPE 360 at L_b= 12.0 m)

h_d \ b_d	$2b_c/5$	$b_c/2$	$2b_c/3$	$3b_c/4$
$h/5$	9.30	10.55	11.96	_12.42_
$h/4$	8.83	10.15	11.76	12.31
$h/3$	8.02	9.31	10.93	11.52
$2h/5$	7.45	8.65	10.17	10.72

Table 6.70 κ values of Delta girders (welded IPE 360 at $L_b = L_{rD}$)

h_d \ b_d	$2b_c/5$	$b_c/2$	$2b_c/3$	$3b_c/4$
$h/5$	7.34	8.74	10.67	11.47
$h/4$	7.17	8.75	11.08	12.09
$h/3$	6.84	8.54	11.20	12.44
$2h/5$	6.60	8.31	11.09	_12.45_

Table 6.71 κ values of Delta girders (welded IPE 450 at $L_b = L_p$)

h_d \ b_d	$2b_c/5$	$b_c/2$	$2b_c/3$	$3b_c/4$
$h/5$	<u>0.70</u>	0.69	0.67	0.65
$h/4$	0.58	0.57	0.56	0.55
$h/3$	0.44	0.43	0.42	0.42
$2h/5$	0.35	0.35	0.35	0.34

Table 6.72 κ values of Delta girders (welded IPE 450 at L_b= 3.0 m)

h_d \ b_d	$2b_c/5$	$b_c/2$	$2b_c/3$	$3b_c/4$
$h/5$	2.32	2.40	<u>2.45</u>	<u>2.45</u>
$h/4$	2.00	2.09	2.17	2.18
$h/3$	1.62	1.70	1.79	1.82
$2h/5$	1.40	1.48	1.56	1.59

Table 6.73 κ values of Delta girders (welded IPE 450 at L_b= L_{rI} = 5.2 m)

h_d \ b_d	$2b_c/5$	$b_c/2$	$2b_c/3$	$3b_c/4$
$h/5$	4.83	5.18	5.46	<u>5.51</u>
$h/4$	4.31	4.64	4.95	5.02
$h/3$	3.61	3.90	4.19	4.27
$2h/5$	3.19	3.44	3.70	3.77

Table 6.74 κ values of Delta girders (welded IPE 450 at L_b= 7.0 m)

h_d \ b_d	$2b_c/5$	$b_c/2$	$2b_c/3$	$3b_c/4$
$h/5$	6.42	7.08	7.72	<u>7.87</u>
$h/4$	5.86	6.50	7.15	7.32
$h/3$	5.06	5.60	6.18	6.35
$2h/5$	4.54	5.01	5.51	5.67

Table 6.75 κ values of Delta girders (welded IPE 450 at L_b= 10.0 m)

h_d \ b_d	$2b_c/5$	$b_c/2$	$2b_c/3$	$3b_c/4$
$h/5$	7.97	9.02	10.22	<u>10.60</u>
$h/4$	7.44	8.49	9.74	10.15
$h/3$	6.62	7.58	8.72	9.11
$2h/5$	6.07	6.92	7.93	8.28

Table 6.76 κ values of Delta girders (welded IPE 450 at L_b= 12.0 m)

h_d \ b_d	$2b_c/5$	$b_c/2$	$2b_c/3$	$3b_c/4$
$h/5$	8.54	9.77	11.24	<u>11.75</u>
$h/4$	8.04	9.29	10.86	11.43
$h/3$	7.25	8.42	9.91	10.46
$2h/5$	6.70	7.76	9.13	9.62

Table 6.77 κ values of Delta girders (welded IPE 450 at $L_b = L_{rD}$)

h_d \ b_d	$2b_c/5$	$b_c/2$	$2b_c/3$	$3b_c/4$
$h/5$	6.67	8.09	10.21	11.14
$h/4$	6.49	8.07	10.52	11.64
$h/3$	6.21	7.86	10.58	11.83
$2h/5$	6.01	7.67	10.46	<u>11.84</u>

Table 6.78 κ values of Delta girders (welded IPE 550 at $L_b = L_p$)

h_d \ b_d	$2b_c/5$	$b_c/2$	$2b_c/3$	$3b_c/4$
$h/5$	<u>0.71</u>	0.70	0.68	0.67
$h/4$	0.59	0.58	0.56	0.56
$h/3$	0.44	0.43	0.43	0.42
$2h/5$	0.35	0.35	0.35	0.35

Table 6.79 κ values of Delta girders (welded IPE 550 at L_b= 3.0 m)

h_d \ b_d	$2b_c/5$	$b_c/2$	$2b_c/3$	$3b_c/4$
$h/5$	1.96	2.03	2.10	<u>2.11</u>
$h/4$	1.68	1.76	1.84	1.86
$h/3$	1.35	1.42	1.50	1.53
$2h/5$	1.16	1.22	1.30	1.33

Table 6.80 κ values of Delta girders (welded IPE 550 at $L_b = L_{rI} = 5.6$ m)

h_d \ b_d	$2b_c/5$	$b_c/2$	$2b_c/3$	$3b_c/4$
$h/5$	4.59	4.97	5.34	<u>5.42</u>
$h/4$	4.08	4.44	4.80	4.90
$h/3$	3.42	3.72	4.03	4.13
$2h/5$	3.02	3.27	3.54	3.63

Table 6.81 κ values of Delta girders (welded IPE 550 at L_b= 10.0 m)

h_d \ b_d	$2b_c/5$	$b_c/2$	$2b_c/3$	$3b_c/4$
$h/5$	7.22	8.22	9.41	<u>9.81</u>
$h/4$	6.69	7.66	8.85	9.25
$h/3$	5.91	6.76	7.80	8.17
$2h/5$	5.39	6.14	7.04	7.36

Table 6.82 κ values of Delta girders (welded IPE 550 at L_b= 15.0 m)

h_d \ b_d	$2b_c/5$	$b_c/2$	$2b_c/3$	$3b_c/4$
$h/5$	8.45	9.82	11.62	<u>12.31</u>
$h/4$	7.96	9.34	11.24	11.99
$h/3$	7.22	8.51	10.32	11.05
$2h/5$	6.71	7.90	9.56	10.23

Table 6.83 κ values of Delta girders (welded IPE 550 at L_b= 20.0 m)

h_d \ b_d	$2b_c/5$	$b_c/2$	$2b_c/3$	$3b_c/4$
$h/5$	8.90	10.43	12.53	<u>13.39</u>
$h/4$	8.44	10.02	12.29	13.26
$h/3$	7.74	9.27	11.54	12.53
$2h/5$	7.26	8.70	10.88	11.82

Table 6.84 κ values of Delta girders (welded IPE 550 at $L_b = L_{rD}$)

h_d \ b_d	$2b_c/5$	$b_c/2$	$2b_c/3$	$3b_c/4$
$h/5$	6.18	7.59	9.81	10.78
$h/4$	5.99	7.51	10.03	11.22
$h/3$	5.72	7.27	10.00	11.29
$2h/5$	5.51	7.13	9.87	<u>11.30</u>

Table 6.85 Recommendations for delta stiffener configurations

Limits	Length	h_d	b_d
$d/b_c \leq 1$	Any	$h/5$ to $h/4$	$2b_c/5$ to $b_c/2$
$1 < d/b_c < 2$	$L_b \leq L_{rI}{}^*$	$h/5$ to $h/4$	$2b_c/5$ to $b_c/2$
	$L_b > L_{rI}{}^*$	$h/5$ to $h/4$	$b_c/2$ to $3b_c/4$
$d/b_c \geq 2$	Any	$h/5$ to $h/4$	$2b_c/3$ to $3b_c/4$
* L_{rI} is L_r of the base I-section given in Eq. (2.17)			

6.9   <u>Summary</u>

In this chapter, an overview of and a comparison between the flexural resistance curves

contained in the AISC (2016a) and EC3 (2005) specifications were presented. While EC3 (2005)

provides four LTB curves based on cross-section types (hot-rolled or welded) and d/b_c ratios,

AISC (2016a) specifications provides only one LTB curve for all cross-sections. The comparison

showed that the AISC (2016a) LTB curve is higher than those of EC3 (2005). For short beams,

the limit state is formation of plastic hinge, therefore a derivation of the plastic neutral axis and

the plastic section modulus for Delta girders were made.

A comparison was then made between the LTB curves of various Class 1 (compact)

Delta girders obtained using FE analysis and from AISC (2016a) and EC3 (2005). The results

showed that the AISC (2016a) specifications overestimate the LTB capacity of Delta girders in

comparison with the FE simulation results by an average of 9% with a maximum value of 21%.

The relatively large differences between the AISC (2016a) and the FE buckling curves mainly

occurred in the inelastic region. On the other hand, EC3 (2005) buckling curves "a" and "b"

predicted the buckling capacity of Delta girders with an average error of 2% (unconservative)

when compared with the FE simulation results for both $d/b_c \leq 2$ and $d/b_c > 2$, and with a

maximum difference of 7% (unconservative). Based on these results, EC3 (2005) buckling

curves "a" and "b" for rolled sections or equivalent welded sections case were recommended for

Class 1 (compact) Delta girders with $d/b_c \leq 2$ and $d/b_c > 2$, respectively. Thereafter, the

proposed model was assessed for Delta girders with $d/b_c = 2$ and $d/b_c < 1$ and showed very

good results with an average difference of 2% (unconservative) and a maximum difference of

5% (conservative and unconservative).

Afterwards, a comparison was made between the LTB curves of Delta girders and their

corresponding I-sections. The results showed that the percent increase in moment capacity is

more pronounced for Delta girders with higher cross-section areas and longer unbraced length

L_b. However, the most effective design, i.e., the one that provides the maximum increase in

flexural capacity to increase in cross-section area ratio, does not correspond to the case of

maximum increase in LTB capacity. As a result, a detailed comparison between the flexural

capacities of Delta girders and their corresponding base I-sections was performed in the last

section of this chapter. The comparison employed 16 different delta stiffener configurations and

various H- and I-sections with a comprehensive range of d/b_c ratio. The factor "κ" was used to

determine the most effective configuration at each unbraced length. Based on the results of this

comparison, design recommendations were proposed for effective selecting of delta stiffener

configurations. These recommendations provide a range for delta stiffener dimensions based on

the d/b_c ratio and the L_r length of the corresponding I-section. In addition, recommendations to avoid local buckling in the delta stiffeners were provided.

Chapter 7

Shear Capacity of Delta Girders

7.1 <u>Introduction</u>

One of the primary functions of the web of an I-section is to resist shear forces. In most practical design situations, particularly when hot-rolled sections are used, flexural strength or capacity govern the design of an I-section. This is because the web of most hot-rolled standard American I-sections (W shapes) and all standard European H- and I-sections are compact for normal strength steel and can develop the full web shear yielding capacity. Small differences exist between the shear resistance equations in AISC (2016a) and EC3 (2005). The main distinction between the two codes is that EC3 (2005) provides two values for the shear resistance capacity, one that is conservative and one that allows for strain hardening effects. On the other hand, AISC (2016a) provides only one value that is in between the two recommended values of EC3 (2005).

The objective of this chapter is to investigate the shear resistance of Delta girders. The chapter starts with providing some background information on the shear capacity of web plates and the shear design equations in AISC (2016a) and EC3 (2005). Thereafter, a nonlinear FE model is created to study the shear resistance of I-sections and Delta girders. The results are then presented and discussed. Based on the FE results, design equations for the shear resistance capacity of Delta girders are then proposed and assessed. It should be noted that the scope of work is limited to webs that are compact in shear (Class 1 cross-sections), i.e., webs that can develop the full shear yielding capacity before web buckling occurs.

7.2   Shear Capacity of I-Sections

7.2.1   Theoretical background

When a transverse load is applied to a beam, both normal and shear stresses are present in cross-sections that are subjected to internal bending moment and shear force. The bending moment M gives rise to the normal stress and the shear force V gives rise to the shear stress. In the case of an I-section, the shear stress over any cross-section of the beam can be obtained using the shear formula (Beer, Johnsotn Jr., & Dewolf, 2006)

$$\tau_{ave} = \frac{VQ}{I_x t} \tag{7.1}$$

where τ_{ave} is the shear stress averaged over the width of a horizontal section in which the x- and y-axis are defined as the longitudinal and vertical (transverse) axes, respectively, V is the vertical shear force, t is the cross-section width at the considered section, I_x is the moment of inertia of the full cross-section about the x-axis and Q is the first moment of the considered area with respect to the neutral axis.

Figure 7.1 shows a typical shear stress distribution over a cross-section of an I-beam. In the case of the web, the shear stress τ_{ave} does not vary appreciably over the depth of the web and is much higher than that of the flanges. As a result, for practical design considerations the shear force V is assumed to be carried only by the web. Thus, a common approximation for the maximum shear stress in the cross-section τ_m is obtained by dividing the shear load by the cross-section area of the web A_w (Beer et al., 2006), i.e.

$$\tau_m \approx \frac{V}{A_w} \tag{7.2}$$

210
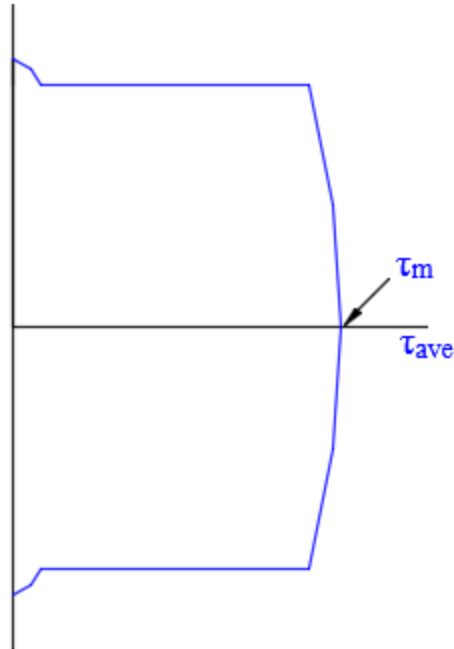
Figure 7.1 Typical shear stress distribution in an I-section

Shear yielding initiates in a cross-section when the maximum shear stress τ_m is equal to the shear yield stress τ_y. If the von Mises yield criterion is used, the shear yield stress can be expressed as a function of F_y, the yield stress of the material, as (Boresi & Schmidt, 2003)

$$\tau_y = \frac{F_y}{\sqrt{3}} \tag{7.3}$$

By setting τ_m equals to τ_y, the shear force V acting on the I-section that causes shear yielding of the web is obtained as

$$V = \frac{F_y A_w}{\sqrt{3}} \tag{7.4}$$

Shear yielding of an I-section can only occur when the web is compact, i.e., the web satisfies some h/t_w ratio specified in various design codes, so its full shear yielding capacity can

be developed. Otherwise, elastic or inelastic web shear buckling will control the design for shear.

The theoretical equation for the elastic critical buckling load V_{cr} of a rectangular plate under

shear loading is given by Timoshenko and Gere (1961) as

$$V_{cr} = \frac{\pi^2 E k_v}{12(1-v^2)\left(h_{pl}/t_p\right)^2}(h_{pl}t_p) \tag{7.5}$$

where h_{pl} is the depth of the plate, t_p is the plate thickness, E is the Young's modulus, v is the

Poisson's ratio and k_v is the elastic shear buckling coefficient.

The elastic shear buckling coefficient k_v is dependent on the boundary conditions and the

span-to-depth ratio (a/h_{pl}) in which a represents the spacing between the transverse (vertical)

stiffeners. For a simply-supported plate on all edges, the coefficient k_v is given by

$$k_v = \begin{cases} 4 + \dfrac{5.34}{\left(a/h_{pl}\right)^2} & \text{for } a/h_{pl} \leq 1 \\[4mm] 5.34 + \dfrac{4}{\left(a/h_{pl}\right)^2} & \text{for } a/h_{pl} > 1 \end{cases} \tag{7.6}$$

and for a plate where opposite edges are simply-supported and fixed, respectively, the coefficient

k_v is given by

$$k_v = \begin{cases} \dfrac{5.34}{\left(a/h_{pl}\right)^2} + \dfrac{2.31}{\left(a/h_{pl}\right)} - 3.44 + 8.39\left(a/h_{pl}\right) & \text{for } a/h_{pl} \leq 1 \\[4mm] 8.98 + \dfrac{5.61}{\left(a/h_{pl}\right)^2} - \dfrac{1.99}{\left(a/h_{pl}\right)^3} & \text{for } a/h_{pl} > 1 \end{cases} \tag{7.7}$$

For I-sections, transverse stiffeners are often assumed to be sufficiently rigid to provide a

simply-supported condition to the web and are designed as such. On the other two edges, the web

is restrained by the flanges. Several assumptions exist for the type of restraint at the web-flange

juncture. The first assumption is that the web panel is simply-supported at the juncture (Basler & Thurlimann, 1959; Porter, Rocky, & Evans, 1975). This conservative assumption was adopted in the development of the AISC (2016a) shear buckling design equations. The second assumption is that the web panel is fixed against the flanges (Chern & Ostapenko, 1969). Other assumptions include a more realistic boundary condition that lies between the simply-supported and fixed conditions (Sharp & Clark, 1971). In recent studies, Lee and Yoo (1998) and Lee, Davidson and Yoo (1996) investigated the flange-web juncture by means of FEM and found simply-supported conditions to be too conservative for many plate girders. Their results showed that the actual boundary condition is closer to a fixed support and is dependent on the flange to web thickness ratio.

7.2.2 Current AISC (2016a) and EC3 (2005) design equations

In the AISC (2016a) specifications, the nominal shear capacity V_n of a singly or doubly symmetric I-section loaded in the plane of the web is given by

$$V_n = 0.6F_y A_w C_v \tag{7.8}$$

where A_w is the web area defined as the overall depth of the section d times the web thickness t_w, and C_v is the web shear coefficient obtained as follows:

a) For webs of hot-rolled I-sections with $h/t_w \leq 2.24\sqrt{E/F_y}$

$$C_v = 1 \tag{7.9}$$

b) For webs of all other I-shaped members

i) when $h/t_w \leq 1.10\sqrt{k_v E/F_y}$

$$C_v = 1 \tag{7.10}$$

ii) when $h/t_w > 1.10\sqrt{k_v E/F_y}$

$$C_v = \frac{1.10\sqrt{k_v E/F_y}}{h/t_w} \tag{7.11}$$

where h is defined as the clear distance between the flanges less the fillet for hot-rolled sections and the clear distance between the flanges for welded sections, and k_v is defined as the web plate shear buckling coefficient and is determined as follows:

a) For webs without transverse stiffeners and with $h/t_w < 260$

$$k_v = 5.34 \tag{7.12}$$

b) For webs with transverse stiffeners

$$k_v = 5 + \frac{5}{(a/h)^2} \tag{7.13}$$

or $\qquad\qquad\qquad k_v = 5.34$ when $a/h > 3.0$ $\tag{7.14}$

where a is the clear spacing between the transverse stiffeners. Note that Eq. (7.13) is an accurate simplification of Eq. (7.6) (AISC, 2016b).

In the EC3 (2005) provisions, the member should be designed for its plastic shear resistance $V_{pl,Rd}$ when

$$\frac{h}{t_w} \le \frac{72}{\eta} \sqrt{\frac{235}{F_y[\text{MPa}]}} \tag{7.15}$$

where η is defined by the National Annex or set equal to 1.2 as recommended by EC3 (2006) for steel grades up to S460 and equal to 1.0 for higher grades.

For convenience, the plastic shear resistance $V_{pl,Rd}$ will be denoted as V_n and is given by

$$V_n = \frac{F_y A_v}{\sqrt{3}} \tag{7.16}$$

where A_v is the shear resistance area determined as follows:

a) For hot-rolled H- and I-sections loaded parallel to the web

$$A_v = A - 2b_f t_f + (t_w + 2r)t_f \text{ but not less than } \eta h t_w \tag{7.17}$$

b) For welded H- and I-sections loaded parallel to web

$$A_v = \eta h t_w \tag{7.18}$$

where A is the full cross-sectional area, b_f and t_f are the width and thickness of the flange, respectively, h is the web depth, and r is the root radius.

η is a factor that takes into account the reduced area and the strain hardening effect of the material. EC3 (2005) states that η may conservatively be taken as 1.0. For cases where shear buckling is expected to cover the shear design, i.e., when $h/t_w > \frac{72}{\eta}\sqrt{\frac{235}{F_y}}$, the code user is referred to Part 5 of EC3 (2006) "Plated Structural Elements" to compute the shear resistance.

From the aforementioned discussion, it can be seen that EC3 (2005) explicitly accounts for material strain hardening by using the coefficient η which can increase the shear resistance by 20%. η also accounts for the reduced area due to using only the web area in shear resistance computation. On the other hand, AISC (2016a) implicitly accounts for some material strain hardening effect through the use of a constant value of 0.6 in Eq. (7.8) instead of $1/\sqrt{3}$ which provides a 4% increase in the shear resistance. Additionally, the full depth of the cross-section d is used to compute the shear resistance area.

7.3   FE Modeling of Delta Girders under a Shear Force

7.3.1   Elastic shear buckling of plates

The finite element model of a member under a shear loading requires different load and boundary conditions than those used in lateral-torsional buckling analysis. Since theoretical solutions exist for the buckling of plates under a pure shear load, two plates with simply-supported boundary conditions will be modeled using Abaqus to demonstrate the accuracy of the modeling techniques. The two plates employ different height-to-width (h_{pl}/a) ratios and different thicknesses (t_p) as shown in the second to fourth columns of Table 7.1. The theoretical elastic buckling loads of the two plates are obtained using Eqs. (7.5) and (7.6) and compared to the eigenvalue solutions of the FE models. The modulus of elasticity E used is equal to 200 GPa and the Poisson's ratio ν is 0.333 ($G = 75$ GPa).

The boundary conditions along the four sides of the plate are shown in Figure 7.2 and summarized in Table 7.2, where u and θ refer to the translational and rotational degrees of freedom, respectively, and "X" indicates the restrained degree of freedom. The shear force V is

applied on side 2 in a vertical direction. S4R shell elements are used to model the plates. A

preliminary convergence study has shown that a mesh size of 3 cm as shown in Figure 7.2 is

enough to produce accurate results. The lowest buckling mode shape for one of the plates is

shown in Figure 7.3. The results show that the errors between the theoretical and numerically

obtained buckling loads for the two plates are 0% and 3% as shown in Table 7.1. These results

demonstrate that the FE modeling of the shear resistance of a plate under pure shear is accurate.

Table 7.1 Shear buckling analysis of plates

Plate	a (m)	h_{pl} (m)	t_p (mm)	V_{cr} (kN)	V_{FEM} (kN)	V_{FEM}/V_{cr}
1	1.0	1.0	15.0	5,832	5,843	1.00
2	2.0	1.0	12.0	2,037	2,099	1.03

Figure 7.2 Mesh and boundary conditions used for the FE modeling of plates

Table 7.2 Boundary conditions used along each edge of the plate shown in Figure 7.2

Side	Translation			Rotation		
	u_x	u_y	u_z	θ_x	θ_y	θ_z
1	X	X	X	X		X
2	X		X	X		X
3	X		X	X	X	
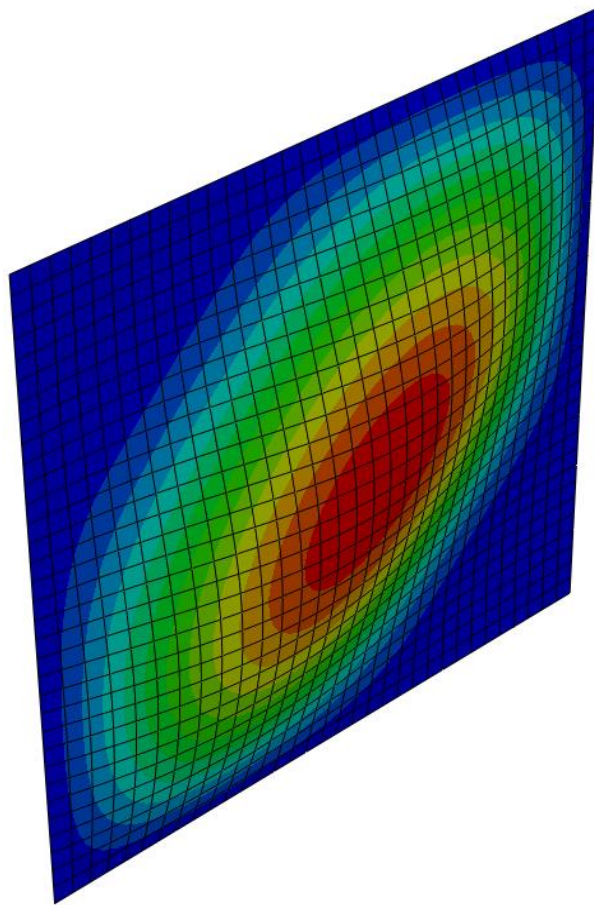
Figure 7.3 First buckling mode of Plate 1

7.3.2   Nonlinear FE model of Delta girders under pure shear

A nonlinear 3D FE model is created to determine the shear resistance of Delta girders under a shear force. The length of each Delta girder model is taken as the height of the web below the delta region, i.e., $L = h - h_d$. The elements type, material properties and analysis procedure are similar to those described in Section 5.2. The maximum mesh size used is 3 cm. The boundary conditions are shown in Figure 7.4 and summarized in Table 7.3. The boundary conditions on sides 1 and 2 are similar to the boundary conditions of section 7.3.1. The flanges are assumed to provide simply-supported boundary conditions at the junction with the web, while the flange ends are allowed to move vertically and rotate around the x-axis. The shear force V is applied on side 2 in a vertical direction. The residual stresses are included in the FE model using the proposed residual stress pattern in Section 5.2.3.

The initial geometrical imperfections are included in the FE model as the eigenmode shape associated with the lowest positive eigenvalue scaled down to $h/150$ where h is the web height. The $h/150$ ratio is the maximum allowable web out-of-flatness for girders without intermediate stiffeners (AWS, 2010). A typical eigenmode shape of a Delta girder is shown in Figure 7.5. The magnitude of the initial imperfections affects mainly the ultimate postbuckling shear capacity of girders while it has negligible effect on the shear yielding capacity. However, initial imperfections are required in the FE model to identify web buckling in the load-displacement curve after yielding occurs and to check that the web does not buckle below the recommended shear yielding capacity. The analysis results will be presented in the following section.

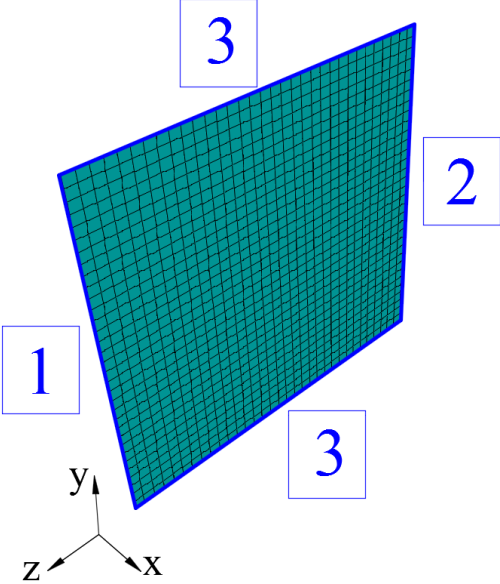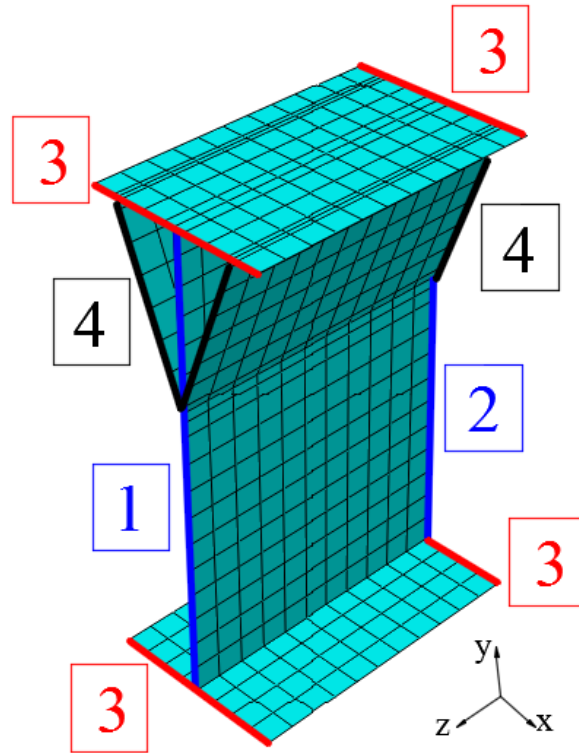Figure 7.4 Mesh and boundary conditions used for the FE modeling of Delta girders

Table 7.3 Boundary conditions used along each edge of the Delta girder shown in Figure 7.4

Side	Translation			Rotation		
	u_x	u_y	u_z	θ_x	θ_y	θ_z
1	X	X	X	X		X
2	X		X	X		X
3	X		X		X	X
4	X		X			X
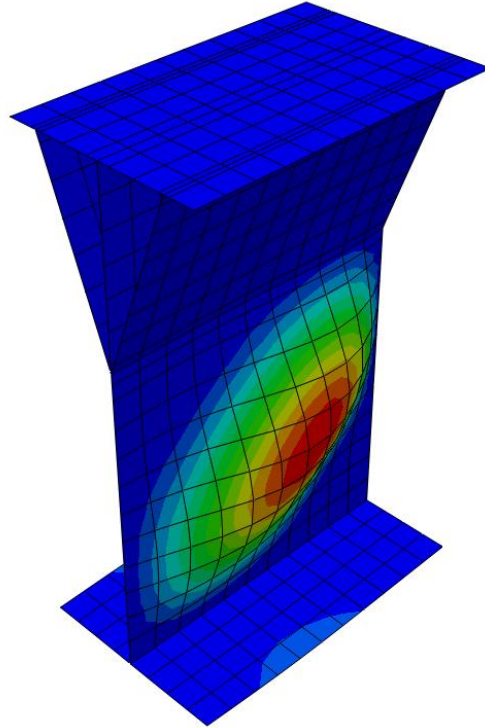
Figure 7.5 Eigenmode shape used as initial imperfections in Delta girders

7.3.3   FE analysis results

Analysis for the shear force are performed on the same Delta girders used in Chapter 6, which were selected to cover a wide range of standard European H- and I-sections with various practical delta stiffeners configurations. The dimensions of the selected Delta girders are provided in Tables 6.4 and 6.19. The FE simulation results are shown in Figure 7.6 to 7.13 where the shear resistance of the Delta girders normalized with respect to that of the base I-section ($V_{FEM}/V_{n,I}$) are plotted against the shear strain γ. $V_{n,I}$ is the EC3 (2005) nominal shear resistance obtained using Eqs. (7.16) and (7.18) with $\eta = 1.0$. The shear strain γ is obtained as the ratio of the vertical displacement of the loaded side, i.e., side 2, to the length of the FE Delta girder model.
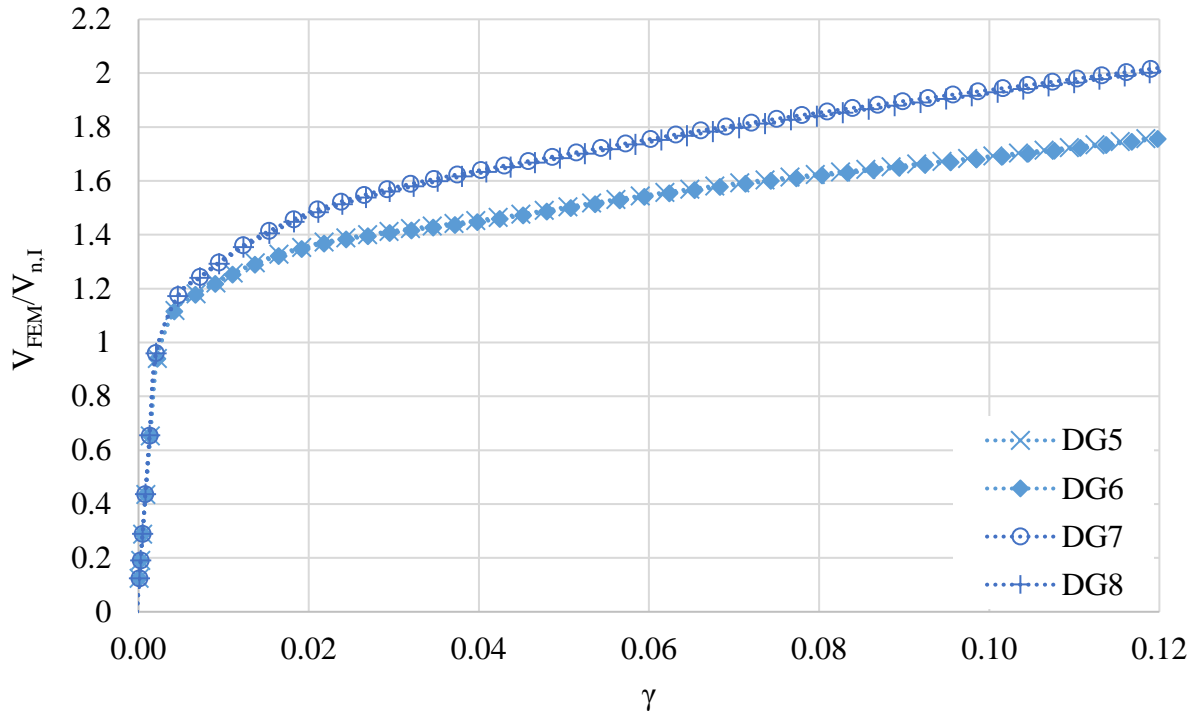
Figure 7.6 FE shear resistance of Delta girders 5, 6, 7 and 8
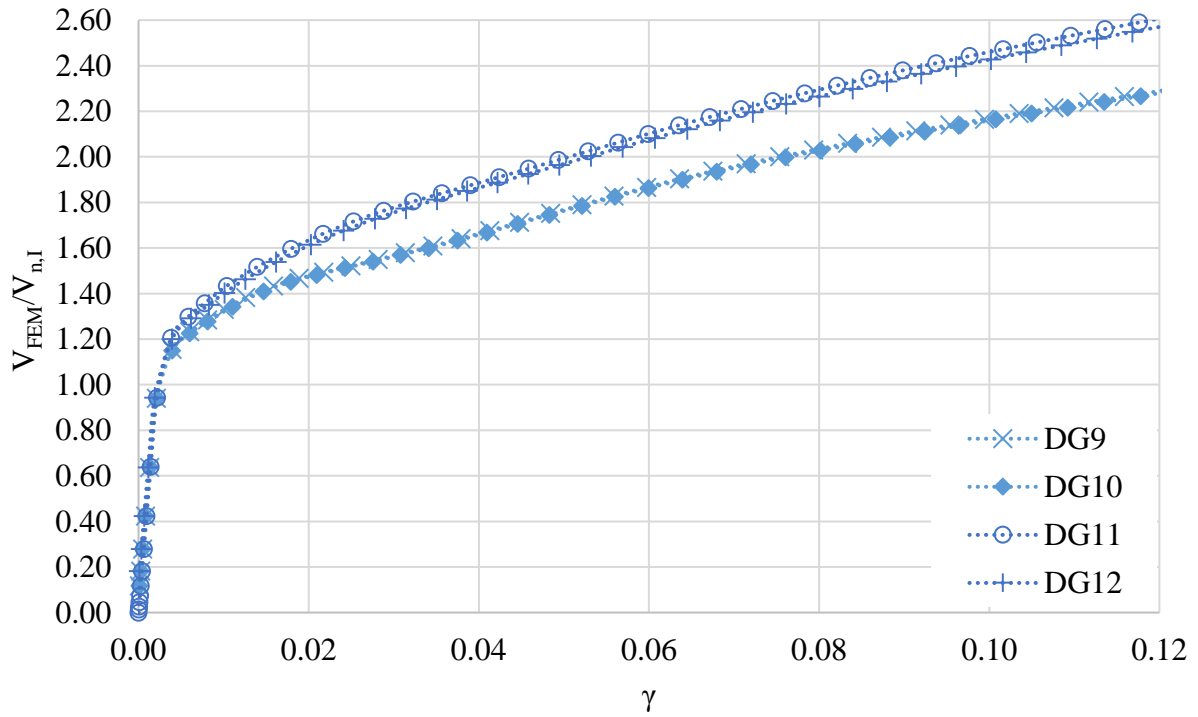
Figure 7.7 FE shear resistance of Delta girders 9, 10, 11 and 12
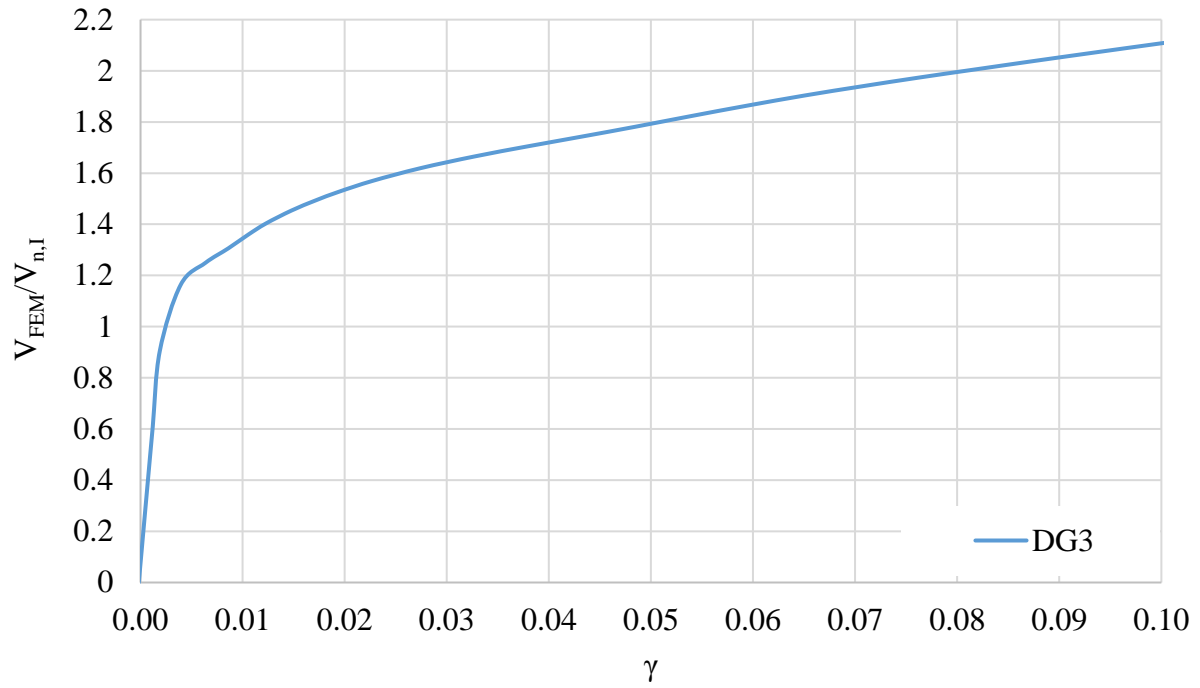
Figure 7.8 FE shear resistance of Delta girder 3
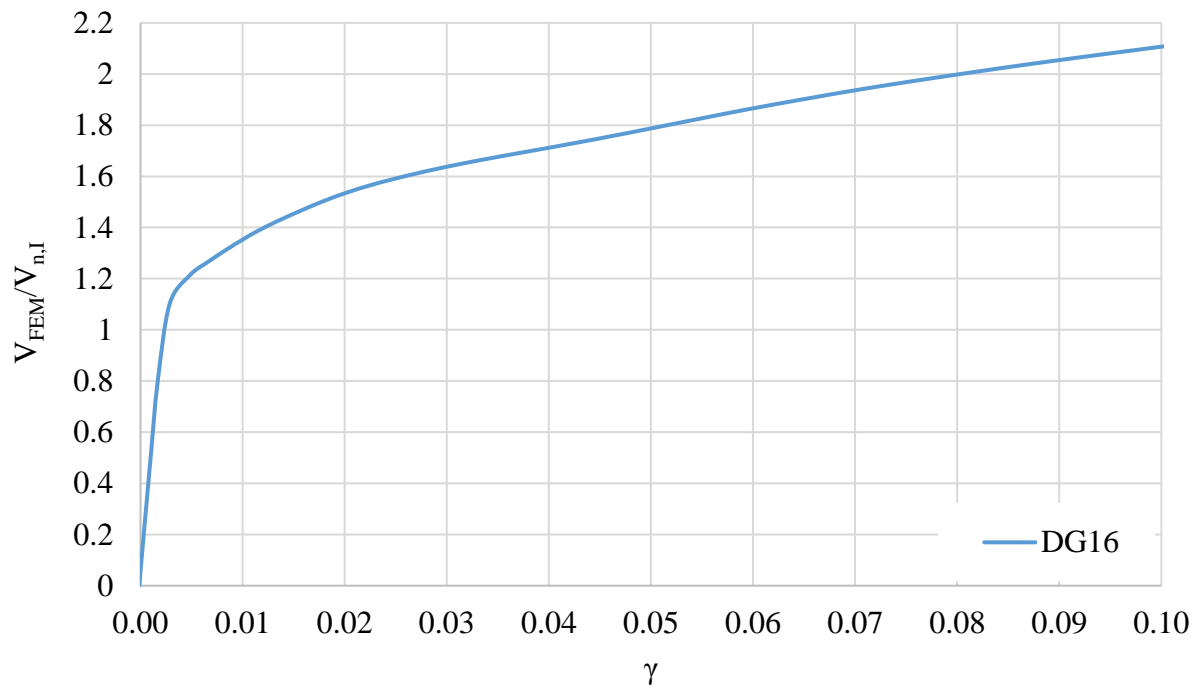
Figure 7.9 FE shear resistance of Delta girder 16
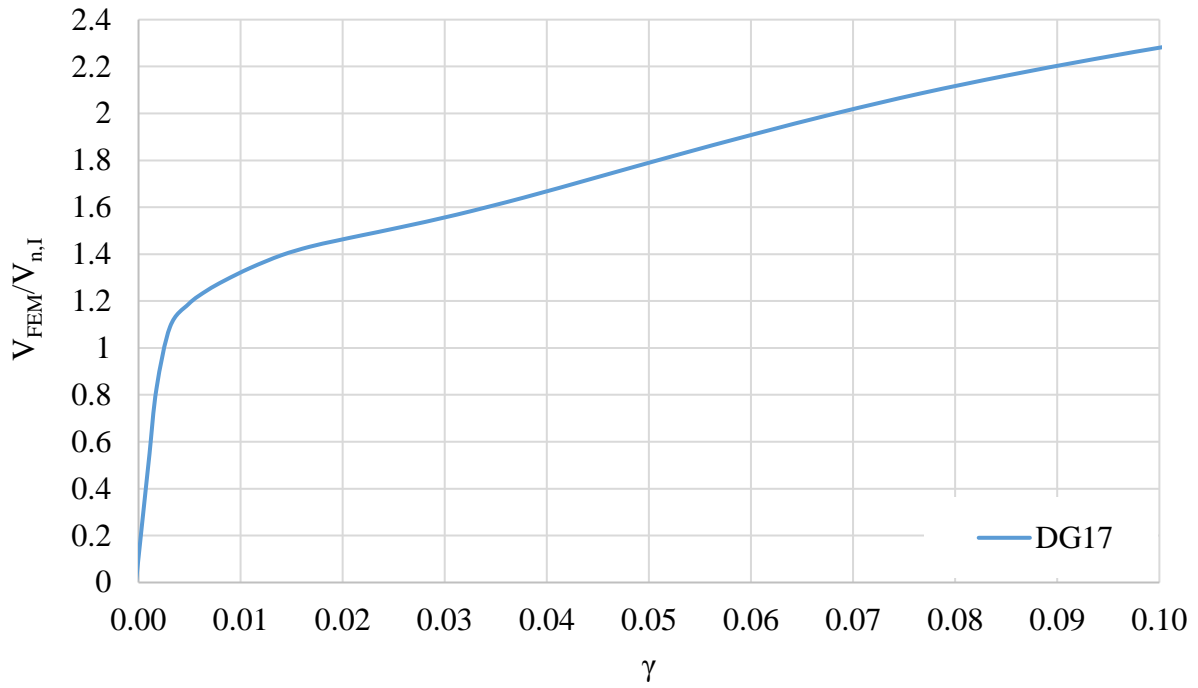
Figure 7.10 FE shear resistance of Delta girder 17
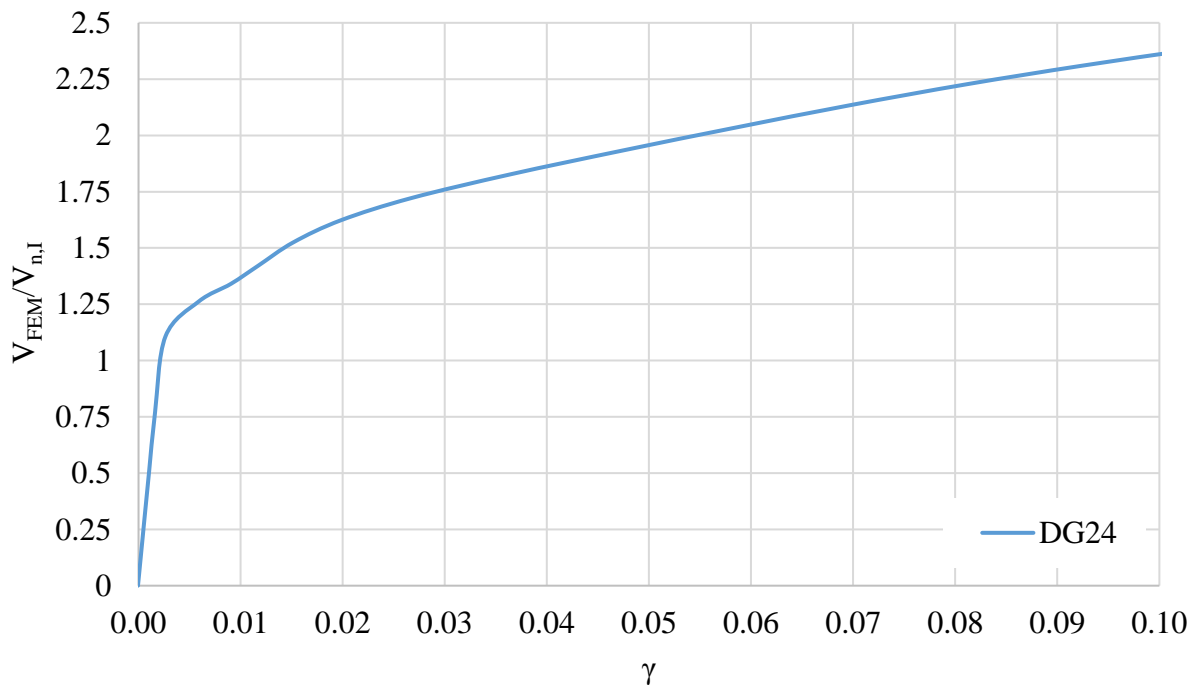
Figure 7.11 FE shear resistance of Delta girder 24
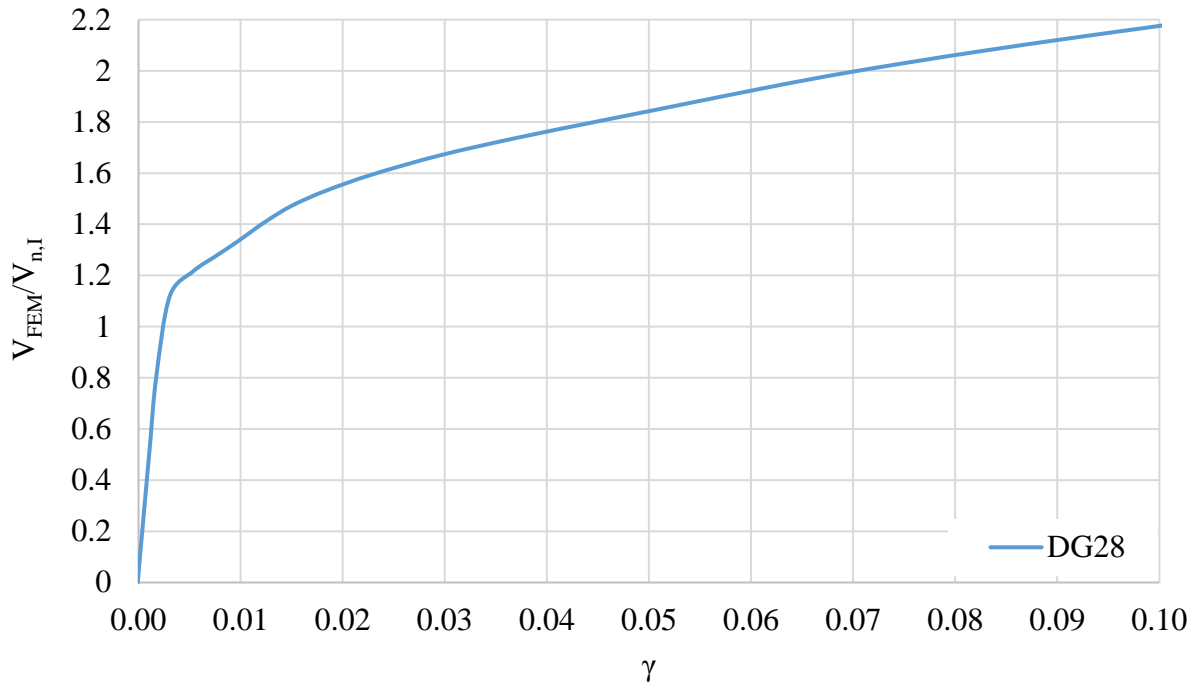
Figure 7.12 FE shear resistance of Delta girder 28
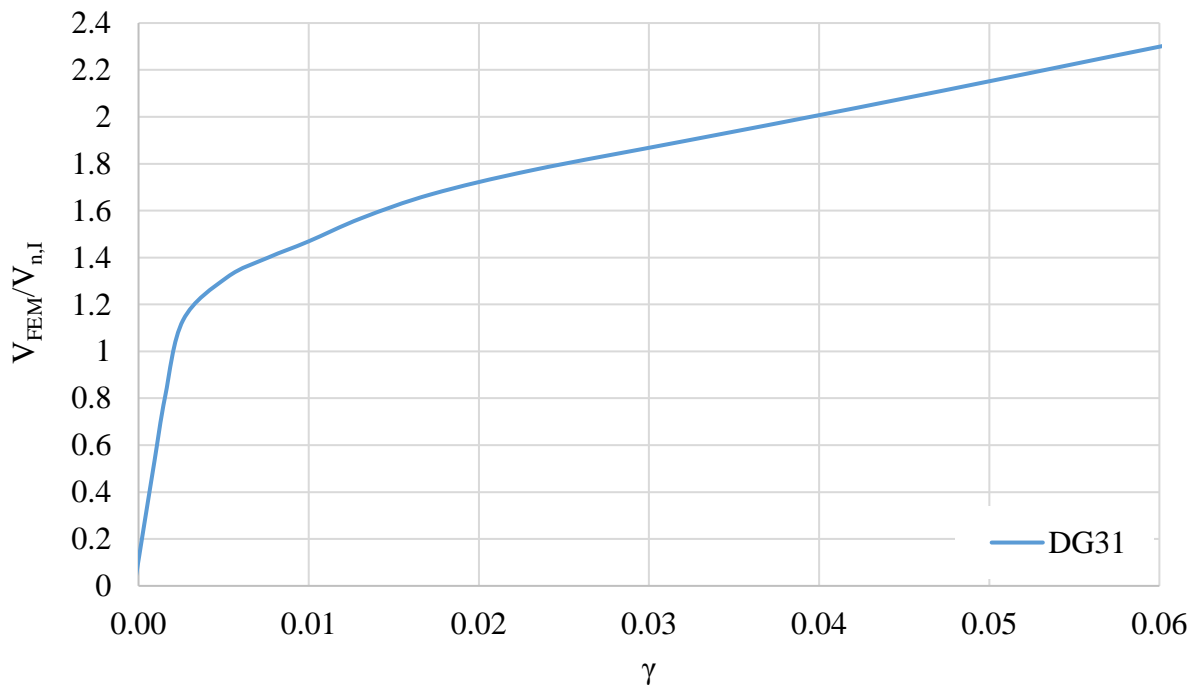
Figure 7.13 FE shear resistance of Delta girder 31

7.3.4 Discussion of results

The results show the expected increase in nominal shear capacity of Delta girders upon comparison with the corresponding base I-sections. Figure 7.6 to 7.13 show that yielding initiates in the Delta girders at a $V_{FEM}/V_{n,I}$ ratio higher than one and a yield plateau is absent in all the sections. This can be explained by the difference in shear stress distribution between Delta girders and I-sections. A typical shear stress distribution in an I-section has been shown in Figure 7.1. The shear stress distribution in a Delta girder can be obtained analytically using Eq. (7.1) or numerically using the FE software ShapeBuilder. The latter is used here and a representative result is shown in Figure 7.14. In the figure, τ_{avg} is normalized against the maximum shear stress τ_m obtained at the centroid of the cross-section under a unit shear force V. Figure 7.14 shows that the maximum shear stress in the delta stiffeners and in the web region between the stiffeners is only around one third the maximum shear stress in the web portion below the delta region. However, depending on the cross-section, this shear stress ration can vary from $0.2F_y$ to $0.4F_y$. This difference in the magnitude of shear stress in the cross-section explains the absence of a yield plateau and that yielding occurs gradually over the cross-section, starting with the web portion below the delta region and progresses toward the delta region as depicted in Figure 7.15. Moreover, it should be pointed out that the configuration of the delta stiffeners will affect the shear resistance only after yielding initiates in the cross-section as can be seen in Figures 7.6 and 7.7. The FE results show that Delta girders with higher h_d/h ratio provide higher post yield shear resistance while the b_d/b_c ratio has negligible effect on the shear resistance. Additionally, web buckling is not a concern as it occurs at a very high shear load V and shear strain γ, as shown in Figure 7.16, after the stresses in the cross-section has reached the ultimate stress F_u.
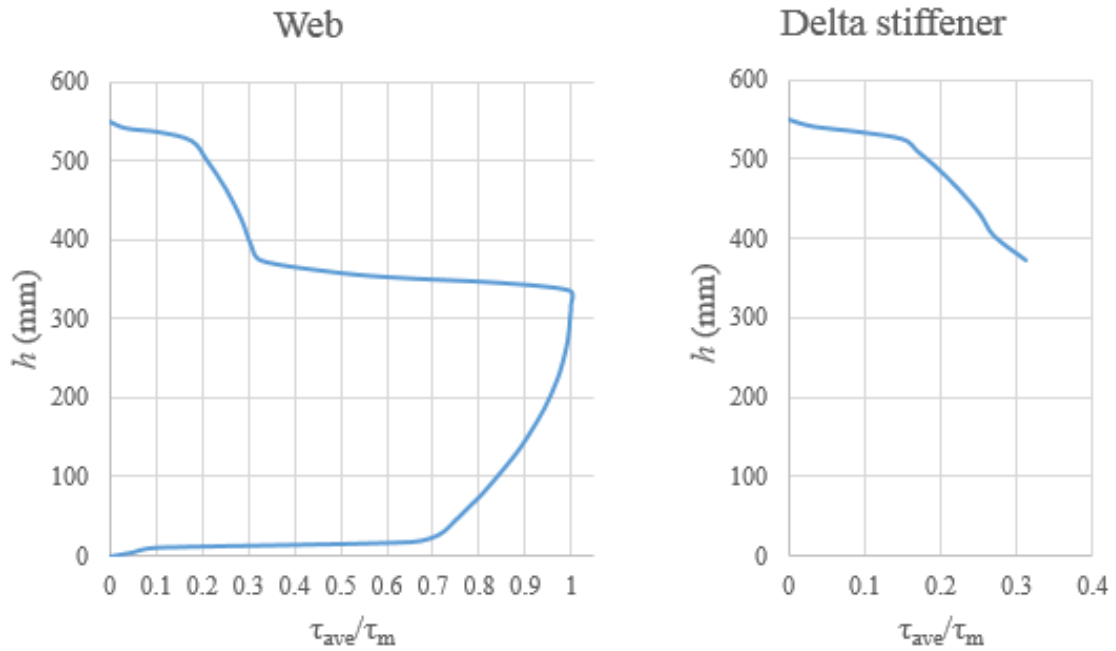
Figure 7.14 Shear stress distribution in Delta girder 8
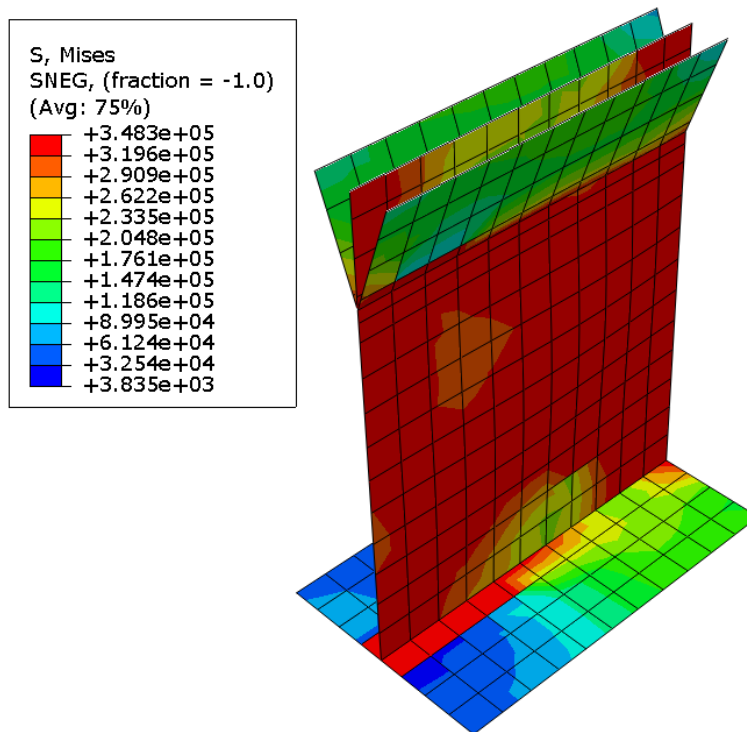
Figure 7.15 von Mises shear stress distribution in Delta girder 8 (unit in kPa)
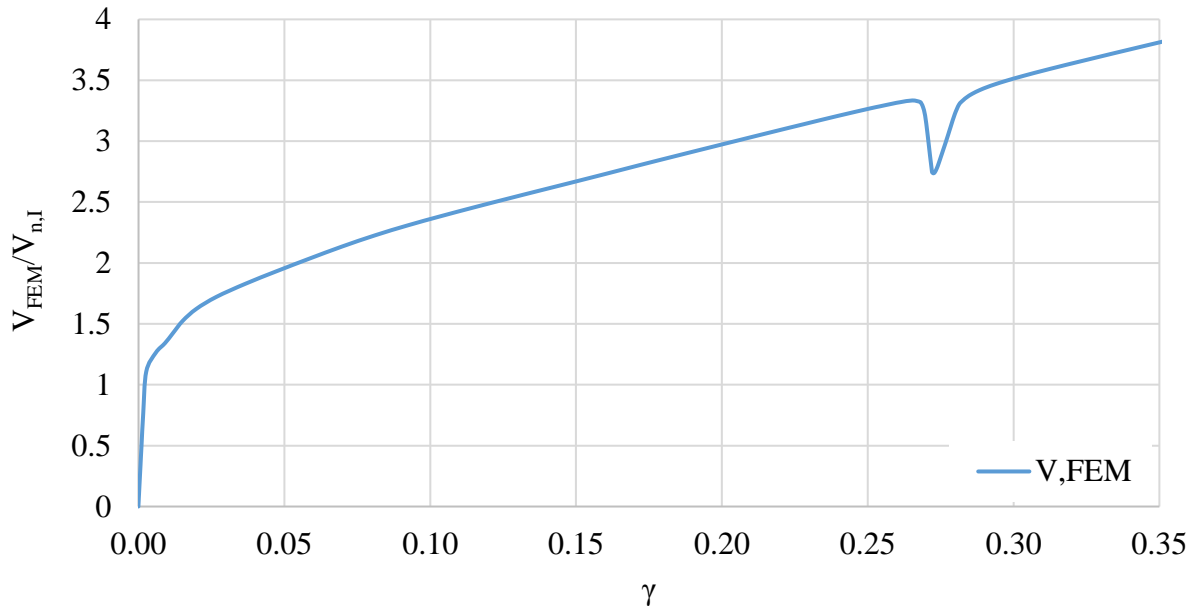
Figure 7.16 Web buckling identified in the shear resistance curve of Delta Girder 24

7.4 Shear Yielding of I-sections

A nonlinear inelastic analysis is performed on I-sections using the same procedure described in

Section 7.2.1 to determine their shear resistance capacity. They are then compared with the AISC

(2016a) and EC3 (2005) provisions. The boundary conditions used for the edges are given in

Figure 7.17 and summarized in Table 7.4. Similar boundary conditions have been utilized for

predicting the postbuckling shear capacity of I-sections (Glassman, Moreyra Garlock, Aziz, &

Kodur, 2016). The load V is applied on side 2 in a vertical direction. The FE analysis is

performed on equivalent welded standard European sections: one I-section (IPE 360) and one H-

section (HEA 400). The FE load-displacement curves are shown in Figures 7.18 and 7.19. These

figures also show the provisions for nominal shear resistance given in AISC (2016a), as well as

EC3 (2005) using η values of 1.0 and 1.2. The results show that the EC3 (2005) shear equations

with $\eta = 1.0$ provide a good estimate for yield initiation in the cross-section. On the other hand,

the EC3 (2005) equations with $\eta = 1.2$ allow the stress in the web to exceed the yield stress. It also allows relatively large vertical displacements with shear strain γ values of 0.048 for IPE 360 and 0.036 for HEA 400. On the other hand, the AISC (2016a) nominal shear resistance equations allow for some strain hardening in the cross-section, as explained in Section 7.2.2, and provide results in between the EC3 (2005) results with the two values of η.
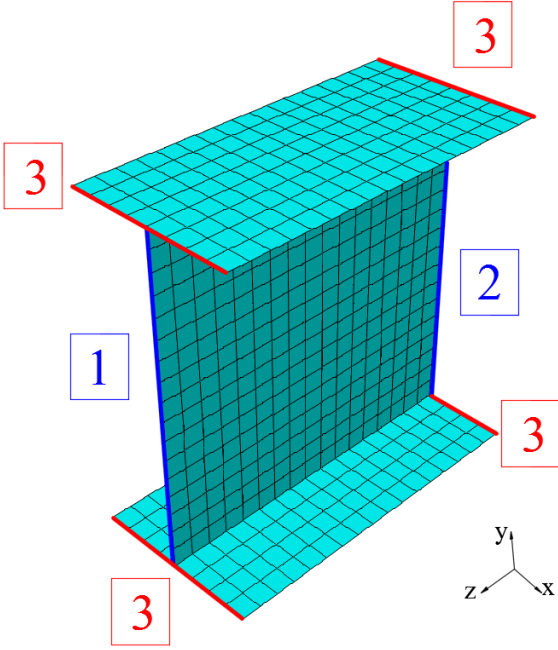
Figure 7.17 Mesh and boundary conditions used for the FE modeling of I-sections

Table 7.4 Boundary conditions used along each edge of the I-section shown in Figure 7.17

Side	Translation			Rotation		
	u_x	u_y	u_z	θ_x	θ_y	θ_z
1	X	X	X	X		X
2	X		X	X		X
3	X		X		X	X

229
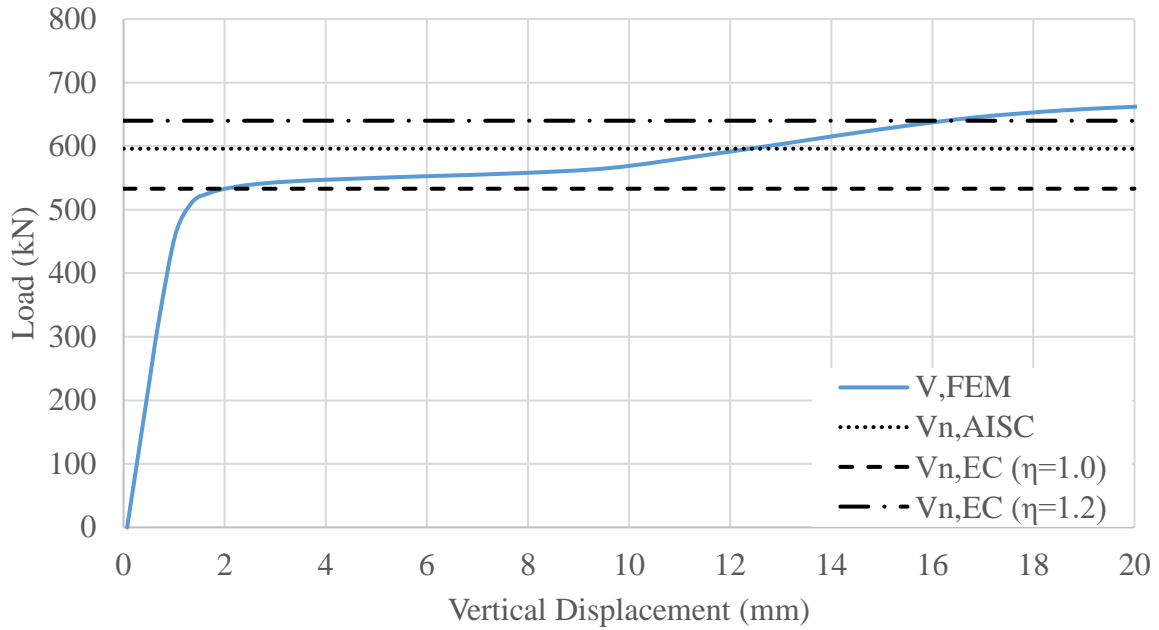
Figure 7.18 Comparison between FE simulations, AISC (2016a) and EC3 (2005) shear resistance

for a welded IPE 360 section
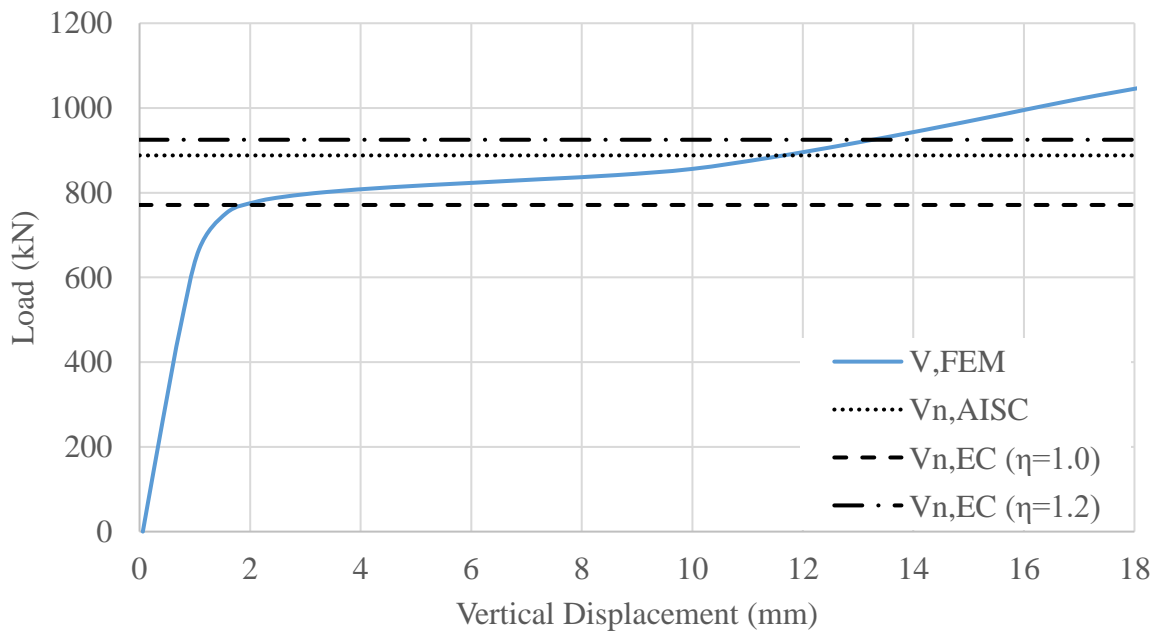
Figure 7.19 Comparison between FE simulations, AISC (2016a) and EC3 (2005) shear resistance

for a welded HEA 400 section

7.5   Recommended Design Equations for the Shear Capacity of Delta Girders

To be consistent with the recommended flexural design equations for Delta girders described in

Chapter 6 where the EC3 (2005) equations have been adopted, the recommended design

equations for the shear capacity of Delta girders will also follow the format of the EC3 (2005)

equations. Presented in Figure 7.20 are the normalized FE results of all the Delta girders that

were analyzed. The FE results are normalized against $V_{n,I}$, i.e., the shear capacity of the

corresponding welded I-section obtained using EC3 (2005) equations with $\eta = 1.0$. The

following equations are recommended for use in determining the shear capacity of Delta girders.

$$V_n = \frac{F_y A_v}{\sqrt{3}} \tag{7.19}$$

in which

$$A_v = \eta (A_{wl} + 0.5 A_d) \tag{7.20}$$

$$\eta = 1 + \frac{0.5 A_d}{A_{wl} + 0.5 A_d} \tag{7.21}$$

$$A_{wl} = (h - h_d) t_w \tag{7.22}$$

$$A_d = h_d t_w + 2 w_d t_d \tag{7.23}$$

where A_v is the shear resistance area, η is a factor that accounts for strain hardening and non-

uniform shear stress distribution and may conservatively be taken equal to 1.0, A_{wl} is the area of

the web portion below the delta region, A_d is the area of the delta region, h is the web height, h_d

is the height of the delta region, w_d is the width of the delta stiffener plate, and t_d and t_w are the thicknesses of the delta stiffener and the web, respectively.

The "0.5" factor in front of A_d in Eqs. (7.20) and (7.21) accounts for the non-uniform shear stress distribution in Delta girders as explained in Section 7.3.4 where it has been shown that lower shear stresses are obtained in the A_d region in comparison with the A_{wl} region. Furthermore, it is assumed that both the web and the delta stiffeners have reached the yield stress when η is obtained using Eq. (7.21); however, only the lower portion of the web A_{wl} is assumed to have yielded when η is conservatively taken as 1.0. Table 7.5 shows the shear resistance capacity of all Delta girders analyzed in this chapter, normalized with respect to the shear resistance of the corresponding I-section ($\eta=1.0$), with η values calculated from Eq. (7.21) and a conservative η value of one. The table also shows the shear strain γ that corresponds to the shear resistance V_n. The results show that using the conservative η value of 1.0 provides a 11% to 26% increase in the nominal shear capacity with respect to the I-section, while using the η value computed using Eq. (7.21) provides a 41% to 89% increase in the nominal shear capacity (18% to 58% increase based on $\eta=1.2$ for I-sections). The shear strains obtained using a η value of 1.0 are relatively small, whereas shear strains of up to 5.3% are obtained using the proposed equation for η. Moreover, by inspecting the $V_n/V_{n,I}$ values of Table 7.5 using Figure 7.20, it can be seen that the Delta girders can actually exhibit additional shear resistance. An assessment of the stress distribution at the proposed shear resistance will be performed in the following section.

As a final note, the analysis performed herein and the recommended design equations assume a monotonically increasing load. However, web yielding behavior is different under a

cyclic load that may occur during a major earthquake and special design considerations may be applied (Popov, 1980).

Table 7.5 Proposed normalized shear resistance capacity and the corresponding shear strain γ

Delta girder no.	$V_n/V_{n,I}$ (η=1.0)	γ (%)	$V_n/V_{n,I}$	γ (%)
3	1.15	0.38	1.63	2.8
5	1.11	0.43	1.41	2.9
6	1.13	0.50	1.46	4.3
7	1.16	0.44	1.65	4.3
8	1.18	0.48	1.70	5.3
9	1.17	0.42	1.54	2.8
10	1.23	0.60	1.65	4.0
11	1.21	0.38	1.76	2.9
12	1.26	0.51	1.86	3.9
16	1.20	0.46	1.74	4.4
17	1.20	0.55	1.60	3.4
24	1.26	0.59	1.85	3.9
28	1.21	0.53	1.76	4.1
31	1.28	0.50	1.89	3.2
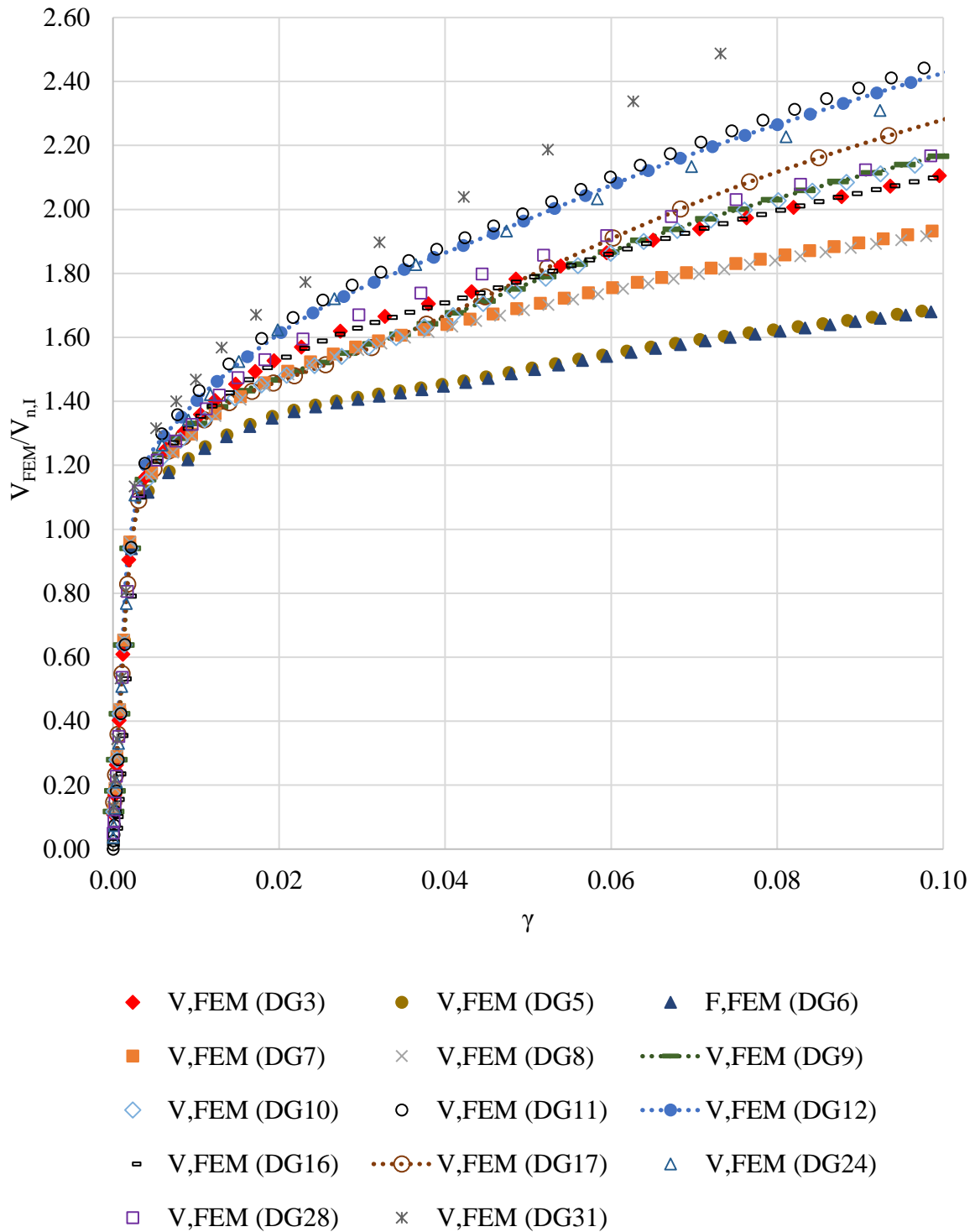
Figure 7.20 Comparison between normalized FE shear resistance results for all analyzied Delta

girders

7.6   Assessment of the Proposed Shear Equations

The shear capacity equations in Section 7.5 are assessed by inspecting the stress distribution in

two analyzed Delta girders when V_n is reached. For the case where η is conservatively taken as

1.0, the FE results show full yielding of the part of the web below the delta region, as shown in

Figure 7.21, while the stresses in the delta stiffeners remain below yield. For the case where η is

computed using Eq. (7.22), Figures 7.22 and 7.23 show the stress distribution in Delta girders 8

and 16, which correspond to the two Delta girders with the largest shear strain γ obtained as per

Table 7.5. The results show yielding of the entire web and the delta stiffeners without exceeding

the ultimate stress F_u. Therefore, the proposed equations provide good estimate of the shear

resistance capacity of Delta girders.
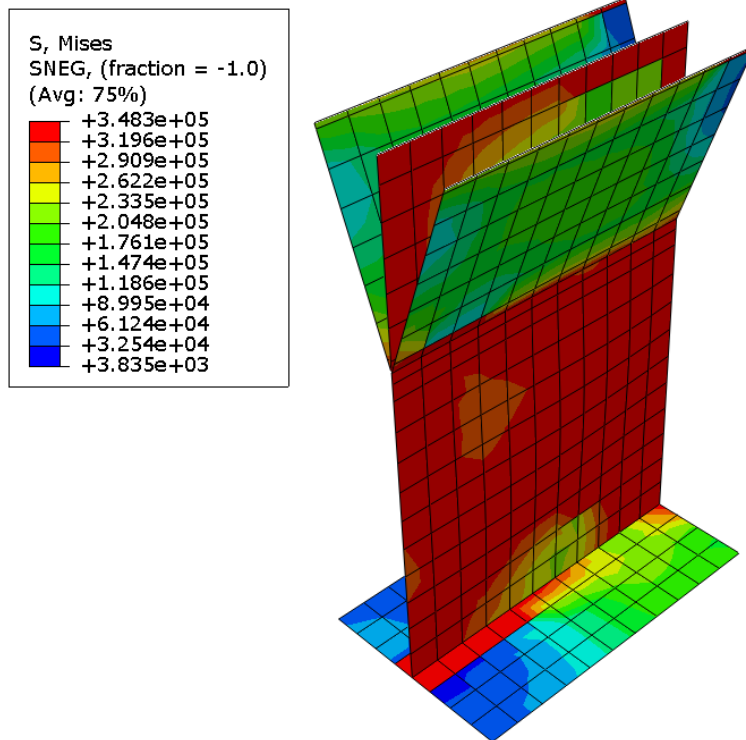
Figure 7.21 von Mises stress distribution at the proposed V_n (η=1.0) for Delta girder 8 (unit in

kPa)

235
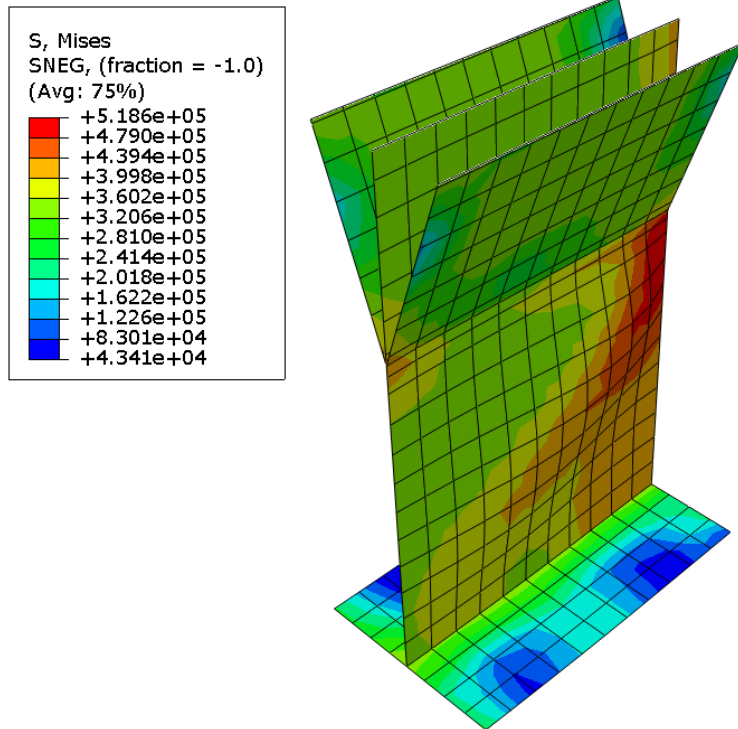
Figure 7.22 von Mises stress distribution at the proposed V_n for Delta girder 8 (unit in kPa)
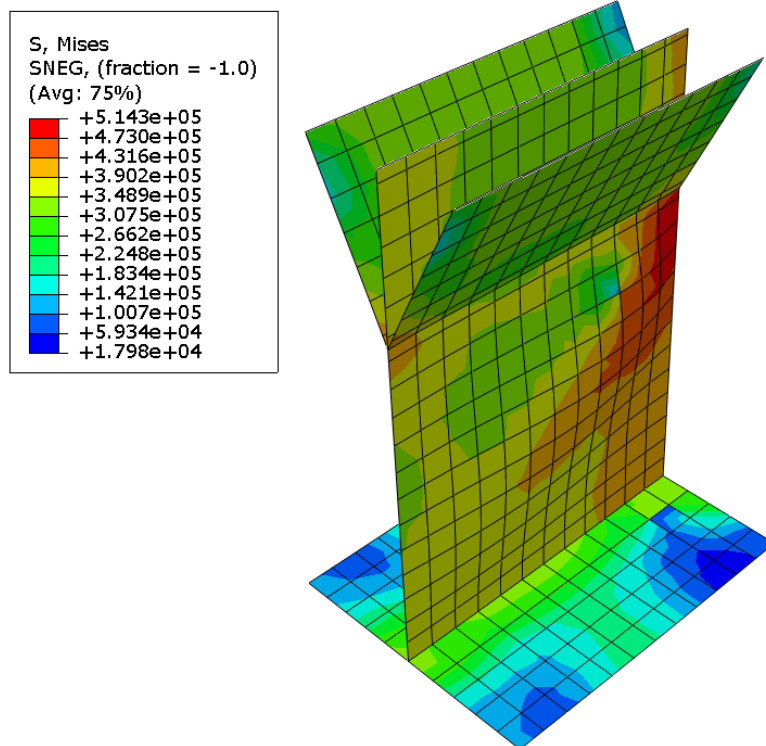
Figure 7.23 von Mises stress distribution at the proposed V_n for Delta girder 16 (unit in kPa)

7.7 <u>Summary</u>

In this chapter, the shear capacity of Delta girders is examined. For I-sections, shear forces are mainly resisted by the web. A comparison between the shear resistance equations in AISC (2016a) and EC3 (2005) was first presented. While AISC (2016a) provides one deign value for the shear resistance of I-sections that implicitly allows for some material strain hardening, EC3 (2005) provides one conservative shear design value and the possibility to increase the shear resistance by 20% to explicitly allow for material strain hardening. A nonlinear finite element model was then developed to determine the shear resistance of I-sections and Delta girders. The FE model includes the effects of initial geometrical imperfections and residual stresses and was verified for the specified boundary conditions and load application by comparing the numerical results obtained against the theoretical buckling loads of rectangular plates under a pure shear condition.

FE simulations were performed on the same set of Delta girders used in Chapter 6. They were selected to cover a wide range of practical European welded standard H- and I-sections under various delta stiffener configurations. Since standard European sections are classified as Class 1 cross-sections and the delta stiffeners satisfy the Class 1 requirements, all analyzed Delta girders can develop their full shear yielding capacity. The FE results showed some differences between the load-displacement curves of Delta girders and I-sections, particularly in the strain hardening region, which was attributed to the non-uniform shear stress distribution in Delta girders. An example of the elastic shear stress distribution in Delta girders was obtained using the FE software ShapeBuilder where it was observed that the maximum shear stress in the delta region is always smaller than the maximum shear stress at the centroid of the cross-section.

Thus, shear yielding in a Delta girder is a gradual process. Yielding starts in the part of the web below the delta region, and progresses into the delta region as the applied shear force increases.

Based on the FE results, equations for the nominal shear capacity of Class 1 (compact) Delta girders were proposed. Among the girders that were analyzed, the increase in shear capacity of a Delta girder with respect to the base I-section varies from 41% to 89%. An assessment of the proposed shear capacity equations using FE simulations showed that the proposed equations provide a good estimate for the shear resistance capacity of Delta girders under monotonically increasing loads.

Chapter 8

Design Examples

8.1   Introduction

This chapter provides two design examples to illustrate how the proposed equations can be used

for the design of Delta girders. The first example is concerned with the design of a new girder

while the second example demonstrates how delta stiffeners can be added to strengthen an

existing girder. These examples will only address those concepts that have been studied in this

dissertation, i.e., flexural and shear capacities, plus a check for deflection.

8.2   Design Example 1: A Simply-Supported Beam under a Uniformly-Distributed Load

The girder shown in Figure 8.1 is to be designed to carry a factored uniformly-distributed load

q_u of 57 kN/m (which includes a 225 kg/m allowance for self-weight and 22 kN/m service live

load). The load is applied on the top flange. The span of the simply-supported girder is 12.0 m.

Due to specific site limits, lateral supports that fully prevent lateral deflections and twisting

rotations can only be provided at the two ends of the girders. The girder is to be designed for

moment and shear, then checked for allowable deflection. The following material properties are

to be used: F_y = 345 MPa, E = 200 GPa, G = 75 GPa.

Solution:

The required moment capacity is

$$M_{Ed} = (1/8)(57)(12)^2 = 1,026 \text{ kN-m}$$

q_u = 75 kN/m

12.0 m
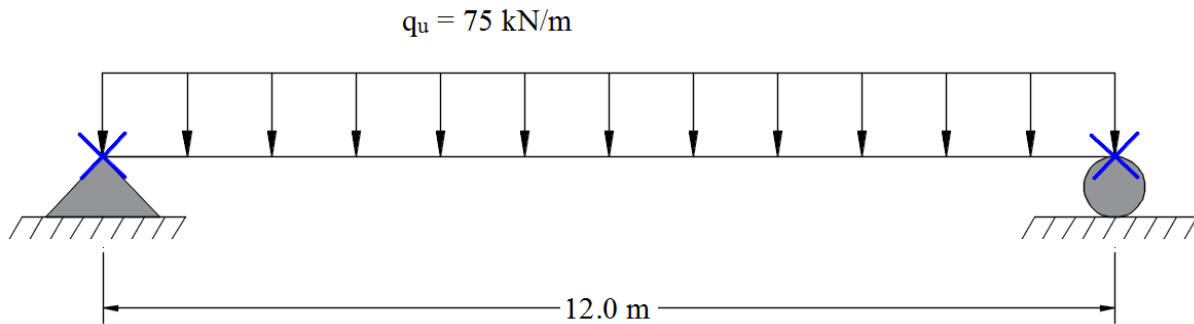
Figure 8.1 Beam of design example 1

Because of the relatively large span and load, we will start with the heaviest available H-section, i.e., HEA 1000. The section is a Class 1 section. The non-uniform moment distribution is accounted for by using $C_b = 1.14$, and the load height is accounted for by using Eq. (2.10) as follows:

$$C_b^* = 1.14\left(1.4^{-2\times495/959}\right)(1) = 0.805$$

The design moment capacity of the section in accordance with EC3 (2005) equations as presented in Section 6.2.2 is

$$M_{b,Rd} = 1{,}078 \text{ kN-m}$$

$$M_{Ed}/M_{b,Rd} = 0.95 \leq 1 \therefore \text{ok}$$

The HEA 1000 section is adequate to carry to the applied loads; however, this section is only available for special orders at a relatively high cost. An alternative solution is to add delta stiffeners to an existing H-section as shown below.

Delta stiffeners are to be added to the HEA 500 section to enhance its flexural capacity. The thickness of the stiffeners is selected to be at least equal to the web thickness. Since the web thickness is 12 mm, the selected delta stiffener thickness is 12 mm. The configuration of the delta stiffeners will be selected based on the recommendations of Section 6.8. For the HEA 500, $d/b_c = 1.63$ and L_{rI} is calculated using Eq. (2.15) as follows:

$$L_{rI} = 1.95 \times \frac{81.52}{10^3} \times \frac{200{,}000}{0.7 \times 345} \sqrt{\frac{2.57}{3.43 \times 467} + \sqrt{\left(\frac{2.57}{3.43 \times 467}\right)^2 + 6.76 \left(\frac{0.7 \times 345}{200{,}000}\right)^2}} = 9.4 \text{ m}$$

From Table 6.42, for $d/b_c \leq 2$ and $L_b > L_{rI}$, try the smallest recommended delta stiffener configuration of $h_d = h/5$ and $b_d = 2b_c/3$. The dimensions and properties of the newly formed cross-sections are obtained using the equations in Tables 3.13 and 3.14 and are summarized as follows: $b_c = b_t = 300$ mm, $b_d = 200$ mm, $d = 490$ mm, $h_d = 88.8$ mm, $w_d = 117.3$ mm, $t_c = t_t = 23$ mm, $t_w = 12$ mm, $t_d = 12$ mm, $\bar{y} = 269.79$ mm, $I_x = 9.27 \times 10^8$ mm⁴, $I_y = 1.15 \times 10^8$ mm⁴, $S_{xc} = 4.21 \times 10^6$ mm³, $J = 2.00 \times 10^7$ mm⁴, $e_y = -17.07$ mm, $C_w = 5.47 \times 10^{12}$ mm⁶, $Z_x = 4.16 \times 10^6$ mm³.

The coefficient of monosymmetry β_x is calculated using Eq. (2.5) as follows:

$$I_{yc} = 1.15 \times 10^8 - (1/12)(23)(300)^3 - (1/12)(444)(12)^3 = 6.32 \times 10^7 \text{ mm}^4$$

$$\beta_x = 0.9(467) \left(\frac{2 \times 6.32 \times 10^7}{1.15 \times 10^8} - 1\right) \left[1 - \left(\frac{1.15 \times 10^8}{9.27 \times 10^8}\right)^2\right] = 41 \text{ mm}$$

The elastic critical buckling moment and C_b^* are computed using Eqs. (2.3) and (2.10), respectively, as follows:

$$C_b^* = 1.14\left(1.4^{-2\times245/467}\right)(1) = 0.801$$

$$M_{cr} = (0.801)\frac{\pi^2(200{,}000)(1.15\times10^8)}{(10^6)(12{,}000)^2}\left\{\frac{41}{2}\right.$$

$$+ \left.\sqrt{\left(\frac{41}{2}\right)^2 + \left[\frac{5.47\times10^{12}}{1.15\times10^8} + \frac{(75)(2.0\times10^7)}{(200)(1.15\times10^8)}\frac{(12{,}000)^2}{\pi^2}\right]}\right\}$$

$$M_{cr} = 1{,}288 \text{ kN-m}$$

The moment capacity of the Delta girder is computed using the equations presented in Section 6.2.2 and the recommendations given in Section 6.5 as follows:

$$\bar{\lambda}_{LT} = \sqrt{\frac{(4.16)(345)}{1{,}288}} = 1.06$$

For Delta girders with $d/b_c \leq 2$, use buckling curve "a" and thus $\alpha_{LT}=0.21$.

$$\Phi_{LT} = 0.5[1 + 0.21(1.06 - 0.4) + 0.75\times1.06^2] = 0.991$$

$$\chi_{LT} = \frac{1}{0.991 + \sqrt{(0.991)^2 - 0.75(1.06)^2}} = 0.733$$

$$M_{b,Rd} = (0.733)(4.16)(345) = 1{,}052 \text{ kN-m}$$

$$M_{Ed}/M_{b,Rd} = 1{,}026/1{,}052 = 0.975 \leq 1.0 \ \therefore \text{ ok}$$

The shear design value is

$$V_{Ed} = \frac{(57\times12)}{2} = 342 \text{ kN}$$

The shear resistance is obtained in accordance with Section 7.5 as follows

$\eta = 1.0$ (conservative)

$A_v = (444 - 88.8)(12) + 0.5(88.8 \times 12 + 2 \times 117.3 \times 12) = 6{,}203 \text{ mm}^2$

$V_n = \dfrac{1}{\sqrt{3}}(345 \times 6{,}203 \times 10^{-3}) = 1{,}236 \text{ kN}$

$\dfrac{V_{Ed}}{V_n} = 0.28 \leq 1.0 \quad \therefore \text{ok}$

Check beam deflection under service live load as follows:

$\Delta_{all} = \dfrac{L}{360} = \dfrac{12{,}000}{360} = 33.3 \text{ mm}$

$\Delta_L = \dfrac{5qL^4}{384EI_x} = \dfrac{5(22)(10^{-3})(12{,}000)^4}{(384)(200)(9.27 \times 10^8)} = 32.0 \text{ mm} \leq \Delta_{all} \quad \therefore \text{ok}$

Check the width-to-thickness ratio of the delta stiffeners as follows

$\dfrac{w_d}{t_d} = \dfrac{117.3}{12} = 9.8 \leq 72\sqrt{\dfrac{235}{345}} = 59.4 \quad \therefore \text{ok}$

Check the dead load of the Delta girder: $180 \text{ kg/m} \leq 225 \text{ kg/m} \quad \therefore \text{ok}$

The final design shows that a Delta girder formed by welding two delta stiffeners to a standard hot-rolled HEA 500 section is adequate. The delta stiffener configurations are $h_d = h/5$ and $b_d = 2b_c/3$ with a plate thickness of 12 mm.

8.3 Design Example 2: Strengthening of a Simply-Supported Beam under a Concentrated Load

The 8.0-m long HEA 400 girder, Class 1 section, in Figure 8.2 is to be retrofitted so it can carry a factored midspan concentrated load Q_u applied on the top flange. The girder is simply-supported at both ends where lateral deflections are effectively restrained and twisting rotations are partially restrained. The $M_{Ed}/M_{b,Rd}$ of this beam is 0.91 based on Q_u=260 kN. The girder needs to be strengthened to carry the factored concentrated load Q_u of 400 kN (which includes a 150 kg/m allowance for self-weight and 190 kN service live load). The girder is to be checked only for its moment, shear and deflection capacities. The following material properties are to be used: $F_y = 345$ MPa, $E = 200$ GPa, $G= 75$ GPa.
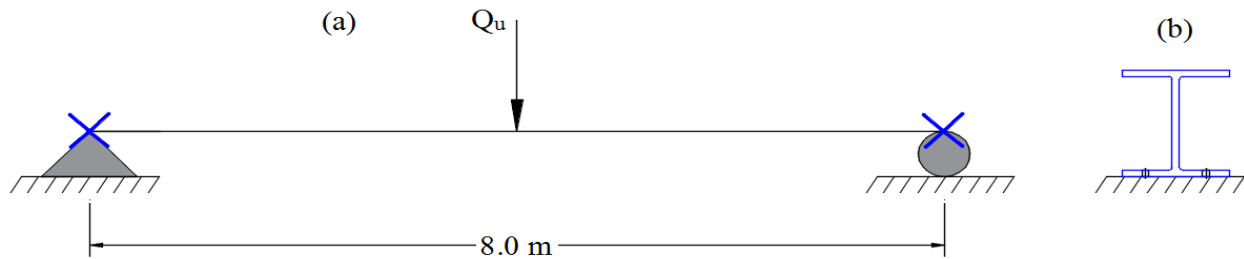
Figure 8.2 (a) Beam of design example 2, (b) End restraints

Solution:

The required moment capacity is

$M_{Ed} = (400)(8)/(4) = 800$ kN-m

The partial torsional end restraints are accounted for as follows (Trahair et al., 2008):

$$k_{cr} = 1 + 0.5 \left(\frac{h_o}{6L}\right)\left(\frac{t_f}{t_w}\right)^3 \left(1 + \frac{b_f}{h_o}\right) = 1 + 0.5 \left(\frac{371}{6 \times 8,000}\right)\left(\frac{19}{11}\right)^3 \left(1 + \frac{300}{371}\right) = 1.036$$

$L_{cr} = k_{cr}L_b = 1.036{\times}8 = 8.29$ m

The non-uniform moment distribution is accounted for by using $C_b = 1.32$, and the load height is accounted for by using Eq. (2.10) as follows:

$$C_b^* = 1.32\left(1.4^{-2{\times}195/371}\right)(1) = 0.927$$

The beam will be strengthened by adding delta stiffeners to the HEA 400 section. The thickness of the stiffeners is selected to be at least equal to the web thickness. Since the web thickness is 11 mm, the selected delta stiffener thickness is 12 mm (based on available increments in steel plate thickness). The configuration of the delta stiffeners will be selected based on recommendations provided in Section 6.8. From Table 6.42, for $d/b_c \leq 2$ and $L_b \leq L_{rI} = 10$ m, try the smallest recommended delta stiffener configuration of $h_d = h/5$ and $b_d = 2b_c/5$. The dimensions and properties of the newly formed cross-sections are obtained using the equations in Tables 3.13 and 3.14 and are summarized as follows: $b_c = b_t = 300$ mm, $b_d = 120$ mm, $d = 390$ mm, $h_d = 70.4$ mm, $w_d = 76.6$ mm, $t_c = t_t = 19$ mm, $t_w = 11$ mm, $t_d = 12$ mm, $\bar{y} = 212.28$ mm, $I_x = 4.71{\times}10^8$ mm^4, $I_y = 8.84{\times}10^7$ mm^4, $S_{xc} = 2.65{\times}10^6$ mm^3, $J = 7.5{\times}10^6$ mm^4, $e_y = -19.27$ mm, $C_w = 2.79{\times}10^{12}$ mm^6, $Z_x = 2.65{\times}10^6$ mm^3.

The coefficient of monosymmetry β_x and the elastic critical buckling moment at $L_{cr} = 8.29$ m are obtained in a similar way as Design Example 1 and are equal to: $\beta_x = 10.2$ mm, $M_{cr} = 1,196$ kN-m.

The design moment capacity of the Delta girder is computed using the equations presented in Section 6.2.2 and the recommendations given in Section 6.5 as follows:

$$\bar{\lambda}_{LT} = \sqrt{\frac{(2.65)(345)}{1,196}} = 0.874$$

For Delta girders with $d/b_c \leq 2$, use buckling curve "a" and thus $\alpha_{LT} = 0.21$.

$$\Phi_{LT} = 0.5[1 + 0.21(0.874 - 0.4) + 0.75 \times 0.874^2] = 0.836$$

$$\chi_{LT} = \frac{1}{0.836 + \sqrt{(0.836)^2 - 0.75(0.874)^2}} = 0.840$$

$$M_{b,Rd} = (0.84)(2.65)(345) = 768 \text{ kN} - \text{m}$$

$$M_{Ed}/M_{b,Rd} = 800/768 = 1.04 > 1.0 \therefore \text{N.G.}$$

Now try the largest recommended delta stiffener configuration as per Table 6.42 which is $h_d = h/4$ and $b_d = b_c/2$. The dimensions and properties of the newly formed cross-sections are obtained using the equations in Tables 3.13 and 3.14 and are summarized as follows: $b_c = b_t = 300$ mm, $b_d = 150$ mm, $d = 390$ mm, $h_d = 88$ mm, $w_d = 99.8$ mm, $t_c = t_t = 19$ mm, $t_w = 11$ mm, $t_d = 12$ mm, $\bar{y} = 214.78$ mm, $I_x = 4.74 \times 10^8$ mm^4, $I_y = 9.10 \times 10^7$ mm^4, $S_{xc} = 2.71 \times 10^6$ mm^3, $J = 1.21 \times 10^7$ mm^4, $e_y = $ -20.52 mm, $C_w = 2.75 \times 10^{12}$ mm^6, $Z_x = 2.65 \times 10^6$ mm^3.

The coefficient of monosymmetry β_x and the elastic critical buckling moment at $L_{cr} = 8.29$ m are obtained in a similar way as Design Example 1 and are equal to: $\beta_x = 19.7$ mm, $M_{cr} = 1,510$ kN-m.

The design buckling resistance moment of the Delta girder is computed as follows:

$$\bar{\lambda}_{LT} = \sqrt{\frac{(2.65)(345)}{1,510}} = 0.778$$

$$\Phi_{LT} = 0.5[1 + 0.21(0.778 - 0.4) + 0.75 \times 0.778^2] = 0.767$$

$$\chi_{LT} = \frac{1}{0.767 + \sqrt{(0.767)^2 - 0.75(0.778)^2}} = 0.882$$

$$M_{b,Rd} = (0.882)(2.65)(345) = 806 \text{ kN-m}$$

$$M_{Ed}/M_{b,Rd} = 800/806 = 0.99 \leq 1.0 \; \therefore \text{ Ok}$$

The shear design value is

$$V_{Ed} = \frac{400}{2} = 200 \text{ kN}$$

The shear resistance is obtained in accordance with Section 7.5 as follows:

$$\eta = 1.0 \text{ (a conservative value)}$$

$$A_v = (352 - 88)(11) + 0.5(88 \times 11 + 2 \times 99.8 \times 12) = 4,586 \text{ mm}^2$$

$$V_n = \frac{1}{\sqrt{3}} (345 \times 4,586 \times 10^{-3}) = 913 \text{ kN}$$

$$\frac{V_{Ed}}{V_n} = 0.22 \leq 1.0 \; \therefore \text{ ok}$$

Check beam deflection under service live load as follows:

$$\Delta_{all} = \frac{L}{360} = \frac{8,000}{360} = 22.2 \text{ mm}$$

$$\Delta_L = \frac{Q_L L^3}{48EI_x} = \frac{(190)(8,000)^3}{(48)(200)(4.74\times10^8)} = 21.4 \text{ mm} \leq \Delta_{\text{all}} \ \therefore \text{ ok}$$

Check the width-to-thickness ratio of the delta stiffeners as follows

$$\frac{w_d}{t_d} = \frac{99.8}{12} = 8.3 \leq 72\sqrt{\frac{235}{345}} = 59.4 \ \therefore \text{ ok}$$

Check the dead load of the Delta girder: 147 kg/m $\leq$ 150 kg/m $\therefore$ ok

The final design shows that strengthening the existing HEA 400 girder by welding to it two delta stiffeners can be a viable solution to resist the increase in the applied loads. The delta stiffener configurations are $h_d = h/4$ and $b_d = b_c/2$ with a plate thickness of 12 mm.

If a HEA section is to be used, the lightest HEA section that can carry the specified load is a HEA 550 section. This represents an increase of weight of 13% over the HEA 400 section with the delta stiffeners. Alternatively, if a compression flange cover plate is to be used, the required size of the cover plate is 30 cm × 2.4 cm. The weight of this plate is three times that of the delta stiffeners, and the resulting girder is 26% heavier than the Delta girder.

8.4   Summary

This chapter presented two illustrative design examples of Delta girders. One example shows the design of a simply-supported girder under a uniformly-distributed load, while the second example shows the retrofitting of an existing simply-supported girder under a midspan concentrated load. The use of delta stiffeners is considered a better alternative for the following reasons:

1. If delta stiffeners were not used for these girders, the lightest sections that would have to be used to carry the specified loads were HEA 1000 and HEA 550, respectively. This would represent an increase in weight over the Delta girders of 51% and 13%, respectively.

2. For the girder in the first example, by using the HEA 500 instead of the HEA 1000 section, the height of the member is reduced from 990 mm to 490 mm. This means a 500 mm increase in vertical clearance.

3. For the girder in the second example, adding delta stiffeners to the existing member may very well result in cost and time savings. Instead of replacing the HEA 400 section with a larger and heavier HEA 550 section, delta stiffeners are to be welded to the existing girder to increase its capacity so it is now capable of carrying the higher load.

4. If the alternative method of providing a cover plate to strengthen the existing beam is to be adopted in the second example, the design shows that the lightest cover plate required is 30 cm wide (equals to the flange width) and 2.4 cm thick. The weight of the cover plate is 300% higher than that of the two delta stiffeners and the resulting girder will be 26% heavier than the Delta girder.

Chapter 9

Summary and Conclusions

9.1   Research Summary and Conclusions

This research focuses on the design and behavior of simply-supported steel Delta girders subjected to uniform bending and pure shear. The work covers a comprehensive range of straight, homogeneous and prismatic Delta girders based on the dimensions of European standard H- and I-sections. The delta stiffener configurations also cover a large range of practical configurations. Refined three-dimensional (3D) finite element (FE) models were developed and verified to determine the flexural and shear capacities of these Delta girders. The following are the main conclusions and key contributions of this research based on their order of appearance in this dissertation:

- Closed-form equations for the geometric and torsional cross-section properties of Delta girders were derived and verified against results obtained using a commercial finite element software. The results have shown that the equations derived for the torsion constant J, the shear center location e_y and the warping constant C_w provide values that have a maximum error of 1.8%, 1.6% and 0.3%, respectively, with respect to the FE results. These equations are summarized in Tables 3.13 and 3.14.

- Based on FE eigenvalue buckling analysis, it was found that the elastic lateral-torsional buckling (LTB) capacity of simply-supported Delta girders under uniform moment can be obtained using the elastic LTB equation derived for open monosymmetric I-sections and given in Eq. (2.3). It was also shown that the approximate form of the

250

monosymmetry coefficient β_x given in Eq. (2.5) can be used for Delta girders as long as the moment of inertia of the delta stiffeners about the weak axis is included in the I_{yc} term.

- A comparison between the effects of adding delta stiffeners to and increasing the web thickness of I-sections has shown that delta stiffeners are much more effective in increasing the elastic LTB capacity of the sections.

- A parametric study that included a comparison of the elastic LTB capacity of 1,024 Delta girders and I-girders has led to the following observations: (a) Within the range of girders studied, the maximum increase in LTB capacity is 1294.2%. This is associated with a 52.6% increase in cross-section weight, (b) delta stiffeners are slightly more effective for larger cross-sections, (c) delta stiffeners provide only a minor advantage when the girder length increases, and better results are obtained when they are added to an initially monosymmetric I-section, (d) increasing the stiffener thickness above the web thickness is not an effective method to increase the LTB capacity of the girder, (e) the combination of $h_d = 2h/5$ and $b_d = 3b_c/4$ provides the largest increase in elastic LTB capacity, and (f) the value of b_d is as important as h_d in affecting the LTB capacity of Delta girders.

- A nonlinear inelastic FE model was developed to study the flexural behavior of simply-supported Delta girders under a uniform bending moment. The FE model included the effects of initial geometrical imperfections and residual stresses. For Delta girders, a residual stress pattern was proposed based on available patterns of welded monosymmetric I-sections and rectangular steel plates. The FE model and modeling techniques were verified by comparing the experimental inelastic buckling load of a test

beam to the numerically obtained buckling load. The FE model predicted the experimental buckling load with a 4.15% error.

- A sensitivity study was conducted to investigate the effects of the magnitudes of initial geometrical imperfections and residual stresses on the LTB capacity of Delta girders. The study included three magnitudes of initial imperfections, L_b/1000, L_b/2000 and L_b/4000, as well as using the full and half magnitudes of the proposed residual stress values. Within the range of the girders analyzed, the results have shown that using reduced imperfection magnitudes increases the LTB capacity by up to 18.2%.

- The numerically obtained flexural capacity curves of Delta girders were compared to the flexural capacity curve of AISC (2016a) and the four flexural resistance curves of EC3 (2005) using the rolled sections or equivalent welded sections case. The results have shown that the recommended LTB curve in AISC (2016a) overpredicts the buckling capacity of Delta girders by an average of 9% and a maximum value of 21%. In contrast, curves "a" and "b" of the EC3 (2005) show a much better fit to the FE results with an average difference of 2% and a maximum difference of 7%. The results have also shown that the LTB capacity of Delta girders is sensitive to the d/b_c ratio.

- Based on nonlinear inelastic FE simulation results, the flexural resistance of simply-supported Delta girders subjected to uniform moment should be computed using EC3 (2005) buckling curves "a" and "b" for rolled sections or equivalent welded sections case were recommended for Delta girders with $d/b_c \leq 2$ and $d/b_c > 2$, respectively. The results have shown that the recommended buckling curves predicted the buckling capacity of Delta girders with an average error of 2% (unconservative) when compared

252

with the FE simulation results for both $d/b_c \leq 2$ and $d/b_c > 2$, and with a maximum difference of 7% (unconservative).

- Design guidelines that can be used to select effective delta stiffener configurations were provided in Table 6.42 based on comparisons between the LTB curves of Delta girders and their corresponding I-sections. These recommendations are based on the d/b_c ratio and the L_r value of the corresponding I-sections.

- The shear capacity of Delta girders was analyzed using a nonlinear inelastic FE model under pure shear. The FE results have indicated that some differences exist between the load-displacement curves of Delta girders and I-sections, particularly in the strain hardening region. This is attributed to the non-uniform shear stress distribution in Delta girders.

- A comparison between the elastic shear stress distribution in I-sections and Delta giders has shown that, while the shear stress is assumed to be uniform over the depth of an I-section, it is non-uniform in Delta girders. It was shown that the maximum shear stress at the centroid is much larger than the maximum shear stress in the delta region of the cross-section. Hence, shear yielding is a gradual process in Delta girders that starts in the part of the web below the delta region and progresses into the delta region under an increasing shear force.

- Equations that follow the EC3 (2005) format were proposed for the nominal shear capacity of Class 1 Delta girders under monotonically increasing loads. The equations provide flexibility for the designer by either allowing strain hardening in the cross-section or conservatively ignore it. Within the range of the analyzed girders, a 41% to 89%

253

increase in the shear capacity of Delta girders with respect to the base I-section was obtained.

9.2 **Recommendations for Future Work**

The research conducted in this dissertation is a systematic study of the flexural and shear capacities of steel Delta girders. The flexural and shear resistance capacities examined in this study are limited to compact sections (Class 1 sections). The work presented herein lays the foundation for a comprehensive number of further research ideas that will provide a more comprehensive understanding of the behavior of Steel Delta girders. Some of these ideas are summarized as follows:

- Since experimental testing was not performed as part of the current study and the work presented in this dissertation is based primarily on analytical formulations and finite element simulation, experimental work is recommended to verify the current findings.

- Experimental measurements of residual stresses are required to verify the adequacy of the proposed residual stress pattern. These measurements should be conducted for cases where delta stiffeners are added to hot-rolled and welded beams. This would result in two residual stress patterns and could lead to different buckling curves as is the case for the existing buckling curves in EC3 (2005).

- Work on the flexural and shear capacities should be extended to cover all section types, particularly cross-sections with slender component elements.

- The current work considered only the cases of pure moment and pure shear, and should be extended to cover various types of loadings and boundary conditions and the effect of load height and moment-shear capacity interaction. At present, coefficients and equations

are available to account for the aforementioned conditions in I-sections; however, the applicability of these coefficients and equations to Delta girders should be examined.

- Examine the required width-to-thickness ratios for the compression flange, web, and delta stiffener for all section classifications.

- The behavior of hybrid Delta girders, i.e., when the component elements have different yield stress warrants some careful study, especially when the delta stiffeners have a different yield stress than that of the base I-section.

- The application of delta stiffeners to other types of beams, such as castellated beams and curved I-sections, to enhance their LTB capacity should be investigated.

- Further work should be conducted to study the effect of using high-performance steel (HPS) on the behavior of homogenous and hybrid Delta girders.

- This study covered prismatic members in which the delta stiffeners are added along the full length of the base I-section. The work should be extended to study the application of delta stiffeners to limited longitudinal sections. This method should be particularly effective for slender beams in which LTB is most likely the governing limit state.

- Finally, the behavior of Delta girders under cyclic loads should also be a topic of interest if these girders are to be used in seismic applications.

Appendix

List of Notations and Symbols

A	Cross-section area
A^*	Percent increase in cross-section area
A_D	Cross-section area of Delta girders
A_d	Area of the delta region
A_I	Cross-section area of I-girder
A_i	Cross-section area of component plate i
$\hat{A}_i$	Area enclosed by the medial line of cell i
A_{MI}	Cross-section area of the modified I-girder
A_v	Shear resistance area
A_w	Web area defined as the overall depth of the section d times the web thickness t_w
A_{wel}	Area of added weld metal
A_{wl}	Area of the web portion below the delta region
B	Welding process constant
C_b	Lateral-torsional buckling modification factor for non-uniform moment diagrams
C_b^*	Modified equation for C_b
C_i	Torsion constant aspect ratio correction factor
C_v	Web shear coefficient
C_w	Warping constant
C_1, C_2, C_3	Coefficients to account for various types of loadings and end-restraint conditions
E	Modulus of elasticity
E_{sh}	Strain hardening modulus
F	Tendon force
F_L	Magnitude of flexural stress in the compression flange at which LTB is influenced by yielding
F_{sh2}	Stress at the end of the initial strain hardening region
F_u	Ultimate stress of the material

F_y	Yield stress of the material
G	Shear modulus
I_c	Moment of inertia for the compression flange about the axis of symmetry
I_t	Moment of inertia for the tension flange about the axis of symmetry
I_{wx}, I_{wy}	Warping products of inertia about the principal axes
I_x, I_y	Moment of inertia about the principal axes
$I_{x,d}, I_{y,d}$	Moment of inertia of the delta stiffener about the principal axes
$I_{x,i}, I_{y,i}$	Moment of inertia of the component plate i about the principal axes
$I_{x',d}, I_{y',d}$	Moment of inertia of the delta stiffener about its local principal axes
I_{xy}	Product of inertia
I_{yc}	Moment of inertia of the compression flange about the minor axis
J	St. Venant torsional constant
J_Δ	St. Venant torsional constant of the delta region
K^{MN}	Tangent stiffness matrix
K_y	Effective-length factor accounting for full cross-section lateral bending restraint at the ends of L_b
K_z	Effective-length factor accounting for the warping restraint at the ends of L_b
L	Span length
L_b	Lateral unbraced length of the compression flange
L_{cr}	Effective length of the beam
L_{ij}	Length of the element connecting points i and j
L_p	Limiting laterally unbraced length for the limit state of yielding
L_r	Limiting laterally unbraced length for the limit state of inelastic lateral-torsional buckling
L_{rD}	L_r value of a Delta girder
L_{rI}	L_r value of an I-section
$M_{b,Rd}$	Design moment capacity
M_{cr}	Elastic lateral-torsional buckling moment
M_{cr}^*	Percent increase in lateral-torsional buckling capacity
M_{crD}	Lateral-torsional buckling moment capacity of a Delta girder

M_{crI}	Lateral-torsional buckling moment capacity of an I-girder
M_{crMI}	Lateral-torsional buckling moment capacity of modified an I-girder
M_{Ed}	Design moment capacity
M_{FEM}	FE simulation flexural capacity
M_n	Nominal flexural resistance
M_o	Uniform bending moment
M_p	Plastic bending moment
M_{yc}	Moment that corresponds to yielding of the extreme compression fibers
$M_{z'}$	Twisting moment about the z' axis
Q	First moment of the considered area with respect to the neutral axis
Q_u	Factored concentrated load
R_m	Parameter used to account for the beam curvature
R_{pc}	Web plastification factor
S_{xc}	Elastic section modulus about the x-axis with respect to the compression flange
S_{xt}	Elastic section modulus about the x-axis with respect to the tension flange
T	Torque applied to a cross-section
V	Shear force
V_{cr}	Elastic critical buckling shear load
V_{Ed}	Design shear capacity
V_{FEM}	FE simulation shear capacity
V_n	Nominal shear capacity
$V_{n,I}$	Nominal shear capacity of an I-section
$V_{pl,Rd}$	Plastic shear resistance
$W_{eff.y}$	Effective section modulus about the strong axis
$W_{el.y}$	Elastic section modulus about the strong axis
$W_{pl.y}$	Plastic section modulus about the strong axis
Z_x	Plastic section modulus about the x-axis
a	Spacing between transverse stiffeners
a_σ	Distance between the shear center and the point where σ acts

b	Total width of a steel plate
b_c	Width of the compression flange
b_d	Distance between the centerlines of delta stiffeners at the intersection with the inside face of the compression flange
b_i	Width of component plate i
b_t	Width of tension flange
b_1	Total width of a rectangular tubular section
b_2	Total height of a rectangular tubular section
c_i	Width of tension residual stress blocks in component plate i
d	Full depth of cross-section
e_x	Horizontal distance from centroid to shear center
e_y	Vertical distance from centroid to shear center
f_{c_i}	Compressive residual stresses in component plate i
f_y	Yield stress of steel
h	Height of web
h_c	Twice the distance from the centroid to the inside face of the compression flange less the fillet for rolled sections, to the inside face of the compression flange for welded sections, and to the nearest line of fasteners for built-up sections
h_d	Vertical distance from the inside face of the compression flange to the point of intersection between the web and centerline of delta stiffener
h_o	Distance between flange centroids
h_p	Twice the distance from the plastic neutral axis to the inside face of the compression flange when welds are used, or to the nearest line of fasteners when bolts are used
h_{pl}	Depth of a rectangular plate
k_{cr}	Factor to account for end restraints
k_v	Elastic shear buckling coefficient
l_i	Length of the midline perimeter of the ith cell
q_i	Shear flow of cell i
q_u	Factored uniformly distributed load
q'	Shear flow for the cell adjacent to the ith cell
$\tilde{q}$	Torsional function

r	Root radius
r_i	Inner radius of a circle
r_o	Outer radius of a circle
r_t	Radius of gyration of the flange components in flexural compression plus one-third of the web area in compression due to application of major axis bending
t	Thickness where dl is located
t_c	Thickness of compression flange
t_d	Thickness of delta stiffener
t_i	Thickness of component plate i
t_{ij}	Thickness of the element connecting points i and j
t_p	Rectangular plate thickness
t_{tb}	Plate thickness of rectangular tubular section
t_w	Web thickness
u	Out-of-plane deflection
v	Vertical deflection
v^M	Non-trivial displacement solution
w	Double sectorial area or unit warping with respect to the centroid
w_d	Plate width of delta stiffener
x, y, z	Cross-section coordinates with respect to the centroid
x', y', z'	Rotated and deflected cross-section coordinates with respect to the centroid
x_d	Horizontal distance between the centroids of the cross-section and delta stiffener
$\bar{y}$	Distance from the bottom of the cross-section to the centroid location
y_c	Distance from the centroid to the centerline of the compression flange
y_d	Vertical distance between the centroids of the cross-section and delta stiffener
y_i	Distance from the bottom of the cross-section to the centroid of component plate i
y_{lc}	Distance between the location of the applied load and the mid-height of the cross-section
y_{ls}	Distance between the point of application of the transverse load and the shear center
$\bar{y}_p$	Distance from the bottom of the cross-section to the plastic neutral axis
y_t	Distance from the centroid to the centerline of the tension flange

y_w	Vertical distance between the centroids of the cross-section and web
β	Angle of twist per unit length
β_x	Coefficient of monosymmetry about the non-symmetry axis
Δ_{all}	Allowable deflection
Δ_L	Deflection under service live load
Φ_{LT}	Value to determine the reduction factor χ_{LT}
α_{LT}	Imperfection factor for lateral-torsional buckling
χ_{LT}	Reduction factor for lateral-torsional buckling
ε_{eng}	Engineering strain
ε_{true}	True strain
ε_{sh1}	Strain at the onset of strain hardening
ε_u	Strain at ultimate stress F_u
ε_y	Yield strain
η	Factor for shear area
γ	Shear strain
γ_{M1}	Partial safety factor for resistance of the member to instability assessed by member checks
γ_t	Angle of twist
κ	Ratio of percent increase in buckling moment capacity to percent increase of cross-section area when delta stiffeners are added to an I-girder
λ	Slenderness parameter
$\bar{\lambda}_{LT}$	Non-dimensional slenderness for lateral-torsional buckling
$\bar{\lambda}_{LT,0}$	Plateau length of the lateral torsional buckling curves
λ_{pw}	Limiting slenderness parameter for compact webs
λ_{rw}	Limiting slenderness parameter for noncompact webs
ν	Poisson's ratio
ρ_{ij}	Perpendicular distance from the centroid of the cross-section to the tangent line joining points i and j
σ	Normal stress
σ_{eng}	Engineering stress
σ_{true}	True stress

θ	Angle measured between the web and delta stiffener
τ_{ave}	Shear stress averaged over the width of a horizontal section
τ_m	Maximum shear stress in the cross-section
τ_y	Shear yield stress

Bibliography

AASHTO. (2014). *AASHTO LRFD Bridge design specifications* (7th ed.). Washington, DC: American Association of State and Highway Transportation Officials.

Abambres, M., & Quach, W. M. (2016). Residual stresses in steel members: a review of available analytical expressions. *International Journal of Structural Integrity, 7*(1), 70-94.

AISC. (2010). *Code of standard practice for steel buildings and bridges, AISC 303-05.* Chicago, IL: American Institute of Steel Construction.

AISC. (2016a). *Specification for structural steel buildings* (ANSI/AISC 360-16 ed.). Chicago, IL: American Institute of Steel Construction.

AISC. (2016b). *Commentary on the specification for structural steel buildings.* Chicago, IL: American Institue for Steel Construction.

Alpsten, G. A. (1968). *Thermal residual stresses in hot-rolled steel members.* Fritz Engineering Laboratory Report 337.3. Bethlehem, PA: Lehigh University.

Alpsten, G. A., & Tall, L. (1970). Residual stresses in heavy welded shapes. *Welding Journal, 49*(3), 93-105.

Andrade, A., Camotim, D., & Providencia e Costa, P. (2007). On the evaluation of elastic critical moments in doubly and singly symmetric I-section cantilevers. *Journal of Constructional Steel Research, 63*, 894-908.

Arabzadeh, A., & Varmazyari, M. (2009). Strength of I-girders with Delta stiffeners subjected to eccentric patch loading. *Journal of Constructional Steel Research, 65*, 1385-1391.

AWS. (2010). *Structural welding code-steel, AWS D1.1: D1.1M* (22nd ed.). AWS Committee on Structural Welding.

Basler, K., & Thurlimann, B. (1959). Plate girder research. *AISC National Engineering Conference.* New York: American Insitute of Steel Construction.

Beckman, F. R., & Mertz, D. R. (2005). *Steel bridge erection practices.* Transportation Research Board.

Beedle, L. S., & Tall, L. (1960). Basic column strength. *Journal of the Structural Division, 86*(5), 139-173.

Beer, F. P., Johnsotn Jr., E. R., & Dewolf, J. T. (2006). *Mechanics of Materials* (4th ed.). New York: McGraw-Hill.

Boissonnade, N., & Somja, H. (2012). Influence of imperfections in FEM modeling of lateral torsional buckling. *Proceedings of the Annual Stability Conference.* Grapevine, TX: Structural Stability Research Council.

Boresi, A. P., & Schmidt, R. J. (2003). *Advanced mechanics of materials.* New York, NY: John Wiley & Sons.

Bradford, M. A. (1989). Inelastic buckling of tapered monosymmetric I-beams. *Engineering Structures, 11*, 119-126.

Camotim, D., Andrade, A., & Basaglia, C. (2012). Some thoughts on a surprising result concerning the lateral-torsional buckling of monosymmetric I-section beams. *Thin-Walled Structures , 60*, 216-221.

Chen, M., & Das, S. (2009). Experimental study on repair of corroded steel beam using CFRP. *Steel and Composite Structures, 9*(2), 103-118.

Chen, W., & Lui, E. (1987). *Structural stability, theory and implementation.* New York: Elsevier.

Cherenko, D. E., & Kennedy, D. L. (1991). An analysis of the performance of welded wide flange columns. *Canadian Journal of Civil Engineering, 18*(14), 537-554.

Chern, C., & Ostapenko, A. (1969). *Ultimate strength of plate girder under shear.* Fritz Engineering Laboratory Report 328.7. Bethlehem, PA: Lehigh University.

Chwalla, E. (1936). Die bemessung der waagerecht ausgesteiften stegbleche vollwandiger trager (Design of horizontally stiffened web plates of plates girders). *IABSE congress report*, (pp. 957-985).

Clarin, M. (2004). *High strength steel - local buckling and residual stresses.* Lic. thesis, Sweden: Lulea University of Technology.

Clark, J. W., & Hill, H. N. (1960). Lateral buckling of beams. *Journal of the Structural Division, 86*(ST7), 175-196.

Durkee, E. L. (1959). Problems in bridge erection as affected by design requirements. *Proceedings of AISC National Engineering Conference.* New York.

Dux, P. F., & Kitipornchai, S. (1983). Inelastic beam buckling experiments. *Journal of Constructional Steel Research, 3*(1), 3-9.

Dwight, J. B. (1981). The effect of residual stresses on structural stability. In A. J. Farlane (Ed.), *Residual stresses and their effects* (pp. 21-27). London: The Welding Institute.

Dwight, J. B., & Moxham, K. E. (1969). Welded steel plates in compression. *The Structural Engineer, 47*(2), 49-66.

EC3. (2005). *Eurocode 3: Design of steel structures.* Part 1-1: General rules and rules for buildings (EN 1993-1-1). Brussels: European Committee for Standardization (CEN).

EC3. (2006). *Eurocode 3: Deisgn of Steel Structures.* Part1-5: General rules - Plated structural elements. Brussels: European Committee for Standardization (CEN).

ECCS. (1976). *Manual on stability of steel strucutres.* Brussels: European Convention for Constructional Steelwork, Technical Committee 8.

Egilmez, O. O., & Yormaz, D. (2011). Cyclic testing of steel I-beams reinforced with GFRP. *Steel and Composite Structures, 11*(2), 93-114.

El-Mahdy, G. M., & El-Saadawy, M. M. (2015). Elastic and inelastic strength of singly symmetrical I-beams. *Proceedings of the Annual Stability Conference.* Nashville, TN: Structural Research Council.

Essa, H., & Kennedy, D. (1993). *Distortional Buckling of Steel Beams, Structural Engineering Rep. No. 185.* University of Alberta, Department of Civil Engineering, Edmonton, Alberta, Canada.

Fukomoto, Y. (1982). Numerical data bank for the ultimate strength of steel stuctures. *Der Stahlbau*, 21-27.

Fukomoto, Y., Itoh, Y., & Kubo, M. (1977). Strength variation of laterally unsupported beams. *Journal of the Structural Division*, 541-562.

Fukumoto, Y., & Itoh, Y. (1981). Statistical study of experiments on welded beams. *Journal of Structural Division, 107*(ST1), 89-103.

Galambos, T. V. (1968). *Structural members and frames.* (W. J. Hall, Ed.) Upper Saddle River, New Jersey: Prentice-Hall, Inc.

Galambos, T. V. (Ed.). (1998). *Guide to stability design criteria for metal structures* (5th ed.). New York, NY: Structural Stability Research Counsil, Wiley.

Galambos, T. V., & Ketter, R. L. (1959). Columns under combined bending and thrust. *Journal of the Engineering Mechanics Division, 85*, 1-30.

Glassman, J. D., Moreyra Garlock, M. E., Aziz, E. M., & Kodur, V. K. (2016). Modeling parameters for predicting the postbuckling shear strength of steel plate girders. *Journal of Constructional Steel Research, 121*, 136-143.

Goodier, J. N. (1942, January). Flexural-torsional buckling of bars of open section under bending, eccentric thrust or torsional loads. *Cornell University engineering experimental station*(28).

Hadley, H. M. (1961, May). Exploratory test on a steel delta girder. *Civil Engineering Magazine*, pp. 50-52.

Hadley, H. M. (1964). The bridge delta girder - single-webbed and doublewebbed. *AISC Engineering Journal*, 132-136.

Hassanein, M., Kharoob, O., & El Hadidy, A. (2013). Lateral-torsional buckling of hollow tubular flange plate girders with slender stiffened webs. *Thin-Walled Structures, 65*, 49-61.

Hatami, F., & Esmaeili, N. (2013). Optimization of height at delta stiffened in steel girders by numerical modeling. *Journal of American Science, 9*(2s), 1-5.

Heins, C. P. (1975). *Bending and torsional design in structural members.* Lexington, MA: Lexington Books.

Helwig, T. A., Frank, K. H., & Yura, J. A. (1997). Lateral-torsional buckling of singly symmetric I-beams. *Journal of Structural Engineering, 123*(9), 1172-1179.

Ioannidis, G. I., & Kounadis, A. N. (1994). Lateral post-buckling analysis of monosymmetric I-beams under uniform moment. *Journal of Constructional Steel Research, 30*, 1-12.

JSCE. (2009). *Standard specifications for steel and composite structures* (1st ed.). Tokyo, Japan: Japan Society of Civil Engineers.

Kim, Y. D. (2010). *Behavior and design of metal building frames using general prismatic and web-tapered steel I-section members.* (Docotoral Dissertation), Georgia Institute of Technology, School of Civil and Environmental Engineering, Atlanta.

Kim, Y. D., & White, D. W. (2013). Transverse stiffener requirements to develop shear-buckling and postbuckling resistance of steel I-girders. *Journal of Structural Engineering, 140*(4), 04013098.

Kitipornchai, S., & Trahair, N. S. (1979). *Buckling properties of monosymmetric I-beams.* Report No. CE 4, University of Queensland, Department of Civil Engineering.

Kitipornchai, S., & Wong-Chung, A. D. (1987). Inelastic buckling of welded monosymmetric I-beams. *Journal of Structural Engineering, 113*(4), 740-756.

Kitipornchai, S., Wang, C. M., & Trahair, N. S. (1986). Buckling of monosymmetric I-beams under moment gradient. *Journal of Structural Engineering, 112*(4), 781-799.

Knight, R. P. (2003). Economical steel plate girder bridges. *Engineering Journal, Second Quarter*, 89-93.

Lee, S., & Yoo, C. (1998). Strength of plate girder web panels under pure shear. *Journal of Structural Engineering, 124*(2), 184-194.

Lee, S., Davidson, J., & Yoo, C. (1996). Shear buckling coefficients of plate girder web panles. *Computers and Structures, 59*(5), 789-795.

Lindner, J. (1976). The ultimate load of monosymmetric sections due to lateral torsional buckling. *IABSE congress report, 10*, 353-357.

Maiorana, E., Pellegrino, C., & Modena, C. (2011). Influence of longitudinal stiffeners on elastic stability of girder webs. *Journal of Constructional Steel Research, 67*(1), 51-64.

McFalls, R. K., & Tall, L. (1969). A study of welded columns manufactured from flame-cut plates. *Welding Journal, 48*(4), 141-146.

Mohebkhah, A., & Azandariani, M. G. (2015). Lateral-torsional buckling of Delta hollow flange beams under moment gradient. *Thin-Walled Structures, 86*, 167-173.

Mohri, F., Brouki, A., & Roth, J. (2003). Theoretical and numerical stability analyses of unrestrained, mono-symmetric thin-walled beams. *Journal of Constructional Steel Research, 59*, 63-90.

Nagaraja Rao, N. R., & Tall, L. (1964). Residual stresses in welded shapes. *Welding Journal, 43*(7), 295-302.

Nakai, H., & Yoo, H. C. (1988). *Analysis and design of curved steel bridges.* TX: McGraw-Hill, Inc.

Nethercot, D. A. (1973). Inelastic buckling of monosymmetric I-beams. *Journal of Structural Division, 99*(ST7), 1696-1701.

Nethercot, D., & Gardner, L. (2005). The EC3 approach to the design of columns, beams and beam-columns. *Steel and Composite Structures, 5*(2-3), 127-140.

O'Connor, C., Goldsmith, P. R., & Ryall, J. T. (1965). The reinforcement of slender steel beams to improve beam buckling strength. *Civil Engineering Transactions, CE7*(11), 29-37.

O'hEachteirn, P., & Nethercot, D. A. (1988a). Lateral buckling behaviour of monosymmetric plate girders. *Journal of Constructional Steel Research, 11*, 261-282.

O'hEachteirn, P., & Nethercot, D. A. (1988b). Lateral buckling tests on monosymmetric plate girders. *Journal of Constructional Steel Research, 11*, 241-259.

Owen, D. R., Rockey, K. C., & Skaloud, M. (1970). *Ultimate load behavior of longitudinally reinforced web plates subjected to pure bending.* Japan: KAJIMA Technical Reseach Institute.

Plum, C. M., & Svensson, S. E. (1993). Simple method to stabilize I-beams against lateral buckling. *Journal of Structural Engineering, 119*(10), 2855-2870.

Popov, E. P. (1980). An update on eccentric seismic bracing. *Engineering Journal, AISC, 17*(3), 3rd Quarter, 70-71.

Porter, D. M., Rocky, K. C., & Evans, H. R. (1975). The collapse behaviors of plate girders loaded in shear. *Structural Engineering, 53*(9), 131-325.

Prawel, S. P., Morrell, M. L., & Lee, G. C. (1974). Bending and buckling strength of tapered structural members. *Welding Journal, 53*(2), 75-84.

Rebelo, C, Lopes, N., Simoes da Silva, L., Nethercot, D., & Vila Real, P. (2009). Statistical evaluation of the lateral-torsional buckling resistance of I-beams, part 1: variability of the Eurocode 3 resistance model. *Journal of Constructional Steel Research, 65*, 818-831.

Righman, J. (2005). *Rotation compatibility approach to moment redistribution for design and rating of steel I-girders.* (Doctoral dissertation), West Virginia University, Department of civil and environmental engineering.

Roberts, T. M., & Burt, C. A. (1985). Instability of monosymmetric I-beams and cantilevers. *International Journal of Mechanical Sciences, 27*(5), 313-324.

Sahnehsaraei, M. J., & Erfani, S. (2014). Analysis of elastic buckling behavior of steel girders. *International Journal of Engineering & Technology, 3*(3), 372-377.

Sahraei, A., Wu, L., & Mohareb, M. (2015). Finite element formulation for lateral torsional buckling analysis of shear deformable mono-symmetric thin-walled members. *Thin-Walled Structures, 89*, 212-226.

Sharp, M. L., & Clark, J. W. (1971). Thin aluminum shear web. *Journal of the Structural Division, 97*(4), 1021-1038.

Simulia. (2014). *Abaqus 6.14 documentation.* Providence, RI, USA: DS Simulia Corp.

Subramanian, L., & White, D. W. (2015). Evaluation of lateral torsional buckling resistance equations in AISC and AASHTO. *Proceedings of the Annual Stability Conference.* Nashville, TN: Structural Stability Research Council.

Subramanian, L., & White, D. W. (2016). Reassessment of the lateral torsional buckling resistance of I-section members: Uniform-moment studies. *Journal of Structural Engineering*, 04016194.

Subramanian, L., & White, D. W. (2017). Resolving the disconnects between lateral torsional buckling experimental tests, test simulations and design strength equations. *Journal of Constructional Steel Research, 128*, 321-334.

Surla, A. S., Kang, S. Y., & Park, J. S. (2015). Inelastic buckling assessment of monosymmetric I-beams having stepped and non-compact flange sections. *Journal of Constructional Steel Research, 114*, 325-337.

Szalai, J., & Papp, F. (2005). A new residual stress distribution for hot-rolled I-shaped sections. *Journal of Constructional Steel Research, 61*, 845-861.

Szewczak, R. M., Smith, E. A., & DeWolf, J. T. (1983). Beams with torsional stiffeners. *Journal of Structural Engineering, 109*(7), 1635-1647.

Takabatake, H. (1988). Lateral buckling of I beams with web stiffeners and batten plates. *International Journal of Solids and Structures, 24*(10), 1003-1019.

Takabatake, H., Kusumoto, S., & Inoue, T. (1991). Lateral buckling behavior of I-beams stiffened with stiffeners. *Journal of Structural Engineering*(117), 3203-3215.

Timoshenko, S. P. (1921). Uber die stabilitat versteifter platten (On the stability of stiffened plates). *Eisenbau, 12*, 147-163.

Timoshenko, S. P., & Gere, J. M. (1961). *Theory of elastic stability* (2nd ed.). Mineola, New York: Dover Publications, Inc.

Trahair, N. S. (1993). *Flexural-torsional buckling of structures.* London: E & FN Spon.

Trahair, N. S. (2012). Inelastic buckling design of monosymmetric I-beams. *Engineering Structures, 34*, 564-571.

Trahair, N. S., Bradford, D. A., Nethercot, D. A., & Gardner, L. (2008). *The behavior and design of steel structures to EC3* (4th ed.). New York: Taylor & Francis.

Vlasov, V. Z. (1940). *Thin-walled elastic beams* (2nd ed.). Moscow: Translated by Israel program for scientific translations, Jerusalem (1961).

Wagner, H. (1936). Torsion and buckling of open sections. (333, Ed.) *NACA technical memorandum 807*.

Wang, C. M., & Kitipornchai, S. (1986). Buckling capacities of monosymmetric I-beams. *Journal of Structural Engineering, 112*(11), 2373-2391.

White, D. W. (2008). Unified flexural resistance equations for staibility design of steel I-section members: Overview. *Journal of Structural Engineering, 134*(9), 1405-1424.

White, D. W., & Baker, M. G. (2008). Shear resistance of transversely stiffened steel I-girders. *Journal of Structural Engineering, 134*(9), 1425-1436.

White, D. W., & Jung, S. -k. (2003). *Simplified lateral-torsional buckling equations for singly-symmetric I-section members. Structural Engineering, Mechanics and Materials Rep. No. 24b.* Georgia Institute of Technology, School of Civil and Environmental Engineering, Atlanta.

White, J. D. (1977a). *Longitudinal shrinkage of a single pass weld.* University of Cambridge. Report CUED/C-Struct/TR.57.

White, J. D. (1977b). *Longitudinal stresses in welded T-sections.* University of Cambridge. Report CUED/C-Struct/TR.60.

Yang, Y., & Lui, E. M. (2012). Behavior and design of steel I-beams with inclined stiffeners. *Steel and Composite Structures, 12*(3), 183-205.

Young, B. W. (1975). Residual stresses in hot rolled members. *IABSE reports of the working commissions, 23*, 25-38.

Young, B. W., & Dwight, J. B. (1971). *Residual stresses and their effect on the moment-curvature properties of structural steel sections.* CIRIA Techical Note, 32. London: Construction Industry Research & Information Association.

Young, B. W., & Schulz, G. W. (1977). *Mechanical properties of residual stresses.* Second International Colloqium on Stability of Steel Structures. Liege: Introductory Report, ECCS and IABSE.

Yu, C. K., & Tall, L. (1971). Significane and application of stub column test results. *Journal of the Structural Division, 97*(ST7), 1841-1861.

Zhao, J. J., & Tonias, D. E. (2012). *Bridge engineering : design, rehabilitation, and maintenance of Modern Highway Bridges.* New York: McGraw-Hill Education.

Ziemian, R. D. (Ed.). (2010). *Guide to stability design criteria for metal structures* (6th ed.). New Jersey: John Wiley & Sons, Inc.

Vita

Omar El Masri was born on June 9, 1988 in Tripoli, Lebanon. He finished high school at École Saint Élie des Pères Carmes, graduating first in his class with the Lebanese Baccalaureate in general sciences (mention très bien). He then attended the Lebanese American University (LAU) in Byblos, Lebanon where he received a Bachelor of Engineering in Civil Engineering in June 2012. Thereafter, he started his graduate studies at LAU where he worked as a laboratory technician for one semester and as a laboratory instructor for three semesters. During this period, he served as a trainer at the Leadership & Constitutional Education Academy, and attended courses on English oral communication skills at Oxford House College in London, UK and St. Giles International in San Francisco, CA. He received his M.S. degree in Civil & Environmental Engineering in June 2014. The title of his thesis was "Effects of Deck transverse Cracks on the Temperature Distribution in Composite Bridges". In August 2014, he joined the Doctoral program at Syracuse University (SU), NY, under the Yabroudi and Al-Bitar Fellowship and is expected to receive his Ph.D. in Civil Engineering for his work on steel Delta girders in May 2017. At SU, he served as a guest lecturer, worked as a teaching assistant for two semesters, and participated in the Future Professoriate Program (FPP) where he received his certificate in university teaching (CUT).

Throughout his ten years of study at university level, the author has been actively engaged in his family company "Masri for Steel Construction", where he prepared proposals, shop drawings, and the design of a number of steel structures. The author is a student member of the following professional societies: AISC, ASCE and SEI, and a member of the international honor society Phi Beta Delta. He has published several papers in the structural engineering field.

272

His main research interests include steel structures, structural stability, computer-aided analysis and design methods, and bridge engineering.